Study on Heat Dissipation and Aeration in Hydraulic Jump through Laboratory Experiments and Simulation

Thesis Submitted by

SAIKAT MONDAL

Index No.: D-7/ISLM/34/18

Doctor of Philosophy (Engineering)

School of Water Resources Engineering

Faculty of Interdisciplinary Studies, Law & Management

Jadavpur University

Kolkata, India

2025

Dedicated to

My Parents

&

Teachers

JADAVPUR UNIVERSITY
KOLKATA – 700 032, INDIA

INDEX NO.: **D-7/ISLM/34/18**

Title of Thesis:

Study on Heat Dissipation and Aeration in Hydraulic Jump through Laboratory Experiments and Simulation

Name, Designation & Institution of the Supervisors

Dr. Subhasish Das
Associate Professor and Joint Director
School of Water Resources Engineering
Jadavpur University
Kolkata 700 032, West Bengal, India

Dr. Sanchayan Mukherjee
Associate Professor
Department of Mechanical Engineering
Kalyani Government Engineering College
Kalyani 741235, West Bengal, India

Dr. Rajib Das
Assistant Professor
School of Water Resources Engineering
Jadavpur University
Kolkata 700 032, West Bengal, India

List of Publications

Journals:

- **Saikat Mondal, Rajib Das, Subhasish Das and Sanchayan Mukherjee**. (2024). Experimental investigation of dissolved oxygen improving aeration efficiency by hydraulic jumps. ***Flow Measurement and Instrumentation***, 100, 102715. (**SCIE** and Scopus Indexed) (Impact Factor: 2.3).

- **Saikat Mondal, Sanchayan Mukherjee and Subhasish Das**. (2020). Experimental Study of Thermal Effect on Oscillating Hydraulic Jump. ***Indian Science Cruiser***, Volume 34, No 4, pp. 15-19.

Conferences:

- **Saikat Mondal, Subhasish Das, Rajib Das and Sanchayan Mukherjee**. (2025). *An Approach to Improve Water Quality by Increasing Aeration Efficiency Through Hydraulic Jumps*. In: Mukhopadhyay, A., Ghosh, K. (eds) Advances in Thermo-Fluid Engineering. INCOM 2024. Lecture Notes in Mechanical Engineering, pp 231–243. Springer, Singapore. https://doi.org/10.1007/978-981-97-7296-4_16

- **Saikat Mondal, Subhasish Das, Rajib Das and Sanchayan Mukherjee**. (2024). *Improving Aeration Efficiency in Hydraulic Jump: An Approach to Improve Water Quality*, 2nd International Conference on Mechanical Engineering (INCOM 2024), Kolkata, India.

- **Saikat Mondal, Rajib Das, Subhasish Das and Sanchayan Mukherjee**. (2023). *Effect of Hydraulic Jump on Aeration Efficiency in Terms of Dissolved Oxygen in an Experimental Channel*, 5th Regional Science & Technology Congress, 2022-2023, Kolkata, India.

PROFORMA – 1

"Statement of Originality"

I, **Saikat Mondal (D-7/ISLM/34/18)** registered on **06th February, 2018** do hereby declare that this thesis entitled "**Study on Heat Dissipation and Aeration in Hydraulic Jump through Laboratory Experiments and Simulation**" contains literature survey and original research work done by the undersigned candidate as part of Doctoral studies.

All information in this thesis have been obtained and presented in accordance with existing academic rules and ethical conduct. I declare that, as required by these rules and conduct, I havefully cited and referred all materials and results that are not original to this work.

I also declare that I have checked this thesis as per the "Policy on Anti Plagiarism, Jadavpur University, 2019", and the level of similarity as checked by iThenticate software is 06 %.

Signature of Candidate: Saikat Mondal.

Date : 27/01/2025

Certified by Supervisor(s):(Signature with date, seal)

1. Subhasish Das 27/01/25
   Dr. Subhasish Das
   Associate Professor & Joint Director
   School of Water Resources Engineering
   Jadavpur University
   Kolkata - 700032

2. Sanchayan Mukherjee 27/1/2025
   (DR. SANCHAYAN MUKHERJEE)
   Associate Professor
   Department of Mechanical Engineering
   Kalyani Govt. Engg. College, Kalyani, Nadia

3. Rajib Das 27/01/2025
   Dr. RAJIB DAS
   Assistant Professor
   School of Water Resources Engineering
   Jadavpur University
   Kolkata-700 032

PROFORMA – 2

CERTIFICATE FROM THE SUPERVISORS

This is to certify that the thesis entitled "**Study on Heat Dissipation and Aeration in Hydraulic Jump through Laboratory Experiments and Simulation**" submitted by **Mr. Saikat Mondal**, who got his name registered on **06th February, 2018** for the award of the Ph.D. degree of Jadavpur University is absolutely based upon his own work under the supervisions of **Dr. Subhasish Das**, Associate Professor and Joint Director of School of Water Resources Engineering, Jadavpur University, **Dr. Sanchayan Mukherjee**, Associate Professor, Department of Mechanical Engineering, Kalyani Government Engineering College, and **Dr. Rajib Das**, Assistant Professor, School of Water Resources Engineering, Jadavpur University and that neither his thesis nor any part of the thesis has been submitted for any degree or any other academic award anywhere before.

1. Subhasish Das 27/01/25

THESIS ADVISOR

Dr. Subhasish Das
Associate Professor and Joint Director
School of Water Resources Engineering
Jadavpur University

Dr. Subhasish Das
Associate Professor & Joint Director
School of Water Resources Engineering
Jadavpur University
Kolkata - 700032

2. Sanchayan Mukherjee 27/1/2025

THESIS ADVISOR

Dr. Sanchayan Mukherjee
Associate Professor
Department of Mechanical Engineering
Kalyani Government Engineering College

Associate Professor
Department of Mechanical Engineering
Kalyani Govt. Engg. College, Kalyani, Nadia

3. Rajib Das 27/01/2025

THESIS ADVISOR

Dr. Rajib Das
Assistant Professor
School of Water Resources Engineering
Jadavpur University

Dr. RAJIB DAS
Assistant Professor
School of Water Resources Engineering
Jadavpur University
Kolkata-700 032

ACKNOWLEDGEMENTS

The author wishes to express his heartfelt gratitude towards his thesis supervisors Dr. Subhasish Das, Associate Professor and Joint Director of School of Water Resources Engineering (SWRE), Jadavpur University (JU), Dr. Sanchayan Mukherjee, Associate Professor, Department of Mechanical Engineering, Kalyani Government Engineering College (KGEC), and Dr. Rajib Das, Assistant Professor, School of Water Resources Engineering (SWRE), Jadavpur University (JU), for their valuable guidance and continuous encouragement in planning, wholehearted involvement, advice, support, execution and presentation of this thesis. It was their initiation, constant encouragement and help rendered in developing the experimental facilities in the Fluvial Hydraulics Laboratory of the School of Water Resources Engineering, Jadavpur University which enabled the author to carry out a major part of the present thesis work. It would also be very difficult to inculcate this work in pen and paper without their valuable advises. The author is also indebted to his supervisors for helping and providing moral support during the tenure of his Ph.D. work.

Heartfelt gratitude to Prof. (Dr.) Asis Mazumdar, Professor & Director, School of Water Resources Engineering, Jadavpur University for his encouragement during the research. Also thank Dr. Gourab Banerjee, Assistant Professor, School of Water Resources Engineering, Jadavpur University for his moral support.

Thanks are also due to all the staff members of the SWRE, JU, for their co-operation during the investigation.

Thanks are also due to Dr. Asim Kuila, Ex-Ph.D. student; Mr. Plaban Sen; Mr. Buddhadev Nandi; Ph.D. students and other Research Scholars; of SWRE, JU, for their unconditional support and help during the preparation of my thesis.

Last but not least, the author would like to dedicate this thesis to his parents, family and friends without whose motivation and constant backup, the completion of this thesis might be a distant dream to the author.

Date: 27/01/2025

Place: SWRE, Jadavpur University

Saikat Mondal.

Saikat Mondal
Ph.D. Student
School of Water Resources Engineering
Jadavpur University

Table of Contents

Abstract

Hydraulic jumps (H-jumps) develop when any upstream super-critical flow starts decreasing rapidly or suddenly to downstream sub-critical flows. The phenomenon usually occurs when the bed slope suddenly changes from steep to flattened, in natural waterways and hydraulic constructions at the base of spillways, and channels below sluice gates. The highly turbulent flow of and H-jump is associated with the formation of large-scale turbulence, air entrainment, surface roller and spray, and dissipation of energy. It is implemented to improve flow re-aeration, fluid mixing, and energy dissipation.

Along with this H-jump, it has a wide application in industries and environmental engineering. Modern society is heavily dependent on power plants and a wide range of industries, which in turn discharge thermally polluted water into the water bodies such as canals, rivers, and lakes. During H-jumps, the energy is lost in the term of heat dissipation from kinetic energy. The H-jump could be an efficient and economical means of dissipating heat from the water discharged from power plants and other industries.

The amount of dissolved oxygen (DO) in a water body is an essential parameter for evaluating the water quality as well as the capability of water to maintain flora and fauna. In order for bacteria and other microorganisms to survive, the DO content in a waterbody must be higher than 5 mg/l. The process of circulating, mixing, or dissolving air in a liquid or substance is known as aeration. In order to effectively treat wastewater and promote microbial growth, this procedure is usually the first significant phase in the oxygen transfer process in drinking water treatment plants. The H-jump is being explored as an aeration agent.

By generating turbulence, the H-jump, a natural mechanical mixer, is used as a more cost-effective and effortless oxygen transfer mechanism than the traditional oxygenation procedure. This transfer of oxygen is mostly due to the air being entrained into the stream by several air bubbles, which facilitates the transfer of air and water. The H-jump position, jump length, energy dissipation amount, and aeration efficiency must all be determined in order to develop and execute a hydraulic setup that will form an H-jump.

In the current analysis, H-jumps were formed in a rectangular laboratory channel, and a number of experiments were conducted to examine jump parameters, energy dissipation in the form of heat, and aeration efficiency with variable discharge, bed slope, bed profile, and ramp slope.

The water temperature varied from lowest to highest within a measuring range in order to perform a forced submerged oscillating H-jump study. Temperature variations between 32°C and 40°C were used to monitor and record various jump characteristics. Temperature variations were recorded during the jump profiles, and the relationship between jump parameters and temperature variations was measured and quantified. The temperature was measured throughout the jump profile with the help of temperature sensors and a temperature controller. Applications, where the jump characteristics are greatly impacted by a varying stream water temperature, may be identified by this investigation. This investigation may help in identifying uses where the jump characteristics are significantly impacted by the change in water temperature in the stream.

A part of the present work focusses on the simulation of H-jumps in a simple flume of rectangular shaped and determination of the ability of H-jump to increase the dissipation of heat from the water to the ambient. The inlet water temperature was kept constant at 40°C while six different ambient temperatures were considered as 10°C, 15°C, 20°C, 25°C, 30°C and 35°C. The H-jump for each of the ambient temperatures was simulated and the drop in average temperature at a section downstream of the H-jump was determined. The decreases in average specific entropy and average specific enthalpy were also determined and these decreases in average temperature, specific enthalpy and specific entropy, for each ambient temperature, were compared with the decrease in the corresponding quantities due to natural convection and conduction without the occurrence of a H-jump.

The heat transfers from the water to the ambient aided by the H-jump resulted in an improvement in the drop in temperature, specific entropy, and specific enthalpy as compared to the drops in these quantities owing to heat transfer due to convection and conduction without the H-jump. This improvement showed a non-linear variation with the ambient temperature and decreased with the increase in ambient temperature. However, to establish the exact association between this increase in the drop in temperature, specific enthalpy, and specific entropy by H-jump with the ambient temperature and also the water temperature, a few more experiments and simulations with different water temperatures and with a few more ambient temperatures have to be performed.

This experimental study aims to investigate the aeration performance using H-jump characteristics on smooth beds, so that their correlations may be used as a basis for measuring aeration efficiency. The relationships between discharge, inlet Froude number, bed slope, jump height, relative jump length, sequent depth ratio (SD-Ratio), and aeration efficiency were identified. The nature of these interactions was investigated by testing the aeration performance of a forced submerged H-jump with five different discharges ranging from 15 lps to 35 lps and five distinct smooth bed slopes ranging from 0° to 6° in a rectangular tilting flume. The DO was measured at the water surface level throughout the jump profile. The inlet Froude number prior to the jump ranges from 2.18 to 8.23. The positive correlation between H-jump controlling parameters and aeration efficiency is confirmed by experimental observation. During the experiment, the aeration efficiency was found to vary from 9.4 to 34.0%. Estimating the ideal aeration efficiency caused by H-jumps is part of this study, which can help hydraulic engineers design structures that can restore any deteriorated stream.

In this study, the impacts of a pebbled rough bed on fundamental parameters of H-jump and aeration efficiency were methodically investigated. The H-jump, herein, was formed by adjusting a tail gate in rectangular flume with five different discharges varying from 15 lps to 35 lps and five different bed slopes fluctuating from 0° to 6° with two distinct ramp slopes of 1:3 and 1:4. The roughness height in the experimental setup was 24.77 mm. Experiments were performed by varying the discharge and bed slope of water from minimum to maximum within the range of measurement and different jump characteristics were observed. The dependence of jump parameters with varying discharge and bed slope was measured and quantified. Aeration efficiency, jump height, relative jump length, bed slope, discharge, inlet Froude number, and SD-Ratio were found to be associated. The research of fundamental flow patterns with aeration efficiency covered a

broad range of Reynolds numbers from 4.7×10^4 to 1.2×10^5 and Froude numbers from 2.24 to 8.40. The observations and outcomes reveal a relationship among the aeration efficiency, energy dissipation rate, discharge, and bed slope. In this rough bed arrangement, the H-jump attained a maximum aeration efficiency of 37.0% using a 1:3 ramp slope and 40.1% using a 1:4 ramp slope which is quite satisfactory. From these results, the H-jump is found to be effective for oxygen transfer and energy dissipation. This study is expected to advance this complex hydraulic process of aeration efficiency and provide strong support for upcoming theoretical and numerical investigations.

Introduction

A conduit with a free top surface through which a liquid flows is revealed to as an open channel. The top free surface, which has a constant pressure, is the interface between a moving liquid and the fluid substrate above it, as shown in Fig. 1.1. In the applications of hydraulic engineering, the most commonly used liquid is water, while air at atmospheric pressure operating as the overlaying fluid. Therefore, the primary focus of our concentration will be on the stream of water with a free surface. In the field of engineering, using water resources involves, in one way or another, open channels of different sizes. Open channels serve many kinds of purposes like flows in naturally occurring rivers and streams; man-made, or artificial, channels for transferring water from an origin to a place of requirements, such as for water supply, irrigation, and hydropower creation; drainage systems that carry waste waters from industry or home; and waterways for navigation. Open channels come in a wide range of sizes, shapes, and roughness, covering several orders of magnitude. In open channels, surface tension effects are minimal and water flow predominantly occurs in the turbulent regime. Furthermore, the incompressible nature of water makes it easy to understand and the primary non-dimensional parameter governing the flow characteristic in open channels is the Froude number.

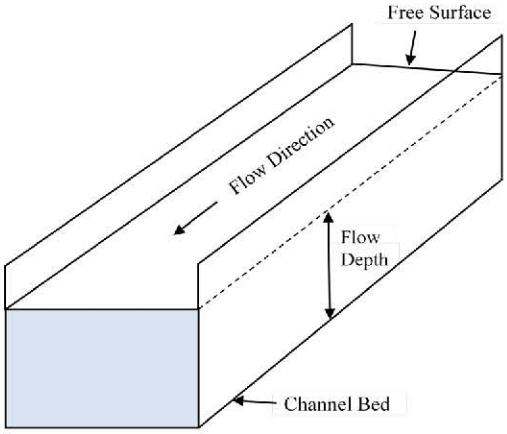

Fig. 1.1. A rectangular shaped open channel.

1.1. Types of Channels

a) Prismatic and Non-Prismatic Channels

Prismatic channels are those in which the bottom slope, cross-sectional form, and size are all consistent. Prismatic channels make up the majority of man-made (artificial) channels over extended lengths and it commonly shaped as rectangular, trapezoidal, triangular and circular.

For the most part, all natural channels are non-prismatic because of their variable cross-sections and bottom slopes.

b) Rigid and Mobile Boundary Channels

Channels like sewers, unlined canals of non-erodible nature, and lined canals that have a rigid boundary are those whose planiform, roughness, and shape magnitudes do not depend on the flow parameters. There is just one degree of freedom for rigid channels; the only possible variation for a given channel shape is the flow depth, which can vary across time and space based on the flow characteristics.

Mobile boundary channels are a lot of unlined alluvium channels, both man-made and natural rivers, where depending on the type of flow, the longitudinal slope, bed width, and depth of the channel can all alter over time and space. The flow causes constant erosion and deposition, causing the borders to deteriorate. In these situations, the edge of the channel is movable, and the flow transports substantial volumes of silt into suspension and into contact with the bed.

1.2. Classification of Flows

a) Steady and Unsteady Flows

When the flow characteristics, like the depth or discharge at a segment, remain constant throughout time, the flow is said to be steady.

A flow is said to as unsteady if the depth or discharge varies with time.

In real world applications, there will always be variations in the flow characteristics over time because of the turbulent character of the flow and the interaction of several forces, such as surface tension and wind. The flow is not considered unstable if there are ripples in a canal caused by wind that blows over the free surface and if the character of the water–surface profile due to the impact of an obstacle is to be examined. In this scenario, a time–average of depth collected over an adequate amount of time would show a consistent depth at a segment, and as a result, the flow would be considered steady to study qualitative characteristics. Unsteady flow examples include flood flows in rivers and significantly fluctuating surges in canals. Analysis of unsteady flows is far more challenging than that of steady flows.

b) Uniform and Non-uniform Flows

An open channel is considered to have uniform flow if its flow characteristics, such as its depth of flow, stay consistent throughout its length.

Non-uniform flow describes a flow where the flow characteristics change as it moves through the channel.

An illustration (Fig. 1.2) of uniform flow is a prismatic channel that conveys a specific discharge at a constant velocity. As it is practically impossible to have an unsteady uniform flow, the word "uniform flow" refers to a steady uniform flow. Examples of non-uniform flow are stream in a prismatic channel with various velocities and flow in a non-prismatic channel. A non-uniform or varying flow may be steady or unsteady.

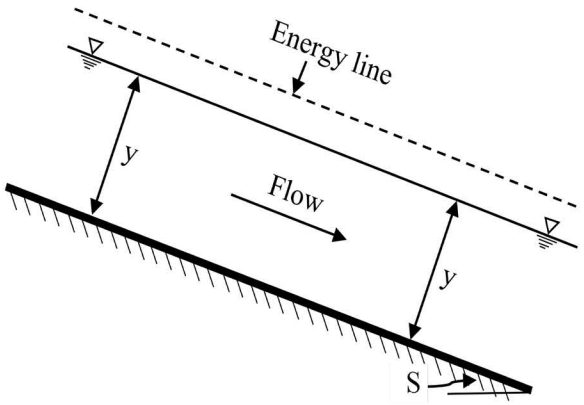

Fig. 1.2. Uniform flow through open channel.

c) Gradually Varying and Rapidly Varying Flows

Gradually varying flow (GVF) and rapidly varying flow (RVF) are two classifications for non-uniform flow. Variable flow presupposes that no flow is introduced into or removed from the channel system externally. In the channel system, the water volume within a given time period is retained.

A varying flow is referred to as GVF if the variation in depth is moderate enough to prevent an excessive curving of streamlines, shown in Fig. 1.3. Examples of a steady GVF include water surface dropping as a result of a dam or an abrupt decrease in a canal bed.

An occurrence known as RVF develops when there is a substantial variation in depth over short distances and a large curve in the varying flow. A steady RVF is exemplified by a hydraulic jump (H-jump) that takes place beneath a spillway or sluice gate. Unsteady RVF can be seen in the movement of a bore up a river or a surge up a canal.

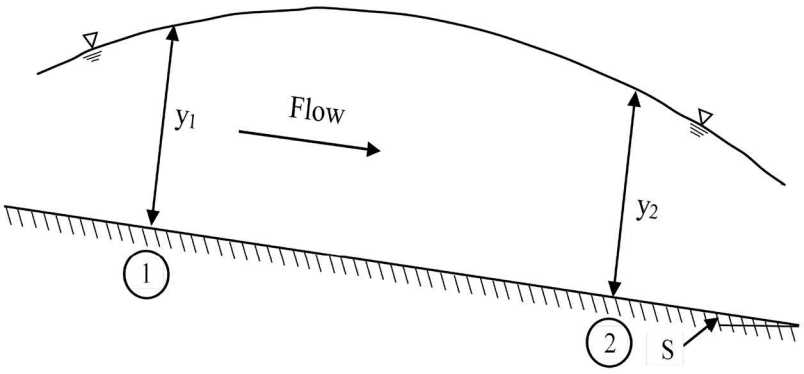

Fig. 1.3. Gradually varying flow through the open channel.

d) Spatially Varying Flow

A spatially varying flow (SVF) is the term used to describe the varying flow that results when a certain amount of flow is added to or eliminated from the system, as in Fig. 1.4. SVF may exhibit steady or unsteady behaviour. Steady SVF can be seen in the flow through a side weir. One common illustration of unsteady SVF is the creation of surface runoff as a result of rainfall, also referred to as overland flow.

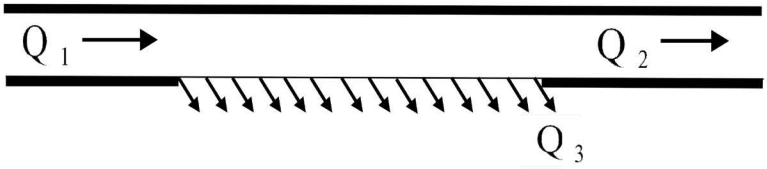

Fig. 1.4. Spatially varying flow through the open channel.

1.3. Specific Energy

In a fluid flow system, specific energy is the energy per unit mass that accounts for variations in pressure, velocity, and elevation. It fluctuates along a channel as a result of variations in bottom elevation and energy losses (E_L), and is comparable to energy per unit mass, using the bottom of the channel as the reference point. In a flow through open channel, the specific energy is utilised to determine the design discharge over a river hydraulic structure in addition to the water depth and critical flow depth through the flow transition while the discharge is given. The specific energy is denoted by E (Eq. 1.1) and is extremely useful in identifying critical depth.

$$E = y + \frac{V^2}{2g} \tag{1.1}$$

The entirety of the kinetic head, potential head, and datum head represent the energy at a section. The potential energy at a segment increases linearly with flow depth, y. As y increases, the kinetic energy at a section decreases parabolically. The correlation between the specific energy and y is represented in the specific energy curve. It is a plot between the specific energy on the abscissa and the depth of flow on the ordinate, shown in Fig. 1.5.

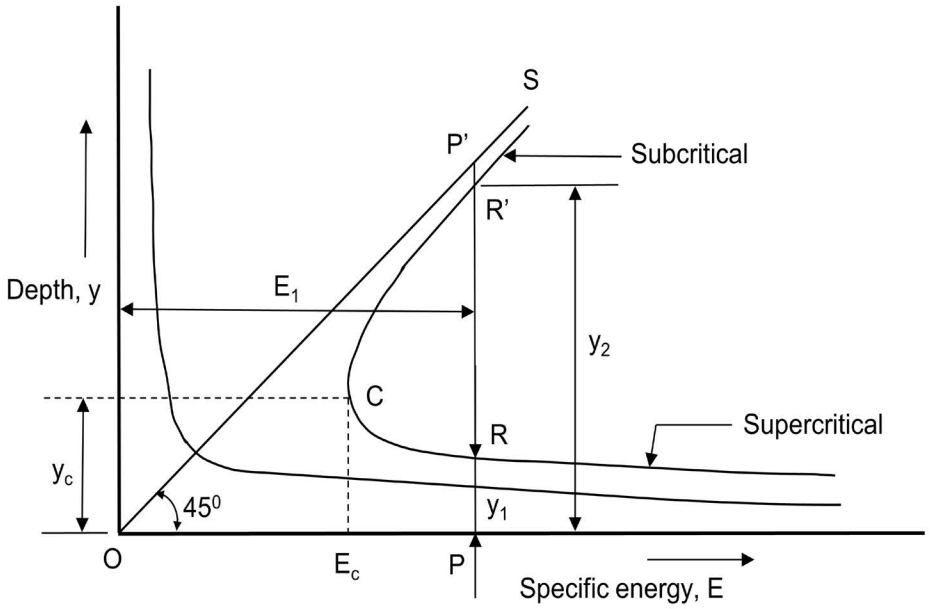

Fig. 1.5. A sketch pertaining to the definition of the specific energy.

The specific energy is unaltered for a uniform flow and can either increase or decrease in a varying flow because it is determined by the elevation of the channel bed in relation to the elevation of the energy line. A line OS is drawn such that the specific energy is equal to the depth. The critical flow condition is the state of having the least amount of specific energy (E_c), and the critical depth is the depth y_c that corresponds to it. The flow velocity at a critical depth is known as the critical velocity. Sub-critical flow is defined as a flow with a depth greater than the critical depth and a velocity lower than the critical velocity. Conversely, in super-critical flow, the velocity exceeds the critical velocity and the flow depth is less than the critical depth. A straight line PP' drawn parallel to the y axis, will intersect the specific energy curve in two points R and R'. In these conditions for a particular discharge, the specific energy (E_1) is the same for two different depths y_1 and y_2. These two depths are referred to be alternate depths since they have the same specific energy. The velocity head is depicted by the point of intercept P'R' or P'R. One (PR = y_1) has a greater velocity head and a smaller depth than the other (PR' = y'_1), which has a larger depth and a lesser velocity head. For a given discharge, the deviation between the two alternative depths increases as the specific energy increases. Conversely, lowering E_1 will result in a smaller difference ($y'_1 - y_1$) and the merging of the two depths at point C, at a specific value $E_1 = E_c$. Only the channel shape and discharge control the critical flow condition. For any given discharge, the critical flow condition is independent of other channel properties like roughness and bed slope.

A dimensionless quantity termed the Froude number (Fr) describes different open channel flow conditions. The Fr represents the ratio between inertia force and gravitational forces (Eq. 1.2).

$$\mathrm{Fr} = \frac{V}{\sqrt{gD}} \tag{1.2}$$

where, V is the average velocity of channel flow, g is gravitational acceleration and D is hydraulic mean depth. Flow types can be categorized according to Fr. If the Fr value is 1, it is defined as critical flow. Supercritical flow is indicated if the Fr value is higher than 1 and if the value is less than 1, it is specified as sub-critical flow.

1.4. Hydraulic Jump

Variable flow occurs when there is a localized disruption of the gravity-friction equilibrium (for example, at a weir, behind a sluice gate, free overfall, or sudden change in slope) or a difference between the depths enforced by upstream and downstream controls. A flow known as GVF occurs when the water depth varies gradually over a considerable distance. Significant changes in water depth or flow velocity over a small distance are referred to as RVF. An example of a rapidly varying flow is an H-jump, in which the liquid free surface level rises abruptly, according to Fig. 1.6. Here, the parameters are flow rate Q, pre-jump and post-jump sequent depths y_1 and y_2, oscillating jet thickness y_{jet}, velocity heads of pre-jump and post-jump conditions $V_1^2/2g$ and $V_2^2/2g$, energy dissipated along the jump H_t, tailwater depth T_w, and longitudinal position x.

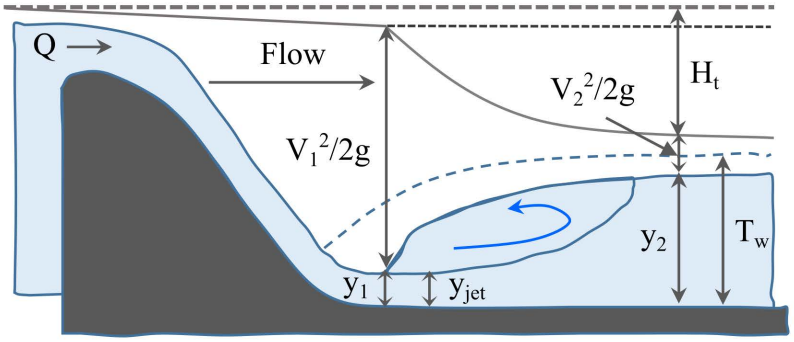

Fig. 1.6. Schematic diagram of H-jump over a typical stilling basin.

One of the most important issues to thoroughly examine in hydraulic engineering is the H-jump. It is a very interesting natural occurrence that has attracted the attention of numerous researchers since its first observation made by Leonardo da Vinci. The depth variations significantly influence the flow velocity across the jump length. The H-jump occurs when a super-critical stream comes into contact with a sub-critical stream that is deep enough, causing energy to be wasted as eddies and an abrupt change in flow depth, as shown in Fig. 1.7. It develops from the interaction of a shallow water stream with super-critical velocity with a deep flow with sub-critical velocity. In the real world, it can be found at the bottom of spillways, downstream of sluice gates on mild slopes, and when a steep slope transitions to a mild slope. The primary purpose of H-jump is to disperse extra energy that flows with water downstream of a hydraulic structure like sluice gates and spillways.

Fig. 1.7. Occurance of H-jump over the concrete stilling basin of Paradise Dam on the Burnett River, Bundaberg, Queensland, Australia (Bahmanpouri 2019).

In order to lower the uplift pressure, a H-jump also aids in raising the height of the apron. Therefore, set up some blocks downstream to lower the uplift pressure. That way, the H-jump will lessen the head difference and lower the uplift pressure. H-jump, which shows up as a standing wave, is the term for the increase in surface-water level that happens when the unstable super-critical type flow pattern changes into the stable sub-critical flow. The water moves with reduced velocity and at a deeper depth beyond the H-jump. There are

numerous beneficial and practical uses for the H-jump. Major applications include (a) effective flow-measurement flume operation, (b) chemical mixing, (c) facilitating vigorous mixing and transfer of gas in chemical processes, (d) desalinating seawater, (e) enhancing the dissipation of heat to the ambient from a flowing stream, and (f) aerating streams contaminated with biodegradable wastes.

In order to increase the removal of turbidity in water treatment, a H-jump is integrated into the coagulation process. Prior to flocculation operations, the mixing through H-jump seeks to quickly and effectively spread coagulant into the raw water. A quick and uniform coagulant dispersion cannot be guaranteed by mechanical mixing with a longer retention time. This issue can be resolved by using a H-jump to mix chemicals instead of an impeller for mechanical mixing. It is simpler and less expensive (Ghawi 2017).

The inlet Froude number (Fr_1) determines the classification of H-jump (Subramanya 2009).

H-jump of undular type ($1.7 \geq Fr_1 > 1.0$)

A minor ripple is seen on the surface of the water, which is undulating. The energy loss relative to E_1 (E_L/E_1) is less than 5%, and the sequent-depth ratio (SD-Ratio) is extremely modest. A typical illustration of an undular jump is depicted in Fig. 1.8(a).

H-jump of weak type ($2.5 \geq Fr_1 > 1.7$)

The surface roller appears at $Fr_1 = 1.7$ and progressively intensifies as it moves approaching the final point of this range, or $Fr_1 \approx 2.5$. At $Fr_1 = 1.7$ and $Fr_1 = 2.5$, the energy dissipation is E_L/E_1, which is approximately 5% and 18%, respectively. The jump leaves the top surface of water smooth as in Fig. 1.8(b).

H-jump of oscillating type ($4.5 \geq Fr_1 > 2.5$)

This type of jump has instable characteristics subjected to high-velocity flow, which causes it to fluctuate randomly across the fixed bed and surface. The surface waves which are large enough are created by these oscillations, and travel a significant distance downstream, as shown in Fig. 1.8(c).

H-jump of steady type ($9.0 \geq Fr_1 > 4.5$)

The H-jump has become established in the specified range of Froude numbers. The complete development of jump action and roller formation is simultaneously occurred, resulting in a noticeable loss of energy. In this type of jump, the percentage of E_L/E_1 varies between 45% and 70%. When it comes to the toe positioning, the "steady jump" is least influenced by little variations in the elevation of the tailwater, shown in Fig. 1.8(d).

H-jump of strong or choppy type ($9.0 < Fr_1$)

The surface of the water is extremely choppy and uneven for this category of jump. There is also turbulent and undulating water downstream of the jump. With E_L/E_1 values above 70%,

the energy dissipation is highly efficient and the sequence-depth ratio is substantial, as shown in Fig. 1.8(e).

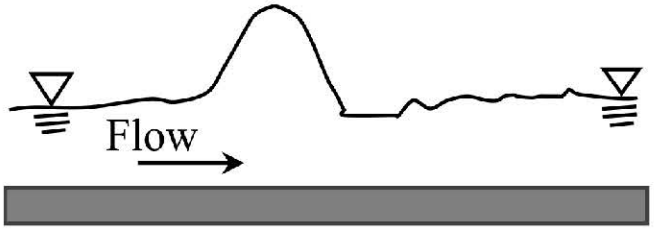

(a) H-jump of undular type

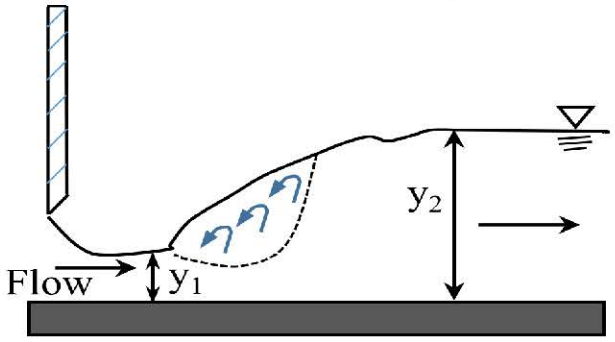

(b) H-jump of weak type

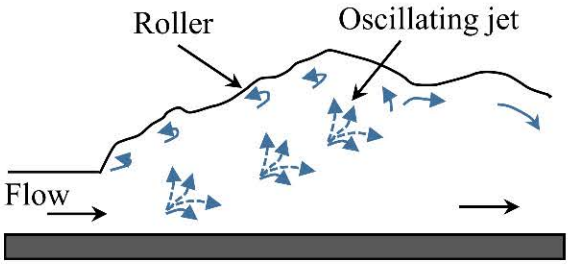

(c) H-jump of oscillating type

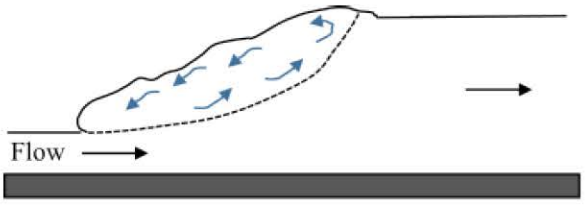

(d) H-jump of steady type

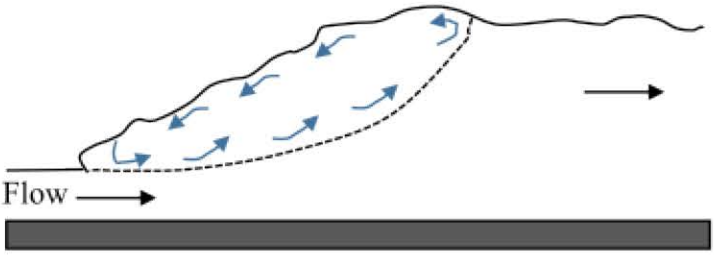

(e) H-jump of strong type

Fig. 1.8. An outline sketch of jump categorization.

1.5. Heat Dissipation

The process by which water releases heat into its surroundings is known as heat dissipation from water. This can happen in several ways, and the temperature gradient, surface area, and ambient circumstances all affect the effectiveness of the process.

The key processes of heat dissipation are as:

- Convection: In the convection process the heat is transferred by the motion of fluids, in this case air and water. Cooler, denser water sinks because it is heavier than warmer, less dense water, which naturally rises due to buoyancy. The heat distribution in the water body is assisted by this movement, which mixes the water layers. Using a pump or mechanical fan during the convection process increases the flow of water and surrounding air, improving heat transmission.
- Conduction: Heat transmission through direct contact is known as conduction. When water comes into touch with another substance, such as air or a metal surface, heat will go from the water that is hotter to the cooler substance. Heat dissipation is more effective when a greater surface area is exposed to air or another substance.
- Evaporation: When water molecules at the surface accumulate enough energy to release as vapour into the atmosphere, this process is known as evaporation. The energy needed for evaporation is latent heat, which is taken up by the water and causes it to cool. Temperature, humidity, available water surface area which is exposed to atmosphere, and airflow, all affect evaporation.
- Radiation: Infrared radiation is another way that water loses heat. Depending on their temperature, all bodies release radiation, and hot water radiates heat to its surroundings in the form of infrared radiation. The amount of heat emitted will depend upon the temperature of the water as well as ambient conditions.

Factors Affecting Heat Dissipation from Water:

- The rate of heat dissipation increases with the temperature differential between water and the surroundings.
- Water dissipates heat more effectively the larger its exposed surface area. For instance, heat will evaporate more quickly in a shallow, wide body of water than in a narrow, deep one.
- Heat dissipation can be greatly impacted by the ambient air's temperature and moisture content. Evaporation will be more effective in a hot, dry environment than in a cool, humid one.
- Water movement accelerates heat transmission by repeatedly exposing various water levels to the surface, which improves heat dissipation.

Applications of Heat Dissipation from Water:

- Water is frequently utilised as a coolant in industrial machinery and power plants.

- One important aspect of preserving the ideal operating temperature is the heat dissipation from water preventing thermal contamination in native water bodies.
- Climate and weather patterns are influenced by the natural heat dissipation that occurs in lakes, rivers, and seas through convection, radiation, and evaporation.

The convection process is supposed to be suitable for the analysis of the current investigation. For this experiment, the testing water is heated using an electric heater. After that, heat is released from the water into the atmosphere by means of the turbulence that the H-jump creates.

1.6. Dissolved Oxygen

The oxygen atom found in water (H_2O) molecules is a component and does not contribute to the amount of dissolved oxygen (DO) in the solution and is not necessary for aquatic life found in natural waters. Water contains a small amount of dissolved oxygen, up to 10 molecules per million of water. The DO is the quantity of oxygen (O_2) which is free and non-compound in water or other liquids. The aerating effect of winds causes oxygen to dissolve in surface water. A significant amount of photosynthes is occurs underneath (by seaweed, subsurface algae, and phytoplankton), whereas most take place at the surface (by low aquatic vegetation and algae). Water can absorb light, but the depth to which it can do so varies depending on the dissolved particles and light-scattering substances. Along with this necessary light, CO_2 is easily absorbed by water (compared to O_2 which is more soluble) and the O_2 that is created as a byproduct stays dissolved in water. The fundamental reaction of aquatic photosynthesis is still the same (Eq. 1.3).

$$CO_2 + H_2O \rightarrow (CH_2O) + O_2 \tag{1.3}$$

The amount of dissolved oxygen generated will increase throughout the day and decrease at night since aquatic photosynthesis is light-dependent. As a consequence of photosynthesis in aquatic plants, oxygen is also added to the water. The dissolved oxygen requirement is varying for each species. The amount of dissolved oxygen per unit volume of water (mg/l) is the expression used to describe dissolved oxygen levels. One of the most crucial factors in assessing the quality of water is the amount of dissolved oxygen present, as this suggests the presence of pollution in an indirect manner. The release of organic materials from industrial or municipal wastes and the warm or hot discharges that come from industrial cooling towers, as well as the runoff from animal farming operations and agricultural fields, are common activities that contaminate surface waters. The amount of dissolved oxygen in water bodies are directly impacted by these discharges, and fish mortality has been linked to excessive pollution. Oxygen is essential for the existence of aerobic organisms and aquatic wildlife. Long-term organic or nutrient releases encourage the process of increased eutrophication or productivity with algal blooms. Dissolved oxygen is a crucial component in limnology, the study of lakes, surpassed only by water.

The air or a byproduct of plants can introduce dissolved oxygen into the water. From the air, oxygen can either swiftly enter the water through natural or artificial aeration, or it can slowly spread across the surface of the water from its surrounding environment.

Waterfalls, groundwater release, wind (which creates waves), and other flowing water can all aerate water. A hand-turned waterwheel, a big dam, or an aquarium air pump are examples of man-made aeration sources. As a byproduct of photosynthesis, phytoplankton, algae, seaweed, and other aquatic plants also produce dissolved oxygen. Toxic chemicals can be inhibited and effectively degraded by water that contains enough oxygen. Ammonia and hydrogen sulphide are difficult to break down and change when there is not enough oxygen present, which will have an impact on biological health and water quality. Different sources of dissolved oxygen in water are shown in Fig. 1.9.

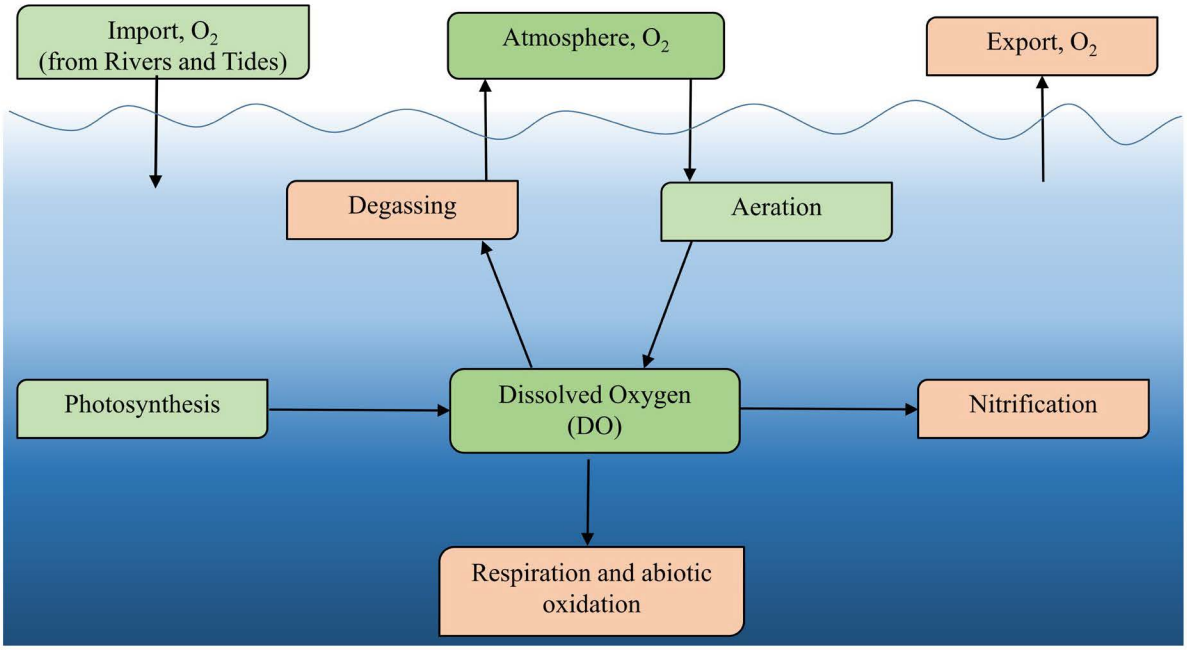

Fig. 1.9. Sources of dissolved oxygen in a water body.

Temperature has a seasonal as well as a daily cycle on the amount of dissolved oxygen in surface water. Compared to warm water, cold water can store more dissolved oxygen. The dissolved oxygen content is highest in the winter and the beginning of spring, while the water temperature is low. When the water is hotter in the summer, there is typically less dissolved oxygen present. The production and consumption of oxygen in the water can be facilitated by the aquatic flora and fauna. The production of oxygen in the presence of light for aquatic vegetation is attributed to the photosynthesis process, which also accounts for variations in DO over the day/night cycle and seasons.

The amount of oxygen that a body of water can hold is also influenced by salinity; freshwater has a higher capacity to hold oxygen than salt water. Excessive amounts of bacteria or algae in water can also lower oxygen levels. Bacteria eat the algae once they die and finish their life cycle. The bacteria also eat the oxygen that has been dissolved in the water during this degradation process. Reduced amounts of biologically accessible oxygen may result from this, which occasionally causes fish kills and the loss of other aquatic life.

The amount of oxygen in the water increases with air pressure because more oxygen molecules may be forced into it. The water can hold more oxygen molecules because of the pressure from above. On the other hand, the oxygen in the water can overflow more easily

when the air pressure is lower. When the air pressure is low, as it usually is before a summer thunderstorm, the dissolved oxygen is typically very low. Many different types of life, such as fish, invertebrates, microorganisms, and plants, depend on DO. The amount of DO needed varies from living being to living being. The generally accepted minimum amount of DO that will support a large population of various fishes is from 4 to 5 mg/l (CWC report 2019).

1.7. Scopes of this Research

Previous studies provide a general indication of the current study areas that need to be investigated.

a) To design a hydraulic structure in which an H-jump is formed, it is necessary to know the location, length of the H-jump and the amount of energy to be dissipated.
b) Carry out a series of experiments in order to find out the characteristics of H-jumps at different discharges and different bed slopes.
c) Carry out another series of experiments by increasing the temperature of water from minimum to maximum and studying the different characteristics of jumps. The density as well as viscosity of the water will also be changed. Water temperature affects its viscosity. So the jump will be conducted at different densities of water. The temperature of the water will be measured by a temperature sensor.
d) H-jumps will be formed by different discharges and different bed slopes. As these parameters change, the height of the jump will also change.
e) Measure the temperature throughout the jump profiles and relate the temperature variations with the basic parameters for the H-jumps. During the experiments, the temperature will also be measured by using temperature sensors at different locations of the jumps. After these measurements, the temperature variations with the different jump parameters will be observed and analyzed.
f) The research will also be extended by the numerical simulation of H-jumps and the creation of a relationship between jump parameters (height, length), temperature, and density.
g) A comparison between the experimentally measured and numerically computed data will also be made.
h) Perform several experiments varying discharge, bed slope and bed profile in order to find out the best possible combination of the H-jump to maximize the aeration efficiency. Results can be used to construct structures that keep the oxygen levels of water at a healthy level.
i) Results of current research and results obtained from previous research (if any) should be obtained to analyse and compare the heat dissipation and aeration efficiency.

It will be much easier for this research to frame H-jumps as an efficient and economical way to dissipate heat from water discharged from power plants and other industries. In addition, this research is designed to analyze the effect of dissolved oxygen on jump characteristics and to correlate changes in aeration efficiency with fundamental parameters of H-jumps under different flow conditions.

Chapter 2:

Basic theories that are related to fluid mechanics, bed roughness, H-jump properties on the smooth–bed and rough–bed, energy dissipation and heat dissipation through the H-jump, aeration efficiency, importance of different non-dimensional parameters have a connection with aeration efficiency and H-jump, Boussinesq assumption, and k-ε turbulence model have been discussed in this chapter. Scale effects are also discussed in this chapter.

Chapter 3:

In this chapter, the temperature of water was increased from the lowest to the highest in the measurement range in order to perform H-jump experiments. Several H-jump characteristics were observed and noted by adjusting the temperature between 32°C and 40°C. During the jump profiles, temperature variations were recorded and the relationship between jump parameters and temperature variations was measured and quantified.

Chapter 4:

Simulations of H-jumps in a rectangular tilting flume were performed in this chapter and determine the ability of the H-jump to improve the dissipation of heat from the water to the surrounding ambient. Six different ambient temperatures from 10°C to 35°C, with an equal interval of 5°C were considered while the inlet water temperatures were kept constant at 40°C. For each of the inlet water temperatures, H-jumps were simulated and the drop in average temperature at a section downstream of the jump was determined. The drops in average specific entropy and average specific enthalpy were also determined.

Chapter 5:

In this chapter, experimental investigations were conducted to determine the relationship between the essential H-jump parameters and the dissolved oxygen variation, as well as to examine the effects of aeration efficiency on jump features. For this purpose, five different bed slopes and five distinct discharges were taken into consideration to carry out 25 H-jump experiments. In the dissolved oxygen experimental study, experiments were carried out on smooth beds, involving measurements of sequent depths, velocity, and jump length.

Chapter 6:

In this chapter of this research, the H-jumps were developed experimentally at five different bed slopes (horizontal, 1.5°, 3°, 4.5°, and 6°) and five different discharges ranging from 15 lps to 35 lps using medium size gravels as bed material. In this rough bed, ramps were used to make the inflow water more super-critical. Two different ramps were used for this experimental investigation, one was in a 1:3 ratio and another was in a 1:4 ratio (both Vertical and Horizontal i.e. V:H). In order to observe various jump characteristics, experiments were conducted by changing the discharge and bed slope from minimum to

maximum within the measuring ranges. During the experiments, the dissolved oxygen of flowing water was measured. Calculations were performed based on experimental data to obtain different H-jump parameters such as jump height, energy loss, sequent depth, length of the roller of the H-jump etc. along with aeration efficiency while the dissolved oxygen was measured using a portable DO meter.

Chapter 7:

This chapter contains the remarks and conclusions from this research, and comparable research discusses the potential future directions of this study. The discharge, bed material, and channel shape may differ from those in our experimental setup in real-world scenarios. Therefore, when the water discharge and bed slope are not constant, further research is needed to identify a more distinct and reliable trend that illustrates the kind of fluctuation in these parameters.

References

Bahmanpouri, F. (2019). Experimental study of air entrainment in hydraulic jump on pebbled rough bed. Doctoral dissertation, Department of Civil, Architectural and Environmental Engineering, The University of Napoli Federico II.

CWC (2019). A Report on "Effect of Time and Temperature on Do Levels in River Waters". Ministry of Jal Shakti, Department of Water Resources, River Development & Ganga Rejuvenation, India.

Ghawi, A. H. (2017). The effect of hydraulic jump coagulation mixer on the performance of drinking water treatment plant. *International Journal of Engineering Technology and Scientific Innovation*, 2, 535-550.

Subramanya, K. (2009). Flow In Open Channels. Third Edition, McGraw Hill Education, Delhi, India.

Basic Theories

2.1. Introduction

In a comparatively "low-loss" approach, the flow through an open type channel can have a transition from sub-critical to super-critical at weirs or gates. Under these circumstances, critical flow conditions accompanied by very little energy loss cause the flow field to transition from sub-critical to super-critical. In contrast, a robust dissipative mechanism is present during the change from super–critical to sub–critical flow, which is called hydraulic jump (H-jump). The turbulence of a H-jump is tremendous. It is distinguished by the emergence of large–scale turbulence, air entrainment, energy dissipation, surface waves and spray. The term "roller" is typically used to describe the large –scale turbulence zone. In the H-jump phenomenon, the white foamy water indicates a zone of turbulent two–phase flow with significant air–entrainment, strong turbulence development, and splashes and droplet projections over breaking surface.

The purpose of energy dissipaters is to release extra kinetic energy at the chute's end before it returns to the natural stream. Mainly three kinds of energy dissipators are frequently used: roller buckets, flip buckets, and stilling basins (Hager 1992). Every dissipater has benefits and drawbacks, and the characteristics of the site may determine which one is best for a given project. In dam spillways, energy dissipation is typically accomplished by (i) a conventional stilling basin at the down-stream of the steep type spillway, where an H-jump is formed in dissipating a great extent of flow energy and transform the subsequent flow condition from super-critical to sub-critical, (ii) a high–velocity water jet that impinges into a downstream plunge pool from a flip bucket, and (iii) a plunging–type jet pool where the concerned spillway flow makes an impact and subsequent kinetic energy is then dissipated in turbulent type recirculation.

A H-jump is used as a component of a dissipater system with high energy beneath a hydraulic structure because of the significant energy loss that takes place during the jump. Sills and baffle blocks are among the accessories that are included with the stilling basin to help dissipate energy. The primary purposes of these accessories are to decrease the length of H-jumps, increase turbulence to release extra energy and stabilise the H-jump in place.

Additionally, free–surface flow can be utilised in industrial facilities and dam spillways to improve aeration and mixing for chemical treatments and/or ecological reasons. For rivers, streams, and lakes to remain healthy, dissolved oxygen (DO) is crucial. Oxygen is used by numerous biological and chemical processes that occur naturally, which lowers the dissolved– oxygen concentration in the waterbody and increases stress. The oxygen is restored by the aeration process. However, by altering the flow profile through these interesting phenomena like H-jump and hydraulic drop, aeration can be improved. Despite the brief time that the water is in touch with hydraulic structures, they can increase dissolved–oxygen concentration in a river network (Raikar and Kamatagi 2015).

2.2. Turbulent flow characteristics

Turbulent fluid motion is defined as an irregular flow situation where different quantities exhibit random variations over time and space, allowing for the determination of statistically unique average values. Turbulence is often described by researchers as an eddying motion, which is a localised swirling motion with potentially extremely strong vorticity. These eddies, which occur in the turbulent motion at different scales, are what give the flow its mixing character. Turbulence is a component of nearly every fluid motion we see in nature and technical applications. Laminar motion becomes unstable at high Reynolds numbers because the inertia of the water surpasses the viscous forces. A two-dimensional motion becomes fundamentally three-dimensional and unstable when rapid changes in pressure and velocity occur. It refers to the motion as turbulent when this happens. Several characteristics define a turbulent flow:

Irregularity: Turbulent flow is characterized by erratic and chaotic eddies of varying sizes. After a particular amount of time, these turbulent eddies are eliminated through the cascade process within that area. They have a distinctive length and speed. The smallest eddies on this spectrum are those that are converted into thermal energy by viscous forces, whereas the largest eddies can be on the order of different flow geometries such as jet width, boundary layer thickness, etc.. Navier-Stokes equations describe the turbulence, which is deterministic despite being chaotic.

Diffusivity: There is an increase in diffusivity in turbulent flow. The momentum exchange between and within boundary layers is accelerated by the turbulence. Heat transfer and resistance (wall friction) are also exacerbated by the higher diffusivity.

Large Reynolds numbers: High Reynolds numbers are associated with turbulent flows. When Reynolds numbers are higher than 1000 but less than 3000, open channel flows undergo a change from laminar to turbulent.

Vortex stretching: Because the vorticity of turbulent flow is three-dimensional, the flow's vortex lines are not parallel. The intense stretching of vortex lines continuously maintains the fluctuating vorticity in turbulent flows.

Continuum: Despite having small turbulent scales, the flow can be treated as continuous because these sizes are far greater than the molecular scale.

Reynolds Averaged Navier Stokes Equations

The Reynolds Averaged Navier Stokes equations for incompressible flow can often be expressed as follows in Eqs. (2.1-2.2):

$$\frac{\partial u_i}{\partial x_i} = 0 \tag{2.1}$$

$$\rho \frac{du_i}{dt} = -\frac{\partial p}{\partial x_i} + \frac{\partial}{\partial x_j}\left[\mu\left(\frac{\partial u_i}{\partial x_j} + \frac{\partial u_j}{\partial x_i}\right)\right] + \rho f_i \tag{2.2}$$

where, u is velocity component, x is direction of flow, p represents pressure, ρ is fluid density, f_i is body force per-unit mass on liquid element acting in three components x,y,z, and μ represents dynamic viscosity.

The instantaneous variables in turbulent flows are decomposed into an averaged value and a fluctuating value, (Eqs. 2.3-2.4), i.e.

$$u_i = \bar{u}_i + u_i' \tag{2.3}$$

$$p = \bar{p} + p' \tag{2.4}$$

where any quantity u'_i or p' represents a fluctuating value and $\overline{u}_i$ or $\overline{p}$ denotes a time average of quantity defined as (Eq. 2.5).

$$\overline{u}_i = \frac{1}{2t}\int_{-t}^{t} u_i dt \qquad \text{or} \qquad \overline{p} = \frac{1}{2t}\int_{-t}^{t} p dt \tag{2.5}$$

where time t is adequately large.

Time averaging all the components of velocities and pressure into Eqs. 2.1-2.2 of Navier Stokes equations and with few amendments, obtain the following sets of equations (Eqs. 2.6-2.7):

$$\frac{\partial \overline{u}_i}{\partial x_i} = 0 \tag{2.6}$$

$$\rho\overline{u_j} \times \frac{\partial \overline{u}_i}{\partial x_j} = \frac{\partial}{\partial x_j} \times \left(\mu \frac{\partial \overline{u}_i}{\partial x_j} - \rho\overline{u_i' u_j'} \right) - \frac{\partial \overline{p}}{\partial x_i} \tag{2.7}$$

Equation 2.6 represents continuity equation averaging with time and Eq. 2.7 represents Navier-Stokes equation averaging with time. These equations are called Reynolds Averaged Navier Stokes equations. New terms $\rho\overline{u_i' u_j'}$ appear on the right side of Eq. 2.7 which are collectively known as stress tensors of Reynolds which are symmetric i.e. $\overline{u_i' u_j'} = \overline{u_j' u_i'}$. The terms that show up in the Reynolds stress tensor are unknown extra terms. Thus, there are seven unknowns (three components of velocity, pressure, and three stresses), while there are four equations (three components of momentum equation and continuity equation). Therefore, some sort of model is required in closing the system of equations (Eqs. 2.6-2.7). Some approaches have evolved for this purpose.

A similar transport equation for temperature, the instantaneous temperature (T) can be written for an incompressible flow (Eq. 2.8) (Davidson, 2022):

$$\frac{\partial T}{\partial t} + \frac{\partial u_i T}{\partial x_i} = \alpha \frac{\partial^2 T}{\partial x_i \partial x_i} \tag{2.8}$$

where, α is the thermal diffusivity.

In a turbulent flow, the instantaneous temperature can be decomposed as Eq. 2.9.

$$T = T' + \overline{T} \tag{2.9}$$

Introducing this relationship in Eq. 2.8, time averaged transport equation for temperature becomes (Davidson 2022) (Eq. 2.10):

$$\frac{\partial \overline{T}}{\partial t} + \frac{\partial \overline{u}_i \overline{T}}{\partial x_i} = \alpha \frac{\partial^2 \overline{T}}{\partial x_i \partial x_i} - \frac{\partial \overline{u_i' T'}}{\partial x_i} \tag{2.10}$$

The final element in Eq. 2.10 is another unidentified term that has the physical meaning of a turbulent heat flux vector. It is necessary to model this considering it is comparable to Reynolds stress concepts.

The RANS-based turbulence models can be thought of as a collection of formulas required to identify the unidentified turbulent correlations that have emerged as a result of the averaging procedure. There are many different types of RANS turbulence models, however, they are broadly divided into 2 categories such as models of (a) Reynolds stress and (b) eddy viscosity. Models of eddy viscosity are dependent on Boussinesq assumptions.

2.3. Rapidly Varying Flow for Hydraulic Jump

A rapidly varying flow is a large shift in surface–water depth over a little distance. It happens when there is a local disruption to the equilibrium between gravity and friction (like, at a sluice gate, venturi, weir, free overfall, or abrupt change in slope) or when the depths enforced by upstream and downstream controls are not consistent as H-jump. A flow transition occurs between low-velocity, high-depth condition and a high-velocity, low-depth condition in this flow phenomenon. Bed friction is irrelevant since it is assumed that the flow fluctuates quickly over a short span. Therefore, the total head has been presumed to be unchanged throughout the whole region for a smooth transition. Significant head loss may occur during a sudden transition, although this is attributed to high turbulence rather than bed friction.

A rapid transition from a shallow, high-speed flow to a deep, low-speed, lower-energy flow is known as an H-jump. It happens when upstream and downstream conditions impose a depth differential. It is preferable to initiate an H-jump near the base of the spillway to eliminate excess kinetic energy and reduce erosion at the downstream. In an H-jump, mass is preserved, the momentum principle is maintained, and the mechanical energy disappears mainly as heat. The main function of an H-jump is in dissipating the surplus energy of the moving water down–stream of different hydraulic structures like sluice gates and spillways. Other practical applications are (i) regulating flow in water treatment plants, (ii) reducing river channel erosion, (iii) mixing in several industrial applications, (iv) improving aeration in the treatment of wastewater, and (v) irrigation and flood control systems. An illustrated diagram of a H-jump in an arbitrary-shaped prismatic channel is shown in Fig. 2.1.

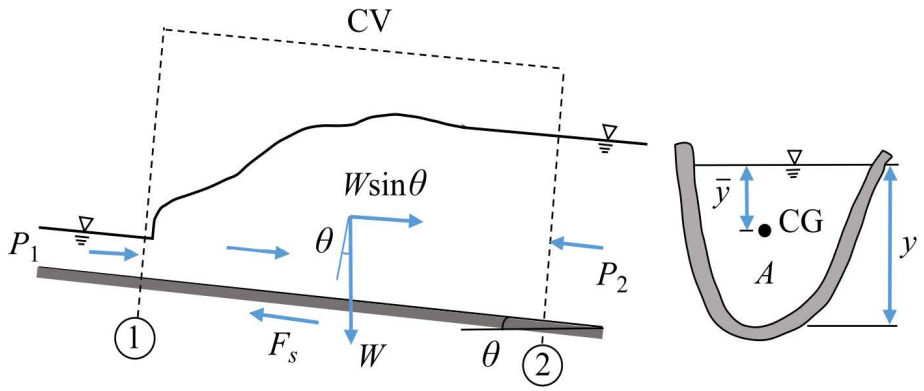

Fig. 2.1. Schematic representations (side-wise and cross-wise) of general momentum equation.

The angle θ is channel tilt with respect to the horizontal direction. The start and finish of the jump are described in Sections 1 and 2, respectively (Subramanya 2009). Here, P_1= pressure force induced at section 1, P_2 = pressure force induced at section 2, W= weight of water content in the control volume (CV), A= area of the control surface, $\bar{y}$ = depth of centroid of area below the water surface.

A control volume is chosen that encloses the H-jump, as indicated by the dotted lines in Fig. 2.1. It is considered that the flow is steady. By implementing the linear momentum equation to the control volume longitudinally, it becomes as Eq. 2.11.

$$W\sin\theta - F + P_1 - P_2 - M_1 + M_2 = 0 \tag{2.11}$$

where, F_s = shear force on control surface, $W\sin\theta$ = longitudinal component of the weight of water, M_1 = momentum flux going in through the control surface in the longitudinal direction, and M_2 = momentum flux going out through the control surface in the longitudinal direction.

In comparison to GVF profiles, the H-jump length is comparatively small of the H-jump, a rapidly varying flow phenomenon. Because frictional force F_s is of secondary relevance, it is typically ignored. Alternatively, ($W\sin\theta - F_s$) can be regarded as extremely little and is therefore ignored for lesser values of θ. Both $W\sin\theta$ and θ are equal to zero for a horizontal channel.

2.4. H-jump over a Rectangular Horizontal Channel

a) Ratio of Sequent Depths (SD-Ratio)

Consider, a frictionless rectangular, horizontal channel. Here, the momentum equation (Eq. 2.11), can be expressed as follows (Eq. 2.12) when taking the unit width of the channel into account

$$\frac{1}{2}\gamma y_1^2 - \frac{1}{2}\gamma y_2^2 = \beta_2\rho q V_2 - \beta_1\rho q V_1 \tag{2.12}$$

Here, γ is specific weight (=ρg), ρ is water density, g is gravitational acceleration and momentum correction factors at two cross sections 1-2 are assumed $\beta_2 = \beta_1 = 1.0$. Considering, q = discharge per– unit width = $V_1 \times y_1 = V_2 \times y_2$, it turns into Eq. 2.13.

$$\left(y_2^2 - y_1^2\right) = \frac{2q^2}{g}\left(\frac{1}{y_1} - \frac{1}{y_2}\right)$$

i.e.
$$y_1^2 y_2 + y_2^2 y_1 = \frac{2q^2}{g} = 2y_c^3 \tag{2.13}$$

Fr_1 = Inlet Froude number of the flow (Eq. 1.2) and y_c = critical depth.
Solving for (y_2/ y_1),

$$\frac{y_2}{y_1} = \frac{1}{2}\left(-1 + \sqrt{1 + 8\mathrm{Fr}_1^2}\right) \tag{2.14}$$

In a frictionless, horizontal, rectangular channel, a momentum equation given by Belanger (Eq. 2.14) is the relationship between the Fr_1 and SD-Ratio or y_2/y_1. Eq. 2.14 can be approximately used to estimate y_2/y_1 for the high values of Fr_1, such as $Fr_1 > 8.0$, as (Eq. 2.15).

$$\frac{y_2}{y_1} \approx 1.41 \mathrm{Fr}_1 \tag{2.15}$$

b) Energy Loss

Using the energy equation implemented in Sections 1 (E_1) and 2 (E_2), energy loss (E_L) in the jump is determined as Eq. 2.16. The relative energy loss can be obtained by calculating Eq. 2.17. The percent of initial energy lost i.e. E_L in the H-jump is provided by Eq. 2.18.

$$E_L = E_1 - E_2$$

$$= \left(y_1 + \frac{q^2}{2gy_1^2} \right) - \left(y_2 + \frac{q^2}{2gy_2^2} \right)$$

Substituting the value q^2/g from Eq. 2.13 and after simplifying, Eqs. 2.16-2.17 are obtained.

$$E_L \times 4 y_1 y_2 = \left(y_2 - y_1 \right)^3 \tag{2.16}$$

The relative energy loss,

$$\frac{E_L}{E_1} = \left(\frac{E_L}{y_1} \right) \Big/ \left(\frac{E_1}{y_1} \right) \tag{2.17}$$

Again,

$$\frac{E_1}{y_1} = 1 + \frac{Fr_1^2}{2}$$

$$\frac{E_L}{E_1} = \frac{\left(\frac{y_2}{y_1} - 1 \right)^3}{4 \left(\frac{y_2}{y_1} \right) \left(1 + \frac{\mathrm{Fr}_1^2}{2} \right)}$$

Substituting y_2/y_1 from Eq. 2.14 and thereafter, simplifying,

$$\frac{E_L}{E_1} = \frac{\left(\sqrt{1 + 8\mathrm{Fr}_1^2} - 3 \right)^3}{8 \times \left(\mathrm{Fr}_1^2 + 2 \right) \times \left(\sqrt{1 + 8\mathrm{Fr}_1^2} - 1 \right)} \tag{2.18}$$

Figure 2.2, illustrates the significant energy dissipation characteristic of the H-jump by displaying the fluctuation of E_I/E_1 with Fr_1. In the super-critical stream, about 55% of the initial energy is lost at $Fr_1 = 6$, and 86% of it is lost at $Fr_1 = 20$. A benchmark for evaluating the effectiveness of different kinds of jumps and energy-dissipating devices is provided in Fig. 2.2.

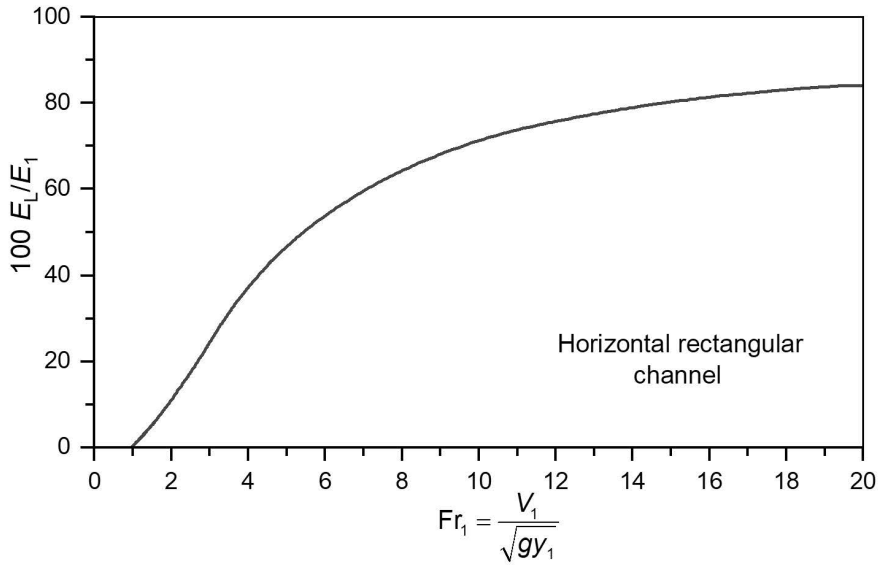

Fig. 2.2. Loss of relative energy with initial Fr in an H-jump over horizontal rectangular channel.

The SD-Ratio and energy loss in an H-jump formed on a horizontal bed are adequately represented by Eqs. 2.14 and 2.15, respectively, according to experimental studies and comprehensive work conducted by numerous researchers precisely by Bradley and Peterka (1957), which covered a range of initial Fr values up to 20.

The following equation (Eq. 2.19) is an intriguing and practical link between Fr_1 and a non-dimensional parameter composed of q and E_L.

$$\frac{E_L}{y_1} = \frac{1}{16}\frac{\left(-3+\sqrt{1+8Fr_1^2}\right)^3}{\left(-1+\sqrt{1+8Fr_1^2}\right)} \tag{2.19}$$

Equation 2.20 is very useful in estimating the components of the H-jump while discharge intensity (given by q) and energy loss (given by E_L) are the only known jump parameters that is a frequent issue in the hydraulic design of different stilling basins for barrages.

Again, $$y_1 = \frac{q^{2/3}}{g^{1/3}Fr_1^{2/3}}$$

Substituting y_1 in the Eq. 2.19, we obtain Eq. 2.20.

$$\frac{16g^{1/3}E_L}{q^{2/3}} = \frac{\left(-3+\sqrt{1+8Fr_1^2}\right)^3}{(Fr_1)^{2/3}\left(-1+\sqrt{1+8Fr_1^2}\right)} = f(Fr_1) \tag{2.20}$$

c) Length of H-jump

The H-jump length i.e. L_j is a crucial factor that influences the stilling basin size, where the H-jump occurs. The horizontal extent from the toe of the H-jump to one section where the water– surface levels out after attaining the highest depth is usually used to calculate the

length of the jump. It is discovered experimentally that $L_j / y_2 = f(\mathrm{Fr}_1)$. Figure 2.3 makes it clear that although L_j / y_2 is dependent on Fr_1 for its small values, the relative H-jump length L_j/y_2 is nearly constant at higher levels (i.e., $\mathrm{Fr}_1 > 5.0$) after Fr_1 of 6. Elevatorski (1959) demonstrated that the data can be written as Eq. 2.21.

$$L_j = 6.9(y_2 - y_1) \tag{2.21}$$

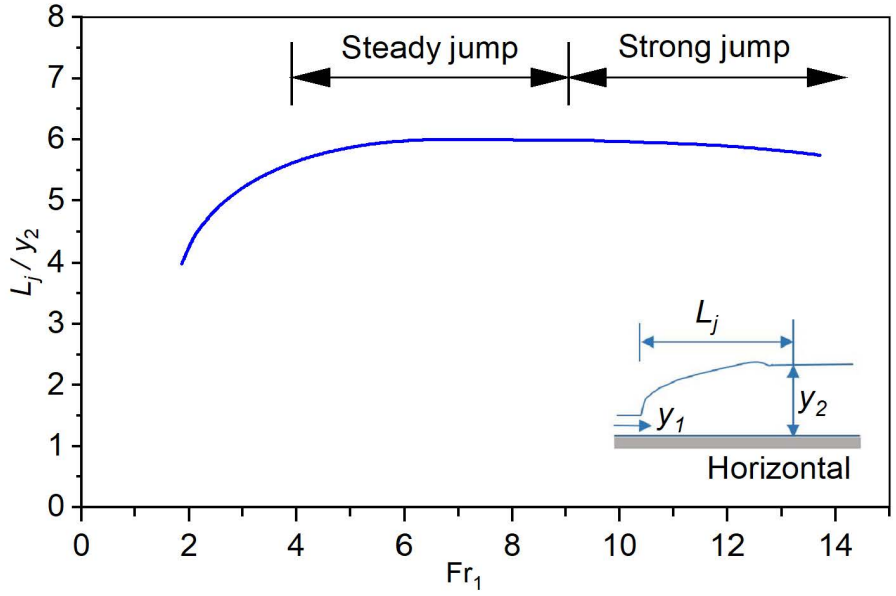

Fig. 2.3. Relative jump length with initial Froude number on a horizontal bed.

d) Pressure Distribution

The hydrostatic pressure distribution is followed by the pressures at toe of H-jump and finish of H-jump. However, the pressures inside the jump body diverge from the hydrostatic distribution due to the severe curvatures of the streamlines. The pressure in the H-jump body is lower than subsequent hydrostatic pressure during first few stages of the H-jump. A rise in the Fr_1, resulting in an increase in that hydrostatic pressure difference. Even so, the pressures are basically hydrostatic at channel bottom and in a small area near the bed.

e) Velocity profile

Shearing activity occurs at both the top and the solid borders when the super-critical stream at toe reaches the H-jump body. High relative velocities are present at the top water–surface of high velocity flow in relation to the fluid mass covering it. The fluid is entrained from the fluid mass above it by the free shear layer created by the strong shear near the surface. The velocity inside the boundary layer is retarded by the boundary shear at the bed. There are two separate parts to the velocity profile, a negative velocity zone at the top and a forward flow in the bottom main body.

The relative roughness of the bed and the initial thickness of the boundary layer have been discovered to be important factors in these characteristics.

2.5. H-jump over Rectangular Sloping Channel

A H-jump in a frictionless rectangular channel on a sloping bed is depicted in an illustration sketch in Fig. 2.4. It is assumed that β_1 or $\beta_2 = 1$. A unit width of the channel is taken into consideration with y_1 being the depth before the H-jump, y_t being the depth at the end of the H-jump, and q being the discharge per unit width. Using the dashed lines to represent a control volume, the momentum equation (Eq. 2.22) in the longitudinal direction is obtained from Eq. 2.11.

$$W\sin\theta + P_1 - P_2 + M_1 - M_2 = 0 \tag{2.22}$$

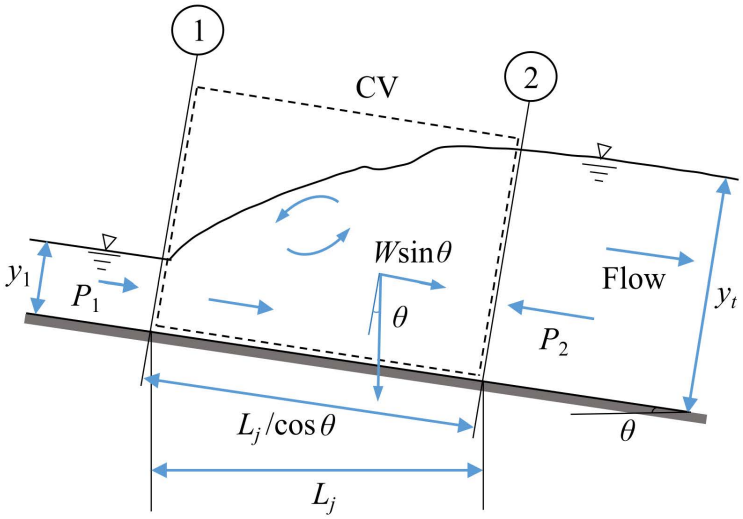

Fig. 2.4. Descriptive sketch of H-jump on sloping bed.

Considering the distribution of hydrostatic pressure in Sections 1 and 2,

$$P_1 = 0.5\gamma y_1^2 \cos\theta$$
$$P_2 = 0.5\gamma y_t^2 \cos\theta$$

If the water surface connected y_1 and y_t in a straight line, the area of the H-jump

$$= 0.5(y_1 + y_t)\frac{L_j}{\cos\theta}$$

Adding a coefficient to take into consideration for curvature of the H-jump profile and $\cos\theta$ term (Eq. 2.23),

$$W = 0.5K\gamma L_j(y_1 + y_t) \tag{2.23}$$

The momentum fluxes $M_1 = \rho q^2/y_1$ and $M_2 = \rho q^2/y_t$.
Equation 2.22 can be written as Eq. 2.24,

$$\frac{1}{2}\gamma\left[y_1^2\cos\theta - y_t^2\cos\theta + KL_j(y_1 + y_t)\sin\theta\right] = \rho q^2\left(\frac{1}{y_t} - \frac{1}{y_1}\right) \tag{2.24}$$

Reorganising Eq. 2.24, it becomes Eq. 2.25.

$$\left(\frac{y_t}{y_1}\right)^2 - 1 - \frac{KL_j \tan\theta}{y_1} \times \left(\frac{y_t}{y_1} + 1\right) - \frac{2\mathrm{Fr}_1^2}{\cos\theta} \times \left(\frac{y_t/y_1 - 1}{y_t/y_1}\right) = 0 \qquad (2.25)$$

If the term (KL_j) is known, the SD-Ratio is estimated using a trial and error process using Eq. 2.26. In general, (KL_j) depends on Fr_1 and θ, and its fluctuation can only be determined experimentally.

$$\left(\frac{y_t}{y_1}\right)^3 - \frac{KL_j \tan\theta}{y_1}\left(\frac{y_t}{y_1}\right)^2 - \left(1 + \frac{KL_j \tan\theta}{y_1} + \frac{2\mathrm{Fr}_1^2}{\cos\theta}\right)\left(\frac{y_t}{y_1}\right) + \frac{2\mathrm{Fr}_1^2}{\cos\theta} = 0 \qquad (2.26)$$

a) Sequent Depth (y_t)

In a horizontal bed jump, y_2 is the equivalent depth to y_1 as $0.5y_1(-1+\sqrt{(1+8\mathrm{Fr}_1^2)})$, and the sequent depth, y_t, is shown to be connected to y_2 as $y_t/y_2 = f(\theta)$.

According to the definition, $y_t/y_2 = 1.0$ when $\tan\theta = 0$ and as can be shown from Fig. 2.5, y_t/y_2 increases as the channel slope increases, typically reaching y_t/y_2 values of 1.4 – 2.7 at $\tan\theta = 1/10$ and 3/10, respectively. Therefore, compared to the corresponding horizontal bed jumps, the sloping bed jumps require greater tail water depths. For the variation of y_t/y_2 with $\tan\theta$ in Fig. 2.5, the best fit line may be written as Eq. 2.27.

$$\frac{y_t}{y_2} = 1.0071\exp\left(3.2386\tan\theta\right) \qquad (2.27)$$

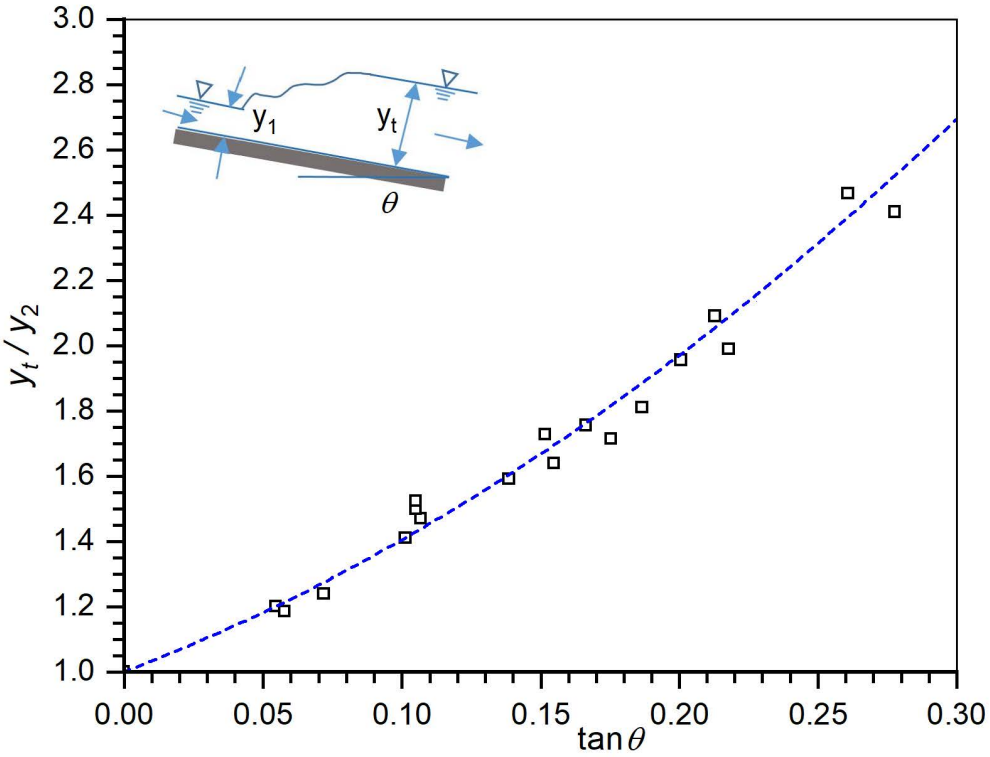

Fig. 2.5. Deviation of y_t/y_2 in H-jumps on sloping bed.

b) H-Jump Length (L_j)

The H-jump length i.e. L_j is horizontal distance, whichever is longer, between the start of the H-jump and either a point on the water surface level just downstream of the roller or a point on sub-critical flow zone where the stream– lines separate from bed.

The comparable L_j of the H-jump on a horizontal bed is shorter than the length of the jump on a sloping bed. The L_j/y_2 variation with Fr_1 for any θ is comparable to Fig. 2.3 fluctuation for the $\theta = 0$ situation. Within the range of $13 > Fr_1 > 4$, L_j/y_2 is a function of θ alone and is practically independent of Fr_1. The deviation can be roughly expressed as Eq. 2.28 in the range of $4.5 < Fr_1 < 13.0$.

$$\frac{L_j}{y_2} = 6.1 + 4.0 \tan\theta \tag{2.28}$$

Analysis by Elevatorski (1959) specified that the H-jump length can be stated as Eq. 2.29.

$$L_j = (y_t - y_1) \times m_s \tag{2.29}$$

in which $m_s = f(\theta)$. The deviation of m_s with $\tan\theta$ is shown in Fig. 2.6. It can be observed that m_s equaling 6.9 for $\tan\theta$ equaling 0 and decreases as the channel slope increases. Equation 2.29 is based on a wider range of Fr_1 values.

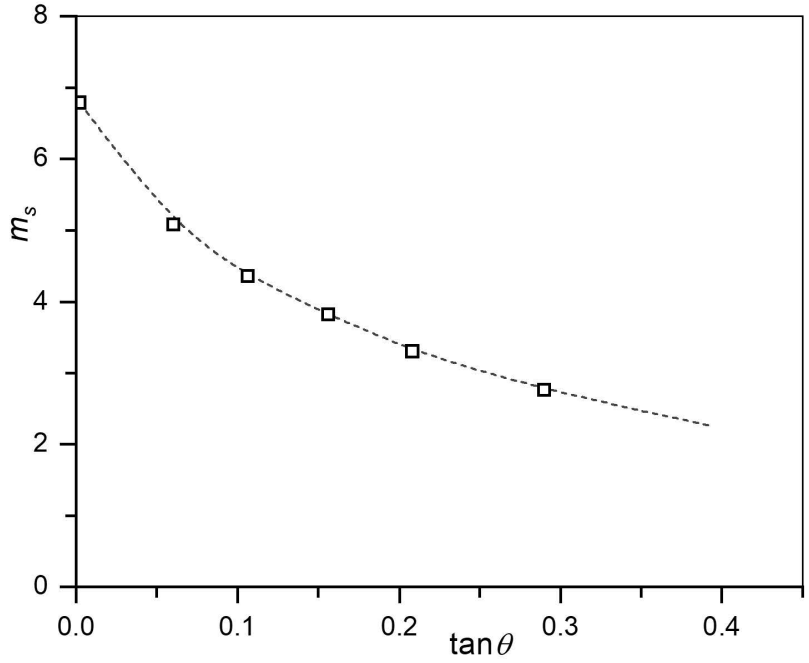

Fig. 2.6. Jump Length on a sloping bed.

c) Energy Loss (E_L)

The energy loss E_L can be computed as $E_L = H_1 - H_2$, using the H-jump length and the sequent depths y_t and y_1. The total energy at a segment is denoted by H. The E_L is calculated by using the Eqs. 2.30 and 2.31.

$$E_L = \left(E_1 + L_f \tan\theta\right) - E_2 \tag{2.30}$$

$$= y_1 \cos\theta + \frac{V_t^2}{2g} + L_j \tan\theta - y_1 \cos\theta - \frac{V_1^2}{2g} \tag{2.31}$$

where y_t is the sequent depth at Section 2 in a sloping channel.

2.6. Bed Roughness

The surface irregularities or roughness of a streambed, riverbed, or channel bed are referred to as bed roughness. These abnormalities, which affect the water flow in the channel, might be brought on by natural objects like rocks, gravel, plants, or sediment deposits. A number of hydraulic properties, including as flow velocity, turbulence, and flow resistance, are impacted by bed roughness. Normally, a rougher bed has more flow resistance, which lowers flow velocity and increases energy dissipation. For hydraulic modelling, flood forecasting, and the design of infrastructure such as bridges and dams, it is essential to comprehend and measure bed roughness.

Several geologists and hydraulic engineers have defined particle size based on measurement along three axes in mutually perpendicular of a particle. If a is longest or the major axis, b is intermediate axis and c is shortest or the minor axis, then one can take the intermediate axis b as the index of size. In such a case correlation can be found between the shape of the particle, nominal diameter and the intermediate axis b. Since, the axes are perpendicular, values of a, b and c for a given particle depending on the axis are chosen first.

It is essential to standardize the terms related to particle size so that they can be used to convey definite ideas regarding the size. The sizes given in Table 2.1 are in terms of triaxial size (b) for boulders, cobbles and up to coarse gravel, and in terms of sieve diameters (d_x) for medium gravel to very fine sand, for the finer material sedimentation diameter is recommended.

Table 2.1. Grade scale for size terms.

Name	Class Size	Range in mm
Boulders	Very large type	Upto 4096 from 2048
Boulders	Large type	Upto 2048 from 1024
Boulders	Medium type	Upto 1024 from 512
Boulders	Small type	Upto 512 from 256
Cobbles	Large type	Upto 256 from 128
Cobbles	Small type	Upto 128 from 64
Gravel	Very coarse type	Upto 64 from 32
Gravel	Coarse type	Upto 32 from 16
Gravel	Medium type	Upto 16 from 8
Gravel	Fine type	Upto 8 from 4
Gravel	Very fine type	Upto 4 from 2
Sand	Very coarse type	Upto 2 from 1

One of the most crucial variables in open channel flow computations that represent the energy loss, is Manning's roughness coefficient (n), denoted by Eq. 2.32 is popularly known as Manning's formula.

$$V = \frac{1}{n} R^{\frac{2}{3}} S^{\frac{1}{2}} \tag{2.32}$$

where R = hydraulic radius, and S = bed slope.

2.7. Heat Dissipation through H-jump

A H-jump occurs when a fast-moving, super-critical flow (with a high Froude number) transitions into a slower, sub-critical flow (with low Fr). The H-jump typically manifests as a turbulent, turbulent roller or wave where flow velocity drops suddenly, and water depth increases. When flow transforms from super–critical to sub–critical, there is a significant loss of kinetic energy. This energy is dissipated primarily through turbulence and vortex formation. In turbulence the chaotic motion of the fluid particles generates friction between them and with the surrounding environment. During vortex formation, the H-jump can induce large eddies and vortices, which further blend the fluid and dissipate energy. The exact amount of heat dissipation due to an H-jump depends on factors such as flow velocity before and after the jump, fluid properties (e.g., viscosity, density), channel geometry, and flow depth and width.

2.8. Air Entrainment in H-jump

Air entrainment into an H-jump refers to the process where air is drawn into the turbulent flow during the jump. This occurs because of the intense mixing and turbulence in the flow, which creates localized low pressure regions that draw in air from the surrounding atmosphere. In an H-jump, the turbulence generated causes intense surface disturbance and the formation of large eddies and vortices. These turbulent vortices create regions of low pressure, which induce air to be drawn into the flow. The resulting air bubbles get trapped in the water, leading to air entrainment. Air entrainment enhances the turbulence which increases the energy dissipation because the interaction between air bubbles and the liquid causes more friction. The entrained air reduces the effective density of flow, which can slightly decrease the velocity of fluid. The presence of air alters the subsequent flow momentum, density, and viscosity, which can influence the downstream behaviour of the flow.

Air entrainment contributes to energy loss which is important for engineers when designing energy dissipation devices in spillways or other hydraulic structures. The entrained air can have significant effects on downstream hydraulic conditions, possibly leading to erosion or scour if not properly managed. Air entrainment is sometimes used deliberately in engineering applications like aerated flow channels or for enhancing mixing in wastewater treatment.

2.9. Boussinesq Assumption

Analogous to the co-efficient of viscosity for laminar–flow, J. Boussinesq assumed a mixing coefficient μ_t for Reynolds stress terms as Eqs. 2.33 and 2.34. The term ν_t (= μ_t/g) appears in Eqs. 2.33 and 2.34 are known as eddy viscosity.

$$\tau_t = -\rho\overline{u_i'u_j'} = \mu_t\left(\frac{\partial\overline{u}_i}{\partial x_j}+\frac{\partial\overline{u}_j}{\partial x_i}\right) = \rho\nu_t\left(\frac{\partial\overline{u}_i}{\partial x_j}+\frac{\partial\overline{u}_j}{\partial x_i}\right) \tag{2.33}$$

So we can write,

$$\overline{u_i'u_j'} = -\nu_t\left(\frac{\partial\overline{u}_i}{\partial x_j}+\frac{\partial\overline{u}_j}{\partial x_i}\right) \tag{2.34}$$

But this equation (Eq. 2.33) is not valid upon contraction (as the right hand side of Eq. 2.33 becomes zero due to the continuity equation but the left hand side may not be zero). So it is rewritten as Eq. 2.35.

$$\overline{u_i'u_j'} = -\nu_t\left(\frac{\partial\overline{u}_i}{\partial x_j}+\frac{\partial\overline{u}_j}{\partial x_i}\right)+\frac{1}{3}\delta_{ij}\overline{u_k'u_k'} \tag{2.35}$$

Noting that $k = \frac{1}{2}\overline{u_k'u_k'}$, the above equation can be modified as Eq. 2.36.

$$\overline{u_i'u_j'} = -\nu_t\left(\frac{\partial\overline{u}_i}{\partial x_j}+\frac{\partial\overline{u}_j}{\partial x_i}\right)+\frac{2}{3}\delta_{ij}k \tag{2.36}$$

which is now valid upon contraction ($\overline{u_i'u_j'} = 2k$).

Equation 2.35 is a result of the Boussinesq assumption. Considering Boussinesq's assumption, Eq. 2.37 can be written.

$$\frac{\partial\overline{u}_i\overline{u}_j}{\partial x_j} = -\frac{1}{\rho}\frac{\partial\overline{p}}{\partial x_i}+\frac{\partial}{\partial x_j}\left\{\left(\nu+\nu_t\right)\left(\frac{\partial\overline{u}_i}{\partial x_j}+\frac{\partial\overline{u}_j}{\partial x_i}\right)\right\} \tag{2.37}$$

The difficulty in using Eq. 2.34 is that ν_t is an additional unknown because, unlike ν which is a property of the fluid considered, ν_t is a quantity derived from the random fluctuations in the turbulent flow. There are ways in which ν_t or μ_t are modelled in terms of other parameters that in turn are expressed with the time-averaged quantities. These models are called eddy viscosity models.

Boussinesq's assumption can also be extended to model the turbulent heat flux appearing in Eq. 2.10 as follows in Eq. 2.38.

$$\overline{u_i'T'} = -\alpha_t\frac{\partial\overline{T}}{\partial x_i} \tag{2.38}$$

where α_t denotes turbulent thermal diffusivity given by $\alpha_t = \frac{\nu_t}{\mathrm{Pr}_t}$, where $\mathrm{Pr_t}$ is a turbulent Prandtl number which is usually set to $0.9 > \mathrm{Pr_t} > 0.7$.

2.10. *k-ε* Turbulence Model

a) Standard type *k-ε* Turbulence Model

Suggested by Launder and Spalding (1983), the standard *k-ε* is a RANS based model that employs Boussinesq's hypothesis to calculate the value of "μ_t" (turbulent viscosity) as function of "*k*" (turbulent kinetic energy) and "*ε*" (turbulence dissipation rate). This model provides two additional transport equations for k and ε apart from the momentum and continuity equation. The transport equation for ε is semi empirical while the transport equation for k is derived from the exact transport equation. While deriving *k-ε* model, it is assumed that the flow is fully turbulent and it is a high Re model. Due to its robustness, economy and reasonable accuracy for a wide range of turbulent flow, the *k-ε* model has gained huge popularity in industrial flow and heat transfer simulations.

The turbulent kinetic energy, k and the turbulence dissipation rate ε are obtained by solving the following transport equations (Eqs. 2.39 and 2.40),

$$\frac{\partial}{\partial x_i}\left(\rho k u_i\right)+\frac{\partial}{\partial t}(\rho k)=G_b+G_k-\rho\varepsilon+S_k-Y_M+\frac{\partial}{\partial x_j}\left[\left(\mu+\frac{\mu_t}{\sigma_k}\right)\frac{\partial k}{\partial x_j}\right] \tag{2.37}$$

$$\frac{\partial}{\partial x_i}\left(\rho\varepsilon u_i\right)+\frac{\partial}{\partial t}(\rho\varepsilon)=C_{1\varepsilon}\frac{\varepsilon}{k}\left(G_k+C_{3\varepsilon}G_b\right)+S_\varepsilon-C_{2\varepsilon}\rho\frac{\varepsilon^2}{k}+\frac{\partial}{\partial x_j}\left[\left(\mu+\frac{\mu_t}{\sigma_\varepsilon}\right)\frac{\partial\varepsilon}{\partial x_j}\right] \tag{2.38}$$

where,

G_k denotes generation of k due to average velocity gradients.

G_b represents generation of k due to buoyancy effects.

Y_M denotes contribution of varying dilatation in compressible turbulence in overall dissipation rate.

S_k and S_ε are source terms defined by users.

$C_{1\varepsilon}$, $C_{2\varepsilon}$, and $C_{3\varepsilon}$ are constants and

σ_k, and σ_ε are turbulent $\mathrm{Pr_t}$ values for k and ε, respectively.

b) RNG k-ε turbulence model

This model is very similar in form to the standard *k-ε* with certain refinements that is achieved using statistical techniques named Renormalisation Group (RNG) theory (Yakhot et. al. 1992) applied to Navier Stokes equations rendering the RNG *k-ε* model more accurate and reliable for a wider class of flow than the standard *k-ε* model. The RNG model has an additional term in its ε equation that significantly improves the accuracy fo r rapidly varying flows. As compared to the standard *k-ε* model that uses either specified or user-specified turbulent Prandtl numbers, the RNG model provides an analytical formula for turbulent $\mathrm{Pr_t}$ values. While the standard *k-ε* model is a high Re model, the RNG model accounts for low Re effects depending upon appropriate near wall region treatment.

The transport equations for k and ε in the RNG k-ε model are as follows (Eqs. 2.41 and 2.42),

$$\frac{\partial}{\partial x_i}\left(\rho k u_i\right)+\frac{\partial}{\partial t}(\rho k)=G_b+G_k-\rho\varepsilon+S_k-Y_M+\frac{\partial}{\partial x_j}\left[\alpha_k\mu_{eff}\frac{\partial k}{\partial x_j}\right] \quad (2.41)$$

$$\frac{\partial}{\partial t}(\rho\varepsilon)+\frac{\partial}{\partial x_i}\left(\rho\varepsilon u_i\right)=\frac{\partial}{\partial x_j}\left[\alpha_\varepsilon\mu_{eff}\frac{\partial \varepsilon}{\partial x_j}\right]+C_{1\varepsilon}\frac{\varepsilon}{k}\left(C_{3\varepsilon}G_b+G_k\right)-C_{2\varepsilon}\rho\frac{\varepsilon^2}{k}+S_\varepsilon-R_\varepsilon \quad (2.42)$$

References

Bradley, J. N., & Peterka, A. J. (1957). Hydraulic design of stilling basins: Hydraulic jumps on a horizontal apron (Basin I). *Journal of the Hydraulics Division*, 83(5), 1401-1.

Davidson, L. (2022). Fluid mechanics, turbulent flow and turbulence modelling. Chalmers University of Technology, Goteborg, Sweden.

Elevatorski, E. A. (1959). Hydraulic Energy Dissipators, McGraw-Hill, New York.

Hager, W. H. (1992). Energy Dissipaters and Hydraulic Jump. Kluwer Academic Publishers, Water Science and Technology Library, Vol. 8, Dordrecht, the Netherlands, p. 288.

Launder, B. E., & Spalding, D. B. (1983). The numerical computation of turbulent flows. In Numerical prediction of flow, heat transfer, turbulence and combustion (pp. 96-116). Pergamon.

Raikar, R. V., & Kamatagi, P. B. (2015). Use of hydraulic phenomena in enhancement of dissolved oxygen concentration. *International Journal of Research in Engineering and Technology*, 4(2), 568-574.

Subramanya. K, (2009). Flow In Open Channels, Third Edition, McGraw Hill Education, Delhi, India.

Yakhot, V., Orszag, S. A., Thangam, S., Gatski, T. B., & Speziale, C. (1992). Development of turbulence models for shear flows by a double expansion technique. *Physics of Fluids A: Fluid Dynamics*, 4(7), 1510-1520.

Thermal Effect on Hydraulic Jump

3.1. Introduction

An open channel allows liquid to flow through a free surface and gravity is the primary factor that causes the flow to move through any open channel. Water behaves as an incompressible fluid in open channel flow, which makes the Froude number (Fr) the primary non-dimensional number governing the flow phenomenon in open channels and the force of gravity the primary force to be considered. Among open channel flow, the hydraulic jump (H-jump) is a significant rapidly varying flow phenomenon with large curvatures, which has non-hydrostatic pressure distribution zones in a significant portion of the flow.

The primary function of an H-jump is to disperse surplus energy from super-critically running water downstream of conventional hydraulic structures, such as sluice gates and spillways. To keep the downstream riverbed from severely scouring and downstream structures from failing, the kinetic energy of the water over the spillway must be released. The chute block in the stilling basin and various shaped sills are utilized to disturb the water and release a significant quantity of water energy by creating an H-jump. The basin should be built to lower the sequent depth of the H-jump and maintain it below the tailwater depth in order to guarantee optimal performance and energy dissipation. If not, the jump will flow out of the basin, making scouring downstream inevitable. The height, location, and arrangement of jumps significantly affect the water energy dissipation.

Pollutant discharges may need to be premixed before being released into a river, lake, or ocean in order to adhere to environmental rules. It is possible to premix dense and frothy discharges in a conduit that is connected to a natural body of water. In recent decades, low-impact river restoration structures have drawn a lot of interest. They maintain ecological balance while causing significant energy loss.

Sea and river water are utilized to lower the temperature of industrial machinery in factories, refineries, and power plants as a result of people using natural resources more frequently for growing economic purposes. The water loses its inherent qualities. Now, there will be serious harm if the outgoing water gets into the environment. As a result, the water that exits should cool down once more before returning to nature. On the other hand, industrial cooling methods such as employing chillers and cooling packages demand a lot of money, therefore it would be beneficial to offer something that allows for temperature regulation based on natural cycles. By looking at several approaches, we have attempted to improve the natural heat transfer between the water and its surroundings and, consequently, the temperature level. The studies are conducted using an experimental model of an open channel where a series of heaters raise the temperature of the water flowing through the channel, causing the water to flow through it at a constant temperature.

3.2. Review of Literature

The oscillating H-jump in an open channel flow is turning out to be an interesting topic in recent researches. Both analytical and experimental methods are used to assess the characteristics of dense and buoyant discharges in a horizontal mixing channel. The mixing channel is attached to a reservoir or stream, is shallow, and has a predetermined length and roughness. A mixing zone and a counter flow that varies gradually make up the flow of the channel. The corresponding mixing modes of four potential interactions are explained. To create synthetic dilution curves, a hydraulic theory is developed. Dilution observations are in line with expected trends, and experiments carried out in a laboratory flume verified the presence of four mixing modes. The theory might be helpful in the actual construction and functioning of a facility like this (Baddour 1987).

A theoretical and experimental investigation was conducted into a thermally stratified internal H-jump in a clean water environment with a temperature of at least 4°C. A comparison was made between the density jump solutions derived from a linear buoyancy function and the thermal jump solutions derived from a nonlinear buoyancy function. In a temperature range above 4°C, the study found a significant difference between thermal and density jump behaviour. Thermal H-jump tests were carried out in water at temperatures of 4°C and 16°C. The Froude number, Reynolds number, and temperature divergence between the two sets of trials were all the same. The thermal jump concept agreed well with experimental findings. The examination of temperature variations indicates that the internal mixing properties of thermal jumps were also altered by ambient temperature (Baddour 1991).

Measurements of the jump profiles in an open rectangular channel, including positive and negative step jumps, were made on a sloping floor. The length and depth of H-jumps on sloping floors were predicted using a set of regression results of the experimental data. The stability and compactness of the H-jump were better with the negative step compared to the positive, according to an analysis of the length characteristics and SD-Ratio. Multiple linear regression analysis has been used to create a group of non-dimensional equations in terms of profile coefficient for H-jumps in sloping channels with or without steps (Husain et al. 1994).

The crucial circumstances for the development of a surface roller just upstream of a sill are known as the incipient jump condition which can be differentiated into two groups. The incipient jump was produced by raising the tail–water level from the splashing flow stage otherwise increasing the sill height from the splashing flow state. Additionally, the impact of the channel width on the incipient jump situation was also discussed and a projection of the jump condition was obtained by applying the momentum equation. The predicted and observed outcomes accord satisfactorily for wide channels, when two-dimensional breaking takes place (Ohtsu et al. 1996).

The work included the turbulence properties of H-jumps with Fr values of 2, 2.5, and 3.32. The highest turbulence intensities and Reynolds stress at any given section were seen to rapidly decline from the toe of the H-jump towards its downstream and to progressively level off in the transition area between the end of the H-jump and the

friction-dominated open downstream channel flow. The greatest turbulent kinetic energy of each section progressively levels out in the transition zone after decreasing linearly with the longitudinal distance within the H-jump. There was some similarity between the Reynolds stress and the turbulence intensities within the H-jump (Liu et al. 2004).

The H-jump that takes place in both homogeneous and non-homogeneous rough bed channels was examined. A methodical investigation was conducted into the parameters that affect the length of the H-jump and the sequent flow depth. The conventional jump equation was utilized to analyze the phenomenon. A new expression of the correction coefficient of the fundamental jump equation that takes into consideration the bed roughness and its non-homogeneity was provided by the experimental data. The proposed formula showed satisfactory agreement with the experimental results (Pagliara et al. 2008).

Based on several real-world investigations, heat transfer from water to the surrounding air occurs during water cooling in open channels either naturally or artificially. The impact of installing different structures in the channels and different flows with varying flow rates on natural cooling are both induced. An open channel model in the laboratory is used for the experiment. The findings suggested that the temperature of water drops naturally through force cooling as it passes through the channel after being heated to 40°C and pushed in a closed cycle. The impact of H-jumps and different structures in channels on heat transfer and temperature distribution was examined in this study using both computational simulation and experimental techniques (Rahbar and Hamzeh 2008).

The work examined H-jumps in an inclined rectangular chute contraction. The effects of contracting breadth and sloping bottom were taken into consideration when developing theoretical equations for the sequent-area and SD-Ratios for H-jumps in the contraction. An altered strategy when analysing H-jumps in the contraction, approach Froude number M was adopted to replace approach Froude number Fr_1, taking into account the impacts of contracting breadth and sloping bottom. The theoretical sequential-area ratio was also confirmed through laboratory experiments with H-jumps in inclined contractions, and empirical equations for the length of jump, start location, flow depth, and energy loss were also developed (Jan and Chang 2009).

Without taking into account the tailwater level, which is variable and entirely influenced by downstream river conditions, experiments are carried out to assess the effects of a single vertical continuous sill and its location on controlling the depth and length of a forced H-jump in a stilling basin. A miniaturized model of a stilling basin was used to position a sill with five distinct heights at three separate longitudinal distances. The hydraulic properties of the H-jump were measured and contrasted with those of the traditional H-jump at different discharge levels. Experiments showed that the sill had a substantial impact on energy dissipation. A new correlation between stilling basin length, SD-Ratio, and sill height and location was established (Alikhani et al. 2010).

A study conducted in a laboratory evaluated how a rough bed affected the roller length and SD-Ratio of an H-jump. H-jump experiments were conducted on smooth and rough beds at four adverse slopes of -0.00125, -0.0025, -0.00375, and -0.005. The findings demonstrated that, given the identical slopes and Froude numbers, the SD-Ratio and jump length over the smooth bed were greater than those of the rough bed. In addition, when

comparing the proportion of energy loss, rough beds lose more energy than smooth beds (Nikmehr and Tabebordbar 2010).

The results of an experimental study on the roller length of B-jumps and classical jumps on smooth beds were presented in this publication. For predicting the roller length of classical and B-jumps on smooth beds, a new relationship was provided based on the measurements made during this study and those found in the literature. Lastly, it was shown that the roller length of H-jumps on uneven horizontal beds may also be estimated using the suggested equation (Carollo et al. 2012).

A comparatively big facility was used for some physical models in the investigation. There was a broad variety of inflow Reynolds numbers and Froude numbers in the flow conditions. Along with the interfacial velocity distributions, the void fraction of the H-jump roller and bubble count rate statistics were recorded. The void fraction and interfacial velocity distribution data were used to determine the rate of air entrainment. Measurements of longitudinal jump front oscillations, free-surface fluctuations, and instantaneous void percentages were made simultaneously. There was discussion of the connection between turbulent fluctuations and the rate of air entrainment (Wang and Chanson 2015).

A set of tests was carried out to investigate the way channel slopes and channel bed roughness affect the properties of an H-jump. The data analysis showed that bed roughness heights had no discernible effect on the properties of a H-jump in sloping channels but the properties were greatly influenced by the channel slope. A new relationship was suggested and the computed values derived from the suggested relationships agreed with the measured values for the SD-Ratio, roller length, and relative energy loss (Kumar and Lodhi 2016).

The study presented experimental research that made it possible to create a semi-theoretical method for assessing the D-jump conjugate depth across different channel bed geometry and boundary configurations. A generic formula for the D-jump sequent depth estimation for low inlet Fr on rocky, positively sloped channels was computed using semi-theoretical method. The data analysis results demonstrated that the suggested methodology agrees well with all of the previously published research on smooth sloping channels. Furthermore, an experimental study showed that the impact of channel bed roughness on the SD-Ratio primarily depended on the relative roughness at relatively low channel slopes (positive or negative). However, the SD-Ratio was decreased due to the increased Reynolds shear stresses on rough beds (Palermo and Pagliara 2017).

For slopes of 1.25°, 2.5°, and 5°, new air-water flow studies including type B and D jumps were carried out. H-jumps on slopes were found more stable, according to comparison studies between the sloped jumps and traditional H-jumps for the same Fr and Re. Type B and conventional H-jumps were shown to have very similar aeration and energy dissipation capabilities. However, type D jumps had decreased aeration and energy dissipation efficiency. The results indicated that a type B jump would be the ideal H-jump since it achieves significant energy dissipation and increases jump toe stability by combining the observations of flow aeration and stability (Montano and Felder 2020).

Another study reported two types of jumps. One is plane type which is conventional H-jumps that occurred on beds with continuous slopes or horizontal beds, and the B

types which occurred partially in the sloping and partially in the horizontal level of plane sections. At several points along the jumps, the velocities and jump profiles were measured. Using the explicit scheme of the McCormack technique for the second–order precision of time and space and the de-Saint Venant hyperbolic equations as governing equations, numerical simulations were performed for both B and planar jumps in order to validate the experimental results. A mixed empirical relation was developed to determine jump profiles that operate both plane and B jumps based on the accuracy attained (Roy et al. 2021).

An investigation of H-jump characteristics was carried out experimentally in order to comprehend the influence of slope in an open channel flume for both smooth bed and rough bed conditions. The results showed that for both horizontal rough beds and smooth horizontal beds, the SD-Ratio (y_2/y_1) increased as the Froude number (Fr_1) increased. Additionally, a drop in y_2/y_1 was noted for smooth sloping beds and a decrease for rough sloping beds with an increase in Fr_1. The experimental results were also used to create new empirical relationships (Laishram et al. 2021).

The H-jump experiments were conducted in smooth, fully and partially grated, and partially vegetated grate rough beds with artificial plants of varying densities. The effects of Fr and inflow roughness conditions, as well as the relationship between the flow and flexible vegetation barrier or roughness, were found as the main areas of attention for the investigation of the free-surface dynamics and air-water flow properties. When the jump roller was diverted across the vegetation layer, the characteristic jump and jump roller lengths it was found to be decreased. When the bed was roughened, the frequency of bubble detection increased in the non-vegetated channels. However, more vegetation on the rough invert resulted in a decrease in the frequency of bubbles and the cross-sectional mean air concentration by causing roller deflection and air bubble detrainment. The findings suggested that the flow-vegetation interaction may compound the consequences of perturbing artificial flexible vegetation with relatively large plant heights, which may differ from uniformly distributed rigid bed roughness elements (Bai et al. 2022).

By creating a variation RANS model that makes use of Kantorovich-Krylov expansions of the flow variables and a unique depth-averaged, eddy viscosity technique appropriate for non-hydrostatic flows, this work offered an alternate method for H-jumps. The validity of the model was confirmed by comparing the outcomes of thorough tests with simulations of both broken and undular jumps. The variational RANS model was found to accurately represent the flow profile over the bar, the H-jump position, and the dynamic pressures over the bar surface in new experiments conducted in a modified bar-built shallow river inlet (Orgaz et al. 2023).

H-jumps were created on the horizontal stilling basin bed in a new set of experiments conducted in a concrete stilling basin prototype downstream of a sloping stepped chute. The H-jumps were characterized by bubbly incoming flow with Froude numbers of 7.6 and 9.3. The jump roller length, H-jump toe oscillations, and air water flow property distributions were the main areas of measurement. The pre-entrained air did not delve very far into the jet shear layer past 0.2 to 0.333 roller length from the H-jump toe, according to the stream-wise evolution of air flux (Bai et al. 2023).

While going through the previous literature it is found that there is an insufficient amount of studies on heat dissipation due to H-jumps. Therefore, to address this research gap the H-jump prediction and its impact on heat transfer are identified as a part of this analysis.

3.3. Need for Thermal Effect Analysis due to Hydraulic Jump

Among the various real-world applications of H-jumps, energy dissipation is one of the major ones. Designing a hydraulic structure that creates an H- jump requires knowing the position, length, and energy dissipation of the jump. An increase in the temperature of water causes both its density and viscosity to vary. As a result, this study compares the length, SD-Ratio, and energy loss of H-jumps at different temperatures. Industrial effluent is usually in high temperatures and is normally discharged into a water body. Aquatic ecosystems may be impacted by rising water temperatures, particularly in critical environments. A significant amount of kinetic energy of the super-critical flow is converted to thermal energy during the H- jump. Managing water quality and ecological health requires an understanding of how H- jumps affect temperature stratification. Therefore, before discharging the effluent in a river if it flows through a H-jump, the water temperature will decrease and maintain the ecological balance. Industrial cooling systems can employ H-jumps to disperse heat. Thermal effects on H-jumps can affect the overall performance and efficiency of power plant cooling systems. Thermal factors must be taken into account when modelling H-jumps accurately in order to produce accurate forecasts. Engineers can enhance system performance, reduce possible hazards, and improve the general health of aquatic ecosystems by taking into account the thermal aspects of H-jumps.

Controlling the tailgate in the flume H-jumps are developed, and various experiments are conducted to determine the characteristics of such H-jumps while causing them to happen at various temperatures. In this study, in order to observe various jump characteristics for a constant discharge, experiments were conducted by increasing the temperature of the water from the lowest to the highest within the measuring range.

3.4. Experimental Setup

In the Fluvial Hydraulics Laboratory of School of Water Resources Engineering at Jadavpur University, an experimental setup was built in the titling flume (Figs. 3.1 and 3.2). This flume was horizontal rectangular Perspex made with smooth glass side walls that were 35 cm wide, 60 cm high, and 7 m long. A vertical sluice gate with a series of fixed baffle plates at the back allowed the water to enter the flume. The water depth was controlled by a tailgate on the flume that was used for raising or lowering. The jump position was changed by varying the depth of the tailwater. A chain pulley system was used in that flume system to alter the bed slope. This slope was a relatively small 1:2400, or 0.0239°. Therefore, the influence of this slope was not taken into consideration in this study. The water was heated to 40°C and circulated down the flume in a closed cycle. A 65 lps centrifugal pump was used to pump water. A bypass system valve was regulated to pump the desired discharge Q.

At the front of the reservoir, six immersion-type electrical heaters with a capacity of 1 kW each and four immersion-type electrical heaters with a capacity of 1.5 kW each were dipped at equal intervals to form a total of 12 kW of immersion heaters (Figs. 3.3-3.4). In addition, to heat the water, two wall mounted type electric heaters, each rated at 3 kW, or a total of 6 kW, were dipped at the hump point of the flume inflow. These heaters were used to heat the water to various necessary experimental temperatures.

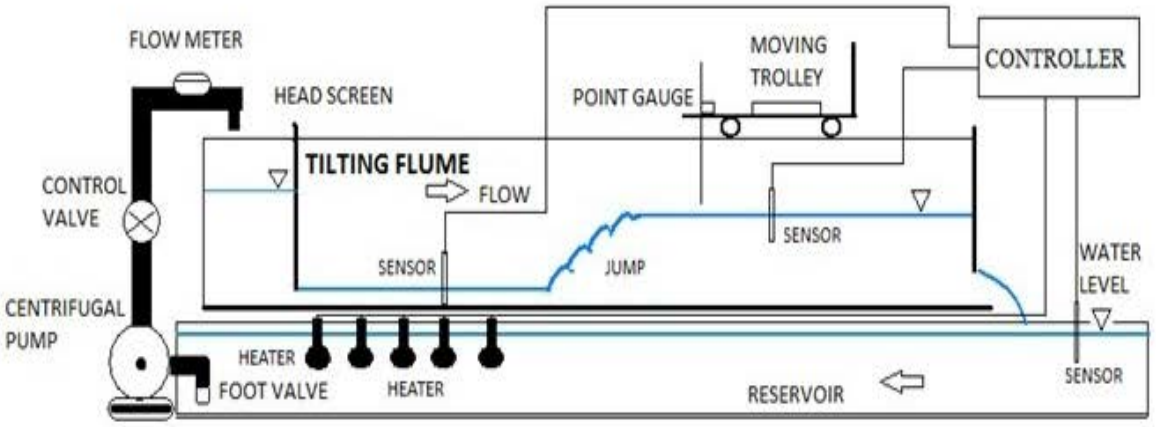

Fig. 3.1. Schematic illustration showing the setup of experiments.

Fig. 3.2. Experimental flume in the laboratory.

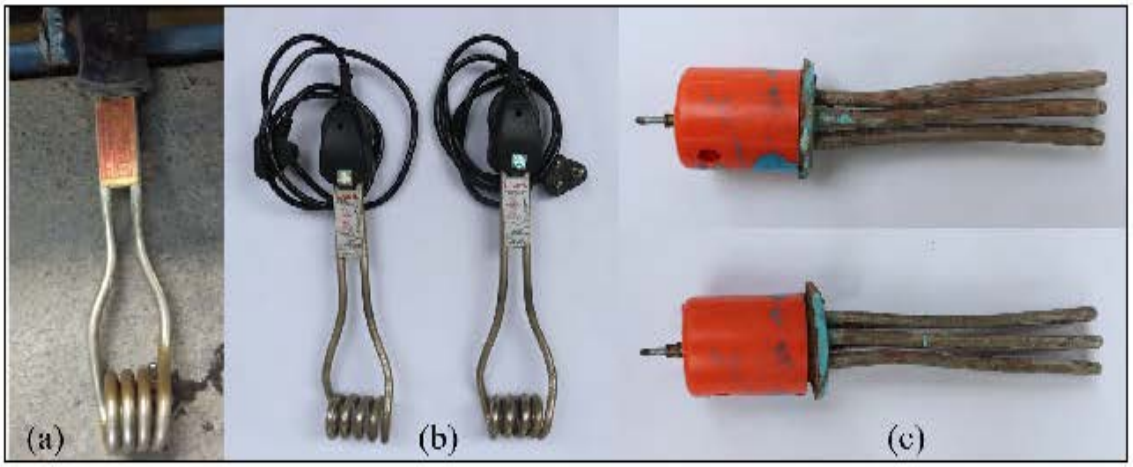

Fig. 3.3. Three types of heaters of (a) Capacity 1 kW, (b) Capacity 1.5 kW, and (c) Capacity 3 kW used for the investigation.

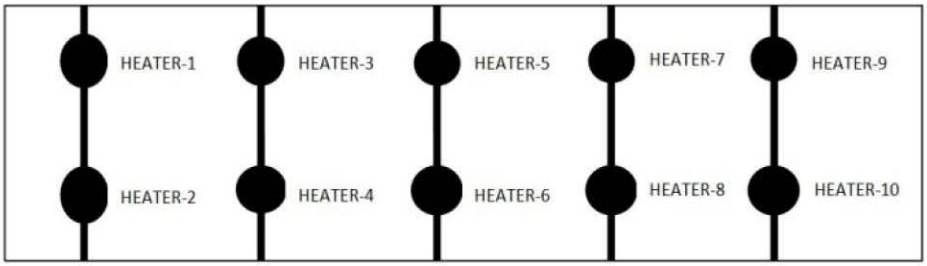

Fig. 3.4. Arrangement of 10 heaters in the reservoir.

One analogue flow meter and one digital flow meter are the two types of flow meters used to measure the pump discharge. The analogue flow meter was manufactured by Dashmesh with an accuracy of ±2% of reading and the digital flow meter was manufactured by Endress & Hauser with an accuracy of ±0.5% of reading (Fig. 3.5). A point gauge was used to monitor the flow depths both before and after the oscillation jump with an accuracy of ±0.5 mm.

Fig. 3.5. Flow measuring instruments: (a) digital type and (b) analogue type.

The temperature in the sub-critical and super-critical zones was measured using two digital thermometers. Along with these two thermometers, one additional digital thermometer was used to measure the water temperature in the reservoir or dumping chamber. Each digital thermometer consisted of a sensor. Therefore, a total three numbers of sensors were utilized in the experiment procedure. This experimental arrangement also included a temperature control unit (Fig. 3.6a). The cylindrical shaped sensor of these thermometers was made of stainless steel and one node of this sensor was connected to the thermometer with a thermistor cable (Fig. 3.6b).

The glass side walls that make up the working component of the flume enable visual observations of the H-jump (Fig. 3.7). A series of electric heaters were used to heat the water. The desired temperature of the water can be previously set with this controlling unit as seen in Fig. 3.8. The measurement took a relatively short time, and the sensor diameter (0.6 cm) was excessively small in comparison to our experimental flume width (35 cm). The flume width was 1.7% more than the sensor diameter. As a result, there might be a little

barrier, so the penetration of the sensor was unlikely to significantly alter the flow characteristics (Fig. 3.8b). Because of this, its impact was ignored.

(a) 

(b) 

Fig. 3.6. Temperature (a) controlling unit, and (b) sensor used for experimentation.

Fig. 3.7. H-jump formation during experimentation in the laboratory.

(a) 
(b) 

Fig. 3.8. Temperature (a) controlling unit with (b) sensor during an investigation.

The water temperature and flow depth were measured in the sub-critical and super-critical zones after it had been pumped out through a closed setup and passed through the flume. Along with this, the ambient temperature was also measured.

3.5. Results and Discussion

For investigation, the experimental flume featured a smooth, horizontal bed. The flume contained a tailgate to regulate the water depth after the jump and a vertical sluice gate for water entry. In this study, forced and submerged type H-jumps were developed by regulating the tailgate in order to establish oscillating H-jumps. The characteristics of H-jumps formed on the flume bed surface were investigated in five experiments (HJ1–HJ5). The temperature in this research ranged from 32°C to 40°C, and the discharge was maintained 37 lps. Electric heaters were used to increase the water temperature and then various jump characteristics have been investigated. In each experiment, the intake gate openings were identical. Along with this, the discharge as well as the inlet velocity was similar for all experiments. The water surface downstream of the H-jump was continually undulating. The maximum and lowest levels of these undulations were marked at specific locations, and the depth at those locations was estimated by averaging individual depths. The depth of the flow is plotted on the vertical axis and the distance from the inlet gate of the flume is plotted on the horizontal axis, as shown in Fig. 3.9.

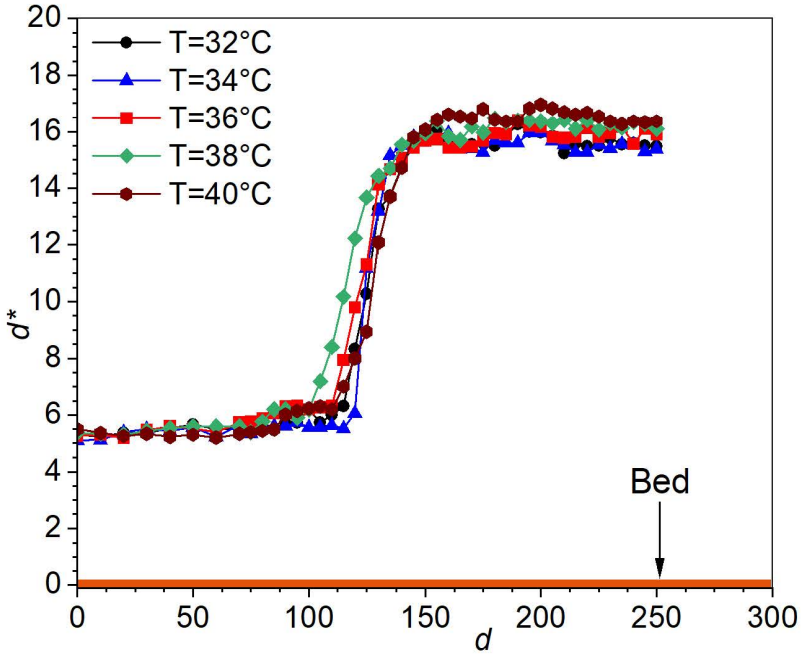

Fig. 3.9. Experimental flow profiles along with the jump for different temperatures.

Here, d and d^* are the distance from the inlet gate and the depth of flow respectively. As the inlet gate opening and the inlet velocity are the same, consequently, as illustrated in Fig. 3.9, the pre-jump depths are nearly the same for the five investigations. Because the density of water varies with temperature, the improvement in post-jump depth

is greater at higher temperatures than at lower ones. In the same manner, it would be more accurate to state that as temperature increases, the SD-Ratio (y_2/y_1) improves.

Before the H-jump, the average Froude number (Fr_1) was 2.55. Following the formation of an oscillating H-jump, a considerable decrease in the post-jump Froude number (Fr_2) is seen. This variation in the Froude number, ΔFr (= Fr_1 - Fr_2) before and after the jump appears to escalate with the increase in water temperature, as shown in Table 3.1. The Reynolds number (Re) of flow which ranges from 133108 to 156221 as indicated in Table 3.2, has increased as the temperature has increased.

Table 3.1. Decrease in ΔFr after the jump at the different water temperatures.

Experiment number	Temperature (°C)	The decrease in Froude number after the jump, ΔFr (%)
HJ 1	32	78.84
HJ 2	34	79.13
HJ 3	36	78.16
HJ 4	38	79.47
HJ 5	40	79.49

Table 3.2. Reynolds number (Re) varying at different water temperatures.

Experiment number	Temperature (°C)	Reynolds number, Re
HJ 1	32	133108
HJ 2	34	138220
HJ 3	36	143741
HJ 4	38	149721
HJ 5	40	156221

The specific energy loss, E_L due to the development of the H-jump is calculated after solving the specific energy Eqs. 3.1-3.4.

$$E = y + \frac{q^2}{2gy^2} \tag{3.1}$$

$$E_L = E_1 - E_2 \tag{3.2}$$

$$= \left(y_1 + \frac{q^2}{2gy_1^2} \right) - \left(y_2 + \frac{q^2}{2gy_2^2} \right)$$

Again,
$$E_L = \frac{(y_2 - y_1)^3}{4 y_1 y_2} \tag{3.3}$$

$$\frac{E_L}{y_1} = \frac{\left(\frac{y_2}{y_1} - 1\right)^3}{4\left(\frac{y_2}{y_1}\right)} \tag{3.4}$$

The relative energy loss (E_L/E_1) is given by Eq. 3.5.

$$\frac{E_L}{E_1} = \left(\frac{E_L}{y_1}\right) \Big/ \left(\frac{E_1}{y_1}\right) \tag{3.5}$$

According to Table 3.3, the relative energy loss in the current work, as calculated using Eq. 3.5, seems to increase as the temperature rises.

Table 3.3. Relative energy loss during a H-jump at different temperatures.

Experiment number	Temperature (°C)	Relative Energy Loss, E_L/E_1 (%)
HJ 1	32	12.90
HJ 2	34	13.12
HJ 3	36	12.64
HJ 4	38	14.00
HJ 5	40	15.34

The specific enthalpy (h) of water at corresponding experimental temperatures has also been computed in pre-jump and post-jump conditions. The specific enthalpy in the H-jump has increased with the increase in temperature (Table 3.4).

Table 3.4. Specific enthalpy during an H-jump at different inlet Froude numbers.

Experiment number	Inlet Froude number, Fr_1	Specific enthalpy, h (kJ/kg)
HJ 1	2.5	134.04
HJ 2	2.56	142.40
HJ 3	2.38	150.77
HJ 4	2.45	159.14
HJ 5	2.39	167.50

3.6. Conclusions

This present work aimed to examine the impact of temperature on H-jump characteristics and establish a relationship between temperature variation and the fundamental H-jump parameters. The five experiments in the thermal experimental H-jump included measurements of sequent depths, temperature, velocity, specific energy, and relative energy loss. The specific energy has altered in this investigation with respect to the depths of the pre-jump location and post–jump location of the H–jump. The difference in the Froude number has increased during the jump. It is evident from this study that in the same flow condition there is a significant change in enthalpy of water as the temperature keeps on varying. Under the same circumstances, the Reynolds number also increases.

To demonstrate the nature of the variation of these parameters as the temperature of water fluctuates, further research is required to establish a clear trend.

References

Alikhani, A., Behrozi-Rad, R., & Fathi-Moghadam, M. (2010). Hydraulic jump in stilling basin with vertical end sill. *International Journal of Physical Sciences*, 5(1), 25-29.

Baddour, R. E. (1987). Hydraulics of shallow and stratified mixing channel. *Journal of Hydraulic Engineering*, 113(5), 630-645.

Baddour, R. E. (1991). Thermal hydraulic jump: theory and experiment. *Journal of fluid Mechanics*, 226, 243-256.

Bai, R., Ning, R., Liu, S., & Wang, H. (2022). Hydraulic jump on a partially vegetated bed. *Water Resources Research*, 58(7), e2022WR032013.

Bai, R., Tang, R., Murzyn, F., & Wang, H. (2023). Pre-aerated classic hydraulic jump downstream a partly-stepped chute. *Journal of Hydraulic Research*, 61(2), 260-271.

Carollo, F. G., Ferro, V., & Pampalone, V. (2012). New expression of the hydraulic jump roller length. *Journal of Hydraulic Engineering*, 138(11), 995-999.

Castro-Orgaz, O., Gamero-Ojeda, P. P., Cantero-Chinchilla, F. N., de Luna, T. M., Hager, W. H., & Bombardelli, F. A. (2023). Variational RANS modeling of hydraulic jumps. *Ocean Engineering*, 283, 115037.

Husain, D., Alhamid, A. A., & Negm, A. A. M. (1994). Length and depth of hydraulic jump in sloping channels. *Journal of Hydraulic Research*, 32(6), 899-910.

Jan, C. D., & Chang, C. J. (2009). Hydraulic jumps in an inclined rectangular chute contraction. *Journal of Hydraulic Engineering*, 135(11), 949-958.

Kumar, M., & Lodhi, A. S. (2016). Hydraulic jump over sloping rough floors. *ISH Journal of Hydraulic Engineering*, 22(2), 127-134.

Laishram, K., Kumar, P. A., & Devi, T. T. (2021, December). Effect of channel slope and roughness on hydraulic jump in open channel flow. *IOP Conference Series: Earth and Environmental Science* 958(1), 012014.

Liu, M., Rajaratnam, N., & Zhu, D. Z. (2004). Turbulence structure of hydraulic jumps of low Froude numbers. *Journal of Hydraulic Engineering*, 130(6), 511-520.

Montano, L., & Felder, S. (2020). An experimental study of air–water flows in hydraulic jumps on flat slopes. *Journal of Hydraulic Research*, 58(5), 767-777.

Nikmehr, S., & Tabebordbar, A. (2010). Hydraulic jumps on adverse slope in two cases of rough and smooth bed. *Research Journal of Applied Sciences, Engineering and Technology*, 2(1), 19-22.

Ohtsu, I., Yasuda, Y., & Hashiba, H. (1996). Incipient jump conditions for flows over a vertical sill. *Journal of Hydraulic Engineering*, 122(8), 465-469.

Pagliara, S., Lotti, I., & Palermo, M. (2008). Hydraulic jump on rough bed of stream rehabilitation structures. *Journal of Hydro-environment Research*, 2(1), 29-38.

Palermo, M., & Pagliara, S. (2017). D-jump in rough sloping channels at low Froude numbers. *Journal of Hydro-environment Research*, 14, 150-156.

Rahbar, N., & Hamzeh, M. (2008). Study of Hydraulic Jump on Heat Transfer at Various Conditions in Open Channels, 5th WSEAS International Conference on Fluid Mechanics (FLUIDS 08) Acapulco, Mexico, 114-120.

Roy, D., Das, S., & Das, R. (2021). Characterisation of B type hydraulic jump by experimental simulation and numerical modeling using MacCormack technique. *Modeling Earth Systems and Environment*, 7, 2753-2768.

Wang, H., & Chanson, H. (2015). Air entrainment and turbulent fluctuations in hydraulic jumps. *Urban Water Journal*, 12(6), 502-518.

Simulation of Hydraulic Jump for Heat Dissipation

4.1. Introduction

The number of thermal, nuclear, and hydroelectric power plants and industrial facilities that have been built and are in operation, both domestically and internationally, has increased dramatically in the 21st century. Aquatic life is harmed when these power plants and several other industrial facilities release thermally contaminated water into natural water bodies like rivers, canals, bays, or lakes. Although there are a number of ways to cool heated water before it is released into bodies of water, using a hydraulic jump (H-jump) to improve heat dissipation to the surrounding environment may have both technological and financial benefits.

There are a number of models available to examine the complex process of heat dissipation between the atmosphere and natural water bodies, which primarily involves turbulent flows. Williams (1963), in his paper, presented measurements of heat losses from a lake through convection and radiations. Spalding (1977) discussed the laws governing heat and mass transfer between rivers, lakes, bays and estuaries. A numerical model for highly transient flow involving mass and heat transfer in rivers was created by Jobson and Keefer (1979). They specifically used this model on the Chattahoochee River in Georgia to forecast and confirm temperature changes in the months of October and March throughout the whole reach of a selected river. The prediction showed good results after verification. Stang (1982) attempted to develop a basic model for heat exchange between flowing water and the atmosphere and then applied this model to the Orkla River to illustrate the ability to analyze diurnal changes in water and air temperature and predict the downstream decay of the temperature changes originating from the man-made releases. Rashidi et al. (1991) studied the mechanism of heat and mass transfer between the gas-liquid interface and the corresponding models. H-jump involves a huge aeration and hence the effect of aeration in heat transfer is also of significance. Some researchers (Ford et al. 1972, Novotny and Krenkel 1973, Talati 1988, Gulliver et al. 1990, Chanson 2007) examined the heat and mass transfer during aeration, as well as air entrainment in free-surface flows, and then attempted to develop appropriate numerical models to represent these processes.

Several computational fluid dynamics (CFD) based models have been developed and put into use to simulate open channel flows with heat and mass transfer in recent years as a result of the tremendous advancements in computation algorithms and capabilities. These CFD algorithms can also accurately resolve the air-water interaction and simulate H-jumps. A few scholars have performed numerical simulations and studies of H-jumps using various turbulence models. Chipadda (1996), Zhao et al. (2004), and Harada and Li (2018) all used conventional k-ε models among the RANS models. Carvalho et al. (2008) and Abbaspour and Farsadizadeh (2009) used the RNG k-ε model to study numerical

simulations of H-jumps. A comparative analysis of numerical simulation of the H-jump utilizing the standard k-ε model, renormalization group (RNG) k-ε model, and shear stress transport (SST) k-ω model was used by Bayon and Jimenez (2015). The ability of OpenFOAM and FLOW-3D CFD software to numerically replicate the H-jump was evaluated by Bayon et al. (2016). A thorough analysis of a number of alternative turbulence models and their relative capacities to replicate the H-jump was provided by Valero et al. (2018).

Investigations into the connection between H-jumps and water temperature have been carried out both in the past and present. Wang and Khayat (2020) studied the influence of H-jumps obtained over a heated circular disc. Mondal et al. (2020) performed experiments in order to study the thermal effect on jump characteristics and correlate the variation of temperatures with several jump parameters. Nandi et al. (2020) conducted numerous experimental investigations and computer simulations focused on submerged H-jumps under various flow conditions.

Although open channel flows with and without involving the H-jumps have been simulated by implementing several turbulence models, the effect of H-jumps on heat transfer between water and the ambient has not been simulated extensively. Given, all the progress achieved to date in simulating the H-jump and heat-mass exchange in turbulent flows using several models and CFD codes, there remains scope for investigating the nature of heat transfer aided by H-jump. The present study focuses on simulating an H-jump in a rectangular flume using Ansys Fluent and thereby observing the effect of heat transfer from the water to the ambient on average thermal quantities of flow such as temperature, specific entropy, and specific enthalpy for six different ambient temperatures. It was found that the H-jump tends to increase the drop in temperature, specific enthalpy and specific entropy at a section downstream of the jump as compared to a drop in the corresponding quantities just with natural convective and conduction heat transfer. However, the reason for this and the exact nature of the H-jump in dissipating the heat for different temperature differences between the ambient and the water remains a matter of further study.

4.2. Review of Published Research

In terms of heat transfer from any open channels, recent research has demonstrated that the thermal effect on H-jumps is an important topic. The study investigated factors that affect heat transfer from open channel flow. The effect of channel roughness was examined so as to find a means of increasing heat transfer by enhanced turbulence. The study suggested the use of artificially roughened channels as an alternative means of accomplishing an increase in evaporative cooling as a consequence of increased turbulent mixing in open channel flow and hence utilizing this result for dissipation of excess industrial heat. Expressions were developed that related the heat transfer rates under several hydraulic conditions and the surface water temperature. An iterative algorithm was proposed for the determination of heat transfer. The model estimated good results of heat transfer in the range of natural water temperatures and raised temperatures found in the discharges from thermal power plants and other chemical plants (Moss 1976).

A comprehensive model for temperature predictions in diffused aeration and sub-surface mechanical aeration systems was presented. During the course of the model development, expressions suggested by Novotny and Krenel (1973) were adopted to account for the heat loss by surface aeration that included heat loss due to evaporation and conduction from water droplets in aerator spray. A steady-state heat balance equation for the aeration basin was considered. The heat balance included heat lost by long wave radiation, the heat lost by evaporation from the basin surface, heat lost by conduction from the basin surface, heat lost by conduction and evaporation by aerator spray, heat gained due to solar radiation, heat gained from mechanical energy input, heat gained from biochemical reaction and heat lost by conduction through basin walls and bottom. The model developed resulted in good agreement between the predicted and measured values of temperatures for two aerated lagoons using surface aerators and diffused air (Yerachmiel and Carl 1978).

Two-component laser Doppler anemometry measurements with high resolution were conducted in a fully formed turbulent channel flow, covering a range of Re from 3000 to 40000. The resulting data rates were high enough to allow for the reconstruction of the velocity signals that varied with time. The time-averaged mean and fluctuation quantities were computed from these reconstructed signals. Over the range under investigation, the inner scaling rules of the changing quantities in the inner region rely on the Re. Additionally, there was a geometry impact that interacts, especially at lower Re, between the inner-region structure from opposing channel walls (Wei and Willmarth 1989). Boussinesq equation was integrated numerically to simulate both sub-critical and super-critical flows as well as the H-jump. For this, the governing equations were solved using the MacCormack (second-order accurate in time and space) and two-four (second-order accurate in time and fourth-order in space) explicit finite-difference schemes, subject to predetermined end conditions, until a steady state was achieved. The significance of the Boussinesq terms was examined, and the Detailed test results were shown for a variation of Fr. The second-order method did not correctly forecast the location of the jump, but a comparison of the calculated and measured data reveals that the fourth-order finite-difference scheme had a sufficient agreement between them. The results of these simulations demonstrate that the Boussinesq terms had minimal impact on the location of the H-jump (Gharangik and Chaudhry 1991).

A prediction model was developed to calculate the sequent depth ratio (SD-Ratio) of the H-jump in an inclined rectangular channel with a positive or negative step. Its basis was the use of continuity and momentum equations in one dimension. Two parameters were defined in the presented model. One of them takes into account the slope of the channel and the other takes into account the existence of a positive or negative step. The effects of the step and bed slope alone or in combination with the SD-Ratio of the H-jumps could be predicted by the model. The created model was calibrated and verified for both horizontal and sloping floors using an extensive series of experimental data (Negm 1996). High-resolution digital elevation models (DEMs) for naturally occurring submerged and unsubmerged H-jump zones were compared to engineering equivalents and the classical H-jump (CHJ). The data demonstrated that, in terms of boundary conditions, the bed and water surface properties of the natural H-jump zones differ greatly from CHJ circumstances and engineered analogues. The results also revealed that, in terms of hydraulic parameters,

the bed and water–surface features of natural H-jump zones differ and are similar to CHJ circumstances and engineered equivalents. The hydraulic properties of the sloped and ballistic jets were found to differ. For the jump areas, updated conceptual models based on idealized corollaries were developed using step geometry and upstream energy head in relation to downstream tailwater depth (Vallé and Pasternack 2006).

Experimental findings from recent measurements in a rectangular horizontal flume with partially imposed inflow conditions. The vertical distribution of the void fraction and the air bubble count rate were recorded. A rapid detrainment process was observed near the toe of the H-jump, but at longer distances the structure of the air diffusion layer was visible. These new data contradict earlier data, which were usually collected at lower Fr values. The comparison showed that the largest percentage of voids C_{max} increases with increasing Fr_1 at a fixed distance from the H-jump toe. Finally, an empirical relationship was established between the distance from the impingement site and the upper boundary of the air diffusion layer (Gualtieri and Chanson 2007). An enhanced Eulerian model was created to simulate the flow field of air-water over the stepped spillways. With the updated drag model, distinct drag coefficients were applied for bubbles and for gas cavities or free surface flows. To find the bubble drag coefficient, turbulence correction and void fraction were applied. The location of the inception point, the distributions of air void fraction, the velocity distributions, and the pressure distributions were all predicted by the Eulerian simulations using the revised drag model. Based on the enhanced computational fluid dynamics model and the transport equation for dissolved oxygen (DO) transferring, the change in the DO concentration from upstream to downstream of the stepped spillways was simulated. The experimental findings and the numerical DO concentration agreed (Cheng and Chen 2013).

At relatively large Re from 2.1×10^4 to 1.6×10^5, new experiments were carried out to quantify the fluctuating characteristics of H-jump in terms of free-surface and two-phase flow properties for a wide range of Fr from 3.8 to 8.5. A self-similar profile was displayed by the time-averaged free-surface profile. Observations of the longitudinal movements of jumps revealed oscillations that were both extremely slow and quick for all Fr. The high aeration of rollers was measured by the air-water flow measurements. Overall, the results showed that free-surface fluctuations and jump roller turbulence interacted strongly (Wang and Chanson 2015). A study of seven turbulence models was done based on RANS equations comparatively to justify their accuracy and suitability as compared to direct numerical simulation (DNS) for turbulent channel flow between two horizontal walls subsequent and heat transfer. The flow in the channel was assumed to be a fully developed turbulent flow and uniform heat flux was applied at the top and bottom walls. Numerical simulations were carried out for four different Re. Different turbulent statistics such as mean streamline velocity, mean temperature and stream wise turbulent heat flux were calculated and compared with the data obtained by DNS. The turbulence models not assuming wall function can determine the near-wall flow and thermal quantities quite accurately. The low Re model k-ε can provide accurate mean flow in the near-wall region within some tolerance. Good accuracy was achieved in the outer wall region. The selected k-ε model was found to be in good agreement with the DNS data for mean velocity and

temperature distributions for different Re and Pr_t. It was further inferred that the turbulent heat flux can be accurately computed by the low Re model (Mollik et al. 2017).

The influence of heat transfers on the axi-symmetrical spreading and structure of the H-jump of a liquid impinging on a circular heated disk was examined theoretically. The disk was maintained at either the prescribed heat flux or temperature. It was assumed that the liquid viscosity and surface tension are dependent on temperature. Across the jump, an energy balance was developed to simultaneously determine the hydraulic and thermal jumps, downstream flow and thermal fields. The jump was found to move outwards (downstream) with the increasing higher wall temperature and heat flux. The jump height decreased with enhanced thermal input at the wall (Wang and Khayat 2020).

The effectiveness of seven machine learning models including Gradient Boosting (GB), Artificial Neural Network (ANN), Least Angle Regression (LARS), Lasso Regression (LASSO), Random Forest (RF), Extra Trees (ET), and Adaptive Boosting (Adaboost) in the context of H-jump roller length forecasting in a rectangular horizontal canal was thoroughly examined in the work. All six of the remaining models aside from Adaboost performed better than the empirical equations, which were overshadowed by the excellent accuracy of ML algorithms. In order to arrive at this conclusion, the study took into account the impacts of fluid viscosity, channel shape, and surface roughness when applying the Buckingham Pi theorem to exactly determine model input and output. Therefore, when the inflow Fr fluctuated between 2.4 and 15.9, the study advised against using empirical equations to anticipate the roller length of the H-jump and instead used the GB, ANN, and ET models (Ho 2024).

4.3. Modelling of a Multiphase Flow

Open channel flow is a multiphase flow as the dynamics of two fluids are involved the water and atmosphere above the water-free surface. As a consequence, the free surface is an interaction of these two phases and hence proper evaluation of the free surface properly becomes essential while simulating an open channel flow. During a H-jump, there is a strong mixing of water and air and when one studies the heat interaction between these two fluids during the H-jump, the modelling of the interaction between these two phases becomes an essential part of the simulation. A large number of multiphase models are present in CFD.

In multiphase flow, a phase can be defined as an identifiable class of material that has a particular inertial response to and interaction with the flow and the potential field in which it is immersed. Multiphase flow regimes can be grouped into four categories such as gas-liquid flows, liquid-liquid flows, gas-solid flows, and three-phase flows. Open channel flow falls under the gas-liquid multiphase flow regime. There are two approaches for the numerical calculation of multiphase flows in CFD, the Euler-Lagrange approach and the Euler-Euler approach.

a) The Euler-Euler Approach

The various phases of the Euler-Euler method are mathematically represented as interpenetrating manifolds. Because the volume of a phase cannot be filled by other phases,

the idea of a volume fraction (of a single phase) is presented. It is assumed that these fractions of volume are continuous functions of time and space and that their aggregate equals one. The conservation equations of each phase are derived to produce a set of equations with a common structure across all phases. By offering constitutive relations derived from empirical data or, in the case of granular flows, by applying kinetic theory, these equations are closed. The Eulerian model, the mixture model, and the volume of fluid (VOF) model are the three distinct Euler-Euler multiphase models that are accessible in Ansys Fluent. The VOF model can be used to simulate liquid motion following a dam collapse, for free surface flows, and for both transient and steady monitoring of any liquid-gas interface.

b) VOF model

The VOF model tracks the volume fraction of each fluid across the domain and calculates a single set of momentum equations to simulate two or more immiscible fluids. Typical uses include tracking any liquid-gas interface both steadily and transiently, predicting the jet breakup, predicting the motion of a huge bubble in a liquid, and predicting the motion of a liquid after a dam breaks. Although the VOF formulation (Hirt and Nichols 1981) is typically used to compute a time-dependent solution, a steady-state computation can be performed for instances where a steady-state solution is all that is needed. Only in situations where the answer is independent of the starting conditions and where the inflow bounds for each phase are well-defined, a steady-state VOF computation can make sense. The steady-state formulation, for instance, can be used to solve the water flow in a channel with an air region on top and a separate air entrance.

The volume percentage of the phase in the computational cell is a variable that is added for every additional phase in the VOF formulation. The total volume fractions of all phases in each cell (control volume) equal one. All variables and attributes have fields that indicate volume-averaged values and are shared by the phases. Therefore, depending on the volume fraction values, the variables and attributes in any given cell are either typical of a combination of the phases or entirely indicative of one of the phases. In a certain way, the following three circumstances could occur if the volume fraction of the q^{th} fluid in the cell is represented by α_q.

- $\alpha_q = 0$ indicates the cell is empty (of the q^{th} fluid)
- $\alpha_q = 1$ indicates the cell is full (of the q^{th} fluid)
- $0 < \alpha_q < 1$ indicates the cell contains the interface between the q^{th} fluid and one or more other fluids.

Each control volume inside the domain will be assigned the proper characteristics and variables based on the local value of α_q.

c) Volume Fraction Equation

In order to track the interface(s) between the phases, a continuity equation for the volume fraction of one or more of the phases must be solved. For the q^{th} phase, this equation has the following form (Eq. 4.1).

$$\frac{1}{\rho_q}\left[\frac{\partial}{\partial t}\left(\alpha_q\rho_q\right)+\nabla.\left(\alpha_q\rho_q\vec{\upsilon}_q\right)=S_{\alpha q}+\sum_{p=1}^{n}\left(\dot{m}_{pq}-\dot{m}_{qp}\right)\right] \tag{4.1}$$

where, m_{pq} = the mass transfer from phase q to phase p, and m_{pq} is the mass transfer from phase p to phase q.

By default, the source term on the right-hand side of Eq. 4.1, $S_{\alpha q}$ is zero but can any user-defined mass source for each phase can be specified. The volume fraction of the primary phase remains unresolved. The following constraint (Eq. 4.2) is used to calculate the primary-phase volume fraction

$$\sum_{q=1}^{n}\alpha_q=1 \tag{4.2}$$

The VOF can be solved by either explicit or implicit time discretization method.

4.4. Thermal Analysis and Modelling

a) Generalized Energy Equation

The following generalized energy equation (Eq. 4.3) is solved by several CFD programs, such as Ansys Fluent.

$$\frac{\partial}{\partial t}\left(\rho E\right)+\nabla.\left(\vec{u}\left(\rho E+p\right)\right)=\nabla.\left(k_{eff}\nabla T-\sum_j h_j\vec{J}_j+\left(\overline{\overline{\tau}}_{eff}.\vec{u}\right)\right)+S_h \tag{4.3}$$

where E is the total energy, k_{eff} is the effective thermal conductivity, defined as $k+k_t$, and k_t is the turbulent thermal conductivity, which is determined by the turbulence model in use. $\vec{J}_j$ is the diffusion flux of species j. Energy transfer resulting from conduction, species diffusion, and viscous dissipation are represented by the first three terms on the right-hand side of Eq. 4.3, respectively. The S_h comprises the heat generated by a chemical reaction as well as any additional volumetric heat sources. Here, ∇ is vector operator $\equiv [i(\delta/\delta x)+ j(\delta/\delta y) + k(\delta/\delta z)]$, τ_{eff} is the effeffective stress tensor and h_j is the enthalpy.

In Eq. 4.3, the E is defined as Eq. 4.4.

$$E=h-\frac{p}{\rho}+\frac{v^2}{2} \tag{4.4}$$

where sensible enthalpy h is defined for ideal gases as Eq. 4.5.

$$h=\sum_j Y_j h_j \tag{4.5}$$

and for incompressible flows as Eq. 4.6.

$$h=\sum_j Y_j h_j+\frac{p}{\rho} \tag{4.6}$$

In Eqs. 4.5 and 4.6, Y_j is the mass fraction of species j and h_j as Eq. 4.7.

$$h_j = \int_{T_{ref}}^{T} c_{p,j} dT \tag{4.7}$$

where T_{ref} is 25°C (298.15 Kelvin) and C_p is specific heat capacity at constant pressure.

b) Natural Convection and Buoyancy-Driven Flows theory

The gravity force acts on density fluctuations as a result flows can be created when heat is applied to a fluid whose density changes with temperature. Ansys Fluent can be used to model these buoyancy-driven flows, which are known as natural-convection (or mixed-convection) flows.

For pure heat transfer, the ratio of the Grashof number (Gr) to the square of the Reynolds number (Re^2), also known as Richardson number (Ri) (Eq. 4.8), can be used to quantify the significance of buoyant forces in a mixed convection flow. The Gr is a special form of Archimedes number (Ar) when the density difference takes place due to temperature difference only, leading to the convective current.

$$\frac{Gr}{\mathrm{Re}^2} = \frac{g\beta\Delta TL}{U^2} \tag{4.8}$$

where g is the gravitational acceleration, β is the thermal expansion coefficient, ΔT is the temperature difference between the hot wall temperature and to reference temperature, L is the characteristic length, and U is the characteristic velocity.

Strong buoyancy contributions from the flow are to be expected when this quantity gets close to or beyond unity. On the other hand, buoyancy forces could be disregarded if it is extremely small. The Rayleigh number (Ra) is used to quantify the strength of the buoyancy-induced flow in pure natural convection (Eq. 4.9).

$$\mathrm{Ra} = \frac{g\beta\Delta TL^3\rho}{\mu\alpha} \tag{4.9}$$

where β is the coefficient of thermal expansion, which is defined as Eq. 4.10.

$$\beta = -\frac{1}{\rho}\left(\frac{\partial\rho}{\partial T}\right)_p \tag{4.10}$$

also, thermal diffusivity is represented by α (Eq. 4.11).

$$\alpha = \frac{k}{\rho c_p} \tag{4.11}$$

A buoyancy-induced laminar flow is indicated by Ra less than 10^8, and the transition to turbulence takes place between $10^8<\mathrm{Ra}<10^{10}$.

c) Modelling Convective heat transfer in k-ε Turbulence Models

Reynolds' analogy to turbulent momentum transfer is used to explain turbulent heat and mass transport. Thus, the following is the modelled energy equation (Eq. 4.12).

$$\frac{\partial}{\partial t}(\rho E)+\frac{\partial}{\partial x_i}\left[u_i(\rho E+p)\right]=\frac{\partial}{\partial x_j}\left(k_{eff}\frac{\partial T}{\partial x_j}+u_i\left(\tau_{ij}\right)_{eff}\right)+S_h \tag{4.12}$$

where, $(\tau_{ij})_{eff}$ is the deviatoric stress tensor and is defined as Eq. 4.13.

$$\left(\tau_{ij}\right)_{eff}=\mu_{eff}\left(\frac{\partial u_j}{\partial x_i}+\frac{\partial u_i}{\partial x_j}\right)-\frac{2}{3}\mu_{eff}\frac{\partial u_k}{\partial x_k}\delta_{ij} \tag{4.13}$$

The effective thermal conductivity for both the standard and the realizable k-ε model is computed as follows (Eq. 4.14).

$$k_{eff}=k+\frac{c_p\mu_t}{\mathrm{Pr}_t} \tag{4.14}$$

where k is the heat conductivity in this instance. The default value of Pr_t is 0.85. For the RNG k-ε model, the effective thermal conductivity is represented as Eq. 4.15.

$$k_{eff}=\alpha c_p\mu_{eff} \tag{4.15}$$

4.5. Methodology

The objectives of this part of the research are to simulate an H-jump in a two-dimensional rectangular flume and to observe the effects of the H-jump on thermal properties such as temperature, specific enthalpy and specific entropy of the flow across a section downstream of the jump. H-jump is characterized by a highly turbulent flow with macro-scale vortices and involves a large amount of kinetic energy dissipation and intense mixing and aeration. The primary objective is to simulate an H-jump to observe its effect on heat transfer from the water to the ambient for six different ambient temperatures.

In the post-processing of the simulations, an attempt has been made to observe and calculate the decrease in the average temperature, specific enthalpy, and specific entropy at a section downstream of the H-jump as compared to a section close to the inlet. Additionally, compare these decreases in temperature, specific enthalpy and specific entropy brought about by the H-jump with respect to the decrease in the same quantities caused by only convection and conduction without any H-jump.

The CFD software Ansys Fluent 17 was used to simulate H-jumps in a two-dimensional rectangular flume. Six simulations were performed with water at 40°C flowing inside the flume in each of the simulations. The ambient temperature was considered from 10°C to 35°C with an equal interval of 5°C for every consecutive simulation. Also, separate simulations for the flow without H-jump were carried out for each of the water temperatures, to compare the effect of heat transfer with H-jump and convection and with only convection. The entire methodology is represented in a nutshell in Fig. 4.1.

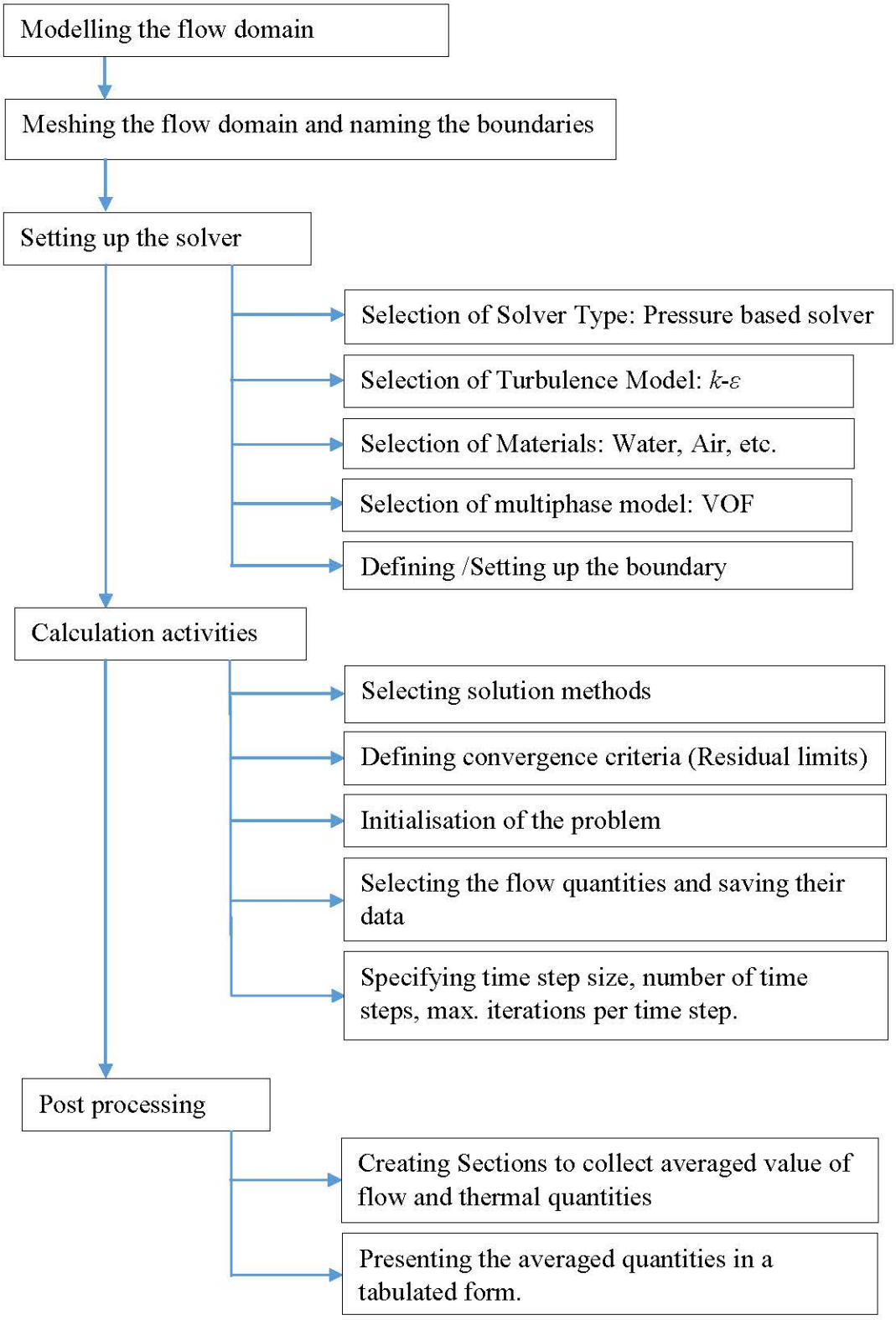

Fig. 4.1. Flow chart representing the methodology adopted in this investigation.

The methodology adopted can be summarized below:

- Modelling the flow domain in a two-dimensional rectangular flume with an inlet gate and the tailgate was developed in the Ansys design modeller.

- The entire domain was meshed and all the boundaries are named conveniently.
- The Fluent solver was set up for calculating the flow. At this stage, several models such as turbulence model, air-water interface tracking model, and energy model were invoked, materials were selected, initial boundary conditions were defined, convergence criteria were set, locations for saving solution files were created etc.
- Suitable solution methods (discretisation schemes) were selected. Selection of quantities that were to be evaluated and stored for post-processing was made. Time step size, number of time steps and maximum number of iterations were set consequently calculating the flow.
- In the post-processing phase, sections were created, averaged flow quantities across the sections were measured and the data thus obtained were analysed.

The detailed methodology is presented below:

a) Modelling the flow domain

The two-dimensional flume was modelled using Ansys Design Modeler in Ansys Workbench. The length of the bed of the channel was taken to be 7 m and the height of the channel was taken to be 0.6 m, shown in Fig. 4.2.

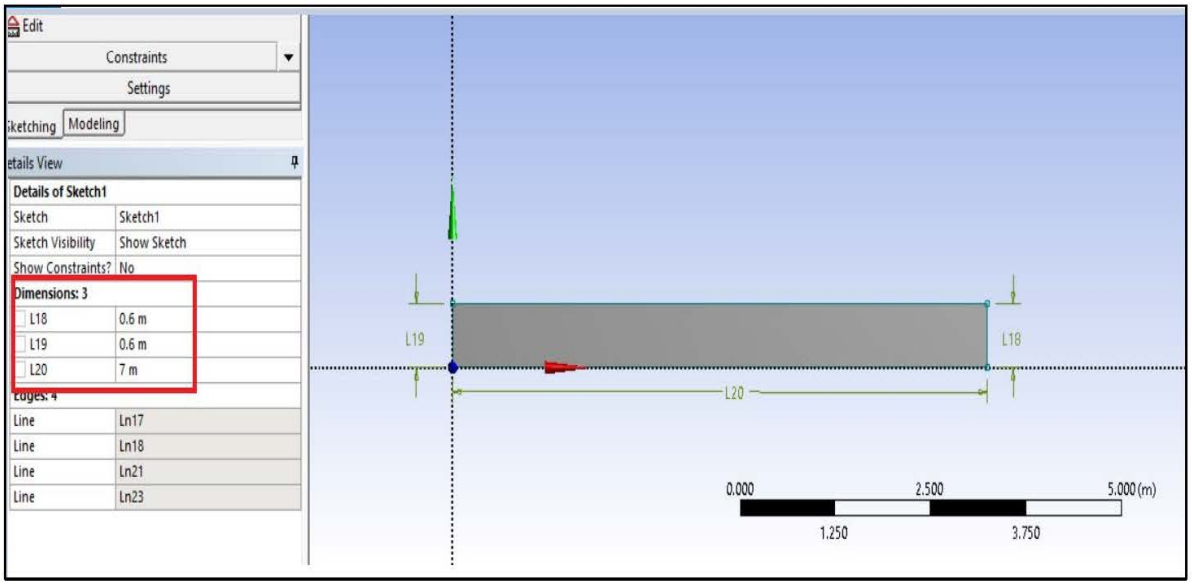

Fig 4.2. Geometry of the rectangular flume with dimensions (enclosed in red box).

Following the laboratory setup, a slope of 1:2400 was provided to the channel bed. The sketch for the channel is shown in Fig. 4.3. The left vertical edge of the channel is the inlet plate that should be kept open to a height of 0.056 m (Fig. 4.3) above the bed, during the simulations. So this edge is split into two parts with the lower part measuring 0.056 m. The right vertical edge is the tailgate (Fig. 4.4). The tailgate is intended to remain closed initially to obstruct the flow and open gradually during the flow. The right edge was split into two parts with the lower part being 0.1 m. This lower part was further split into sixteen equal parts (slots) as shown in Fig. 4.5. The same geometry file was used for all the simulations.

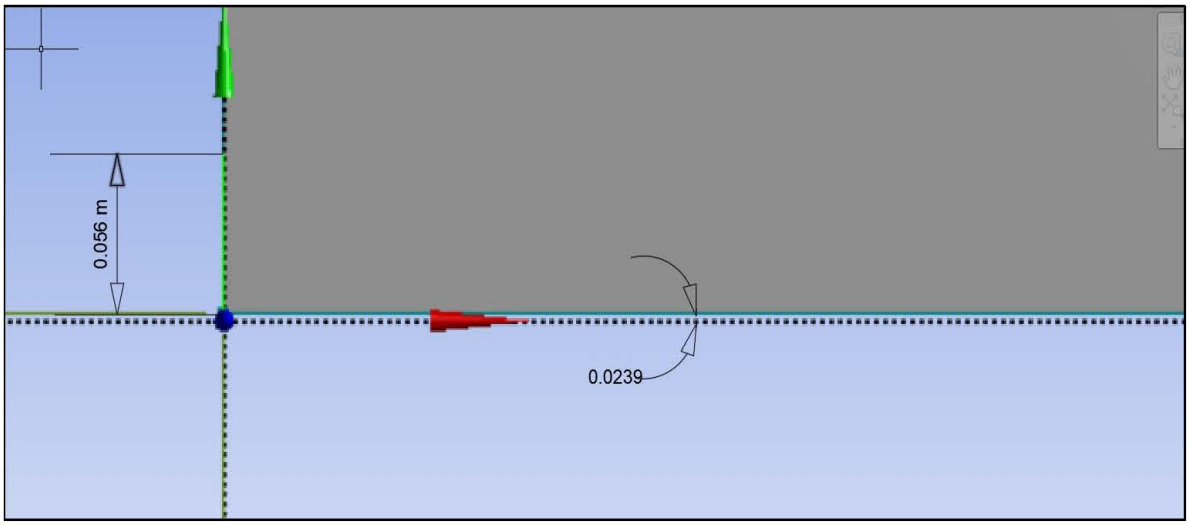

Fig. 4.3. Bed slope (in degrees) and the dimension of the inlet opening.

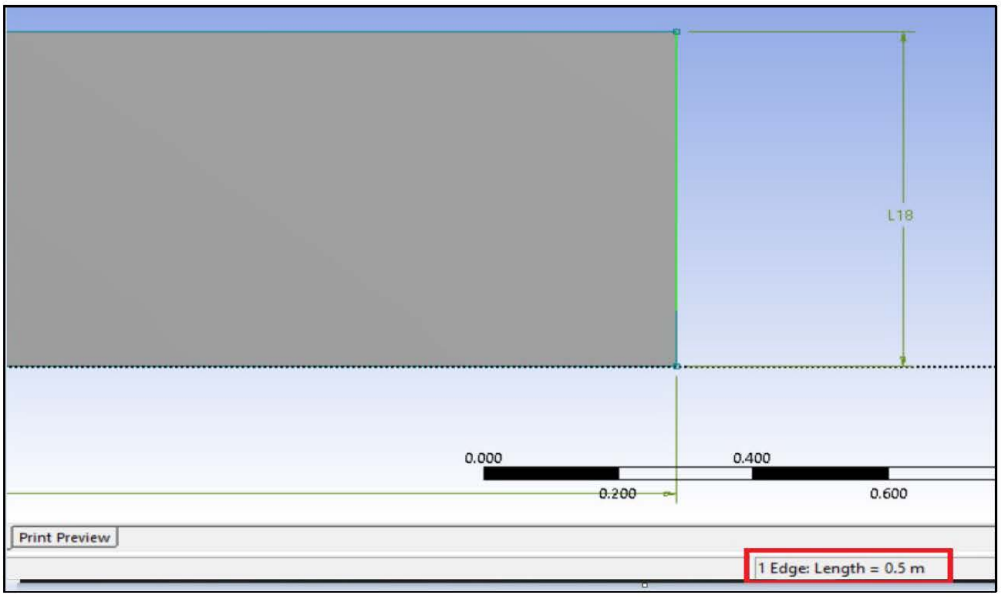

Fig. 4.4. Upper portion of tailgate shown in green and its dimensions enclosed in red box.

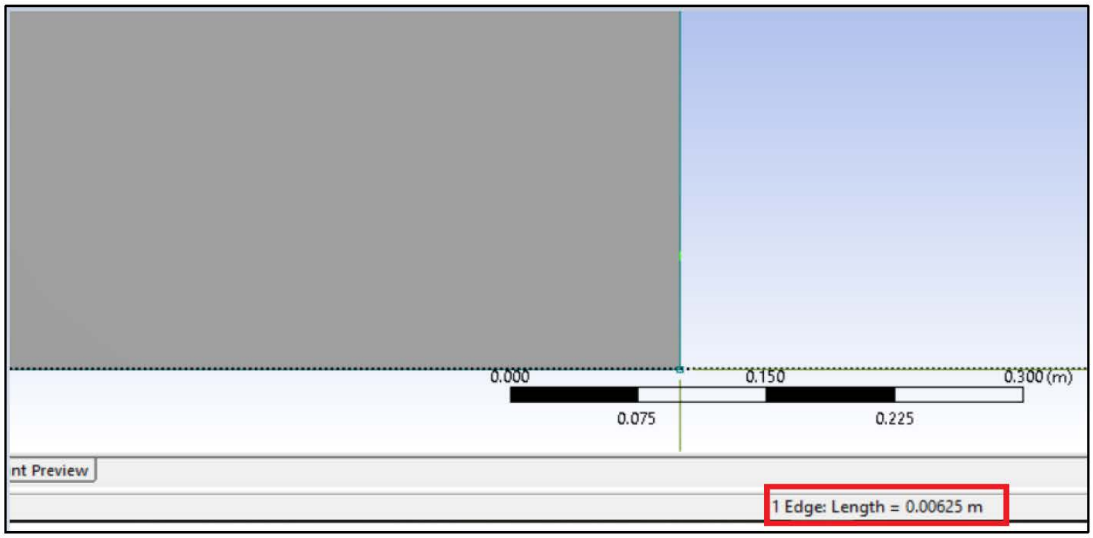

Fig. 4.5. One of the 16 slots highlighted in green and its dimensions enclosed in red box.

b) Meshing the flow domain and naming the Boundaries

Since in the mesh properties table, physics was set to CFD and the solver was set to Fluent, the Ansys meshing software (available within the Ansys Workbench) automatically sets many meshing settings at suitable default. Initially, a default mesh was generated. To refine the mesh further, the maximum face size was reduced to 0.01 m. The exact cell (element) size cannot be provided as the default size function was set to curvature (for CFD physics preference). Nevertheless, the size function was set to adaptive and the mesh was regenerated to check the element size keeping the other mesh settings at default. The element size was found to be 0.01 m. After reverting, the mesh to curvature (default for CFD) size function, inflation with 5 inflation layers with a default growth rate of 1.2 (Fig. 4.6) was provided at the bed and the mesh structure in comparison to the dimensions of the flume. Mesh reports regarding mesh statistics, memory usage and mesh quality were obtained in the Ansys "Fluent" solver console. The advanced mesh, mesh statistics, and mesh quality check parameters were performed. Along with this all the boundaries and the flow domain were named accordingly (Fig. 4.7).

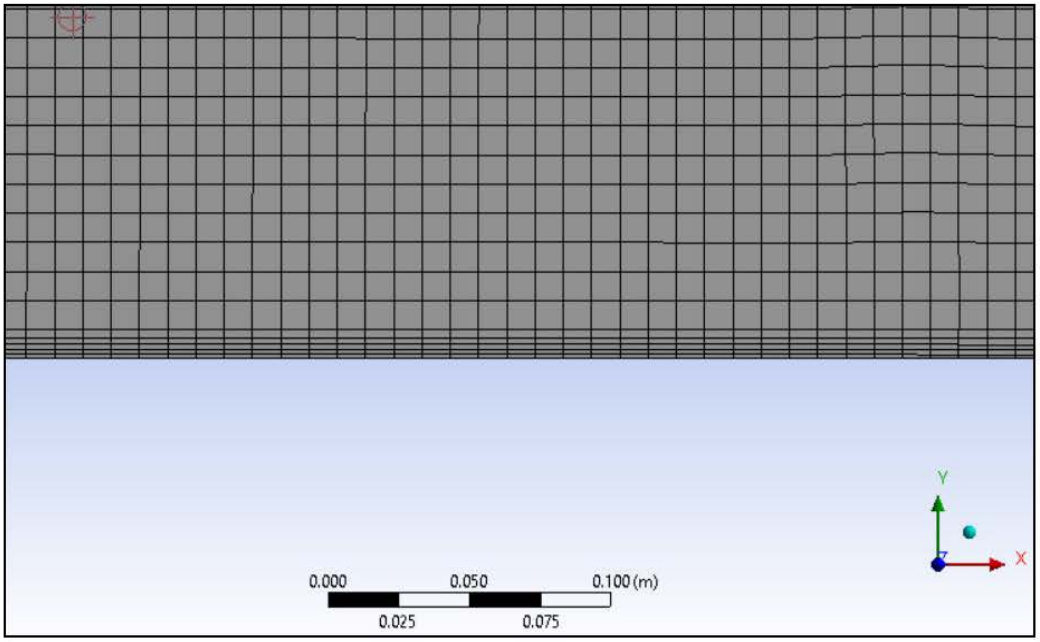

Fig. 4.6. Mesh structure and Inflation layers at the bed.

c) Setting up the Solver

In the general setup (Fig. 4.8), for the solver settings, the "pressure based" type was selected and the "Absolute" velocity formulation was selected, both by default. Under the time settings "transient" option was selected for 2D Space "Planar" was selected. "Gravity" was activated and a value of 9.81 m/s^2 was assigned in the Y component of gravity. Units were set to S.I. by default.

In Ansys Fluent, for the selection of various mathematical models the desired turbulence model may be selected using the "Viscous Model" option under the "Models"

option. The "*k*-*ε*" turbulence model was activated. The "standard" *k*-*ε* model was selected. As for near-wall treatment "Standard" wall treatment was chosen. "Viscous heating" was also activated. The constants involved in *k*-*ε* turbulence models were left with their default values as shown in Fig. 4.9. The "Energy" Model was activated for activating the thermal analysis of the flow for the consideration of the convection heat transfer effects particularly.

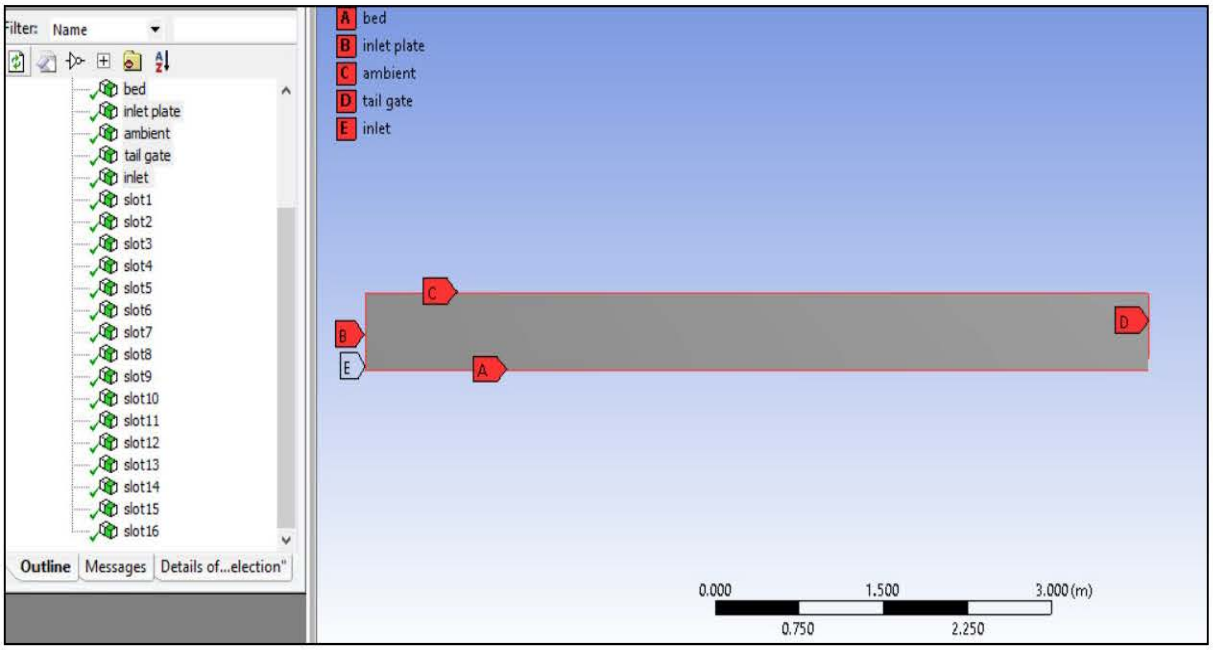

Fig. 4.7. Boundaries and their respective "named selections".

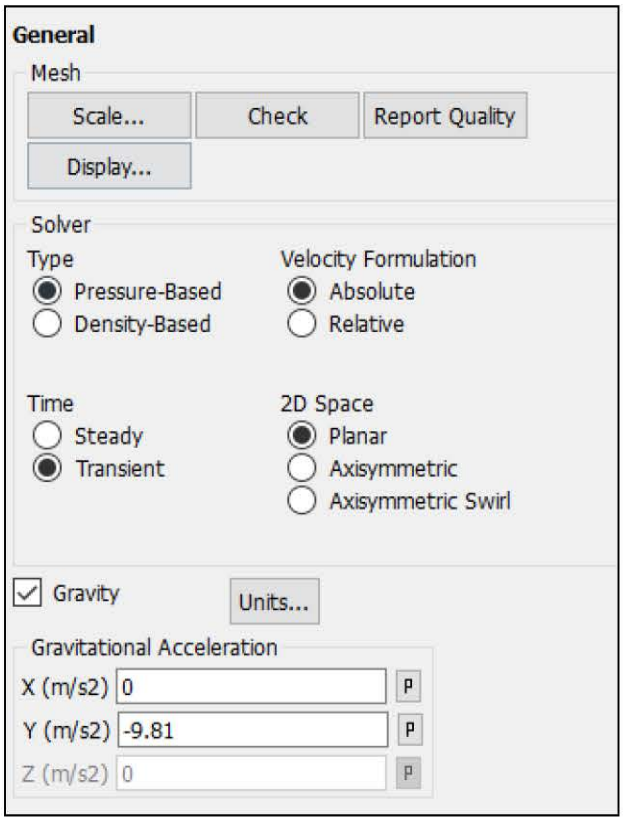

Fig. 4.8. General settings for the solver.

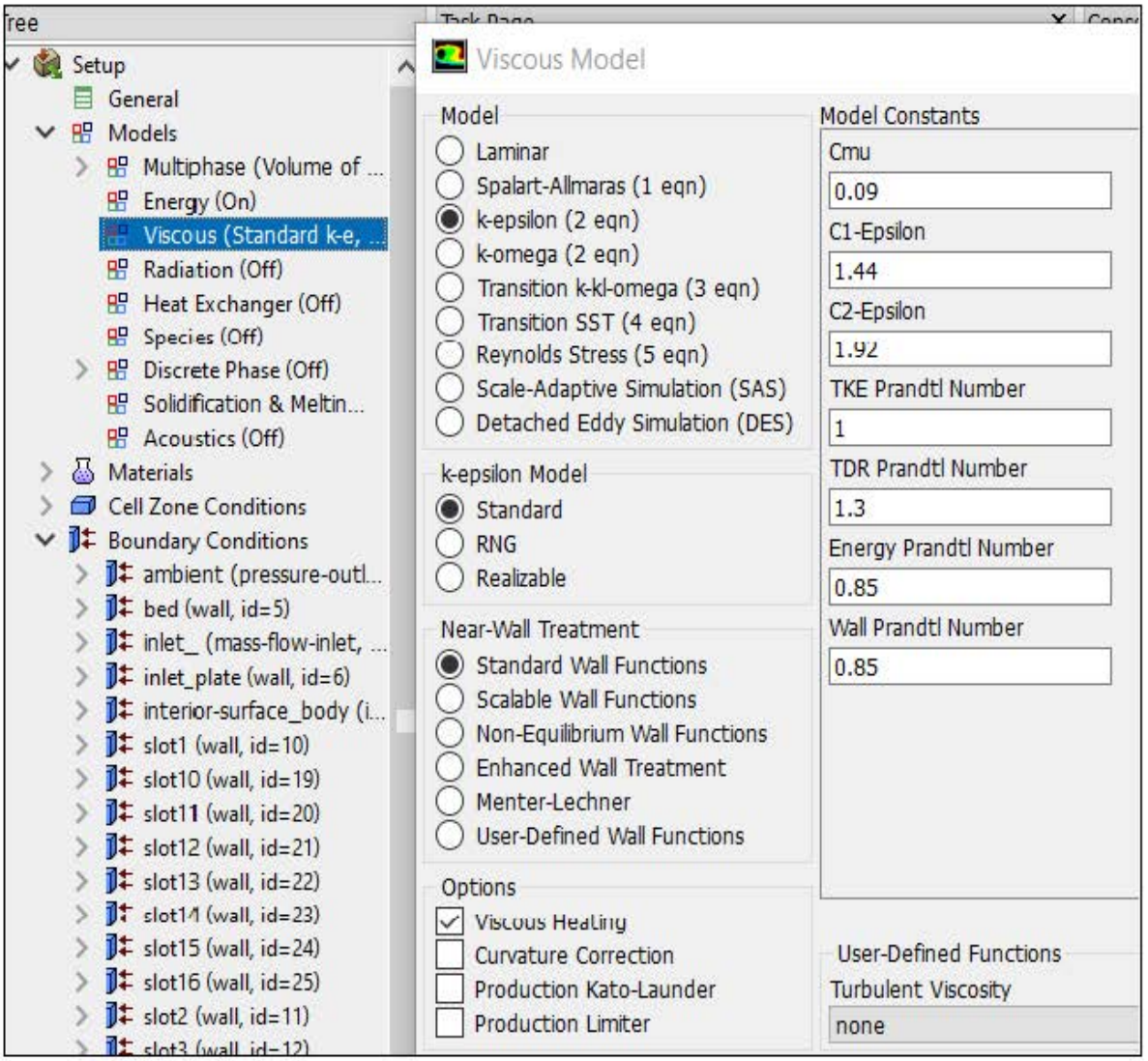

Fig. 4.9. Viscous model dialogue box showing settings for *k-ε* turbulence model.

"Radiation", "Heat Exchanger" and other models that are of very minimal to no significance, were kept inactivated as shown in Fig. 4.9. The "Volume of fluid" was selected as the multiphase model for the present simulation. Volume fraction parameters formulation was set to "implicit". The value for volume fraction cut-off was 10^{-6}. The "Implicit" scheme was adopted for body force formulation. In interface modelling, the "sharp" option was selected. Finally, the number of Eulerian phases was set to 2 (Fig. 4.10).

From the materials panel, water and air with their specified physical properties are selected as fluids. As for solids, steel and wood are selected. Steel is selected as materials to be applied to the inlet gate and the entire tailgate. Wood is selected to act as a hypothetical material for a bed with the thermal properties of wood but with different friction properties that are specified later. It is intended to minimize the conduction of heat from the water to the bed surface so that most of the heat transfer (loss) from the water could occur only due to convection to the ambient and H-jump effects. Water is assigned as the secondary phase and air is assigned as the primary phase in the "phases" section under the "multiphase" tab.

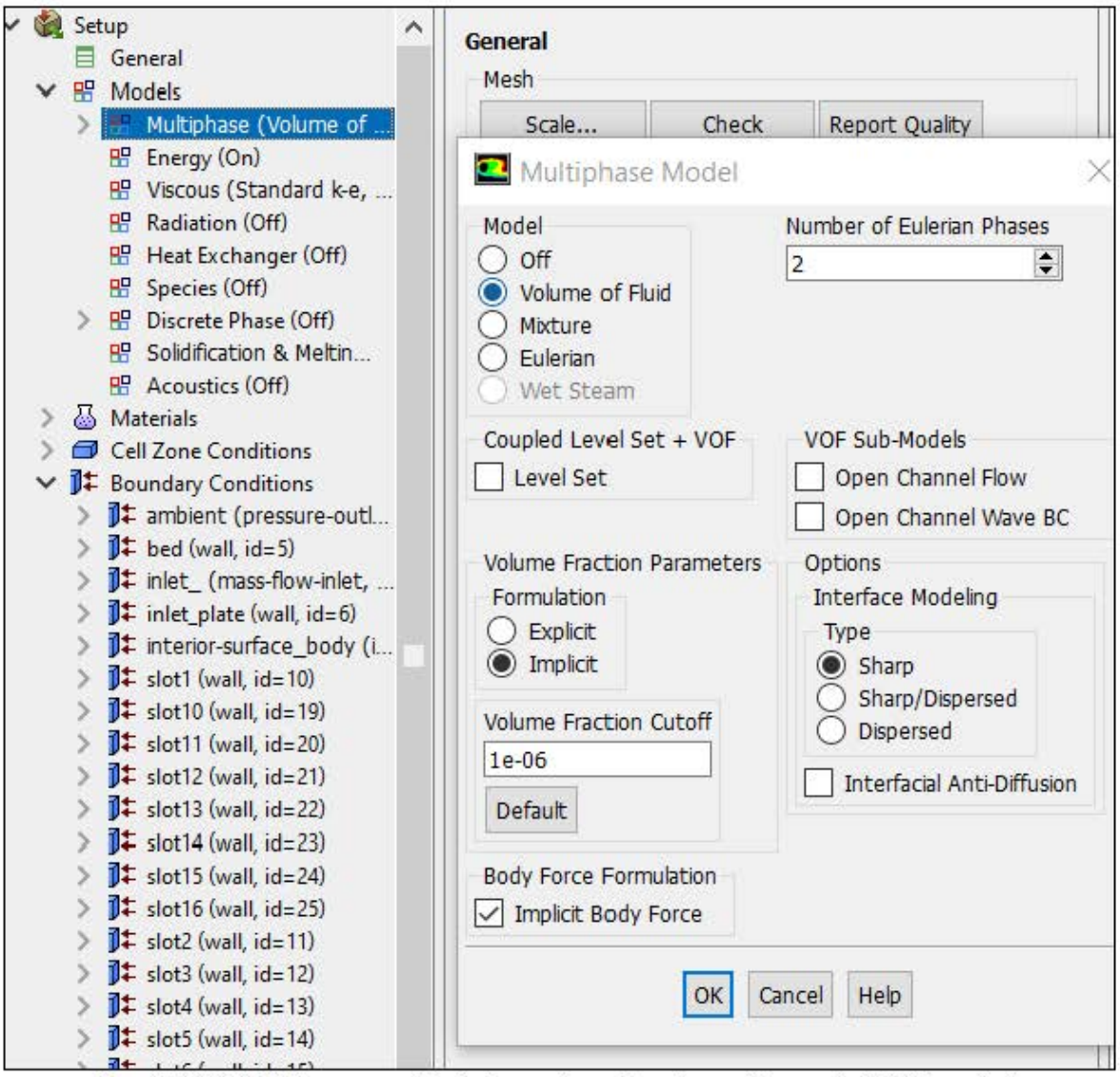

Fig. 4.10. Multiphase model dialogue box showing settings for VOF model.

d) Setting the Boundary conditions and Cell zone conditions

Ansys Fluent solver automatically lists all the boundaries that were named in the mesh module previously. These boundaries are now called zones. Also, the solver assigns default boundary conditions-e.g. materials, friction etc. and the initial conditions volume fraction of each phase, temperature, velocity etc. to each of these zones. Most of these default values had to be changed to their proper values for each zone in the following manner:

Setting up the Inlet Boundary

- For the "inlet" zone, corresponding to the mixture phase, the following edits were done:
- The boundary "type" was changed to "mass-flow inlet" from its default value of "wall".
- In the Momentum tab, the Reference frame was kept at its default value of "Absolute".
- The initial gauge pressure was set to zero.

- "Direction vector" was selected for the direction specification method for which the X-component of flow direction was assigned a value of 1 and the Y-component of flow direction was assigned a value of 0.
- For "Turbulence", default settings were kept for the specification method, intensity and viscosity and hence for the turbulent intensity and turbulent viscosity ratio.
- Under the "Thermal" tab, a total temperature of 40°C (313 Kelvin) was set. This temperature was the inlet water temperature i.e. 40°C and remained the same for all the simulations.
- For the same "inlet" zone, selecting the water phase enabled us to enter the "mass flow rate" of 106 kg/s. This value of mass flow rate was calculated based on the velocity, intended initial water depth of the super-critical flow, inlet opening dimension, density, and width of the channel (flume) as in experiments carried out by Mondal et al. (2020).
- For the air phase, the mass flow rate value was assigned a value of zero.

Setting up the "Bed" Boundary

- The boundary "type" is kept as "wall" which was the default "type" assigned by the solver.
- For the "phase" selected as "mixture", the following edits were done:
- In the "Momentum" tab, "Stationary Wall" was selected for "Wall motion".
- "Shear Condition" was set to "no-slip".
- "Standard" Roughness Model was selected for "Wall Roughness". Corresponding to this a "Roughness Height" of 4.5×10^{-5} m was assigned. This value of roughness height corresponds to a Perspex bed (Marriott and Jayaratne 2010). "Roughness constant" was left at its default value of 0.5.
- Under the "Thermal" tab, "Temperature" was selected for the "Thermal" Conditions. Since at initial conditions, the temperature of the bed was equal to the ambient temperature. So for every new simulation with a different ambient temperature, the "Temperature" value was changed. As, an example, if a simulation corresponds to an ambient temperature of 10°C, the value for the "Temperature" of the bed was 10°C (283.15 Kelvin). Obviously, this was the initial temperature of the "Wall" and changed as the calculations proceeded due to heat transfer from the water. Since there was no heat source associated with the bed, the "heat generation" value was left at zero.

Setting up the "inlet plate" Boundary

Since the inlet plate was a vertical wall, therefore the boundary "type" was left at its default selection of "wall". In the "Momentum" tab, "Stationary Wall" was selected for "Wall motion". "Shear Condition" was set to "no-slip", though it was of no significance in this case. "Standard" Roughness Model was selected for "Wall Roughness" and roughness height was assigned a value of zero. Under the "Temperature" tab, under the "Thermal" tab, "Temperature" was selected for the "Thermal" Conditions. As explained in the previous section, the value of temperature was that of the ambient temperature and the heat generation rate was zero.

Setting up the "tailgate" Boundary

The zone named "Tailgate" refers to the upper portion of the tailgate that was not further split into smaller sections. For this boundary "type" was selected as "wall". In the "Momentum" tab, "Stationary Wall" was selected for "Wall motion". "Shear Condition" was set to "no-slip", though it was of no significance in this case. "Standard" roughness model was selected for "Wall Roughness" and roughness height was assigned a value of zero. Under the "Temperature" tab, under the "Thermal" tab, "Temperature" was selected for the "Thermal" Conditions. As explained in the previous section, the value of temperature was that of the ambient temperature and the heat generation rate was zero.

Setting up the "tailgate slots" Boundary

The lower portion of the tailgate was split up into 16 parts (slots). All the slots were initially set as a "wall" type boundary as the tailgate was fully closed initially. As in any "wall" boundary, excluding the bed, "stationary wall", "no-slip condition" and zero "roughness height" were specified. "Temperature" was selected in the "thermal conditions" and its value was set equal to the ambient temperature. As the calculation proceeded, the slots were changed from a "wall" type boundary condition to an "outlet" type boundary condition.

Setting up the "ambient" Boundary

The upper horizontal edge of the rectangular flume geometry was named "ambient" since this zone was indicative of the ambient. This zone was set up as a "pressure outlet" type boundary. For the "phase" selected as "mixture", the temperature was assigned the value for the ambient temperature considered. Other settings were left unchanged at their default values.

e) Calculations

Once the selection of the desired models, materials and setting up of the boundary conditions were done, it was necessary to select the solution method, set the criteria for residuals, specify the calculation activities, the path for saving the calculation data, create the contours for water volume fractions, creates solution animations and specifying time step size, number iterations etc. as explained in the sections below:

Selecting the Solution methods

- On the "solution methods" task page, various methods and/or schemes for the calculations were selected.
- Firstly, the scheme for "pressure-velocity" coupling was selected as "SIMPLE". Besides being the default value for the pressure-based segregated solver, this scheme has the ability to converge fast.
- Under spatial discretisation, for the calculation of gradients of various quantities, the "Least-squares Cell-Based" method was used as it required lesser computational power but gave acceptable accuracy.

- For pressure interpolation "PRESTO!" scheme was selected as the simulation of an H-jump involves intense turbulence and high swirls.
- The "Second-Order Upwind" scheme was selected for spatial discretisation of the momentum equation for its improved accuracy.
- A "Compressive" scheme was selected for spatial discretisation of the volume fraction of phases.
- "First order upwind" scheme i.e. the default scheme for the pressure-based solver, was selected for spatially discretising the transport equations for k (turbulence kinetic energy) and ε (turbulence dissipation rate).
- For the discretisation of the energy conservation equation, a "Second-order upwind scheme was used".

Setting the Residual Monitor

The convergence criteria i.e. the acceptable residual limits were set by selecting "Residual" in the "Monitor" option under "Solution" in the tree (navigation pane). In the residual monitor section, the "absolute criteria" for the scaled residuals related to continuity, x-velocity, y-velocity, k, ε, and VOF equations, were all set to 0.0001 but for the residual related to energy equation was kept at its default value of 10^{-6}. All the other parameters were kept unchanged at their default values.

Initializing the solution

The initialization of the solution was done by opening the "initialization" from the navigation pane. "Standard Initialization" was selected for the initialization method. All the variables were computed from the "Inlet" zone. Values for all the variables such as x-velocity, y-velocity, temperature, turbulence kinetic energy, turbulence dissipation rate and water volume fraction are computed at time $t = 0$ automatically. However, the water volume fraction was computed as 1 which had to be changed to 0 manually. Also, any non-zero value for the y-component of the velocity has to be changed to zero. Finally, the solution was initialized by clicking "initialize".

Calculation activities and path for saving the case and data files

The solution data and the setup data were exported from the solver to specific files for the convenience of using them during post-processing in CFD post.

The calculation activities task page was opened and the "automatic export" window was opened by "creating" solution data export. The file type was selected as "CFD-Post Compatible". This was done in order to export the case files and data files together in .cdat format that was readable by CFD post (Fluent post-processing software). "write case file every time" was ticked though this was completely optional.

- The frequency time step was set to 10 so as to save the data and case files at an interval of 10 time steps. "Time-step" was selected to append with the file name.
- In the "cell zones" panel, "surface_body" was pre-selected as there is only one cell zone. The surfaces were also pre-selected by default.

- In the "Quantities" panel the following quantities like temperature, entropy, enthalpy, and static pressure that were of importance for post-processing were selected.
- The data files were also exported in .dat.gz format to the same location because these data files were only readable by the Fluent solver (stand-alone application) and not the data files in .cdat format. To save the data file in this format, the autosave dialogue box was opened by clicking "autosave (Every Time Steps)" in the calculation activities. Since the data files occupy a huge memory in the disc, "Retain only most recent files".

Creating Contours of water volume fraction

As the solution proceeded, information regarding the iterations was displayed on the console but at a very fast rate. Also, transient graphs for the scaled residuals were plotted but apart from this information, it is always advisable to graphically visualize the flow development. So the contours of the volume fraction of phases were generated that would graphically give us the idea of the amount of water that has entered the channel in the course of the calculation. Contours of "phases" was selected and "Water" was selected as the phase. All the surfaces were selected. If all the previous setup and initialisation are done correctly, the minimum and the maximum values for the volume fraction of water would be automatically computed as 0 and 1 respectively. Figure 4.11 shows the contours of the water volume fraction for a flow time of t = 0 s and Fig. 4.12 shows the contours of the water volume fraction for a flow time of t = 4.56 s.

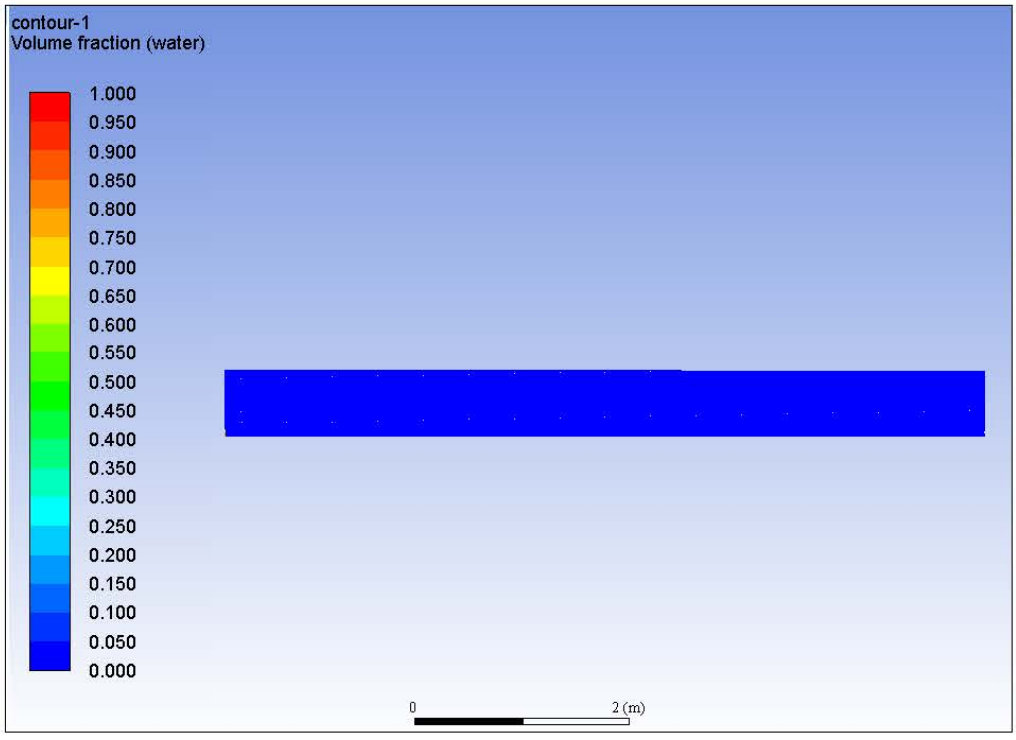

Fig. 4.11. Contours of water volume fraction at flow time t = 0.0 s.

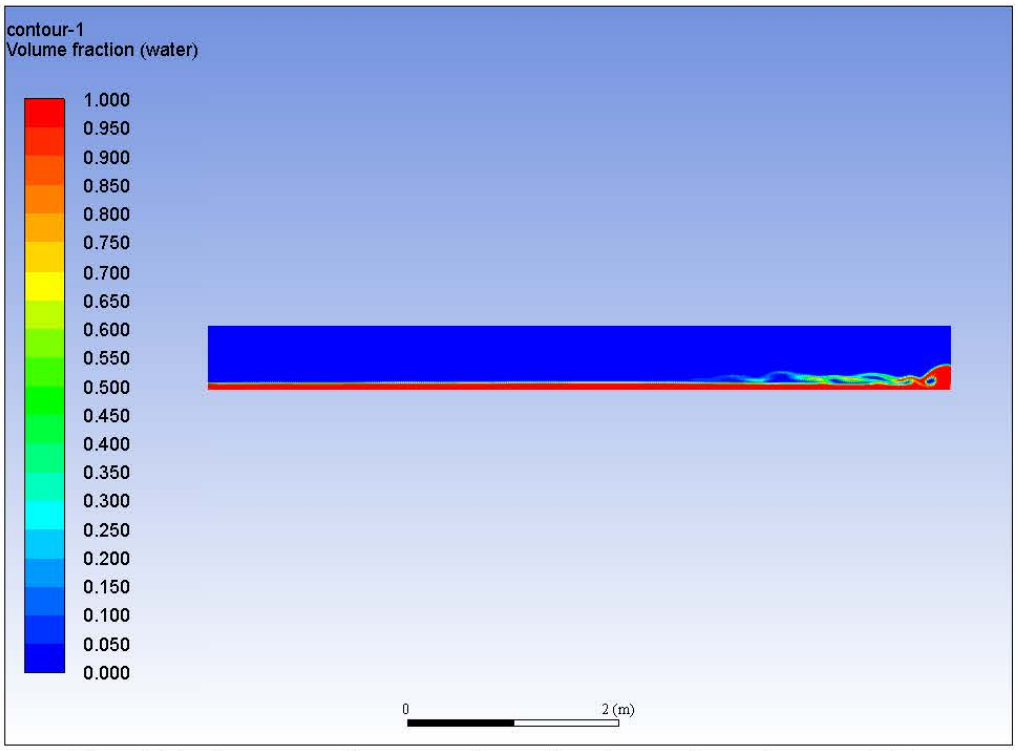

Fig. 4.12. Contours of water volume fraction at flow time t = 4.56 s.

Specifying the Time-Step size and Number of time steps

To specify the time step size, the number of time steps and the maximum number of iterations, the "Run Calculations" task page was opened. Even though for many of the quantities such as volume fraction, an "implicit" scheme for the solution is adopted and from literature, implicit schemes are stable even for large time steps, still the time step considered in this simulation is small enough so as to remain close to the Courant number=1.

Considering a time step of 0.01 seconds, assuming an average grid size of 0.01 m and inlet velocity of 1.89 m/s, the Courant number was found to be 1.89.

Initially, the calculations were carried out for 500 to 600 time steps i.e. a flow time of 5 seconds to 6 seconds till the water reaches the tailgate and gets obstructed.

A maximum of 300 iterations per time step were considered but it is found that the solutions converged much earlier. So after a few time steps, 200 number of iterations were considered. Reporting intervals and profile update intervals were both kept at 20.

f) Post Processing

Post-processing of the results of the calculations was done using the "CFD-Post" application of Ansys Fluent. For the flows involving a H-jump, two sections were considered one section just downstream of the inlet of the flume and one section downstream of the H-jump. Averaged quantities-temperature, specific enthalpy, and specific entropy were measured in a tabulated form. Froude numbers in these two sections were also measured. These are achieved in the following manner:

Creating contours of water volume fraction

Figure 4.13a and Fig. 4.13b show the contour of water volume fraction with and without H-jump respectively, corresponding to a flow time of 12.10 seconds and ambient temperature of 35°C, generated with the above settings respectively.

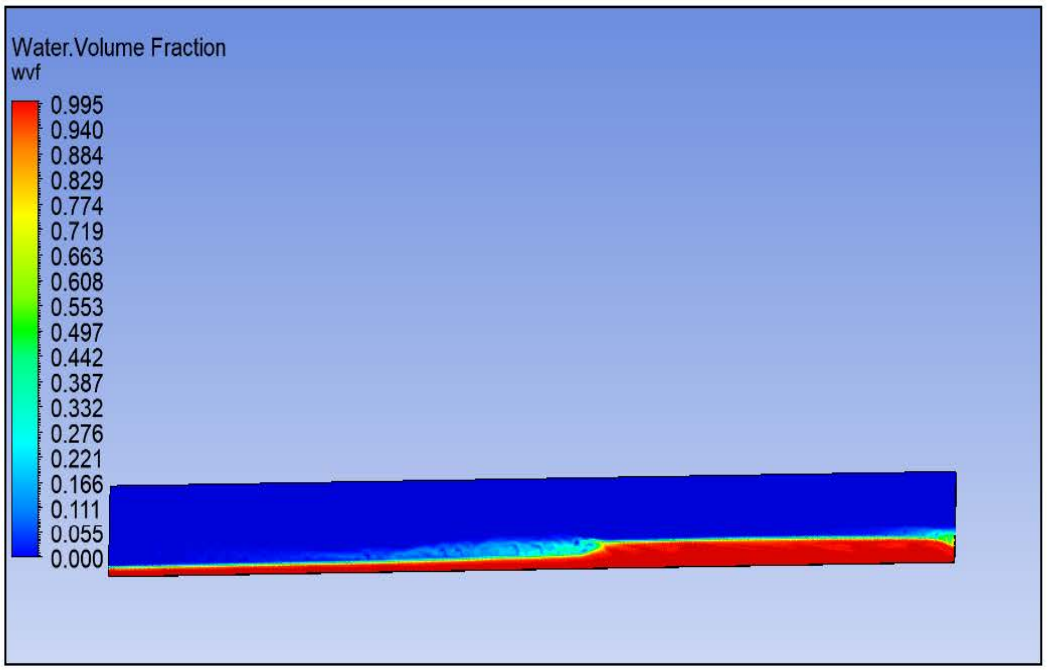

Fig. 4.13a. Contours of water volume fraction with a H-jump for flow-time=2.10 s and ambient temperature=35°C.

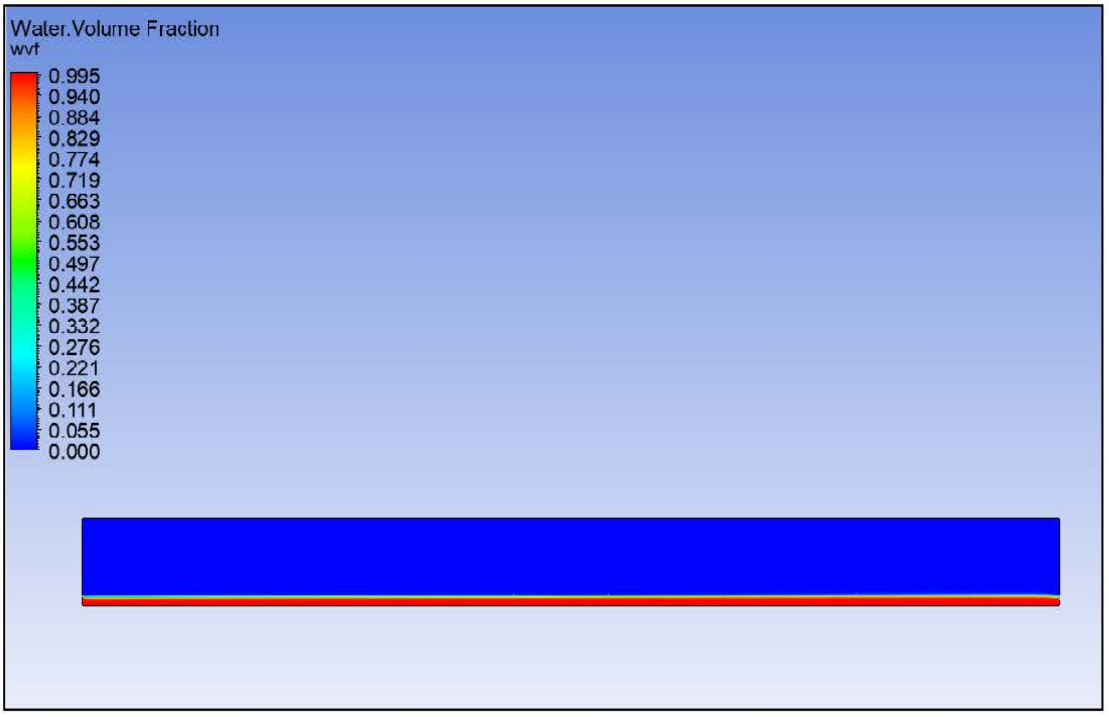

Fig. 4.13b. Contours of water volume fraction without H-jump for flow-time=2.10 s and ambient temperature=35°C.

Creating the sections

In order to create the two sections, we needed to determine the coordinates of the endpoints of each of the sections. After determining the coordinates of the endpoints of a section, a line was created between these two points to create the section. To determine the coordinates of the upper-end point, the "probe" tool was used. The upper-end point is chosen to be somewhere within the air-water interface as shown in Fig 4.14a and 4.14b.

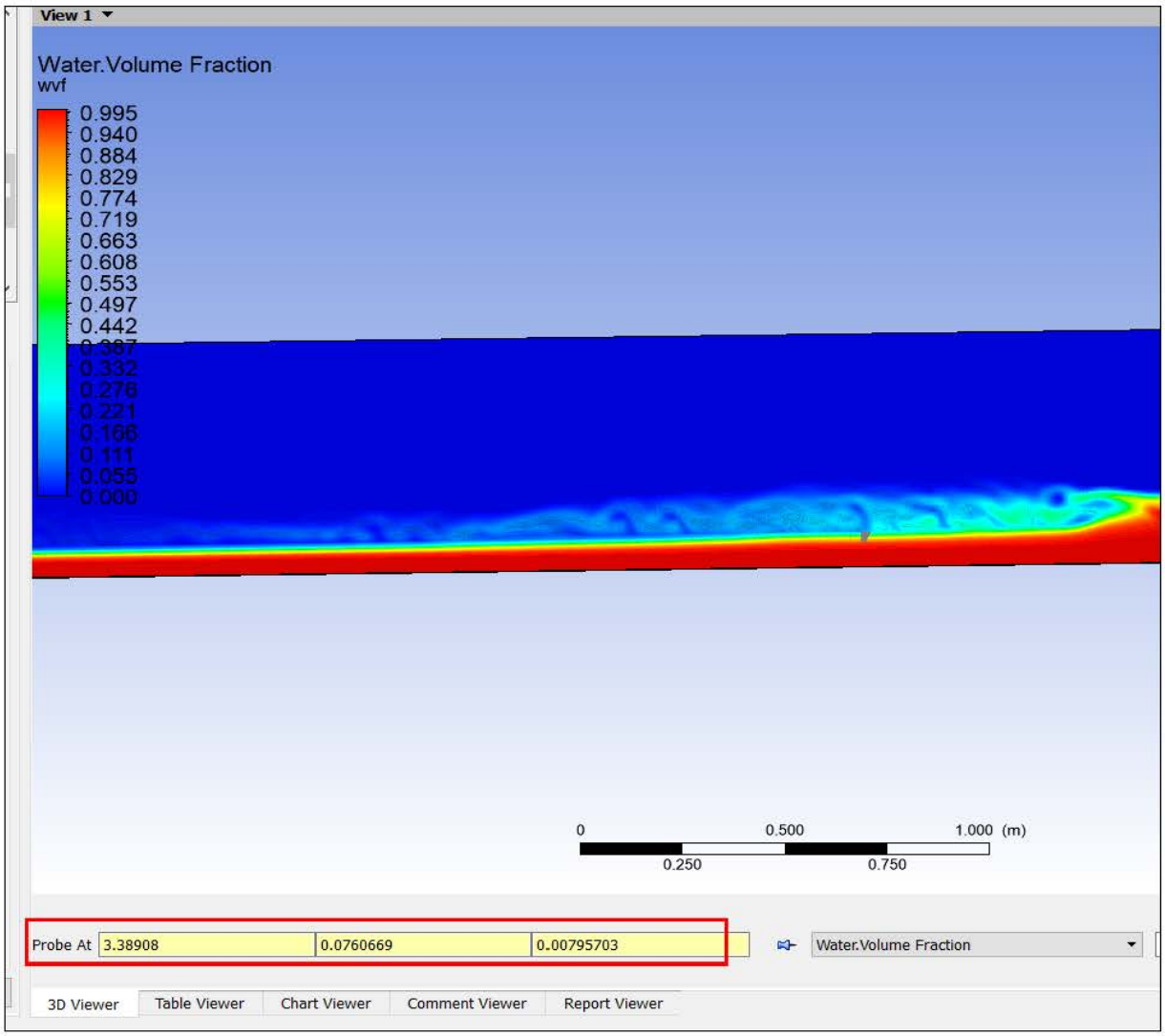

Fig. 4.14a. The point "probed" at the toe of the jump for contours of water volume fraction for flow-time=2.10 s and ambient temperature=35°C. Coordinates of the point shown within the red box.

Generating the table for thermal quantities averaged across the sections

A table is created using the "table" tool. Rows and columns are named appropriately. For obtaining the average temperature across section 1 (pre-jump section), and similar for section 2 (post-jump section).

- Clicking on the appropriate cell, the "CFD-post" "function" is selected from the "insert" ribbon. From the CFD-post selection toolbox, "lenghAve" is selected.

- From “Variable”, “Temperature” is selected.
- From “Location”, “inlet section” is selected.
- Alternatively, the following command is typed in the command/formula box of the table, to get the average temperature in section 1: =lengthAve(Temperature)@inlet section.

The values of average temperature, specific enthalpy, and specific entropy are the same in section 1 for all the simulations. So these values are evaluated only for one simulation.

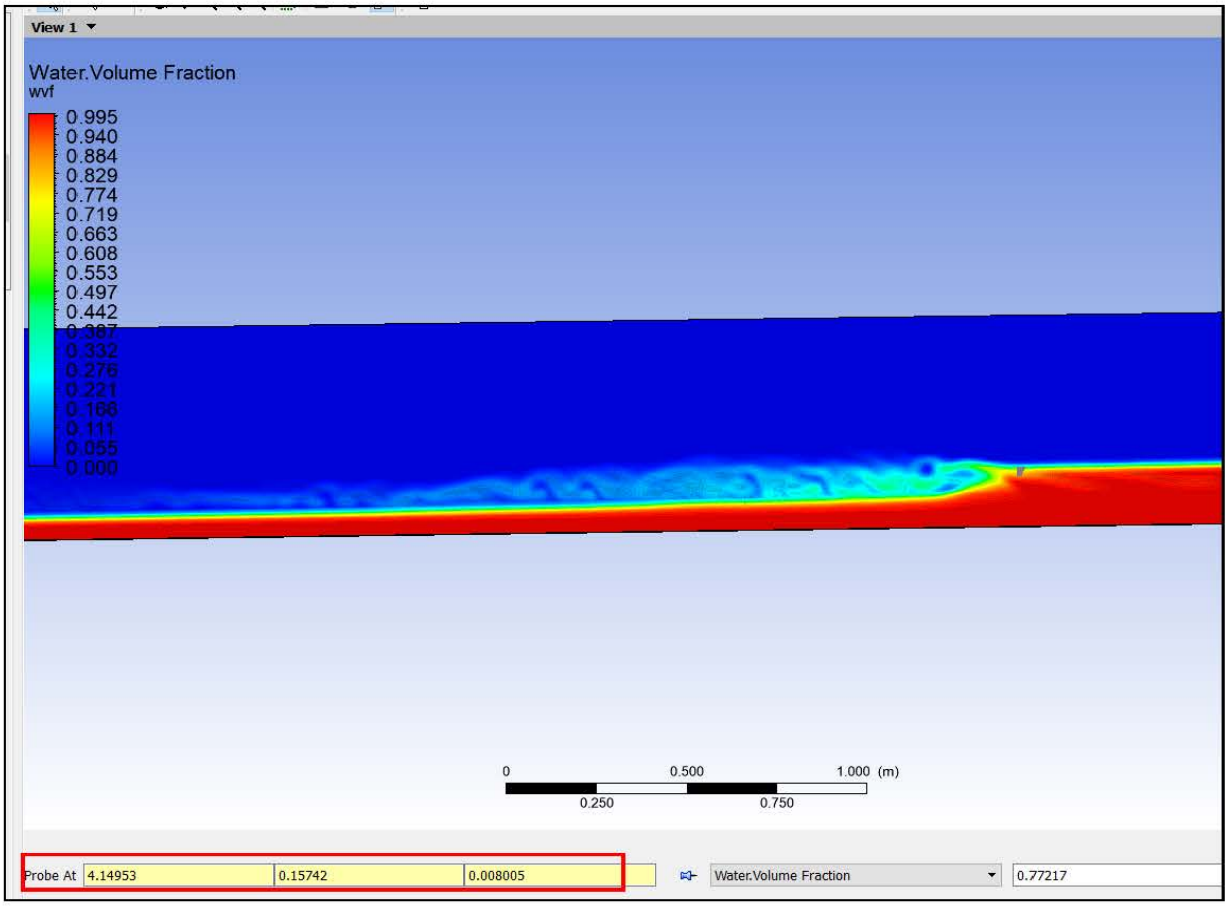

Fig. 4.14b. The point “probed” downstream the jump for contours of water volume fraction for flow-time=2.10 s and ambient temperature = 35℃. Coordinates of the point shown within the red box.

4.6. Results and Discussion

All the simulations are carried out considering the inlet water temperature to be fixed at 40℃. Six different ambient temperatures from 10℃ to 35℃ with an equal interval of 5℃ are considered for the six simulations. The mass flow rate for all six simulations is kept constant at 106 kg/s resulting in a constant inlet velocity(V_1) of 1.893 m/s. A stable H-jump is obtained for a tailgate opening of either 0.062 m (i.e. for all 10 slots open) or 0.068 m (i.e. for all 11 slots open). The depth of the super-critical flow is 0.056 m for all cases and the sub-critical flow depth is found to be within the range of 0.16 to 0.15 m. Inlet Froude number for all the simulations is 2.55. For all the simulations, ΔT_{jk} denotes, the temperature

drop occurring with the H-jump in the k^{th} simulation while ΔT_k is the corresponding temperature drop occurring without the H-jump in the k^{th} simulation. The change in temperature, specific enthalpy and specific entropy are observed as discussed in the following sections.

a) Simulation 1

The ambient temperature is set to 10°C. The Froude number corresponding to the sequent depth is found to be 0.565. The data for the simulation with a H-jump is presented in Table 4.1 and the data for the simulation without the formation of a H-jump is presented in Table 4.2. Section 2 (section downstream of the H-jump) is named as the post-jump section and is taken at the same for both simulations.

The following Tables 4.1 and 4.2 show the average temperature, specific enthalpy, and specific entropy at the section downstream of the H-jump (post-jump section) and at the same location, for the flow without the H-jump.

Table 4.1. Average temperature, specific enthalpy, specific entropy at inlet section and Section 2 for the flow with an H-jump for 10°C ambient temperature.

Sl. no.	Flow Property	Section 1 (Inlet Jump Section)	Section 2 (Post Jump Section)	Difference $\Delta T_{j1} = T_0 - T_{j1}$ $\Delta h_{j1} = h_0 - h_{j1}$ $\Delta s_{j1} = s_0 - s_{j1}$
1	Temperature (°C)	$T_0 = 40$	$T_{j1} = 38.278$	$\Delta T_{j1} = 1.722$
2	Specific enthalpy (J/kg)	$h_0 = 62093.330$	$h_{j1} = 55526.900$	$\Delta h_{j1} = 6566.4$
3	Specific entropy (J/kg-K)	$s_0 = 345.767$	$s_{j1} = 324.730$	$\Delta s_{j1} = 21.037$

Table 4.2. Average temperature, specific enthalpy, specific entropy at inlet section and Section 2 for the flow without H-jump for 10°C ambient temperature.

Sl. no.	Flow Property	Section 1 (Inlet Jump Section)	Section 2 (Post Jump Section)	Difference $\Delta T_1 = T_0 - T_1$ $\Delta h_1 = h_0 - h_1$ $\Delta s_1 = s_0 - s_1$
1	Temperature (°C)	$T_0 = 40$	$T_1 = 38.409$	$\Delta T_1 = 1.591$
2	Specific enthalpy (J/kg)	$h_0 = 62093.330$	$h_1 = 56076.5$	$\Delta h_1 = 6016.83$
3	Specific entropy (J/kg-K)	$s_0 = 345.767$	$s_1 = 326.497$	$\Delta s_1 = 19.27$

It can be observed that the drop in temperature from the inlet section to Section 2, with the H-jump is, $\Delta T_{j1} = 1.722$°C and the temperature drop due to only convective, other modes of heat loss from water and without H-jump effects is, $\Delta T_1 = 1.591$°C. So there is an increase of 8.2% in temperature drop in water due to the H-jump.

Specific enthalpy drop, Δh_{j1} = 6566.4 J/kg is observed with the H-jump. Specific enthalpy drop without H-jump is found to be Δh_1 = 6016.83 J/kg. So there is an enhancement of drop-in specific enthalpy with an H-jump by 9.1%.

Drop-in specific entropy with the H-jump is Δs_{j1} = 21.037 J/kg-K and without a H-jump, the specific entropy is Δs_1 = 19.27 J/kg-K. Thus the H-jump resulted in an increase in the drop of specific entropy by 9.2%.

b) Simulation 2

The ambient temperature is set to 15°C. The Froude number corresponding to the sequent depth is found to be 0.585. The data for the simulation with a H-jump are shown in Table 4.3 and the data for the simulation without forming the H-jump are shown in Table 4.4. Section 2 (section downstream of the H-jump) is named as the post H-jump section and is treated the same for both simulations.

The following tables (Tables 4.3 and 4.4) show the average temperature, specific enthalpy, and specific entropy at the section downstream of the H-jump (post H-jump section) and at the same location for the flow without the H-jump.

Table 4.3. Average temperature, specific enthalpy, specific entropy at inlet section and Section 2 for H-jump flow for ambient temperature of 15°C.

Sl. no.	Flow Property	Section 1 (Inlet Jump Section)	Section 2 (Post Jump Section)	Difference $\Delta T_{j2} = T_0 - T_{j2}$ $\Delta h_{j2} = h_0 - h_{j2}$ $\Delta s_{j2} = s_0 - s_{j2}$
1	Temperature (°C)	T_0 = 40	T_{j2} = 38.51	ΔT_{j2} = 1.49
2	Specific enthalpy (J/kg)	h_0 = 62093.330	h_{j2} = 56527.3	Δh_{j2} = 5566.03
3	Specific entropy (J/kg-K)	s_0 = 345.767	s_{j2} = 327.943	Δs_{j2} = 17.824

Table 4.4. Average temperature, specific enthalpy, specific entropy at inlet section and Section 2 for the flow without H-jump for 15°C ambient temperature.

Sl. no.	Flow Property	Section 1 (Inlet Jump Section)	Section 2 (Post Jump Section)	Difference $\Delta T_2 = T_0 - T_2$ $\Delta h_2 = h_0 - h_2$ $\Delta s_2 = s_0 - s_2$
1	Temperature (°C)	T_0 = 40	T_2 = 38.636	ΔT_2 = 1.364
2	Specific enthalpy (J/kg)	h_0 = 62093.330	h_2 = 57025.1	Δh_2 = 5068.23
3	Specific entropy (J/kg-K)	s_0 = 345.767	s_2 = 329.542	Δs_2 = 16.225

It is observed that the drop in temperature with the H-jump is ΔT_{j2} = 1.49°C while the drop in temperature with only heat loss due to conduction and convection without considering the H-jump is ΔT_2 = 1.364°C. Thus the H-jump enhanced the temperature drop by 9.2%.

A decrease in specific enthalpy with the H-jump is found to be Δh_{j2} = 5566.03 J/kg whereas the decrease in specific enthalpy without the H-jump is Δh_2 = 5068.23 J/kg. An increase of 9.8% in specific enthalpy drop due to the H-jump is observed.

The drop in specific entropy with the H-jump is Δs_{j2} = 17.824 J/kg-K and the drop in specific entropy without considering the H-jump is Δs_2 = 16.225 J/kg-K. Thus the H-jump enhanced the drop in specific entropy by 9.9%.

c) Simulation 3

The ambient temperature is set to 20°C. The Froude number corresponding to the sequent depth is found to be 0.543. The data for the simulation with a H-jump is presented in Table 4.5 and the data for the simulation without the formation of a H-jump is presented in Table 4.6. Section 2 (section downstream of the H-jump) is named as the post H-jump section and is taken at the same for both simulations.

The following tables (Table 4.5 and 4.6) show the average temperature, specific enthalpy, and specific entropy at the section downstream of the H-jump (post-jump section) and at the same location, for the flow without the H-jump respectively.

Table 4.5. Average temperature, specific enthalpy, specific entropy at inlet section and Section 2 for the flow with an H-jump for 20°C ambient temperature.

Sl no.	Flow Property	Section 1 (Inlet Jump Section)	Section 2 (Post Jump Section)	Difference $\Delta T_{j3} = T_0 - T_{j3}$ $\Delta h_{j3} = h_0 - h_{j3}$ $\Delta s_{j3} = s_0 - s_{j3}$
1	Temperature (°C)	T_0 = 40	T_{j3} = 38.721	ΔT_{j3} = 1.279
2	Specific enthalpy (J/kg)	h_0 = 62093.330	h_{j3} = 57385.9	Δh_{j3} = 4707.43
3	Specific entropy (J/kg-K)	s_0 = 345.767	s_{j3} = 330.699	Δs_{j3} = 15.068

Table 4.6. Average temperature, specific enthalpy, specific entropy at inlet section and Section 2 for the flow without H-jump for 20°C ambient temperature.

Sl no.	Flow Property	Section 1 (Inlet Jump Section)	Section 2 (Post Jump Section)	Difference $\Delta T_3 = T_0 - T_3$ $\Delta h_3 = h_0 - h_3$ $\Delta s_3 = s_0 - s_3$
1	Temperature (°C)	T_0 = 40	T_3 = 38.812	ΔT_3 = 1.188
2	Specific enthalpy (J/kg)	h_0 = 62093.330	h_3 = 57721.53	Δh_3 = 4371.8
3	Specific entropy (J/kg-K)	s_0 = 345.767	s_3 = 331.932	Δs_3 = 13.835

In this simulation, the observed temperature drop with an H- jump is ΔT_{j3} = 1.279°C and without the H-jump is ΔT_3= 1.188°C. The H-jump resulted in a 7.7% increase in temperature drop.

A decrease in specific enthalpy with the H-jump is found to be Δh_{j3} = 4707.43 J/kg and without the H-jump, the enthalpy decrease is Δh_3 = 4371.8 J/kg. The increase in specific enthalpy drop due to H-jump is 7.7%.

A decrease in specific entropy with the H-jump is found to be Δs_{j3} = 15.068 J/kg-K and without the H-jump, the entropy decrease is Δs_3 = 13.835 J/kg-K. The increase in specific entropy drop due to H-jump is 8.9%.

d) Simulation 4

The ambient temperature was set to 25°C. The Froude number corresponding to the sequent depth was found to be 0.551. The data for the simulation with the H-jump is presented in Table 4.7 and the data for the simulation without the formation of the H-jump is presented in Table 4.8. Section 2 (section downstream of the H-jump) was named as the post-jump section and was taken at the same for both simulations.

The following tables (Table 4.7 and 4.8) show the average temperature, specific enthalpy, and specific entropy at the section downstream of the H-jump (post-jump section) and at the same location, for the flow without the H-jump respectively.

Table 4.7. Average temperature, specific enthalpy, specific entropy at inlet section and Section 2 for the flow with the H-jump for 25°C ambient temperature.

Sl no.	Flow Property	Section 1 (Inlet Jump Section)	Section 2 (Post Jump Section)	Difference $\Delta T_{j4} = T_0 - T_{j4}$ $\Delta h_{j4} = h_0 - h_{j4}$ $\Delta s_{j4} = s_0 - s_{j4}$
1	Temperature (°C)	T_0 = 40	T_{j4} = 39.096	ΔT_{j4} = 0.904
2	Specific enthalpy (J/kg)	h_0 = 62093.330	h_{j4} = 58862.8	Δh_{j4} = 3230.53
3	Specific entropy (J/kg-K)	s_0 = 345.767	s_{j4} = 335.432	Δs_{j4} = 10.335

Table 4.8. Average temperature, specific enthalpy, specific entropy at inlet section and Section 2 for the flow without H-jump for 25°C ambient temperature.

Sl no.	Flow Property	Section 1 (Inlet Jump Section)	Section 2 (Post Jump Section)	Difference $\Delta T_4 = T_0 - T_4$ $\Delta h_4 = h_0 - h_4$ $\Delta s_4 = s_0 - s_4$
1	Temperature (°C)	T_0 = 40	T_4 = 39.129	ΔT_4 = 0.871
2	Specific enthalpy (J/kg)	h_0 = 62093.330	h_4 = 59085.9	Δh_4 = 3007.43
3	Specific entropy (J/kg-K)	s_0 = 345.767	s_4 = 336.149	Δs_4 = 9.618

The observed temperature drop with the H-jump is ΔT_{j4} = 0.904°C and without the H-jump is ΔT_4 = 0.871°C. The H-jump resulted in a 3.8% increase in temperature drop.

A decrease in specific enthalpy with the H-jump is found to be Δh_{j4} = 3230.53 J/kg and without the H-jump, the enthalpy decrease is Δh_4 = 3007.43 J/kg. The increase in specific enthalpy drop due to H-jump is 7.4%.

A decrease in specific entropy with the H-jump is found to be Δs_{j4} = 10.335 J/kg-K and without the H-jump, the entropy decrease is Δs_4 = 9.618 J/kg-K. The increase in specific entropy drop due to H-jump is 7.5%.

e) Simulation 5

The ambient temperature is set to 30°C. The Froude number corresponding to the sequent depth is found to be 0.519. The data for the simulation with a H-jump is presented in Table 4.9 and the data for the simulation without the formation of the H-jump is presented in Table 4.10. Section 2 (section downstream of the H-jump) is named as the post-jump section and is taken at the same for both simulations.

The following tables (Tables 4.9 and 4.10) show the average temperature, specific enthalpy, and specific entropy at the section downstream of the H-jump (post-jump section) and at the same location, for the flow without the H-jump respectively.

Table 4.9. Average temperature, specific enthalpy, specific entropy at inlet section and Section 2 for the flow with the H-jump for 30°C ambient temperature.

Sl. no.	Flow Property	Section 1 (Inlet Jump Section)	Section 2 (Post Jump Section)	Difference $\Delta T_{j5} = T_0 - T_{j5}$ $\Delta h_{j5} = h_0 - h_{j5}$ $\Delta s_{j5} = s_0 - s_{j5}$
1	Temperature (°C)	T_0 = 40	T_{j5} = 39.318	ΔT_{j5} = 0.682
2	Specific enthalpy (J/kg)	h_0 = 62093.330	h_{j5} = 59880.0	Δh_{j5} = 2213.33
3	Specific entropy (J/kg-K)	s_0 = 345.767	s_{j5} = 338.689	Δs_{j5} = 7.078

Table 4.10. Average temperature, specific enthalpy, specific entropy at inlet section and Section 2 for the flow with the H-jump for 30°C ambient temperature.

Sl no.	Flow Property	Section 1 (Inlet Jump Section)	Section 2 (Post Jump Section)	Difference $\Delta T_5 = T_0 - T_5$ $\Delta h_5 = h_0 - h_5$ $\Delta s_5 = s_0 - s_5$
1	Temperature (°C)	T_0 = 40	T_5 = 39.34	ΔT_5 = 0.659
2	Specific enthalpy (J/kg)	h_0 = 62093.330	h_5 = 60091.9	Δh_5 = 2001.43
3	Specific entropy (J/kg-K)	s_0 = 345.767	s_5 = 339.370	Δs_5 = 6.397

The observed temperature drop with the H-jump is ΔT_{j5} = 0.682°C and without the H-jump is ΔT_5 = 0.659°C. The H-jump resulted in a 3.5% increase in temperature drop.

A decrease in specific enthalpy with a H-jump is found to be Δh_{j5} = 2213.33 J/kg and without the H-jump, the enthalpy decrease is Δh_5 = 2001.43 J/kg. The increase in specific enthalpy drop due to H-jump is 10.6%.

A decrease in specific entropy with a H-jump is found to be Δs_{j5} = 7.078 J/kg-K and without the H-jump, the entropy decrease is Δs_5 = 6.397 J/kg-K. The increase in specific entropy drop due to H-jump is 10.6%.

f) Simulation 6

The ambient temperature was set to 35°C. The Froude number corresponding to the sequent depth was found to be 0.447. The data for the simulation with the H-jump is presented in Table 4.11 and the data for the simulation without the formation of the H-jump is presented in Table 4.12. Section 2 (section downstream of the H-jump) was named as the post-jump section and was taken at the same for both simulations.

The following tables (Table 4.11 and 4.12) show the average temperature, specific enthalpy, and specific entropy at the section downstream of the H-jump (post-jump section) and at the same location, for the flow without the H-jump respectively.

Table 4.11. Average temperature, specific enthalpy, specific entropy at inlet section and Section 2 for the flow with H-jump for 35°C ambient temperature.

Sl no.	Flow Property	Section 1 (Inlet Jump Section)	Section 2 (Post Jump Section)	Difference $\Delta T_{j6} = T_0 - T_{j6}$ $\Delta h_{j6} = h_0 - h_{j6}$ $\Delta s_{j6} = s_0 - s_{j6}$
1	Temperature (°C)	T_0 = 40	T_{j6} = 39.587	ΔT_{j6} = 0.413
2	Specific enthalpy (J/kg)	h_0 = 62093.330	h_{j6} = 61003.9	Δh_{j6} = 1089.43
3	Specific entropy (J/kg-K)	s_0 = 345.767	s_{j6} = 342.286	Δs_{j6} = 3.481

Table 4.12. Average temperature, specific enthalpy, specific entropy at inlet section and Section 2 for the flow without H-jump for 35°C ambient temperature.

Sl no.	Flow Property	Section 1 (Inlet Jump Section)	Section 2 (Post Jump Section)	Difference $\Delta T_6 = T_0 - T_6$ $\Delta h_6 = h_0 - h_6$ $\Delta s_6 = s_0 - s_6$
1	Temperature (°C)	T_0 = 40	T_6 = 39.608	ΔT_6 = 0.392
2	Specific enthalpy (J/kg)	h_0 = 62093.330	h_6 = 61090.9	Δh_6 = 1002.43
3	Specific entropy (J/kg-K)	s_0 = 345.767	s_6 = 342.566	Δs_6 = 3.201

The observed temperature drop with the H-jump is ΔT_{j6} = 0.413°C and without the H-jump is ΔT_6 = 0.392°C. The H-jump resulted in a 5.4% increase in temperature drop.

A decrease in specific enthalpy with the H-jump is found to be Δh_{j6} = 1089.43 J/kg and without the H-jump, the enthalpy decrease is Δh_6 = 1002.43 J/kg. The increase in specific enthalpy drop due to H-jump is 8.7%.

A decrease in specific entropy with the H-jump is found to be Δs_{j6} = 3.481 J/kg-K and without the H-jump, the entropy decrease is Δs_6 = 3.201 J/kg-K. The increase in specific entropy drop due to H-jump is 8.7%.

For simulation 1 with an ambient temperature of 10°C, ΔT_{j1} = 1.722°C and ΔT_1 =1.591°C. So, an increase of 0.131°C in temperature drop due to H-jump is observed. Similarly, for simulation 2 (S-2), simulation 3 (S-3), simulation 4 (S-4), simulation 5 (S-5), and simulation 6 (S-6) the observed temperature drop due to H-jump is 0.126°C, 0.091°C, 0.033°C, 0.023°C, and 0.021°C respectively.

Considering only the average temperature of flow across section 2, it is observed that this temperature increased with an increase in ambient temperature (Fig. 4.15). Without any H-jump, this temperature also increases with the ambient temperature simply because of the reduced heat transfer rate owing to the decreasing temperature difference between the water and the ambient (Fig. 4.15). The variation of ΔT_{jk} and ΔT_k with ambient temperature is plotted in Figs. 4.16-4.17 shows the variation of the increase in temperature drops with the ambient temperature. It is witnessed that the increase in temperature drop, occurring due to the effect of H-jump decreased with the increase in ambient temperature or with the decrease in temperature gap between water and the ambient. The temperature drop for 10°C ambient temperature is slightly greater than the drop in temperature for 15°C ambient. There is a sharp decrease in the improvement of temperature drop due to H-jump after 15°C ambient temperature and the rate of decrease in the improvement of temperature drop became lesser at 25°C and still lesser at 30°C and 35°C.

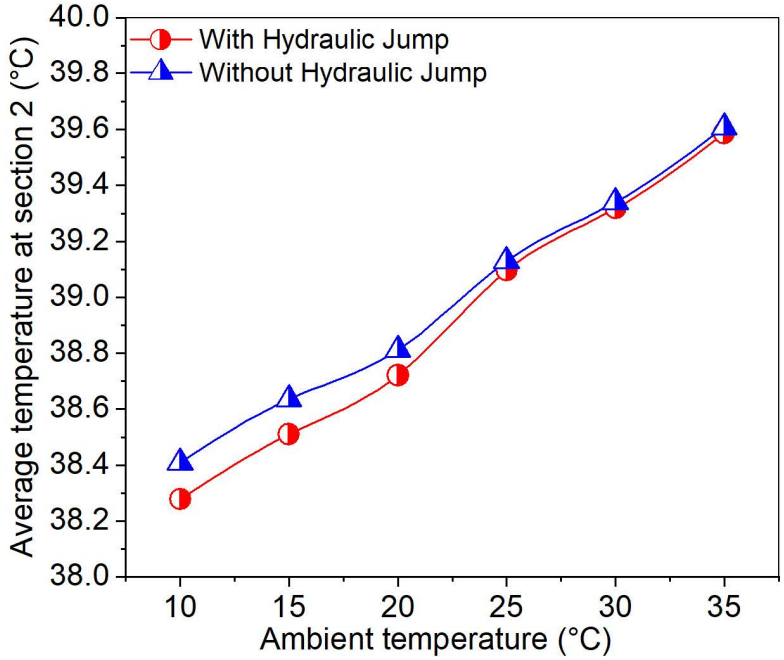

Fig. 4.15. Variation of average temperature at section 2 for the flows with and without H-jump.

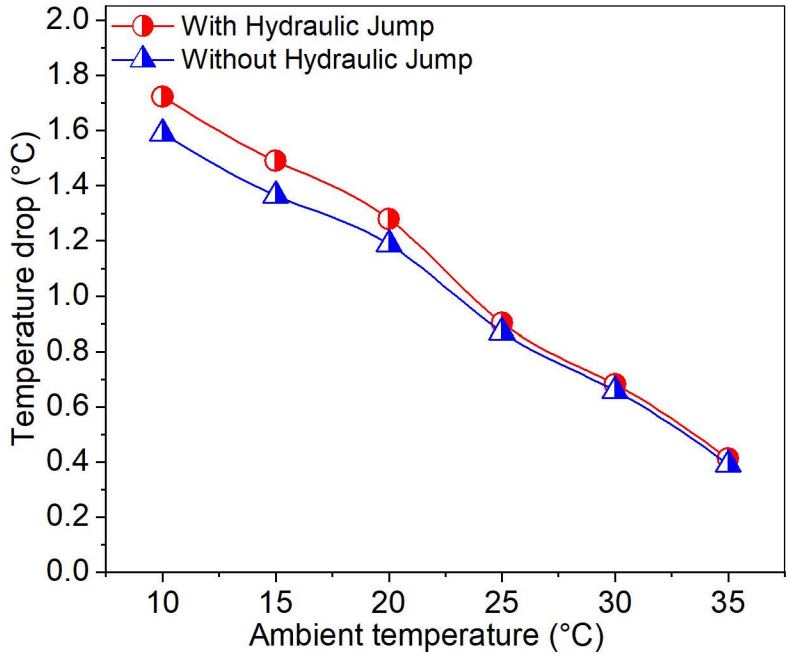

Fig. 4.16. Variation of temperature drop due to H-jump (ΔT_{jk}) and without H-jump (ΔT_k).

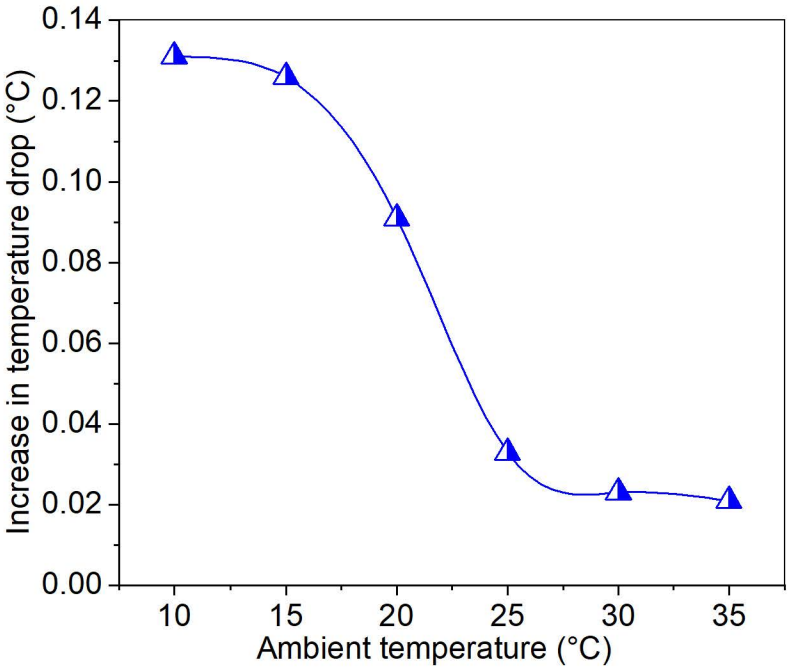

Fig. 4.17. Variation of increase in temperature drop (ΔT_{jk} - ΔT_k) due to H-jump.

For all the simulations, Δh_{jk} denotes, the specific enthalpy drop occurring with the H-jump in the k^{th} simulation while Δh_k is the corresponding specific enthalpy drop occurring without the H-jump in the k^{th} simulation.

For simulation 1 with an ambient temperature of 10 °C, Δh_{j1}= 6566.4 J/kg and Δh_1= 6016.83 J/kg. So, an increase of 549.6 J/kg in specific enthalpy drop due to H-jump is observed. Similarly, for S-2, S-3, S-4, S-5, and S-6 the observed specific enthalpy drop is 497.8 J/kg, 335.6 J/kg, 223.1 J/kg, 211.9 J/kg, and 87.0 J/kg respectively.

Figure 4.18 illustrates the average enthalpy in section 2 for flow with the H-jump and without the H-jump. Figure 4.19 illustrates the specific enthalpy drops for the simulation with the H-jump (Δh_{jk}) and without the H-jump (Δh_k) for all six ambient temperatures.

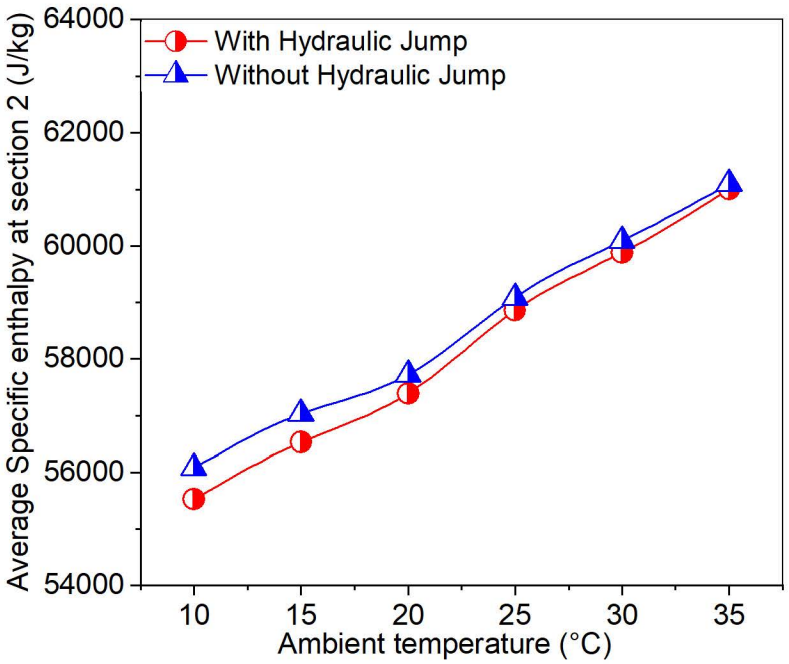

Fig. 4.18. Variation of average specific enthalpy at section 2 for the flows with and without H-jump.

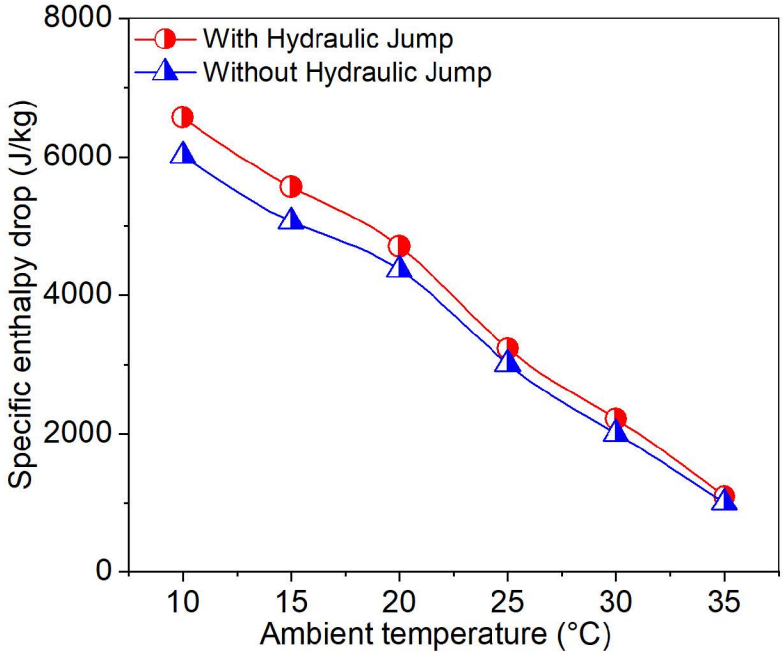

Fig. 4.19. Variation of specific enthalpy drop due to H-jump (Δh_{jk}) and without H-jump (Δh_k).

Figure 4.20 shows the variation of increase in specific enthalpy drop due to the H-jump as compared to the specific enthalpy drop without the H-jump. It is observed that the

specific enthalpy drop is enhanced due to the H-jump effect but this enhancement in enthalpy drop decreased with the increase in ambient temperature. The decrease in enthalpy drop increase is lesser from 10°C to 15°C ambient. From 15°C to 25°C, there is a sharp decrease in the enthalpy drop enhancement. From 25°C to 30°C, the decrease in enthalpy drop increase is much less but is again more from 30°C to 35°C.

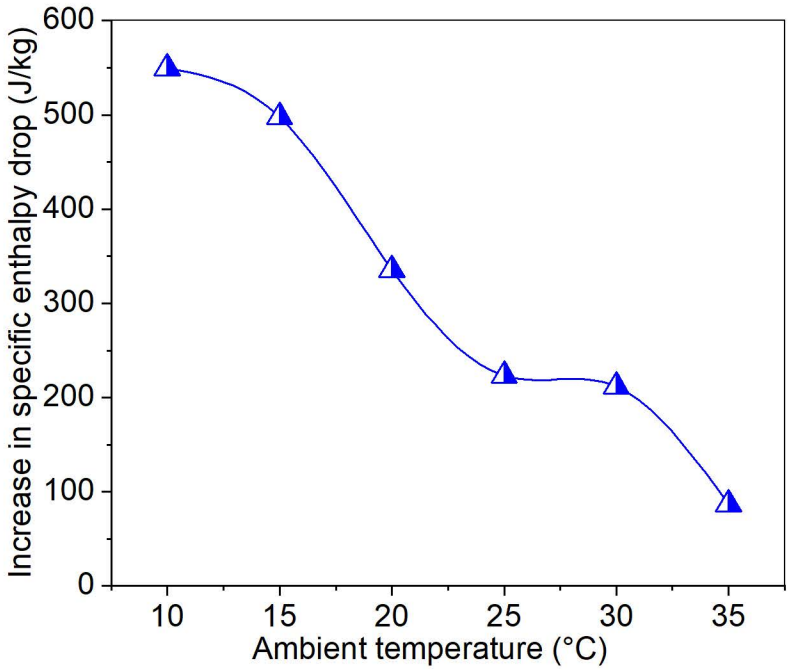

Fig. 4.20. Variation of increase in specific enthalpy drop (Δh_{jk}-Δh_k) due to H-jump.

For all the simulations, Δs_{jk} denotes, the specific entropy drop occurring with the H-jump in the k^{th} simulation while Δs_k is the corresponding specific entropy drop occurring without the H-jump in the k^{th} simulation.

For simulation 1 with an ambient temperature of 10°C, Δs_{j1}=21.037 J/kg-K and Δs_1=19.27 J/kg-K. So, an increase of 1.767 J/kg-K in specific entropy drop due to H-jump is observed. Similarly, for S-2, S-3, S-4, S-5, and S-6 the specific entropy drop is observed 1.599 J/kg- K, 1.233 J/kg- K, 0.717 J/kg- K, 0.683 J/kg- K, and 0.280 J/kg- K respectively.

Figure 4.21 represents the variation of average specific entropy at section 2 with and without H-jump for different ambient temperatures. Figure 4.22 represents the variation of specific entropy drop (Δs_{jk}) with the H-jump and specific entropy drop (Δs_k) without the H-jump for different ambient temperatures.

With the occurrence of the H-jump, the improvement in specific entropy drop by H-jump is observed to decrease as the ambient temperature increases. As shown in Fig. 4.23, the increase in specific entropy drop decreases rapidly between ambient temperatures of 10°C to 25°C. The rate of drop in specific entropy becomes less at 25°C and 30°C. From 30°C to 35°C, the drop in specific entropy is found to increase again.

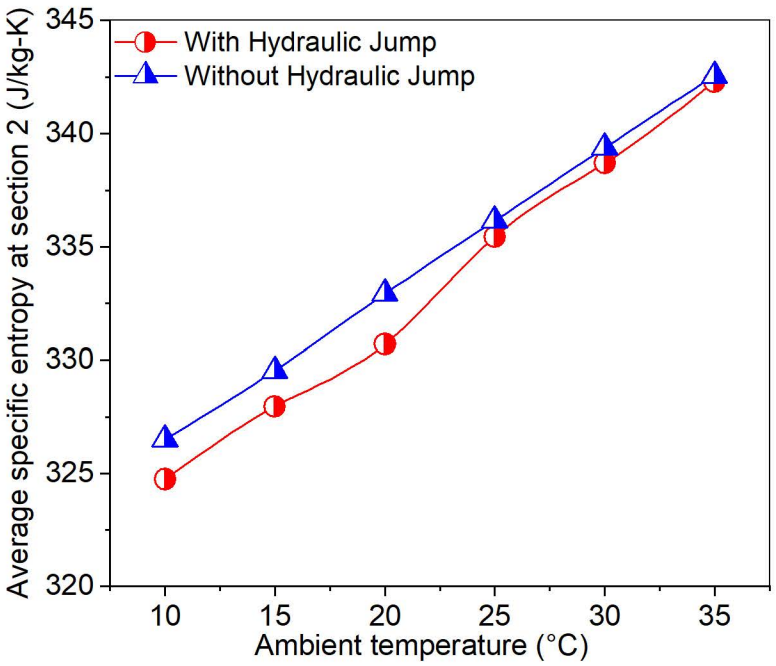

Fig. 4.21. Variation of average specific entropy at section 2 for the flows with and without H-jump.

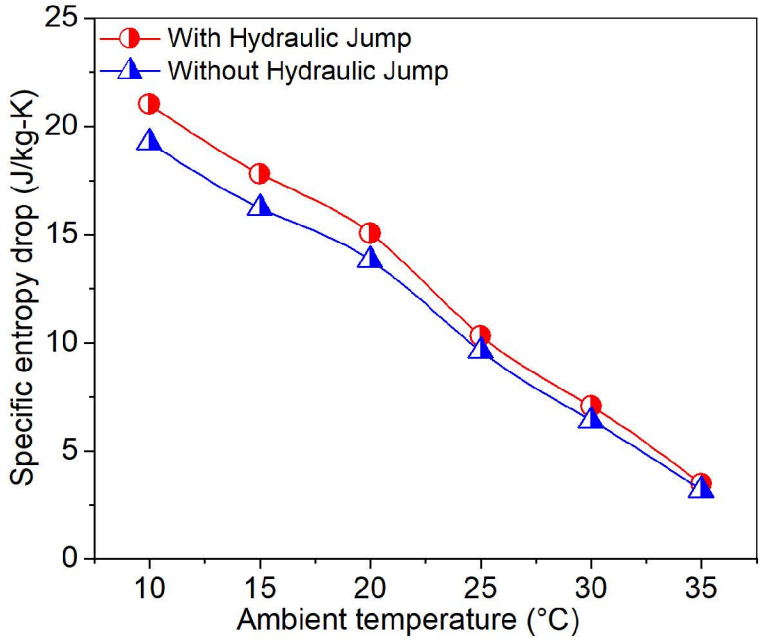

Fig. 4.22. Variation of specific entropy drop due to H-jump (Δs_{jk}) and without H-jump (Δs_k).

4.7. Conclusions

H-jumps in a rectangular flume with a mild slope of 1:2400 have been simulated using Ansys Fluent. This study aims to identify the capabilities of the H-jump to dissipate heat from water at the constant inlet water temperature of 40°C and for different ambient temperatures.

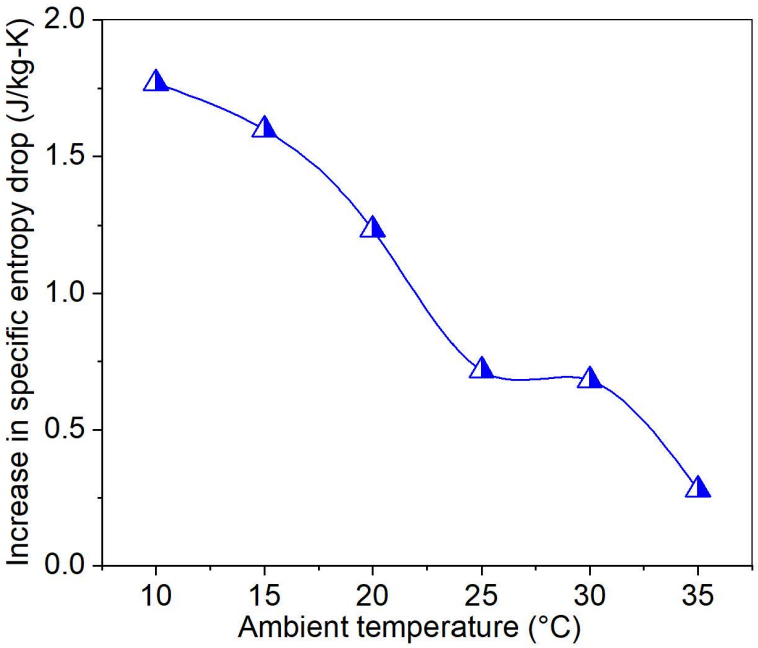

Fig. 4.23. Variation of increase in specific entropy drop (Δs_{jk}-Δs_k) due to H-jump.

Six different ambient temperatures, from 10°C to 35°C with the steps of 5°C, are considered. "Standard k-ε" turbulence model with standard wall function is adopted for simulation and "Energy" model is activated for incorporating the heat transfer by convection and conduction in the simulations. The "Volume of Fluid" model is used for tracking the free surface of flow and to simulate the roller. Considering a section downstream of the H-jump, the temperature, specific enthalpy, and specific entropy drops are measured with respect to the inlet conditions. These drops in the mentioned physical thermal quantities are compared with the corresponding drops occurring due to only convection at the free surface and conduction at the walls.

The most significant results of this investigation can be summed up as:

- The H-jump increases the heat dissipation from the water to the ambient i.e. the mean temperature at a cross-section downstream of H-jump is found to be less than the average temperature across the same section for a flow without the H-jump.
- Improvement in average temperature drop by the H-jump decreases with the increase in ambient temperature. The same can be concluded for the specific enthalpy and specific entropy. In other words, the more is the difference in temperature between the water and the ambient, the more is the enhancement of heat dissipation by the H-jump.
- The increase or improvement in temperature drop is found as a non-linear function of ambient temperature for a constant water inlet temperature.
- The maximum improvement in the temperature drop (0.131°C) is obtained for the low ambient temperature of 10°C.
- The enhancement in temperature drop fell rapidly for ambient temperatures greater than 15°C and became constant at approximately 0.02°C for ambient temperatures of 30°C and 35°C.
- The increases in specific enthalpy and specific entropy drops due to H-jumps are also a nonlinear function of ambient temperature, for the constant temperature of water. Both

the increase in specific enthalpy drop and specific entropy drop follow almost the same variation with ambient temperature.

- Maximum improvement in specific enthalpy drop and specific entropy drop occurred at the low ambient temperature of 10°C and decreased rapidly for temperatures less than 15°C.

References

Abbaspour, A., Farsadizadeh, D., Dalir, A. H., & Sadraddini, A. A. (2009). Numerical study of hydraulic jumps on corrugated beds using turbulence models. *Turkish Journal of Engineering and Environmental Sciences*, 33(1), 61-72.

Bayon, A., Valero, D., García-Bartual, R., & López-Jiménez, P. A. (2016). Performance assessment of OpenFOAM and FLOW-3D in the numerical modeling of a low Reynolds number hydraulic jump. *Environmental Modelling & Software*, 80, 322-335.

Bayon-Barrachina, A., & Lopez-Jimenez, P. A. (2015). Numerical analysis of hydraulic jumps using OpenFOAM. *Journal of Hydroinformatics*, 17(4), 662-678.

Carvalho, R. F., Lemos, C. M., & Ramos, C. M. (2008). Numerical computation of the flow in hydraulic jump stilling basins. *Journal of Hydraulic Research*, 46(6), 739-752.

Chanson, H. (2007). Bubbly flow structure in hydraulic jump. *European Journal of Mechanics-B/Fluids*, 26(3), 367-384.

Cheng, X., & Chen, X. (2013). Numerical simulation of dissolved oxygen concentration in water flow over stepped spillways. *Water Environment Research*, 85(5), 434-446.

Chippada, S. (1996). Numerical study of thin-film flows and open-channel flows. Rice University, Contract No. 94-483-010, Texas Water Development Board.

Ford, D. L., Chih, S. S., & Sobosta, E. C. (1972). Temperature prediction in activated sludge basins using mechanical screens. In Proceedings of the 27th Industrial Waste Conference, Purdue University, West Lafayette, Indiana, Vol. 27, p. 587.

Gharangik, A. M., & Chaudhry, M. H. (1991). Numerical simulation of hydraulic jump. *Journal of Hydraulic Engineering*, 117(9), 1195-1211.

Gualtieri, C., & Chanson, H. (2007). Experimental analysis of Froude number effect on air entrainment in the hydraulic jump. *Environmental Fluid Mechanics*, 7, 217-238.

Gulliver, J. S., Thene, J. R., & Rindels, A. J. (1990). Indexing gas transfer in self-aerated flows. *Journal of Environmental Engineering*, 116(3), 503-523.

Harada, S., & Li, S. S. (2018). Modelling hydraulic jump using the bubbly two-phase flow method. *Environmental Fluid Mechanics*, 18, 335-356.

Ho, H. V. (2024). Determination of the surface roller length of hydraulic jumps in horizontal rectangular channels using the machine learning method. *Stochastic Environmental Research and Risk Assessment*, 38, 2539–2562.

Jobson, H. E., & Keefer, T. N. (1979). Modeling highly transient flow, mass, and heat transport in the Chattahoochee River near Atlanta, Georgia. Vol. 1136. US Government Printing Office.

Marriott, M., & Jayaratne, R. (2010). Hydraulic roughness–links between Manning's coefficient, Nikuradse's equivalent sand roughness and bed grain size. *Advances in Computing and Technology 2010*, London. pp. 27-32.

Mollik, T., Roy, B., & Saha, S. (2017). Turbulence modeling of channel flow and heat transfer: A comparison with DNS data. *Procedia Engineering*, 194, 450-456.

Mondal, S., Mukherjee, S., & Das, S. (2020). Experimental Study of Thermal Effect on Oscillating Hydraulic Jump. *Indian Science Cruiser*, 34(4), 15-19.

Moss, M. D. (1976). The Effects of Roughness on Heat Transfer from Open Channel Flow. Doctoral dissertation, Georgia Institute of Technology.

Nandi, B., Das, S., & Mazumdar, A. (2020). Experimental analysis and numerical simulation of hydraulic jump. *IOP Conference Series: Earth and Environmental Science*, 505(1), 012024.

Negm, A. A. M. (1996). Hydraulic jumps at positive and negative steps on sloping floors. *Journal of Hydraulic Research*, 34(3), 409–420.

Novotny, V., & Krenkel, P. A. (1973). Evaporation and heat balance in aerated basins. *AIChE Symposium Series*, 70(136), 150-159.

Rashidi, M., Hetsroni, G., & Banerjee, S. (1991). Mechanisms of heat and mass transport at gas-liquid interfaces. *International Journal of Heat and Mass Transfer*, 34(7), 1799-1810.

Spalding, D. B. (1977). Heat and Mass Transfer in Rivers, Bays, Lakes, and Estuaries. *Advances in Heat Transfer*, 13, pp. 61-117.

Stang, O. (1982). On the Heat Exchange Between Rivers and Atmosphere. *Hydrology Research*, 13(2), 65.

Talati, S. N. (1988). Heat loss in aeration tanks. Master's thesis, University of California.

Valero, D., Viti, N., & Gualtieri, C. (2018). Numerical simulation of hydraulic jumps. Part 1: Experimental data for modelling performance assessment. *Water*, 11(1), 36.

Vallé, B. L., & Pasternack, G. B. (2006). Submerged and unsubmerged natural hydraulic jumps in a bedrock step-pool mountain channel. *Geomorphology*, 82(1-2), 146-159.

Wang, H., & Chanson, H. (2015). Experimental study of turbulent fluctuations in hydraulic jumps. *Journal of Hydraulic Engineering*, 141(7), 04015010.

Wang, Y., & Khayat, R. E. (2020). The influence of heating on liquid jet spreading and hydraulic jump. *Journal of Fluid Mechanics*, 883, A59.

Wei, T., & Willmarth, W. W. (1989). Reynolds-number effects on the structure of a turbulent channel flow. *Journal of Fluid Mechanics*, 204, 57-95.

Williams, G. P. (1963). Heat transfer coefficients for natural water surfaces. National Research Council Canada, Division of Building Research. pp. 203-212.

Yerachmiel, A., & Adams Jr, C. E. (1978). Comprehensive temperature model for aerated biological systems. Proceedings of the 8th International Conference on Water Pollution Research, Sydney, Australia, 1976. pp. 397-409.

Zhao, Q., Misra, S. K., Svendsen, I. A., & Kirby, J. T. (2004, June). Numerical study of a turbulent hydraulic jump. In Proceeding of 17th Engineering Mechanics Conference, University of Delaware, New York.

Aeration Efficiency due to Hydraulic Jump on Smooth Bed

5.1. Introduction

The movement of liquid does not necessarily require enclosure by a solid boundary on all sides. An open channel is an interface with a free surface that allows liquid to flow. The contact between the moving liquid below and the fluid medium above is practically defined as a free surface. The free surface of liquid acts as an uppermost boundary in these flow conditions. In hydraulic engineering applications, air at atmospheric pressure serves as the overlaying fluid while water is the most often used liquid. The only acting force on the free surface is the constant pressure of the atmosphere. Rivers, streams, irrigation ditches, artificial canals, and flumes are examples of open channels. Therefore, the main focus is on the flow of water with a free surface. Hydraulic jumps (H-jumps) are thoroughly studied in the field of hydraulic engineering because of their numerous applications. A H-jump is the phenomenon of a sudden conversion from a rapid flow with a super-critical velocity to a tranquil flow with a sub-critical velocity in an open channel. In a river/ canal/ channel beneath a sluice gate or at the base of steep spillway, a fast-moving liquid release could cause a rapid flow. The only method to slow this flow to a uniform tranquil flow if an impediment downstream or the roughness of the boundary of a long channel necessitates it is to abruptly change from rapid to tranquil flow at a certain point instead of progressively passing through the critical condition. The water surface unexpectedly stops at the jump location during this shift from super–critical to sub–critical flow, and turbulence dissipates a large amount of energy. Its distinguishing features include entrainment of air, dissipation of energy, surface waves and spray, and large scale turbulence (Mondal et. al. 2020). In H-jumps, the name "roller" usually refers to this enormous turbulence zone. Oxygen transfer is ensured in H-jumps by the air-water contact created by strong mixing and highly turbulent flows.

Dissolved oxygen (DO) is supplied to any body of water by atmospheric aeration and the photosynthesis of aquatic plants. It is an important consideration when assessing the quality of the water because of its effect on aquatic life. Excessively high or low DO levels can harm the aquatic organisms and degrade water quality. For a wide variety of life forms, including fish, invertebrates, microbes, and plants essentially DO is required. Each creature requires a different amount of DO. Hydraulic characteristics are responsible for an increase in the DO concentration in a river system. There might not be an equal amount of DO in two bodies of water that are fully saturated with air. In addition to temperature stratification, a waterbody may also feature oxygen stratification. Temperature, pressure, and salinity will all affect the DO concentration (measured in mg/l). The ability of oxygen to dissolve decreases as temperature increases. This suggests that deeper, cooler water requires more DO than warmer surface water to get 100% air saturation. The amount of DO will increase

in parallel with the pressure. Compared to water at higher elevations, water at lower elevations can hold more DO. At the same pressure and temperature, the amount of DO decreases exponentially as salinity increases. Many forms of aquatic life are unable to survive in low DO conditions, making it essential to evaluate and identify the various re-oxygenation processes in order to create structures that would increase DO. The only way to re-oxygenate is through aeration. It is the act of taking in oxygen straight from the surroundings. This oxygen absorption is caused by the diffusion of molecules from the atmosphere through the air-water contact, followed by turbulence and molecular diffusion throughout the water. In the majority of hydraulic systems, such as hydraulic structures, the rate of aeration is mostly determined by turbulent dispersion.

5.2. Literature Review

Fluid-structure interactions that occur in various engineering environments have been a potential research topic. Since Leonardo da Vinci first described the H-jump in 16^{th} century, this fascinating phenomenon has attracted the interest of many researchers. The first experimental study of this phenomenon was attributed to the Italian engineer Bidone (1818). Since then, a significant amount of research has been done on this subject. The body of research on this subject is extensive and constantly growing. It has incredibly useful practical applicability in water engineering and related fields are the main reason for continued interest in this subject.

A series of systematic experimental studies with six different bed slopes explained the H-jump in sloping channels that would allow engineers to draw useful conclusions. Four sets of experimentations were carried out, with the method consisting of recording the profiles and bottom pressures for all or part of the slopes, keeping consistent discharge and initial depth in each group. The experimental and theoretical agreement is quite satisfactory, especially when one considers that the relatively small size of the flume requires an exceptionally strong frictional effect. Theoretical equations and empirical data should agree more closely in larger channels (Bakhmeteff and Matzke 1938).

The transfer of oxygen, represented as a ratio of deficit, was demonstrated to fluctuate as a simple function of scale when modelled according to Froude's similarity law. The free overflow and H-jump oxygen transfers were described by the provided equations. The resulting equation was shown to successfully correlate model studies and measurements on several prototype structures. Its application to various scenarios including multiple jet weirs, spillway jets and the cascade in pools, was also detailed. A formula was provided to calculate ideal pool conditions for oxygen transfer (Avery and Novak 1978). Measurement data from various field weirs, including a weir on the Meuse River in Netherlands and a cascade of the drinking water plants associated with the city of The Hague, were used to verify the validity of Nakasone's equation, which was developed based on laboratory tests in Japan. Upto a certain point, aeration efficiency increased with increased discharge before decreasing again. Aeration was increased with increasing tailwater depth up to the point where optimal aeration efficiency was reached (Nakasone 1987).

Measurements of jump profiles in an open rectangular channel, including positive and negative step jumps, were performed on an inclined floor. The length and depth of jumps on the inclined floor were predicted using a set of regression results of experimental data. The stability and compactness of the H-jump, according to the analysis of the length characteristics and the SD-Ratio, was better with a negative step compared to a positive one. Multiple linear regression analysis was used to create a non-dimensional set of equations in terms of profile coefficients for H- jumps in inclined channels with as well as without steps (Husain et al. 1994). New experimental data with a slope of 4° and length of 25 m channel were described in another study. Data analysis provided new information about the interface of air-water region in distribution and flow characteristics of air-water. Despite the small amount of entrained air, surface area of air-water interface can exceed 100 m^2 for its each unit volume. When these findings were compared with a previous predictions, it was evident that air entrainment played a major role in air-water gas transfer in super-critical chute flows (Chanson 1997).

A study examined the impact of changing the step height and the chute angle on aeration efficiency of stepped spillways. Empirical relationships between aeration efficiency and the length of non-aerated flow zone were established. The outcomes showed that stepped spillways work well for the transfer of oxygen. This study revealed that because of the significant air entrainment and strong turbulence mixing that occurred, stepped spillways were incredibly effective at transferring oxygen. Occasionally downstream oxygen saturation was reached super--saturation condition. As a result of the increased turbulence, the flow over the stepped spillway was significantly more aerated than over standard chutes (Baylar et al. 2006). A model of fuzzy logic was created to estimate the effectiveness of H-jump aeration. A significant relationship between Froude number and aeration efficiency was observed. Reynolds numbers and inlet Froude numbers were chosen as model input parameters. This study related Fr_1 and Re to aeration efficiency in an if–then format using linguistic terms rather than mathematical calculations. The proposed fuzzy model represented the dynamic behaviour of the system and gave good predictions (Kucukali and Cokgor 2007).

To reveal a positive relationship between energy dissipation and aeration efficiency, the self-aeration efficiency of H-jump was studied in relation to the dispersion of energy rate per unit width. The aeration efficiency and energy dissipation rate had a positive linear relationship according to the H-jump data. The practical implications of this new approach for predicting the aeration efficiency of H-jumps may be significant. The kinetic energy of the turbulence can be represented by the energy dissipation rate, which suggests that turbulence plays a major role in the self-aeration process (Kucukali and Cokgor 2009). Another study predicted the aeration efficiency of baffled chutes in different experimental settings. Variations in aeration efficiency of trapezoidal, T-shaped, wedge, and stepped and baffle blocks were examined in conjunction with unit discharge, chute angle, and chute height. The results of this method demonstrated the efficiency of baffled chutes in the transmission of oxygen. As a result, an empirical correlation was established to predict aeration efficiency. Practical implications of this new equation included the prediction of baffled chute aeration efficiency (Kaya and Emiroglu 2010).

A revised model was introduced to predict the efficiency of oxygen transfer at gated sills. A revised model is introduced to forecast the efficiency of oxygen transfer at gated sills. Investigation of field data from eight gated sill structures were utilised to establish a dimensionless link in between oxygen transfer efficiency, inflow conditions and dam geometry. The oxygen transfer efficiency relationship between gate opening and sill dam design parameter was presented. One technology that could be used to effectively control gate structures to meet oxygen concentration criteria and support the design of restoration technologies is improved field oxygen transfer prediction (Witt and Gulliver 2012). In 2015, an experimental investigation was carried out to examine the effect of H-jumps and different types of weirs on aeration efficiency. The research utilized two types of weirs: triangular and rectangular. (Raikar and Kamatagi 2015).

In 2016, hydraulic experiments were conducted at the stepped weir structure to dissipate energy according to flow types and transfer oxygen by air entrainment (Kim et al. 2016). A research examined various air entrainment comparisons between H-jumps, plunging jets, and plunging breaking waves, as well as exploring contemporary techniques. To better understand about gas exchange occurrences through an interface of air-water, the measured data were re-examined and anatomized. The findings showed that in both breaking waves and plunging jets, the oxygen transfer efficiency decreased with increasing energy dissipation rate. In addition, the jet impingement velocity affected aeration lengths for the H-jumps and the penetration depths for both plunging breaking waves and plunging jets (Hoque and Paul 2022). The aim of this investigation was to assess the aeration performance of hydraulic mixer during photo-oxidation treatment. Before the sewage entered a reactor, an H-jump was performed to aerate it, and the amount of DO produced was monitored. These findings indicated that in developing countries with long sunshine hours, induced aeration is a cost-effective way to improve wastewater treatment (Nwajuaku and Agunwamba 2023).

The influence of H-jumps on aeration efficiency in different types of jumps has not been given sufficient attention according to a thorough analysis of the literature from the past years. Therefore, the purpose of this study is to fill this gap. When the discharge and bed slope increase from minimum to maximum, the upstream Froude number increases from 2.18 to 8.23 and the SD-Ratio increases as well. The current study therefore addresses how forced H-jumps on a smooth bed affect energy dissipation and aeration efficiency on a horizontal bed and an inclined bed at different discharges. Five different bed slopes ranging from horizontal to 6° and five different discharges ranging from 15 to 35 lps have been investigated during this study.

5.3. Need to Evaluate Aeration Efficiency for Hydraulic Jump

The most energy-intensive procedure in wastewater treatment facilities is aeration. Compared to traditional oxygenation systems, H-jump aeration is a simpler and more affordable way to achieve oxygen transfer. In practice, the H-jump is naturally an energy dissipation process that converts kinetic energy of the high velocity flow to a turbulent kinetic energy and heat. Through turbulence and difference in flow depths, H-jump

promotes the air-water mixing. The aeration efficiency is benefitted in this process. The amount of entrained air that contributes to energy dissipation can be measured by calculating the aeration efficiency, and the relationship between energy loss and aeration efficiency can be drawn.

The water quality is improved by the aeration process introduced by the H-jump, which improves the level of DO in water. It is important for sustaining aquatic organisms in places where the oxygen level in rivers and streams is too low. The ability of fish and other aquatic animals to survive can be increased through an effective aeration process that benefits ecosystems.

Increasing the oxygen content of water is critical to reducing biochemical oxygen demand (BOD) in wastewater treatment facilities that are used in the open-channel flow. This requires an understanding of aeration efficiency through H-jumps. The H-jump could therefore be used to create more environment-friendly treatment procedures for reoxygenation. The efficiency of the H-jump aeration process is a fundamental factor in hydraulic modelling that influences flow pattern, velocity, and turbulence models. Better modelling of real-world situations is possible through accurate predictions of aeration efficiency and energy dissipation, which benefit the construction of infrastructure such as spillways, dams, and water treatment plants. The waste stabilization pond is one of the most basic biological treatment methods utilized in the tropics for sewage treatment. The purpose of the H-jump is to provide DO to the pond by creating turbulence. Adding an H-jump to the waste stabilisation pond can improve treatment efficiency and consequently reduce the amount of land required (Agunwamba and Ogarekpe 2010). This study therefore discusses the effect of H-jumps on their aeration efficiency and energy dissipation at different bed slopes and discharges.

5.4. Experimental Setup and Methodology for Smooth Bed

Typical H-jumps on a smooth, straight channel are illustrated with schematics for both a horizontal bed and a sloping bed (with bed slope θ) shown in Fig. 5.1 (Subramanya 2009). The toe of the jump, which indicates cross-section 1, is the point at which the incoming super-critical flow (with velocity V_1) abruptly rises to the depth that acts as the beginning of the normal jump. Cross-section 2 with sub-critical velocity V_2, the nearly level water surface adjacent to the roller after the turbulence zone, is the terminal point of the jump. The distance between these two parts is known as jump length L_j. The y_1 to y_2 at the formed jump is known as the SD-Ratio. A considerable energy loss occurs between cross-sections 1 and 2 as a result of the reversing rollers shearing during intense turbulence. This reverse roller entrains a lot of air, which causes the surface of water to become uneven, white, and frothy.

Compared to traditional oxygenation systems, aeration through H-jumps is a simpler and more affordable method of achieving oxygen absorption. Measurements of DO and H-jump parameters have been investigated multiple times with different slopes and discharges. A new experimental setup (Fig. 5.2) was developed in the Fluvial Hydraulics Laboratory of School of Water Resources Engineering in Jadavpur University.

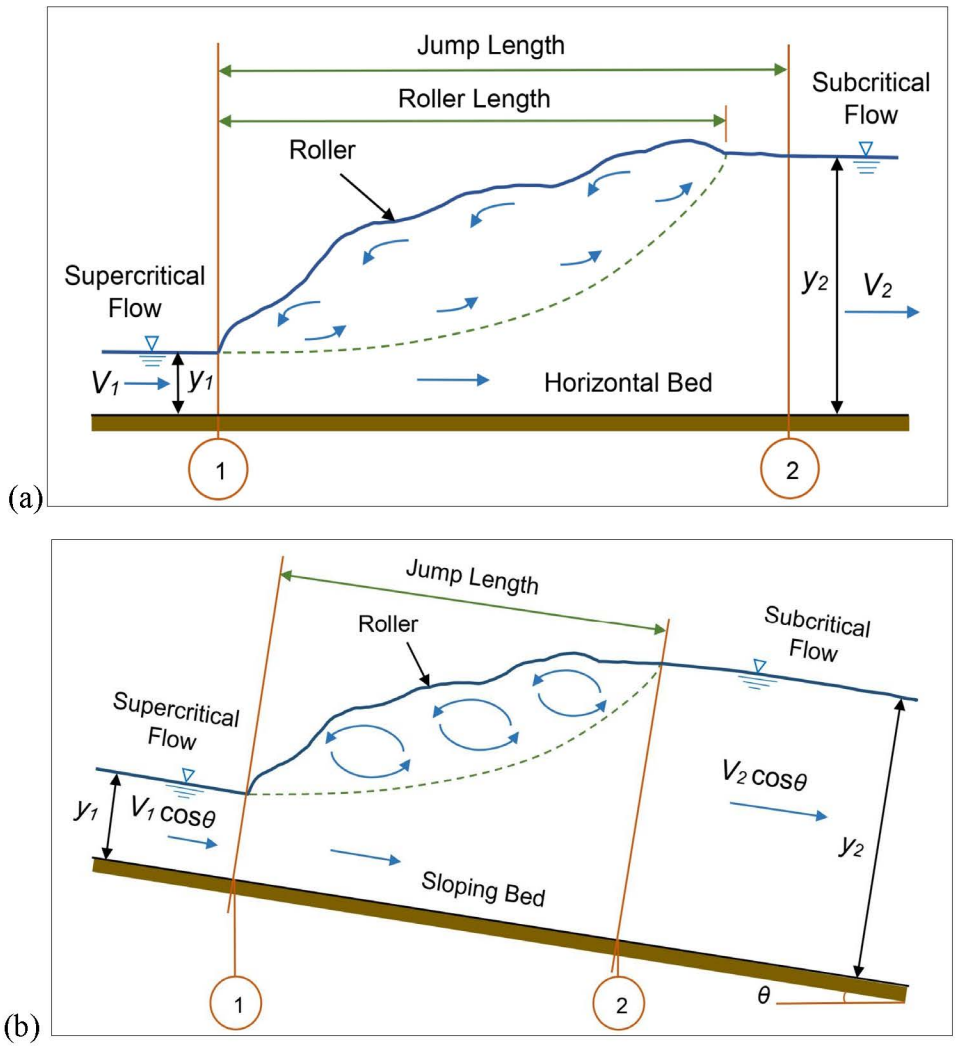

Fig. 5.1. Sectional flow representations of H-jump characteristics that form on (a) horizontal bed and (b) sloping bed.

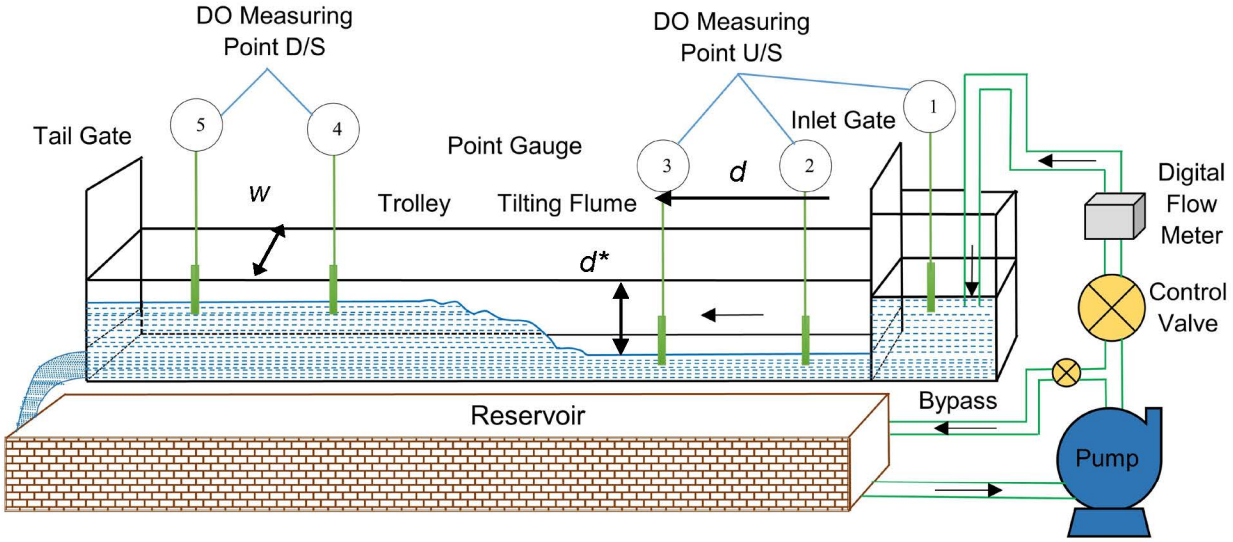

Fig. 5.2. Illustrative diagram of laboratory experimental arrangement highlighting five cross sections for DO measurement.

A straight rectangular Perspex-walled flume of 0.35 m wide, 0.60 m in heigh, and 7 m long was utilized for the tests. This experimental flume was fitted with flat glass surface walls of 5 m long from the outlet for clear observation and measurement of the jump and aeration phenomenon. The bed of the flume was made of galvanized iron. Through an upright sluicegate with a fixed baffle plate at its rear, water enters the investigational flume (Fig. 5.3). The tailgate on the flume can be raised or lowered to regulate the water depth after the jump. The jump location can be changed by controlling the tailwater depth. A chain pulley system was used to change the inclination of the flume.

(a) (b) (c)

Fig. 5.3. Experimental flume (a) Flume bed, (b) Inlet gate, and (c) Outlet gate.

The flume inlet portion received water from the source pump through a conduit and a gate valve. This water went through the transparent investigation portion and back to the reservoir tank after going through the stabilization zone. There was a bypass or return line attached immediately after the pump outlet accompanied by a flow control valve (Fig. 5.2). The return line pipe diameter and the valve size were comparatively less than the main pipe and gate valve. The pump discharge flow was controlled by the bypass system valve. A digital flow meter at inlet pipe was used to measure the discharge.

A 15-horsepower centrifugal pump with a 65 lps maximum discharge was used for water recirculation in all these experimentations. A point gauge with an accuracy of ±0.5 mm was utilised to measure flow depths throughout the flume at evenly spaced intervals. There were continuous undulations in water surface downstream of the H-jump. The maximum and minimum levels of these undulations at a location were marked and an average of these levels was considered the depth at that location. A digital thermometer with an accuracy of ±0.1°C was used to measure water temperature and ambient temperature, as the DO saturation level varies with temperature.

The concreted water reservoir had a capacity of 2200 litres of water. A chain pulley system was used to change the bed slope (θ). Flow was measured using a digital flow meter manufactured by Endress & Hauser (Switzerland) with an accuracy of ±0.5% of reading (Fig. 5.4). The amount of DO in the flow zone, comprising pre-jump and post-jump sections of the H-jump, as well as before the inlet gate, was measured with a portable DO meter manufactured by Hach (USA) with an accuracy of ±0.1 mg/l.

(a)  (b) 

Fig. 5.4. Water discharge measuring instruments used in experimentation: (a) Digital flow meter, and (b) Point gauge.

Stagnant surface water from a water body was used for this current experimental investigation. Initially, water was pumped from an adjacent water body located right next to the laboratory to fill the laboratory tank. We then waited 3-4 hours before starting the experiment. The DO in water in the tank was measured before starting the experiments. Each time, this observed DO value was found to be much lower than the saturation value. While the experiment was in progress, the DO meter probe was launched at five different locations as shown in Fig. 5.2 to measure the values. The probe was not continuously laid down to allow measurements to be taken. To verify the probe values, the DO level was measured several times before the experiment in stagnant water, in super-critical and sub-critical flow, and it was found to be perfectly sensed. The diameter of the probe (1.5 cm) was too small compared to the internal width of the channel (35 cm) and the measurement took a very short time. The diameter of the probe was only 4.3% of that internal width. It was, therefore, a small obstacle, therefore it was expected that the flow characteristic would not change significantly due to the penetration of the probe (Fig. 5.5).

Fig. 5.5. DO measurement during an experiment.

For this reason, its effect was neglected. Hach's product technical datasheet on their website verifies that according to the ISO 17289 standard, the portable DO meter has been reliable and stable over a short period of time for measuring DO in laboratory and field conditions.

After a fixed H-jump profile was maintained during each experiment by controlling the flow through the outlet valve, measurements of oxygen concentrations at different locations were initiated by immersing the same sensor in water. The accuracy of the sensor remained the same at all five monitoring points. The aeration efficiency was then calculated by independently averaging the upstream and downstream measurements. We averaged the values of cross sections 2 and 3 to obtain the upstream DO and averaged the values of cross sections 4 and 5 to obtain the downstream DO.

The aeration efficiency (E) through H-jumps is solved using the Gameson equation (Eq. 5.1) (Gameson 1957). Here, k is air-water mass transfer coefficient, a_w is air-water contact area per volume unit, and t_b is bubble residence time.

$$E = \frac{C_d - C_u}{C_s - C_u} = 1 - \frac{1}{\exp\left(k \times a_w \times t_b\right)} \tag{5.1}$$

The amount of DO (measured in mg/l) varies with water temperature, pressure, and salinity. Aeration efficiency, E can range from 0 (nonappearance of aeration) to 1, (complete saturation in the downstream). In this equation, the C_u and C_d indicate the measured DO values in the pre-jump and post-jump sections respectively. The C_s is the saturation point of DO concentration for a certain temperature.

Water temperature affects the solubility of oxygen into the water. A standard temperature correction factor is used because oxygen transfer efficiency is sensitive to water temperature. Using Eq. 5.2, the aeration efficiency calculated at different temperatures is converted to aeration efficiency at a reference temperature of 20°C (Gulliver et al. 1998).

$$1 - E_i = (1 - E_T)^{1/f} \tag{5.2}$$

where E_T is aeration efficiency at water temperature T during measurement, E_i is equivalent aeration efficiency at indexed temperature (20°C) and f is exponent, described by (Eq. 5.3), where the indexed temperature is 20°C.

$$f = 8.261 \times 10^{-5}\left(T - 20\right)^2 + 0.02103\left(T - 20\right) + 1.0 \tag{5.3}$$

During the H-jump experiments, we measured the DO at the pre-jump and post-jump divisions. Therefore, we have used Eq. 5.1 in this work to determine E. According to the definition of E, the calculated E now becomes E_{20} using Eqs. 5.2 and 5.3.

The sub-critical and super-critical zones were used to measure the water temperature, DO content, and flow height after it was pumped out through a closed setup and travelled through the flume. In this case, the maximum speed and water depth of 0.70 m/s and 0.23 m, respectively were restricted by limiting the discharge capacity, while the operational tailgate was kept fully open. If the tailgate is fully closed and 52 lps of water is discharged through the flume, then the total water depth that can be reached is roughly 0.45 m.

a) Dimensional framework

In many cases, it is not possible to perform experiments in the laboratory at the same setup in conjunction with the operating parameters prevailing in practice for reasons of financial convenience, time saving and ease of investigation. As a result, laboratory testing is usually performed under different operational variable circumstances than those found in practice. These factors include velocity, pressure, geometric dimensions of operating systems, and physical properties of working fluid in case of fluid flow problems. Instead of the original dimensional variables, a set of dimensionless similarity parameters or variables can be used to describe a physical problem. This suggests that fewer parameters need to be considered separately in an experimental study.

Dimensional analysis is a different approach that uses a mathematical technique to determine these dimensionless properties. Dimensional analysis relies heavily on the constraints imposed by the dimensional homogeneity criterion, which takes the form of an algebraic function and limits the quantities involved in the physical problem. Mass, length, time, temperature, current and intensity of light are the main physical quantities that give basic dimensions. The first four of these, represented by the letters M, L, T, and Θ, are used in fluid mechanics. In order to theoretically and numerically analyse H-jumps at small scales, a number of relevant equations that describe structures of turbulent gas-liquid or two-phase flow as well as interactions between trapped bubbles and coherent structures must be taken into account (Chanson 2013). In order to use dimensional analysis to determine the parameters that are of predominant importance, several simplifications can be considered.

Along with geometrical and hydraulic factors, the relevant data needed for the dimensional analysis in this study are the air and water flow characteristics. Under current circumstances, the aeration efficiency (E) is considered to be the properties of air and the remaining properties of water. Inlet velocity, water density, and channel slope are the main determinants of the hydraulic head. E strongly depends on H-jumps. Consequently, E also depends on the parameter controlling H-jumps. E can be expressed using the following functional analogy (Eq. 5.4).

$$f\left(y_1, y_2, V_1, g, L_j, \rho, \mu, S, E\right) = 0 \tag{5.4}$$

where, y_1= pre-jump depth, y_2= post-jump depth, V_1= average velocity of the super-critical stream, g= gravitational acceleration, L_j= jump length , ρ= water density, μ= dynamic viscosity and S= bed slope.

Here, Buckingham's π theorem can be used to express the number of independent variables (m = 9) in terms of three basic dimensions (n = 3), M, L, and T. As a result, number of π terms appears equal to ($m - n$) = (9 – 3) = 6. These six terms are denoted as π_1 to π_6. An implicit relationship of function between the controlling variables, provides an analytical representation of the phenomena, as shown in Eq. 5.5.

$$f_1\left(\pi_1, \pi_2, \pi_3, \pi_4, \pi_5, \pi_6\right) = 0 \tag{5.5}$$

The following non-dimensional groups can be demonstrated using the π theorem (Eq. 5.6):

$$f_1\left\{\begin{array}{l}\pi_1=\left(\frac{y_2}{y_1}\right),\pi_2=\left(\frac{V_1}{\sqrt{y_1 g}}=\mathrm{Fr}_1\right),\pi_3=\left(\frac{L_j}{y_1}\right),\\ \pi_4=\left(\frac{y_1V_1\rho}{\mu}=\mathrm{Re}\right),\pi_5=(S),\pi_6=(E)\end{array}\right\}=0 \tag{5.6}$$

The SD-Ratio is recognized as the first non-dimensional group. The second group is known as the inlet Froude number (Fr_1), and the fourth group is known as Reynolds number (Re). The E can be expressed as a function of the initial five π terms, as shown in Eq. 5.7.

$$E=f_2\left(\frac{y_2}{y_1},\mathrm{Fr}_1,\frac{L_j}{y_1},\mathrm{Re},S\right) \tag{5.7}$$

In the section that follows the impact of these non-dimensional characteristics on the E is carefully examined.

b) Scale Effect

The force ratios of a laboratory setup model diverge from its real-world prototype, which causes scale effects to produce discrepancies between the up-scaled laboratory setup and prototype observations. Upstream flow velocity, upstream flow depth, discharge, channel shape, bed roughness, and channel slope are the primary dependent characteristics of H-jump.

All experiments were performed in the laboratory using a smooth-bed rectangular flume of fixed dimensions. However, in the real world, the channel bed is not always absolutely smooth, although the channel cross-section may be somewhat close in certain situations. Along with flora and fauna, the bed may actually contain many irregular particles of sediment. Changes in flow characteristics and the way atmospheric air is entrained by flowing water can result from the presence of all these bed materials. The DO concentration is also influenced by the presence of flora and fauna. Because the laboratory has a smooth bed, these properties do not affect DO concentration or air entrainment. In addition, our laboratory setup differs from the real flow field in terms of flow and upstream flow depth. In addition to upstream flow and depth, the cross-section is significantly larger in real flow than in the laboratory setting. For this purpose, the air-water interaction zone is larger and the turbulence occupies a large area. As a result, there is significant entrapment of air in flowing water and improvement of DO concentration in real channel flow is significantly greater than in the laboratory.

Under real-world, upstream velocity, flow conditions, and channel slope are quite comparable for our experimental setup. Therefore, for these two factors, air entrainment in a laboratory environment is not significantly different from air entrainment in a real channel.

5.5. Results and Discussion

A rectangular laboratory flume with a smooth bed made of perspex and a chain pulley system for tilting was used for the tests. The flume contained a tailgate to regulate the water depth after the jump and a vertical sluice gate at its rear with fixed baffle plates for water intake. The baffle plates were used for neutralizing surface turbulence or surges from a moving liquid. The H-jump in this study was formed experimentally by adjusting the tailgate, facilitating submerged and forced H-jumps. In the current investigation, a total of 25 tests (Table 5.1) were carried out to assess the aeration efficiency and jump characteristics for a series of bed inclinations and discharges (Fig. 5.6). By adjusting the flow control valve, the channel discharge was achieved. The pump discharge was measured by a digital flow meter attached to the inlet pipeline. Five individual set points of (i) 15 lps, (ii) 20 lps, (iii) 25 lps, (iv) 30 lps, and (v) 35 lps were used to select the discharge of the recirculating pump for these experiments. Five distinct bed slopes selected for this study were (i) horizontal, (ii) 1.5°, (iii) 3°, (iv) 4.5°, and (v) 6°.

(a)

(b)

(c)

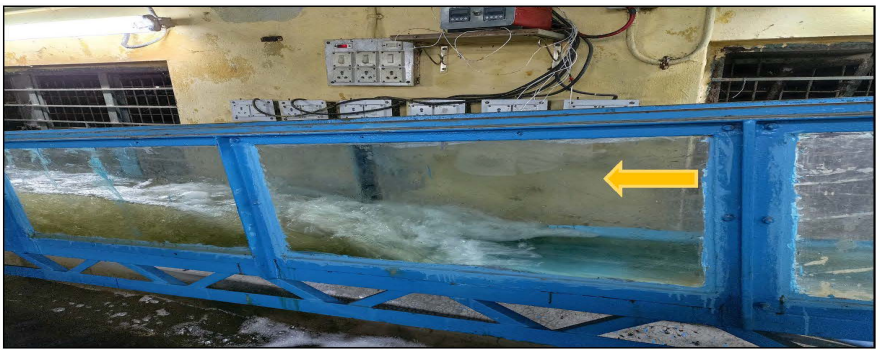

(d)

(e)

Fig. 5.6. H-jumps formation during experiments when (a) discharge 20 lps, bed slope horizontal; (b) discharge 15 lps, bed slope 1.5°; (c) discharge 35 lps, bed slope 3°; (d) discharge 25 lps, bed slope 4.5°; (e) discharge 30 lps, bed slope 6°.

The Fr_1 varied from 2.18 to 8.23, and approach flow depths from 2.3 to 3.7 cm. A mean velocity at inlet (V_1) of 2.4 m/s was set prior to the jump. After the H-jump was developed, huge foams were developed, and the post-jump velocity (V_2) was significantly found to be decreased. Trends in the percentage change in velocity, $\Delta V_{1\text{-}2} = (V_1 - V_2)/V_1$, before and after the jump are shown in Table 5.1. As the discharge and bed slope increases, the $\Delta V_{1\text{-}2}$ increases. In pre-jump conditions, increasing the inlet discharge increases the Fr_1. For every inlet discharge, the Fr_1 increases while the bed slope increases. From Table 5.1 it is quite clear that the H-jump induced velocity drop is maximum for a 35 lps discharge on a 6° bed slope and minimum for a 15 lps discharge on a horizontal bed. Therefore, an H-jump with a 35 lps discharge on a 6° bed slope is ultimately developed for a better velocity reduction in a super-critical flow.

Immediately behind the jump, the water surface is constantly undulating. When these undulations were marked at a particular location, the depth was calculated by averaging the highest and lowest values. As shown in fig. 5.7, vertical axis represents the ratio of channel width (w) to flow depth, while horizontal axis represents the relative distance along the channel. Here, d^* and d represent the flow depth and distance from the inlet gate, respectively. As the discharge increases for a given bed slope, the jump profiles show that the water depth after the H- jump increases. Similarly, when the bed slope changes from small to large, the tail-water depth increases. Consequently, for this submerged forced jump, the y_2/y_1 increases with increasing bed slope and discharge. As the

bed slope increases, the inlet flow velocity starts increasing. This causes the tail-water depth to rapidly increase.

Table 5.1. Variation in velocity ($\Delta V_{1\text{-}2}$) following H-jumps at various experimental discharges and bed slopes.

Experiment ID	Bed slope (Degree)	Discharge (lps)	Decrease in velocity after the jump, $\Delta V_{1\text{-}2}$ (%)
HJ1-15-S0	Horizontal	15	58.91
HJ2-20-S0	Horizontal	20	69.79
HJ3-25-S0	Horizontal	25	74.62
HJ4-30-S0	Horizontal	30	81.38
HJ5-35-S0	Horizontal	35	83.53
HJ6-15-S1.5	1.5°	15	74.44
HJ7-20-S1.5	1.5°	20	75.77
HJ8-25-S1.5	1.5°	25	78.30
HJ9-30-S1.5	1.5°	30	82.78
HJ10-35-S1.5	1.5°	35	85.53
HJ11-15-S3	3°	15	79.35
HJ12-20-S3	3°	20	80.89
HJ13-25-S3	3°	25	82.90
HJ14-30-S3	3°	30	84.27
HJ15-35-S3	3°	35	87.14
HJ16-15-S4.5	4.5°	15	82.10
HJ17-20-S4.5	4.5°	20	84.51
HJ18-25-S4.5	4.5°	25	86.62
HJ19-30-S4.5	4.5°	30	87.29
HJ20-35-S4.5	4.5°	35	87.97
HJ21-15-S6	6°	15	84.53
HJ22-20-S6	6°	20	86.32
HJ23-25-S6	6°	25	87.75
HJ24-30-S6	6°	30	88.13
HJ25-35-S6	6°	35	88.96

Each experimental condition has the same intake gate openings. Consequently, as illustrated in Fig. 5.7, the inlet depth and the relative depth (d^*/w) are almost the same. The post-jump d^*/w is about the same for the discharge of 30 lps and 35 lps, and the jump of 15 lps and 35 lps are in a saturated state as the tail-water d^*/w approaches a nearly straight line, as shown in Fig. 5.7(a). The discharge of 35 lps is found to have the maximum d/w improvement for the horizontal bed slope. Considering the maximum d^*/w improvement, the discharge of 15 lps and 20 lps results in d^*/w improvements of roughly 248.7% and 101.8%, respectively. In comparison to the improvement of 35 lps discharge, the d^*/w increase for the discharge of 25 lps and 30 lps is 48.5% and 3.4%, respectively. According to the Fig. 5.7(b), the sloping channel causes the post-jump d^*/w to increase.

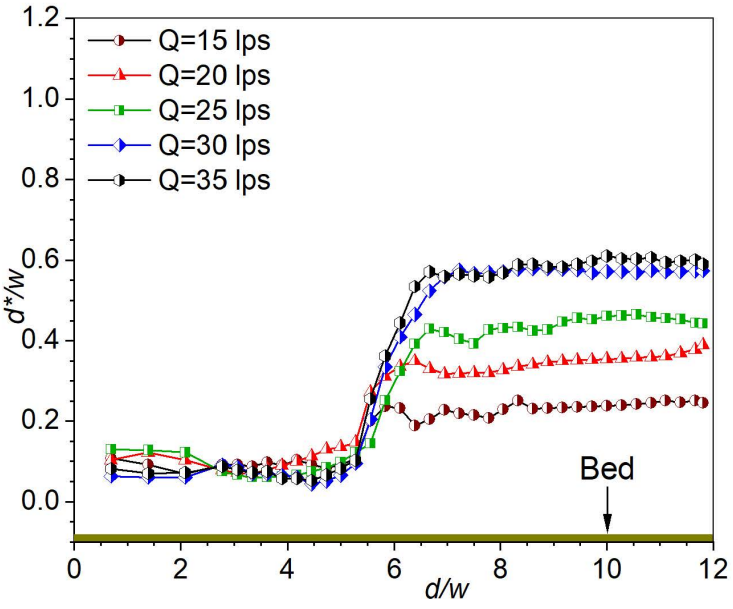

(a) bed slope horizontal

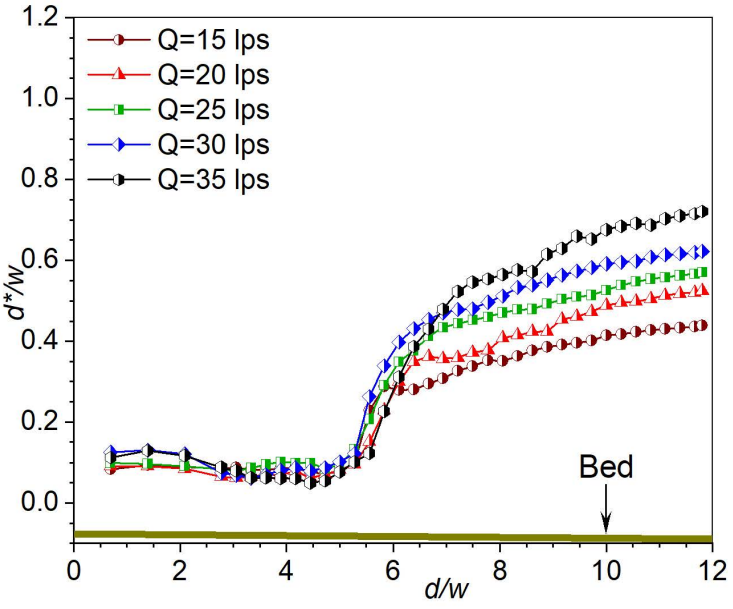

(b) bed slope 1.5°

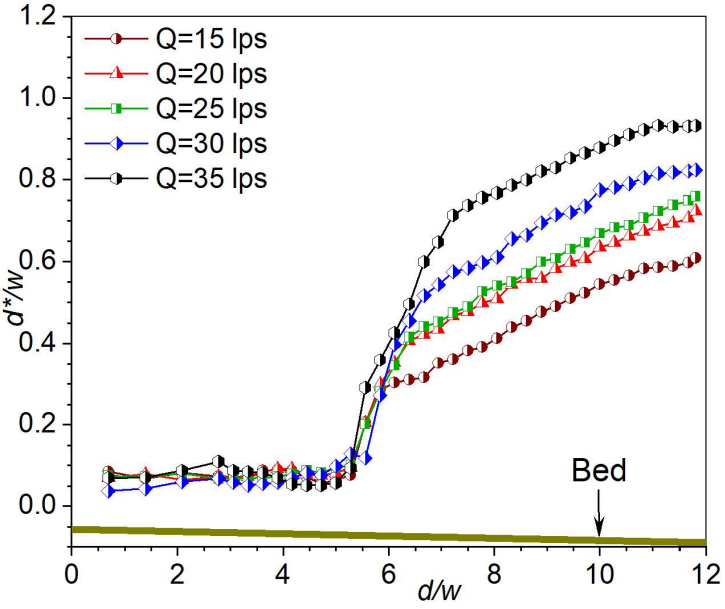

(c) bed slope 3°

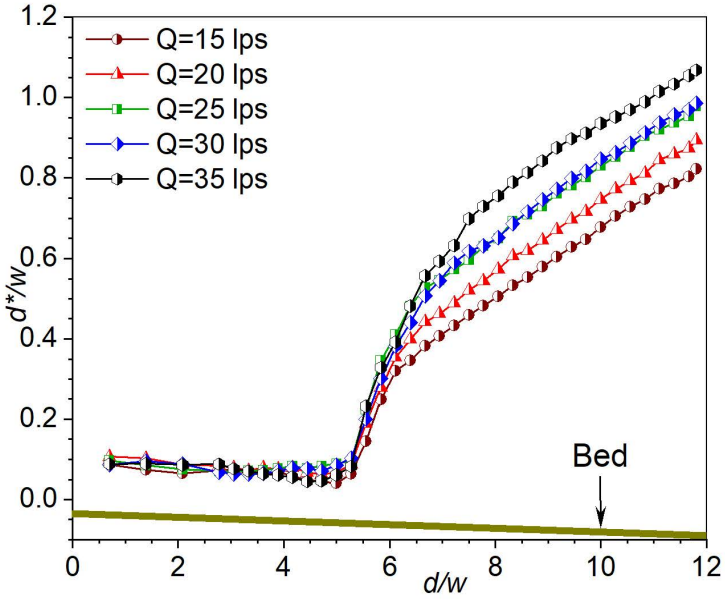

(d) bed slope 4.5°

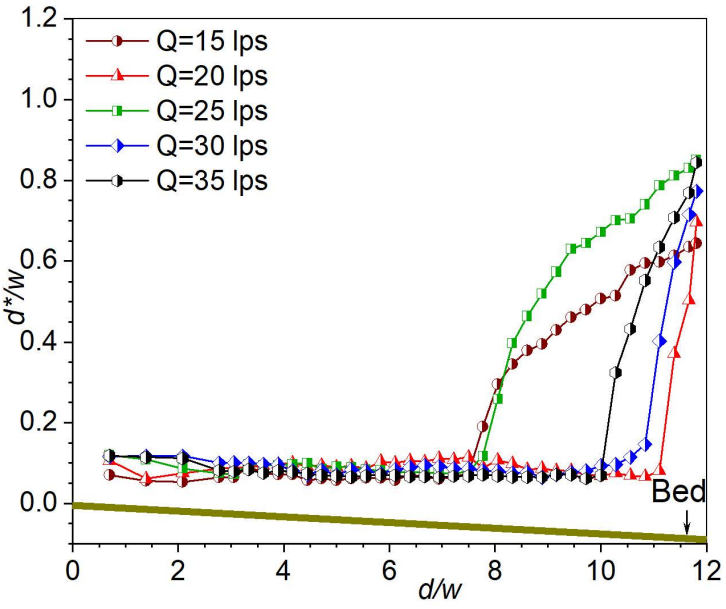

(e) bed slope 6°

Fig. 5.7. Flow profiles of H-jumps for different bed slopes and discharges

The d^*/w increment for the highest increase of 35 lps discharge for the 1.5° bed slope is at least 11.6% for a 30 lps discharge and 70.2% for a 15 lps discharge. It can be inferred from Figs. 5.7(a) and 5.7(b) that the jump at 1.5° bed slope has a relatively larger jump length. The jump profile in Fig. 5.7(c) shows that the post-jump trends for the 20 lps and 25 lps discharge are almost identical. For the jump on the 3° bed slope, the d^*/w increase is the smallest for the minimum discharge and the largest for the maximum discharge. Considering the highest d^*/w increase, the improvement is 80.4% for the discharge of 15 lps, 47.5% for the discharge of 20 lps, 40.4% for the discharge of 25 lps, and 19.4% for the discharge of 30 lps.

According to Fig. 5.7(d), it is seen that the sloping bed causes H- jump shape to increase at post- H-jump zone. The inclination of the post-jump data is almost the same for the 25 lps and 30 lps discharges. Regarding the extreme increase, the lowest d^*/w increment

is for a discharge of 30 lps, around 13.3%, and the highest increment is for a discharge of 15 lps, of 43.1%. In comparison to Figs. 5.7(a),(b), and (c), the jump length is comparatively greater for the 4.5° bed slope. Figure 5.7(e) displays the jump profile for the 6° bed slope at different discharges. In contrast to the other jump scenarios, such as those shown in Figs. 5.7(a-d), the toe of the jump is shifted into the forward direction for this bed slope. The steepness of the jump profile advances with the increasing slope for high discharge. In terms of the maximum d^*/w increase, the 6° bed slope has a minimum d^*/w gain of 0.6% and a maximum of 56.1%.

The surface profile is designated by using Eq. 5.8 (Wang and Chanson 2015).

$$\frac{\eta - y_1}{y_2 - y_1} = \left(\frac{x - x_1}{L_r} \right)^{0.54} \tag{5.8}$$

In this equation, η= the free-surface elevation above invert, x= depth measuring position, x_1= jump toe position, and L_r= jump roller length.

Plotting observed values with the calculated values comes after we convert the η values using It can be seen from the graph (Fig. 5.8) that the calculated values and the observed values agree well. Of the displayed values, 43% of the data fall within the ±15% error range and 66% within the ±30% error range.

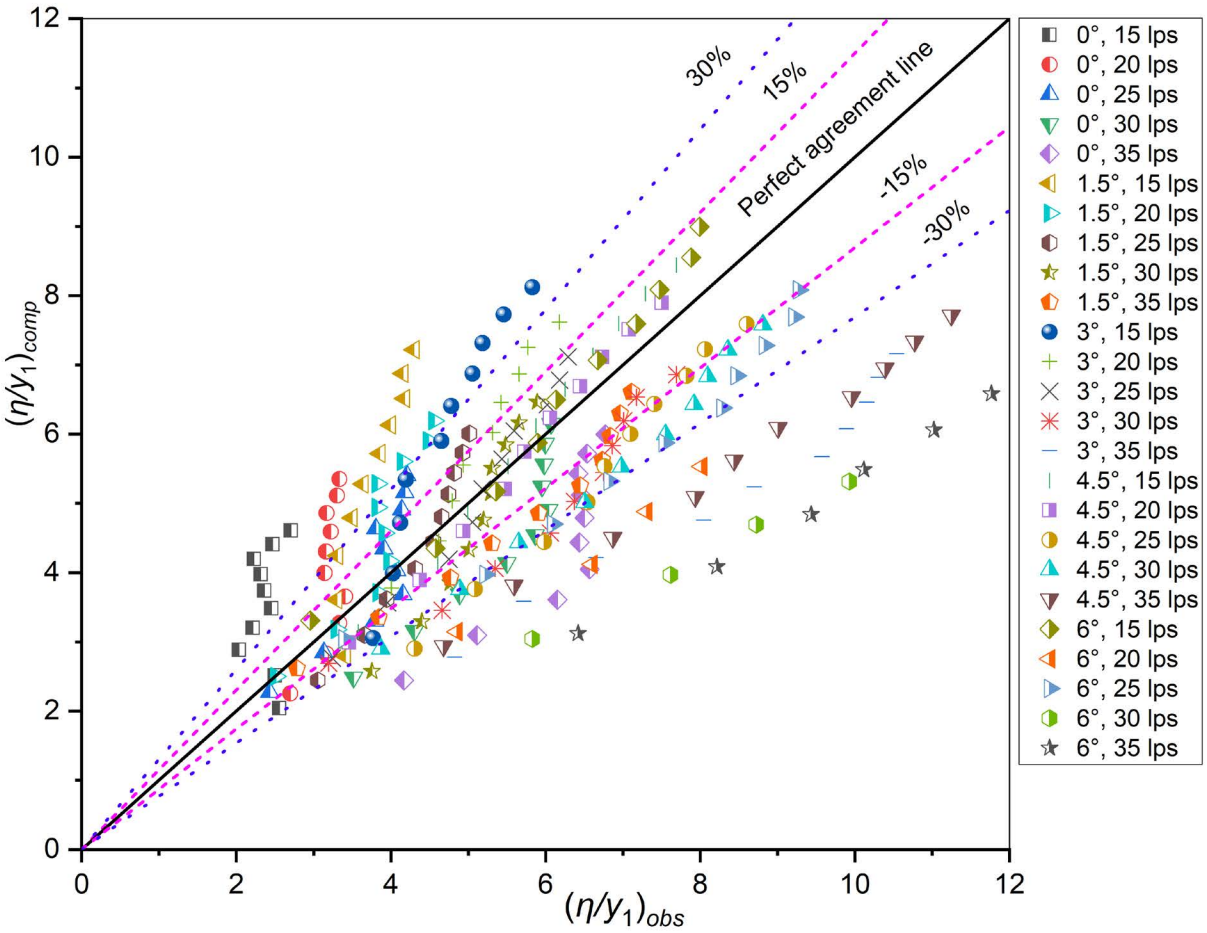

Fig. 5.8. The ratio of free surface profiles to initial depth: comparison between observed data and computed data.

Equation 5.1 is used to solve the E due to H-jumps. To determine the E in water under the appropriate experimental conditions, the DO was measured during the pre-jump and post-jump phases. Then, at a baseline temperature of 20°C, the E is changed (Eq. 5.2). It has been observed that the E in the H-jump increases with increasing bed slope and discharge. For the H-jump, it is found that the efficiency of water aeration varies with the SD-Ratio. Here Fig. 5.9(a) shows a plot of E_{20} with y_2/y_1 for different discharges, and Fig. 5.9(b) displays the same plot for different discharges related to the bed slope. It is observed that as the Fr_1 increases with rising bed slope and discharge, the SD-Ratio also increases. More turbulence and the production of air foam are indicated by an increase in the SD-Ratio.

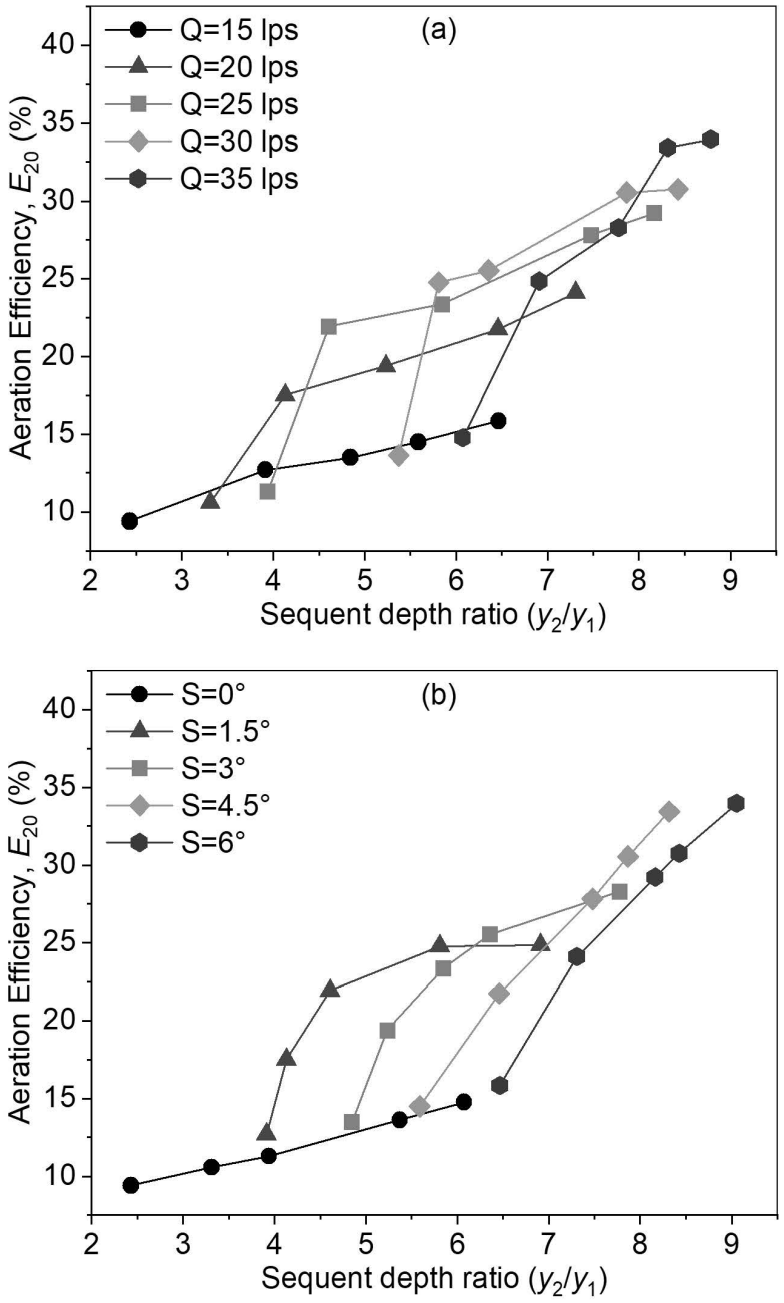

Fig. 5.9. Aeration efficiency variation during H-jumps for various SD-Ratios depending on (a) different discharges and (b) different bed slopes.

Therefore, with increasing bed slope and discharge, it is also shown that the aeration efficiency and the SD-Ratio are also shown to increase (Fig. 5.9). According to Fig. 5.9(a), the E_{20} improvement trend appears to be the same for discharges of 20 lps, 25 lps, and 30 lps. With different bed slopes, the E_{20} enhancement is lowest for 15 lps discharge at about 68.4% and highest for 25 lps discharge at approximately 159.2%. The E_{20} improvement tendency appears to be nearly identical for bed slopes of 1.5° and 3° in Fig. 5.9(b), and it also follows the same pattern for bed slopes of 4.5° and 6°.

The H-jump shows that Fr_1 strongly influences E (Fig. 5.10). It is clear that E increases with Fr_1 due to the increasing mass transfer from air to water through the H-jump. In Fig. 5.10a, E_{20} with Fr_1 is plotted against discharge for various bed slopes. In Fig. 5.10b, it is plotted against the bed slope for various discharges.

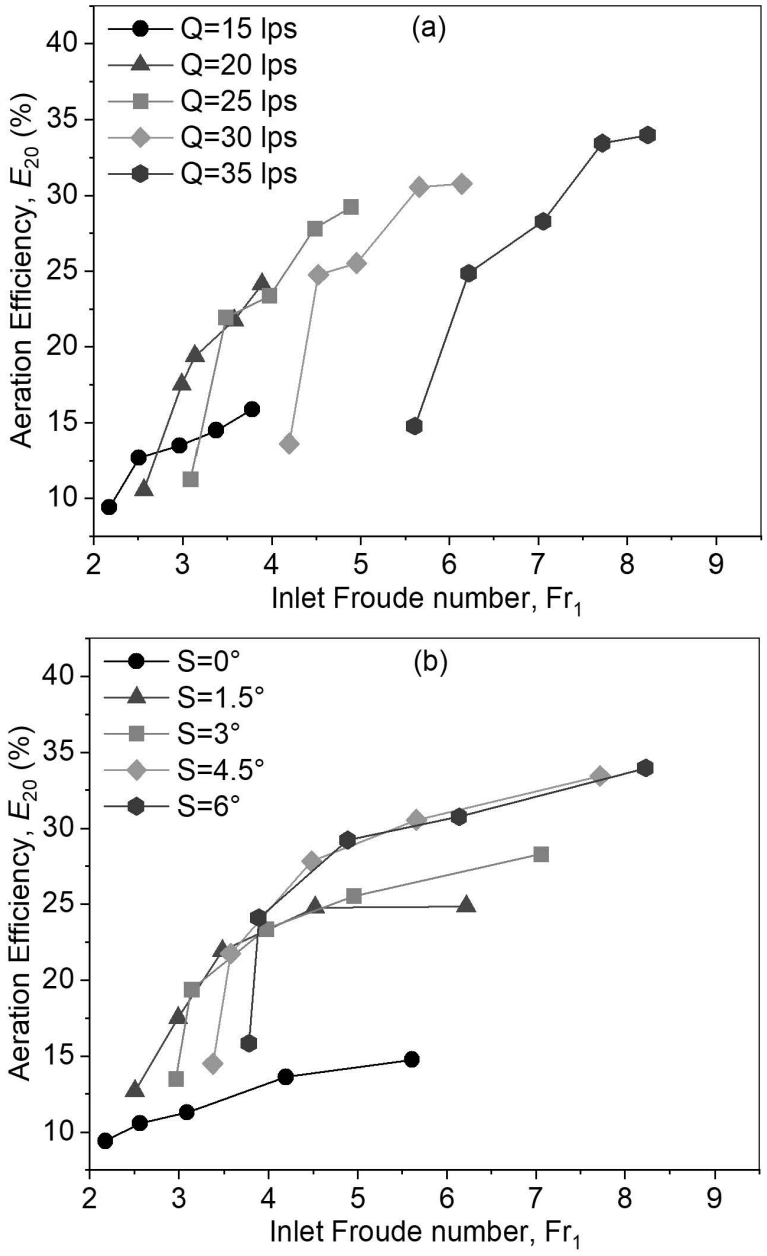

Fig. 5.10. Aeration efficiency variation during H-jumps for various inlet Froude numbers depending on (a) different flows, and (b) different bed slopes.

It is evident that the E_{20} and the Fr_1 increase in super-critical zones as the bed slope and discharge increase, as does the inlet velocity of water. Figure 5.10 shows trends of E_{20} changes with Fr_1. The discharge of 25 lps, 30 lps, and 35 lps shows a similar trend to the improvement of E_{20} (Fig. 5.10a). The evolving pattern for bed slopes of 3° and 4.5° is nearly identical, according to the plot of E_{20} with Fr_1 with varying bed slopes. The lowest E_{20} enrichment percentage is observed with lower discharge and lower bed slopes.

Plotting relative jump length (L_j/y_1) along the abscissa and aeration efficiency along the ordinate in Fig. 5.11 illustrates the correlation between the two variables in the H-jump for different bed slopes and discharges.

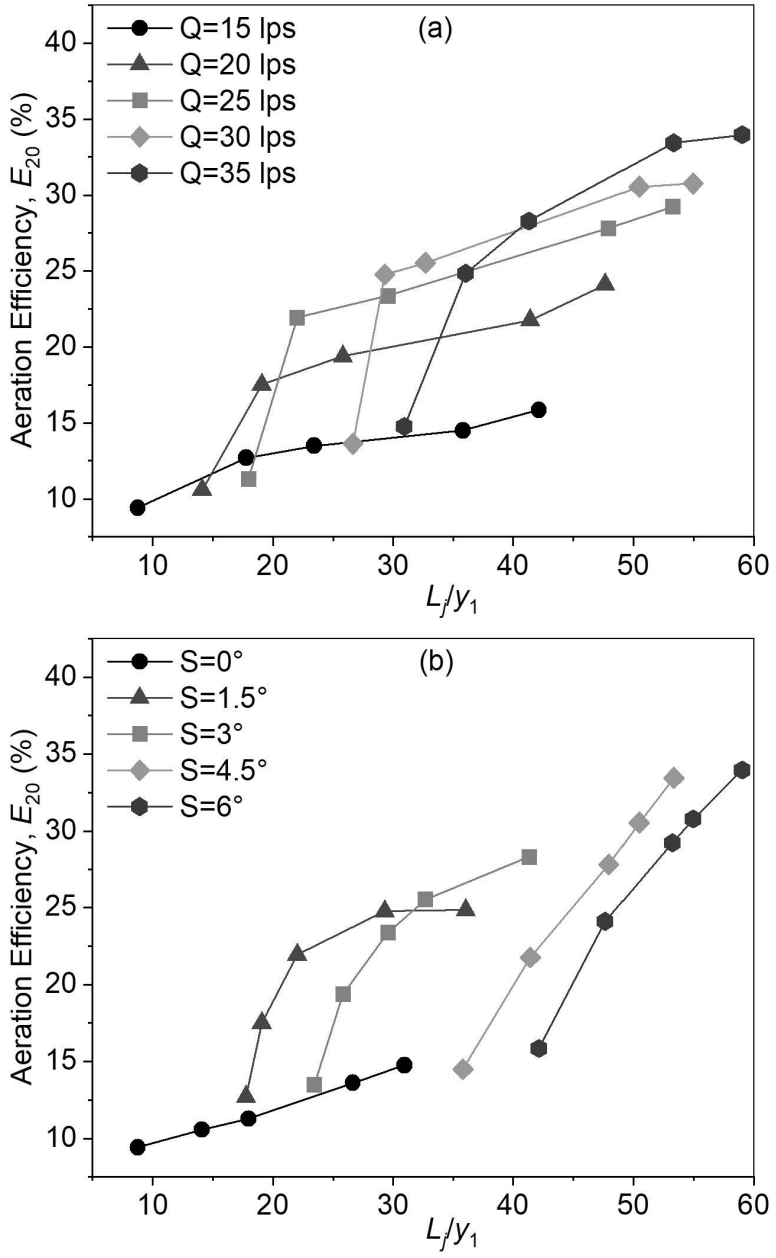

Fig. 5.11. Aeration efficiency variation during H-jumps for various L_j/y_1 depending on (a) different discharges and (b) different bed slopes.

An increase in Fr_1 results in a larger relative jump length. The increase in bed slope and discharge is expected to improve the relative jump length. It also shows that the relative jump length increases the E_{20}. Higher discharge and higher bed slope cause to result in the greatest increase in E_{20}.

One significant non-dimensional parameter in this research is Re which is computed under pre-jump conditions. Increasing the discharge increases Re, which can vary from around 44,000 to 126,000 for any bed slope. As shown in Fig. 5.12, it is evident that H-jump results in an increase in E_{20} with a diverging pattern with Re. The Re growth pattern is almost the same for the higher discharge and higher bed slope, as observed in Fig. 5.12(b). Obtaining a suitable trend of E_{20} improvement with the Re for various discharges requires further investigation in this direction.

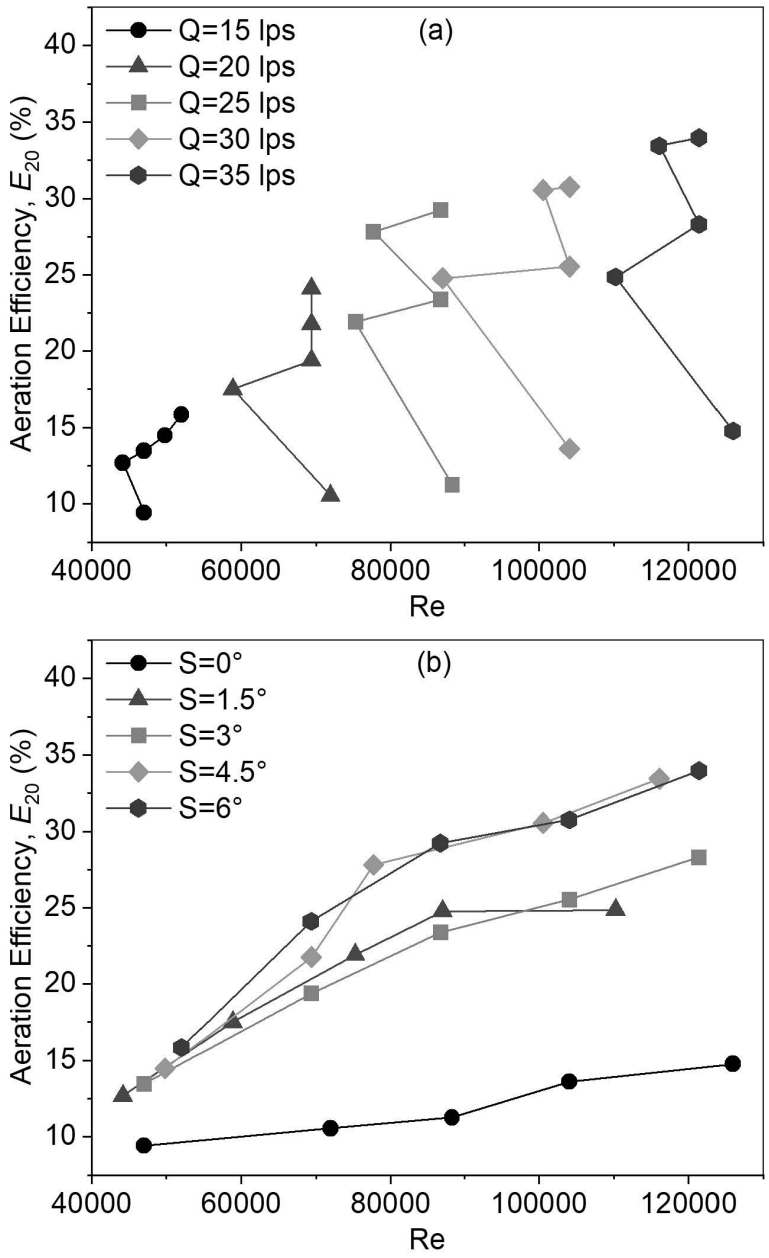

Fig. 5.12. Aeration efficiency variation during H-jumps for various Reynolds numbers depending on (a) different discharges and (b) different bed slopes.

The E for different discharges and bed slopes is compared as a function of energy loss (Fig. 5.13). The bed slope and discharge of the H-jump have an impact on E, which, in turn, affects the energy loss. For H-jumps, energy dissipation rate per unit width is compared to E_{20}. The smallest $\Delta E_{loss}/H_1$ is 0.06 and the maximum is 0.9 due to variations in discharges and bed slopes. The correlation between the E_{20} and the $\Delta E_{loss}/H_1$ is significant. It is discovered that the E_{20} increases in line with the increase in $\Delta E_{loss}/H_1$ in every instance when bed slopes and discharges are improved. The E_{20} improvement trend is nearly the same for discharges of 15 lps, 20 lps, and 25 lps among the various discharges (Fig. 5.13a). Similarly, for bed slopes in relation to $\Delta E_{loss}/H_1$, the E_{20} improvement trend is nearly the same for 3°, 4.5°, and 6° bed slopes (Fig. 5.13b).

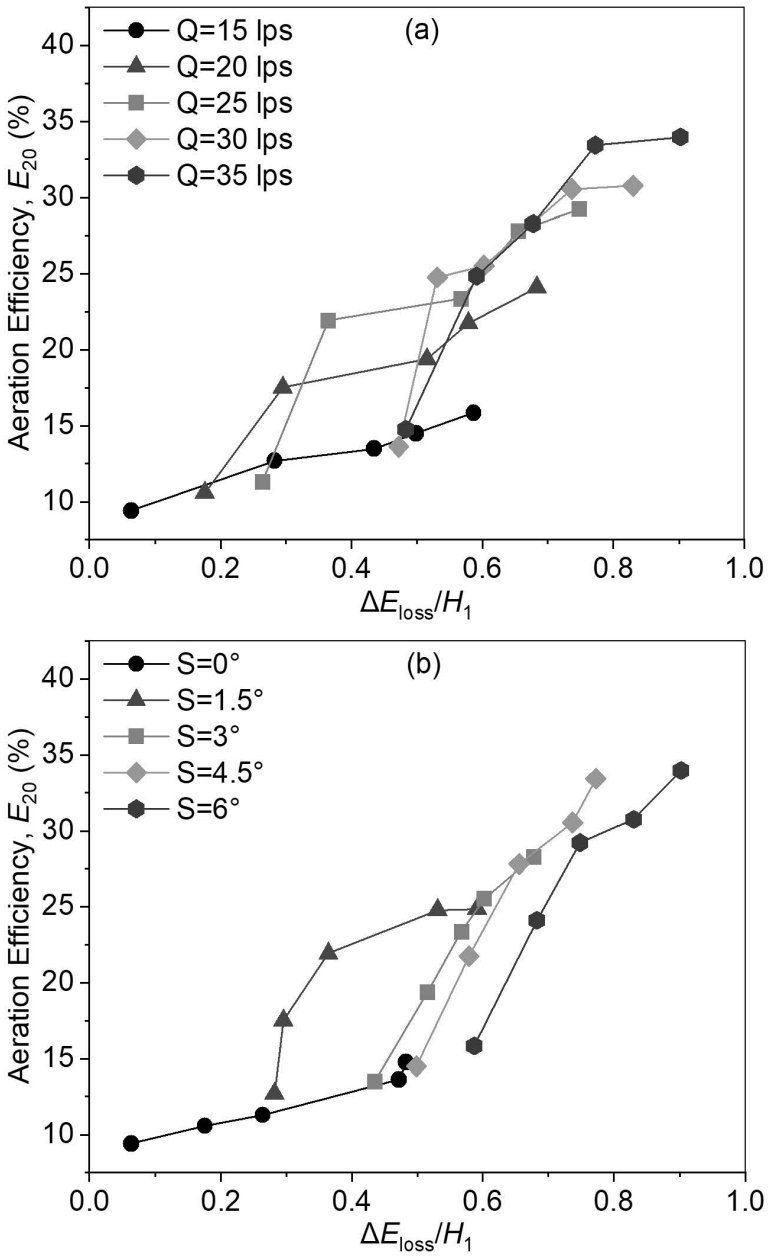

Fig. 5.13. Aeration efficiency variation during H-jumps for various energy dissipation rates per unit width depending on different (a) discharges and (b) bed slopes.

As seen in Fig. 5.14(a), the bed slope is plotted along the x-axis, and the E_{20} percentage is plotted along the y-axis. As illustrated in Fig. 5.14(b), the discharge is once more plotted along the abscissa, and the E_{20} percentage is presented along the ordinate. Likewise, for certain discharges, the E_{20} is enhanced at a specific bed slope. The increasing trend of E_{20} for various bed slopes appears to be the same for the discharge of 15 lps and 20 lps, as shown in Fig. 5.14(a). Once more, the patterns for the discharge of 25 lps, 30 lps, and 35 lps are nearly identical. As observed in Fig. 5.14(b), improvement forms for the various discharges are almost the same for the bed slopes of 1.5°, 3°, and 4.5°. A bigger flow results in a higher E_{20} for a given bed slope because of improved water-air interaction. E_{20} increases from 9.4% to 15.9% for minimum to maximum bed slopes at 15 lps discharge.

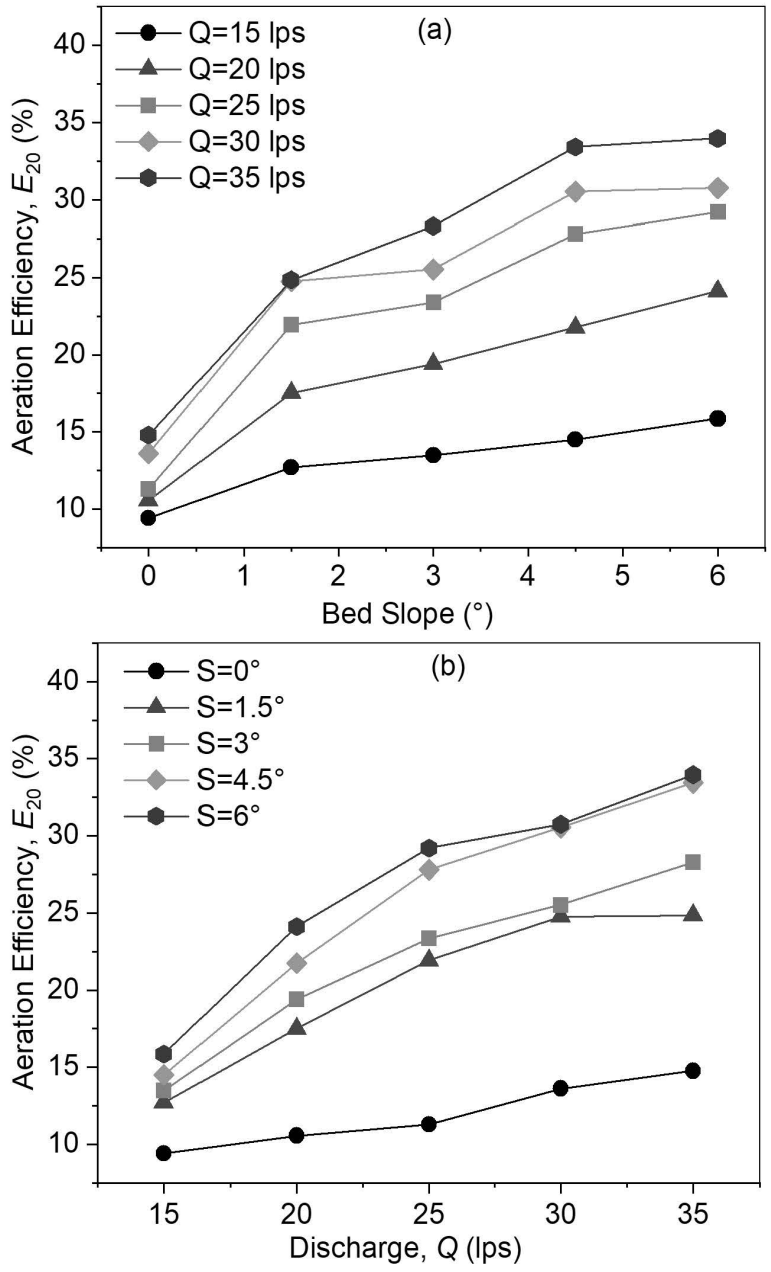

Fig. 5.14. Deviation of aeration efficiency during H-jumps for (a) different flows, and (b) different bed slopes.

Additionally, E_{20} increases from 15.9% to 34.0% for discharge of 15 lps to 35 lps when discharge is increased for a specific bed slope, such as 6°.

This research focuses on the ways that bed slope and discharge affect aeration efficiency. The discharge and the Fr_1 are strongly correlated. Furthermore, as results are displayed in Fig. 5.15, additional predictive correlations proposed by different researchers are also taken into account. The literature data obtained from Chanson (1995) indicates that, for a given Re, the E_{20} is comparable to Fr_1. Three constant values of Re were given in the literature data. The correlation between an increase in Fr_1 and an increase in E_{20} is observed for each case. E is also computed in the current investigation as a function of Fr_1. Re, however, is not maintained constant in the experimental setup The data are therefore divided into three sets of data for comparison purposes, which are almost identical to the Re value from the literature. Plotting these three data sets shows that Fr_1 also improves E_{20}. Moreover, the experimental data are categorised in relation to the literature data. However, since all the boundary conditions are different for the two scenarios, the increasing pattern is different.

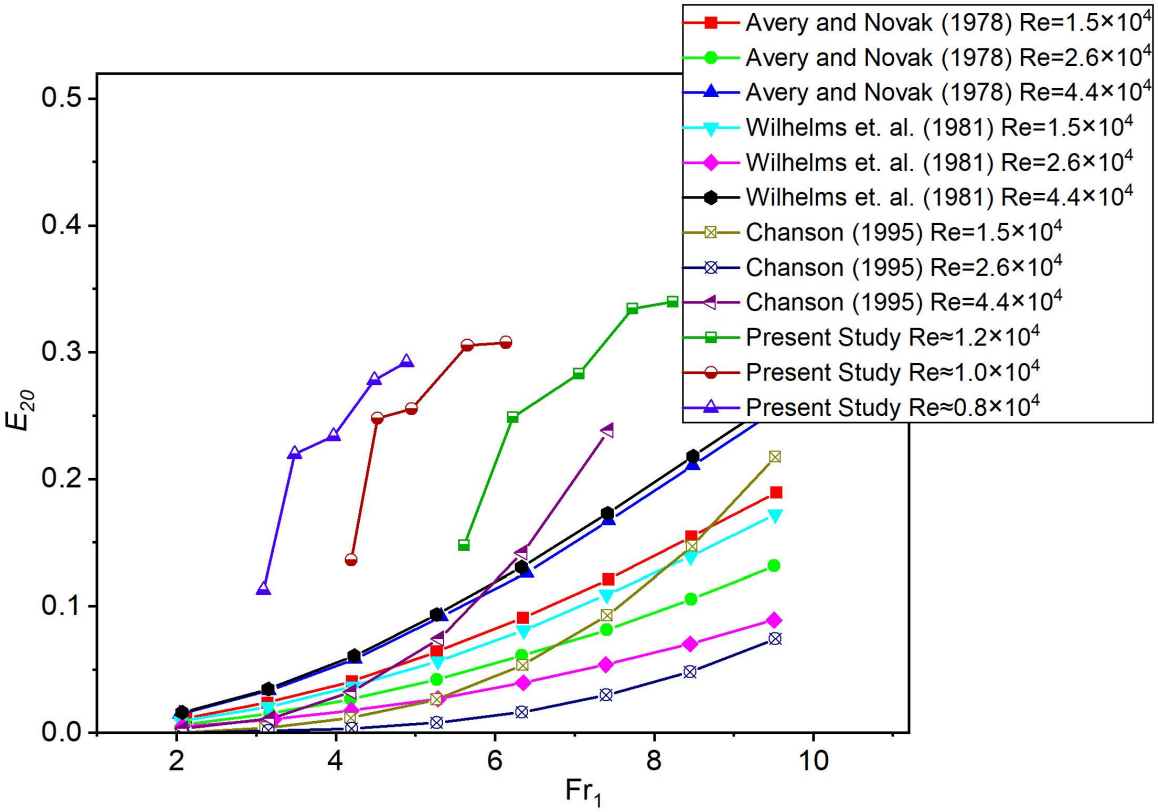

Fig. 5.15. Comparison between the current investigation with data from the previous literature (Avery and Novak 1978, Wilhelms et al. 1981, and Chanson 1995) about aeration efficiency as a function of inlet Froude number.

The relationship between E_{20} and energy loss is compared. The bed slope and discharge of the H-jump had an impact on the E_{20}, which in turn had an impact on the energy loss. The E_{20} and the relative energy loss have a close relationship. In addition, as the results shown in Fig. 5.16, other predictive correlations proposed by various researchers

are also taken into account. Energy dissipation rate per unit width and E_{20} for H-jumps are compared according to the literature data obtained from Zhao et al. (2022). These literature data are plotted for various flow conditions. For all cases, the correlation between the E_{20} and the increase in $\Delta E_{loss}/H_1$ is observed. E_{20} is also computed in the current investigation as a function of $\Delta E_{loss}/H_1$. A plot of the current data sets allows comparison and shows that the E_{20} is also improved by $\Delta E/H_1$. The experimental results are also increased when the literature data are considered, and the increased pattern is almost the same.

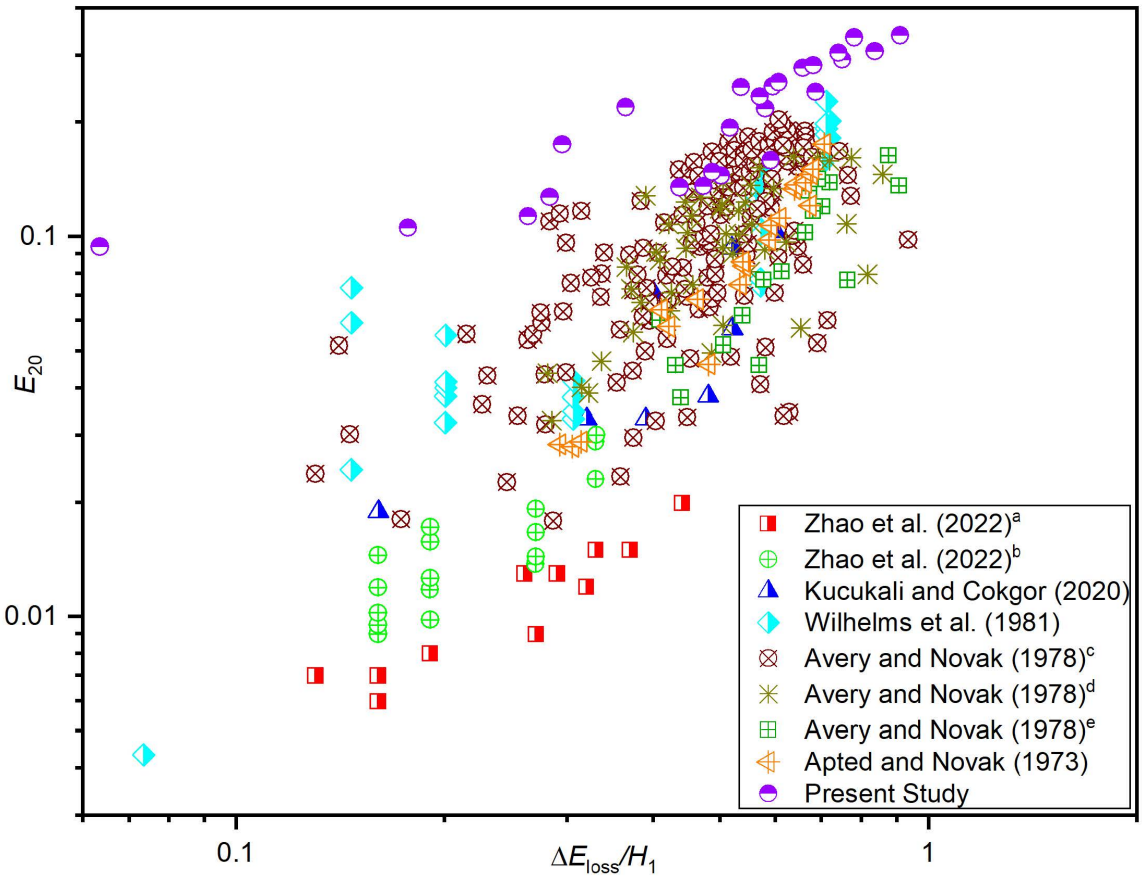

Fig. 5.16. Comparison of identified literature data on aeration efficiency as a function of energy dissipation rate per unit width (Zhao et al. 2022, Kucukali and Cokgor 2020, Wilhelms et al. 1981, Avery and Novak 1978, and Apted and Novak 1973) with the present study ([a]hydraulic jump only, [b]hydraulic jump with L_{sup} upstream, [c]tap water with 0.6% $NaNO_2$, [d]tap water with 0.3% $NaNO_2$ and [e]tap water with 0% $NaNO_2$).

a) Percentage of thermal energy dissipated from specific energy

In this research, thermal energy dissipation through H-jump is investigated with respect to specific enthalpy. As shown in the simulation table (Table 4.9) in the previous chapter for the jump at an ambient temperature of 30°C, the specific enthalpy loss due to the H-jump is 3.6%. From Fig. 5.13, it is evident that the specific energy loss is 48.3% due to H-jump on the horizontal bed and 35 lps discharge. With almost comparable flow parameters and similar boundary conditions, the thermal dissipation is close to 7% of the total energy dissipation.

5.6. Conclusions

The objective of this experimental study is to find a correlation between change in dissolved oxygen (DO) and important parameters of the H-jump and also to analyse the effect of aeration efficiency on characteristics of H- jump. To achieve this goal, 25 H-jump experiments were performed in the laboratory using five different bed slopes and five different discharges. Measurements of sequent depths, velocity, jump length, water temperature, and DO were taken during all experiments conducted on smooth beds to experimentally investigate DO.

- The H-jump was observed to cause large eddies to form. In order to bring air into the water as it flows, ripples are necessary.
- The amount of DO measured after the H-jump in open channel flows increases rapidly in the first minutes and then decreases after several occurrences.
- As the experimental parameters increase, the SD-Ratio is found to increase as well. As the SD-Ratio increases, the aeration efficiency also increases because the inlet velocity increases due to the increase in discharge and bed slope.
- For the same reason, oxygen transport is significantly influenced by the relative jump length. Aeration efficiency is directly related to the Reynolds number, which is also affected by bed slope and discharge.
- The main element affecting the aeration efficiency during the H-jump is determined to be the upstream Froude number (Fr_1). There are always fully developed H-jumps for different Fr_1. It has been found that the development of the H- jump can increase the efficiency of aeration by increasing the displacement and the bed slope.
- The HJ25-35-H6 experiment achieved the highest velocity drop by about 89%. For an optimal result in increasing the aeration efficiency, it is recommended to proceed according to experiment HJ25-35-H6 while maintaining similar boundary conditions.
- Under the current experimental conditions, the experiment HJ25-35-H6 has a maximum energy dissipation rate per unit width is 90.2%.
- H-jumps in the experimental flume have aeration efficiencies ranging from 9.4% to 34.0%. The results of this experiment show that the most important factors influencing the efficiency of aeration are discharge and bed slope.
- To maintain a healthy DO concentration, wastewater can be re-aerated using these techniques to increase aeration efficiency.

In real-world scenarios, the discharge, bed material, and channel shape may differ from those in our experimental setup. Therefore, when water flow and bed slope are not constant, further research is needed to identify a more distinct and reliable trend that illustrates the kind of variation of these parameters.

References

Agunwamba, J. C., & Ogarekpe, N. M. (2010). The effect of hydraulic jump on the performance of waste stabilization ponds. *Journal of Waste Water Treatment & Analysis*, 1(1), 1000102.

Avery, S. T., & Novak, P. (1978). Oxygen Transfer at Hydraulic Structures. *Journal of the Hydraulics Division*, 104(11), 1521-1540.

Bakhmeteff, B. A., & Matzke, A. E. (1938). The Hydraulic Jump in Sloped Channels. *Transactions of the American Society of Mechanical Engineers*, 60(2), 111-118.

Baylar, A., Emiroglu, M. E., & Bagatur, T. (2006). An experimental investigation of aeration performance in stepped spillways. *Water and Environment Journal*, 20(1), 35-42.

Chanson, H. (1997). Measuring air-water interface area in supercritical open channel flow. *Water Research*, 31(6), 1414-1420.

Chanson, H. (2013). Hydraulics of aerated flows: Qui pro quo?. *Journal of Hydraulic Research*, 51(3), 223-243.

Chanson, H. (1995). Air-water gas transfer at hydraulic jump with partially developed inflow. *Water Research*, 29(10) 2247-2254.

CWC report (2019). A Report on "Effect of Time and Temperature on Do Levels in River Waters"; Ministry of Jal Shakti, Department of Water Resources, River Development & Ganga Rejuvenation, Central Water Commission.

Gameson A.L.H. (1957). Weirs and aeration of rivers, *Journal of the Institution of Water Engineers*, 11(5), 477–490.

Gulliver, J. S., Wilhelms, S. C., & Parkhill, K. L. (1998). Predictive Capabilities in Oxygen Transfer at Hydraulic Structures. *Journal of Hydraulic Engineering*, 124(7), 664-671.

Hoque, A., & Paul, A. K. (2022). Experimental investigation of oxygen transfer efficiency in hydraulic jumps, plunging jets, and plunging breaking waves. *Water Supply*, 22(4), 4320-4333.

Husain, D., Alhamid, A. A., & Negm, A. A. M. (1994). Length and depth of hydraulic jump in sloping channels. *Journal of Hydraulic Research*, 32(6), 899-910.

Kaya, N., & Emiroglu, M. E. (2010). Study of oxygen transfer efficiency at baffled chutes. *Proceedings of the Institution of Civil Engineers - Water Management*, 163(9), 447-456.

Kim, J., Kim, S., & Li, M. J. (2016). Oxygen Transfer and Energy Dissipation by Nappe and Skimming Flow over Stepped Weir Structure. Proceedings of the 2016 International Conference on Education, Management, Computer and Society, pp.1691-1695.

Kucukali, S., & Cokgor, S. (2007). Fuzzy logic model to predict hydraulic jump aeration efficiency. *Proceedings of the Institution of Civil Engineers - Water Management*, 160(4), 225-231.

Kucukali, S., & Cokgor, S. (2009). Energy concept for predicting hydraulic jump aeration efficiency. *Journal of Environmental Engineering*, 135(2), 105-107.

Kucukali, S., & Cokgor, S. (2020). An Experimental Investigation of Reaeration and Energy Dissipation in Hydraulic Jump. In: Kalinowska, M., Mrokowska, M., Rowiński, P. (eds) Recent Trends in Environmental Hydraulics. GeoPlanet: Earth and Planetary Sciences. Springer, Cham. pp. 127-136.

Nakasone, H. (1987). Study of aeration at weirs and cascades. *Journal of Environmental Engineering*, 113(1), 64-81.

Nwajuaku, I. I., & Agunwamba, J. C. (2023). Evaluating the aeration efficiency of hydraulic flume on photo-oxidative disinfection of wastewater. *Results in Engineering*, 20, 101455.

Raikar, R. V. & Kamatagi, P. B. (2015). Use of Hydraulic Phenomena In Enhancement of Dis-solved Oxygen Concentration. *International Journal of Research in Engineering and Technology*, 4(2), 568-574.

Subramanya. K. (2009). Flow in Open Channels. Third Edition. McGraw Hill Education, Delhi, India.

Wilhelms, S. C., Clark, L., Wallace, J. R., Smith, D. R. (1981). Gas transfer in hydraulic jumps. Technical Report E-81-10, U.S. Army Engineer Waterways Experiment Station, CE, Vicksburg, MS.

Witt, A. M., & Gulliver, J. S. (2012). Predicting oxygen transfer efficiency at low-head gated sill structures. *Journal of Hydraulic Research*, 50(5), 521-531.

Zhao, W., Prata, A., Peirson, W., Stuetz, R., & Felder, S. (2022). Reaeration in Supercritical Open Channel Flows: An Experimental Study. *Journal of Hydraulic Engineering*, 148(10), 04022016.

Aeration Efficiency due to Hydraulic Jump on Rough Bed

6.1. Introduction

An important field of fluid mechanics, mainly when considering open-channel flow dynamics, is the investigation of aeration efficiency (E) in connection to hydraulic jumps (H-jumps) on rough beds. The abrupt flow change from super– critical to sub– critical in H-jump causes turbulence, energy dissipation, and frequently the development of a turbulent surface. When an abrupt slope shift occurs, this phenomenon is seen in rivers, spillways, and other water engineering applications. The process of artificially or naturally mixing air with water to improve flow stability, decrease cavitation, or enhance oxygen transfer rate is known as aeration. The turbulent mixing of water during an H-jump results in high air entrainment near the water surface, which can have a big impact on the flow characteristics of the H-jump and overall effectiveness. The construction of any hydraulic structures and the ecological effects can both be significantly impacted by the E or the accurate level to which air is mixed into the water.

In contrast to a smooth bed, the flow characteristics alter significantly when the channel bed is rough due to obstructions, abnormalities, or roughness factors like gravel, boulders, or any developed roughness. The bed roughness has an impact on the character and intensity of H- jump along with flow restriction and energy dissipation. The impact zone of the jump is benefitted from increased turbulence and improved air-water mixing caused by a rough bed. This has significant potential to alter the stability of H-jump, and E. Aeration efficiency on rough– bed depends on flow–velocity and depth at the super-critical zone, jump position, turbulence intensity, and roughness element geometry.

Improving oxygen transmission for aquatic ecosystems, reducing cavitation induced damage to hydraulic structures, and managing sediment transport are the engineering domains where optimising E is essential. Furthermore, the relationship between rough beds and H-jumps, spillways, energy dissipaters, and channels in both natural and artificial watercourses can be better designed. In order to predict the E and establish its relation with jump performance under varied hydraulic conditions is the main objective of this investigation. The jump is formed to occur at five different bed slopes varying from 0° to 6°, five different discharges ranging from 15 lps to 35 lps and two different sloped ramps, using gravel of roughness height of 24.77 mm as bed material.

6.2. Review of Published Research

Although H-jumps in inclined channels have been studied in the past, there is still a large gap in the understanding that changes in bed material size directly that affect the relative

height of the H-jump and subsequently affect energy dissipation. This disparity makes it difficult to design open channels to increase the efficiency of aeration and energy dissipation. Therefore, the purpose of this chapter is to look at H-jump characteristics, particularly relative jump height and E as a function of bed material size.

Oxygen transport properties of several low-head hydraulic structures were investigated. A conceptual explanation of gas transfer physics was provided, and a mathematical explanation of the process was established. Significant physical processes were recognized along with how they affected related variables in gas– transfer equation. The hydraulic circumstances that lead to these physical processes for oxygen transport or reaeration have also been discussed and applied. Field engineers should be able to approximate the oxygen transfer occurring in a particular structure using a mathematical representation of oxygen–transfer for a "generic" type of structure and an awareness of how hydraulic conditions contribute in transferring oxygen (Wilhelms et al. 1993). A study was made of entrapment of air bubbles in H-jumps with partially formed inflow conditions. The turbulent shear region with high air content described the air-water flow, which helped to improve the air-water interface and air-water gas transfer in the H-jump. Based on the behaviour of air and water flow in the turbulent shear zone, a gas transfer model was created. With partially developed inflows, the model allowed predictions of dissolved gas levels and water quality down–stream of an H- jump reported by Chanson and Qiao (1994). Entrapment of air bubbles during partially formed H-jumps with inflow conditions was investigated. The air water flow was categorized by turbulent– shear zone with high air content, which accelerated the air water gas transfer and the air–water interface region in the H-jump. Based on empirical data, the model made it possible in predicting dissolved gas levels and water quality below H-jumps with inflows developed partially (Chanson 1995).

Air entrainment was investigated under falling water droplets in a lab setting, in a laboratory environment, focusing on the drop number ($D=q^2/gh^3$) ranging from 0.0007 to 0.0046 where h is the drop height. An approximate formula was developed for air entrainment rates, particularly at the point where a free jump occurs, with particular attention to the tailwater depth (y_t) and the condition when the jet becomes a parallel stream (y_t^*). The study reported that rates of air entrainment were low during the upper phases of plunging flows. These findings suggested that air entrainment is associated with the drop number and may be useful for designing flow drops, particularly for aeration purposes in contaminated water, as suggested by earlier research (Rajaratnam and Kwan 1996). Twelve equations from the literature were compared with field data of oxygen transfer on four different types of hydraulic structures. Weirs, gated and un-gated spillways, gated type sills, and gated type conduit outlets comprised the hydraulic structures. The Avery and Novak equation was found to offer the most accurate prediction of oxygen transfer for weirs. The most accurate predictions for spillways and gated sills, respectively, come from Wilhelms's equation and Rindels and Gulliver's equation. Due to the wide range of hydraulic conditions observed in these structures, no equation was able to predict oxygen transfer at gated conduit outlets in a manner that would be considered acceptable. The prediction of the transport of other substances from these equations was also discussed. If the Henry's law constant exceeded 10, it appeared that it was at that time possible to forecast the transfer of

a different volatile compound using these oxygen transfer equations for such hydraulic structures (Gulliver et al. 1998).

Several laboratory studies were conducted to measure aeration performance at flow rates between 1 and 4 lps. This study investigated the effects of different weir cross-sectional geometries on aeration performance. It was shown that, on average, the E of the triangular notch exceeded that of the other weirs, and tail–water depth, height for the drop, and discharge were the determining factors for weir aeration (Baylar and Bagatur 2000). Experimental research investigated the interaction of boulder flow in a 0.5 m wide flume related to the self aeration process. The placement of boulders in the flow field has been shown to directly affect changes in local dissolved oxygen (DO) by plume formation, H-jump, and flow acceleration based on size, distribution, and flow conditions. A rapid decrease in peak local aeration efficiency (E_{max}) was observed as the boulder immersion ratio increased above 1. Furthermore, the power function described a constructive relationship between blocking ratio and E_{max} of the boulder(s) (Kucukali 2005). The effect of free over–fall jets from sharp–crested weirs on air entrainment and E was examined. As a consequence of the findings, triangular sharp–crested weirs were reported to have significantly higher air entrainment rates and E values than other kinds of sharp–crested weirs. Triangular sharp–crested weirs could be used to effectively aerate streams, rivers, man-made canals, fish hatcheries and water treatment plants. For the triangular sharp-crested weirs, regression equations were derived that related the air entrainment and E to the angle of the weir, drop height, and discharge. The values calculated from the predicted equations and the measured values agreed quite well (Baylar and Bagatur 2006).

The effect of stepped chutes on E was examined. It was shown that the intense turbulent mixing coupled with significant air bubble– entrainment made stepped– chutes extremely effective at transferring oxygen and that this benefit intensifies in the nappe flow regime. An analytical correlation was created to forecast the E of each step in the nappe flow regime. The values calculated from the prediction equation and the measured E values of a single step agree perfectly. Using this empirical correlation, the E of a stepped chute design could be optimized (Baylar et al. 2007). A hybrid theoretical and experimental method was used to explore the problem of bed friction influence on the rigidity of stationary H-jump in rectangular shaped channel with upward slope. A thorough description of the experimental protocol was followed, and the results were compared with theoretical estimations. At least for smaller bed slopes, the proposed stability criterion was shown to accurately predict both steady and unsteady jump performance for both smooth and rough wall flow. Moreover, it was found that for both hydraulically smooth and completely rough wall flow, the theoretical prediction and experimental findings were compared very well. (Defina et al. 2008). In another study, an experimental flume was used to examine the boulder-flow interaction related to the self-aeration process. Using Reynolds numbers ranging from 5×10^3 to 5×10^4, experiments were conducted with three different boulder layouts and four different relative boulder submergences. The E_{max} and flow resistance tend to drop down quickly as the barriers are submerged in water. Moreover, there exists a positive correlation between the blockage ratio of the boulder(s) and E_{max}. The head loss appears to be represented by the blockage ratio, indicating a potential relationship between energy dissipation and E (Kucukali and Cokgor 2008).

The impact of discharge values and tailwater depths on E of stepped and smooth spillways modelled in a laboratory was examined. Tail water depth variations had a greater than 100% impact on E and DO transfer rates, which led to super-saturated DO content. Weir aeration was significantly impacted by tailwater depth. The depth of the tailwater boosted E. According to the study, in both the flat and stepped spillways, the concentration of DO increased as discharge increased (Aras and Berkun 2012). A study was done on the oxygen saturation contribution from three stepped spillway and smooth spillway structures at different flow rates. According to the tests, for all flowrate scenarios that were examined, stepped spillways offered superior E over smooth spillways. Furthermore, it was noted that the E of stepped spillways differed based on the stream flow regime and flow rate. In the nappe flow regime, the most aeration occurred, according to the results. This was due to the fact that turbulence and contact time are higher in nappe flow regime because aeration occurs at every step through the employment of a plunging jet and H-jump. Aeration efficiency declined within the same system as flow rates increased and as flow regimes varied (Sari et al. 2014). A dispersed aeration mechanism with interchangeable perforated plates was installed in a laboratory setup and airflow was injected through the perforated plates to disperse bubbles of various sizes at various air flow rates. The effectiveness of aeration was tested using four scattered aeration devices that were installed non-invasively on a pipeline wall. The volumetric mass transfer, rate of oxygen transfer, oxygen transfer efficiency, power consumption for air injection, and E were measured after the aeration devices were tested for various void fractions (Bunea et al. 2017). Another work aimed to provide a comprehensive summary of state–of–the–art concerning H-jump qualities across a broad spectrum of boundary– conditions and geometric– configurations. The investigation included particular attention to how relative– roughness and bed– slope affect the sequent depth– ratio (SDR), as well as how air entrainment affects effective depth estimate. A comparison and discussion of some forecasting relationships put out by other authors was performed (Palermo and Pagliara 2017).

The dynamics of the bubble size distribution across bubble height columns at various air–flow rates were investigated through experiments using both tap water plus solutions that replicate the viscosity of activated sludge at various sludge concentrations to maximize oxygen transport and therefore save energy. The findings indicated that because bubble size was influenced by hydrodynamics and liquid viscosity, it was quite dynamic in both space and time. As a result, oxygen transfer was similarly dynamic in nature. As an alternative, a modelling technique based on observations of the size of bubble dispersion dynamics was presented to ascertain the K_L locally (Amaral et al. 2018).

Research was done to find out how block carpet affects the scouring phenomenon, H-jump, and changes in the hydro-environmental parameters. The E produced by the H-jump in flows over block carpet was also examined in the study. Upstream of block carpet, along it (toe, mid, and heel), and following the H-jump in channel bed, DO was measured and examined. The flow reached a maximum E of 0.181 in the measured slope ranges like 0.2, 0.25, and 0.3 and block–carpet material, according to the data. The H-jump characteristics were observed for two sediment sizes for channel bed and block carpets with varying slopes (Rawat et al. 2022). Another study reported an experimental assessment of the DO efficiency in block–ramps that were bonded to large–scale granular materials with

various arrangement patterns and different bed slopes. Based on a comparative analysis of the data, block ramps with a 1:3 slope and large–scale roughness improved the DO efficiency by over 20% over identical smooth block ramps for both free H-jump and ramp H-jump. Block–ramps with high surface roughness had DO efficiency of 3 and 0.19 for free H-jump and ramp H-jump, respectively, when their slope was reduced to 0.20. However, the comparable DO efficiency of such block–ramps with a 1:7 slope was 19 and 32%, respectively (Varaki et al. 2022).

Various hydraulic structures including venturi flumes, weirs, conduits, stepped channels and their DO dissolving performance were explored in a review study. After completing the literature research, an artificial– neural– network (ANN) model was established. The standard aeration efficiency value in venturi aeration increased rapidly with the number of air holes in each increasing throat length and angle of diverging and converging parts. It was found in weir aeration that triangular notch weirs yielded the best air entrainment outcomes. The tailwater depth (T_w) and discharge (Q) parameters used in model development demonstrated that Q has a greater influence than T_w. The most important parameter in E_{20} was Q, followed by the number of steps, according to the sensitivity analysis. High-head gated conduits and bubble size were the most crucial parameters for improved aeration based on data from the literature about conduit structure and bubble diffusers. Oxygen–transfer–efficiency (OTE) in jet– diffusers was estimated using ANN. Analysis of sensitivity revealed that the input variable "velocity" is very sensitive to OTE (Puri et al. 2023).

A complex relationship was investigated between the fundamental characteristics of H-jumps and the size of the bed material, offering information on the relative H-jump length, H-jump height, and H-jump energy efficiency. An open–channel flow with four bed– slopes from zero degree to six degrees and three roughness–heights from 10mm to 30mm was used for the investigation. During the research, Fr varied from 2.3 to 8.85 and Re varied from 5450 to 25500. Correlations for various H-jump characteristics were determined in channels with a rough bed slope. The study looked at the combined effects of bed slope and roughness. It was found that when the bed slope increased from zero to six degrees, the relative jump length decreased by 23.1%, while the relative jump height and H-jump efficiency increased by 19.4% and 8.4%, respectively. The relative H-jump length decreased by 29.1% when the bed roughness increased from 0 to 30 mm, but the relative jump height and H-jump efficiency increased by 14.2 and 21.1%, respectively (Gupta and Dwivedi 2024).

H-jumps in inclined channels have been studied in the past, but a thorough evaluation of the direct effects of bed material on energy dissipation through H-jumps and subsequently its impact on E is still clearly lacking. Their resulting impact on E is noticeably absent, despite the fact that some studies have addressed the effects of bed material on H-jumps. Currently, insufficient information is available on the optimal discharge and bed stiffness for H-jumps in coarse-bed sloping channels to maximize energy dissipation and E. This disparity makes it difficult to design channels for better E and energy dissipation. The purpose of this research is to investigate the effects of bed material on H-jump characteristics, specifically focusing on SD-Ratio, energy dissipation, and E.

6.3. Experimental Setup for Rough Bed

In systems with rapidly moving water, H-jumps are essential for dissipating excess energy. These dissipations are crucial in hydraulic engineering developments because they assist in stopping erosion and damage downstream. The turbulence nature of the H-jump is responsible for this. In comparison to a smooth bed profile, more turbulence occurs in a rough bed surface. The size of the bed material has an impact on the energy dissipation of the H-jump. Due to greater turbulence, coarser material may improve energy dissipation and result in more efficient energy loss, while finer material may not do so as well. Size of bed material can affect the stability of the H-jump. While larger particles may cause more abnormalities and oscillations in the jump, finer material can result in a steadier jump.

Descriptive diagrams of typical H-jumps on a straight channel for both a horizontal and a sloping rough bed (with bed slope θ) are shown in Fig. 6.1. In this illustration there are two sections, Section– 1 is toe of the H-jump and section– 2 is the end of H-jump. In section– 1, velocity of super–critical flow is V_1 and the flow depth is y_1. Similarly, in section– 2, velocity of sub–critical flow is V_2 and flow depth is y_2.

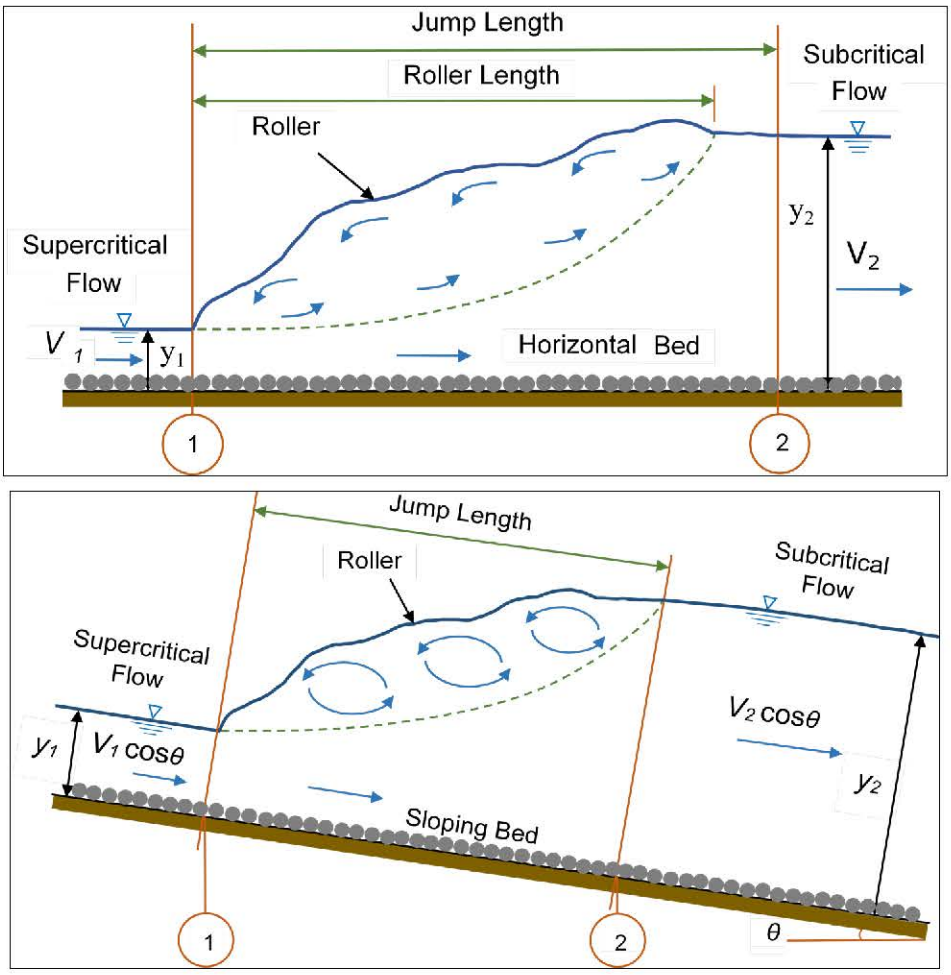

Fig. 6.1. Flow-wise sectional outlines of H-jump profiles developing over (a) horizontal rough– bed, and (b) sloping rough– bed.

The experimental study was conducted utilising a rectangular channel flow test setup in the Fluvial Hydraulics Laboratory of School of Water Resources Engineering, Jadavpur University (Fig. 6.2). It is possible for the channel flume to reach both horizontal and sloping channels. The dimensions, inflow outflow mechanism, and tilting characteristics of the experimental flume are already discussed in the previous section (Section 5.3).

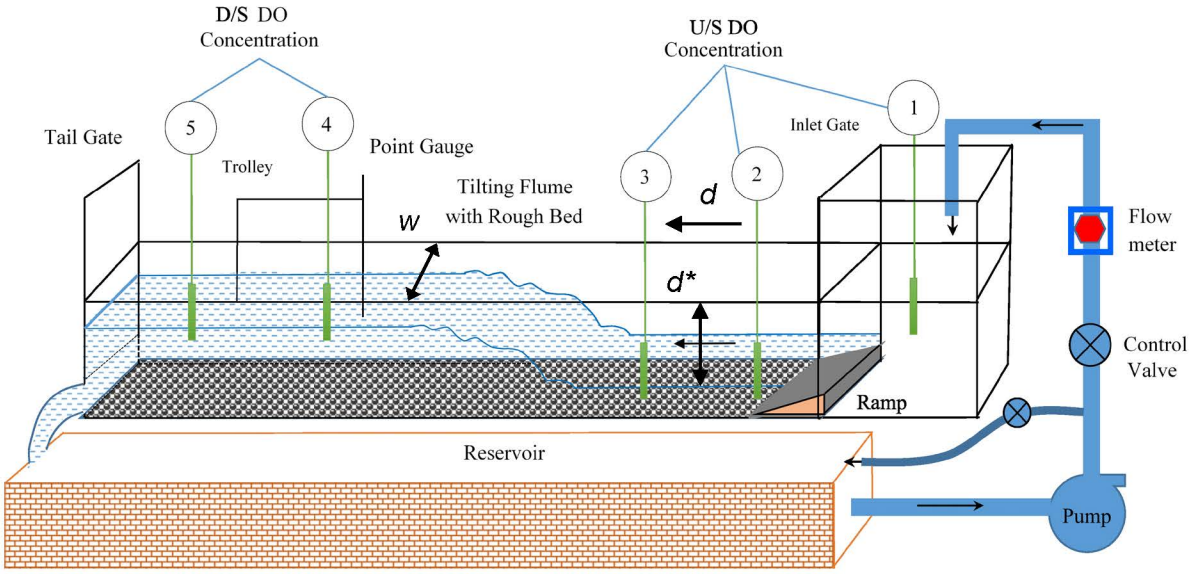

Fig. 6.2. Diagrammatic illustration of the experimental setup with rough bed and ramp arrangement highlighting DO measuring points.

The bed has been paved with gravel to provide the required roughness. To prevent corrosion and make it easier to place gravel on the steel bed, a rectangular tray constructed of acrylic perspex sheet measuring 5.0 × 0.36 × 0.06 m×m×m in length× width× thickness is utilised (Fig. 6.3).

Fig. 6.3. Preparation of the arrangement with gravel bed materials.

The gravel was fixed on the perspex sheet with the help of glue. Then the gravel arranged acrylic perspex sheet was fitted on the experimental flume bed (Fig. 6.4). In this present experimental investigation five different bed slopes and five distinct discharges were selected.

Fig. 6.4. Experimental flume arrangement with gravel bed materials.

In this new gravel bed profile, the roughness height was measured using a laser distance sensor (Leica DISTOTM D110) with a measurement accuracy of ±1.5 mm. The sensor was clamped on the moving carriage of the point gauge and measured the longitudinal distance of the gravel bed at transverse intervals of 2 cm (Fig. 6.5). Then, from these data series, the roughness height in this setup was calculated as 24.77 mm.

Fig. 6.5. Roughness height measurement using laser distance sensor.

In this medium gravelled bed, for minimum discharge and minimum slope, the jump was not properly developed. A ramp was used in this arrangement to overcome this

difference. The ramp was installed just before the entrance gate was placed. The inflowing water thus reached the pre-jump section through this ramp (Figs. 6.6-6.7). These two ramps were used for this experimental work, one was in the ratio of 1:3 in V:H and the other was in the ratio of 1:4. The vertical height of both ramps was the same. The opening of the entrance gate was the same in all experiments.

Fig. 6.6. Ramp fitted at the inlet for jump development.

Fig. 6.7. Ramp with gravelled bed arrangement for the experimentation.

Dissolved oxygen and H-jump parameters were measured several times with varying discharges, bed slopes, and ramp slopes. The jump profiles, inlet flow and DO measuring instruments used for these experiments are discussed in the previous section 5.3. Rough beds and a chain pulley system for tilting the rectangular experimental flume were used for this research. The H-jump in this study was created experimentally by adjusting the tailgate to develop submerged and forced H-jumps.

6.4. Results and Discussion

For this study, a total 50 numbers of laboratory experiments were conducted in two different ramp setups with different discharges and bed slopes. Total 25 numbers experiments were conducted using a ramp of 1:3 slope (Table 6.1 and Fig. 6.8) and another 25 experiments were carried out using a ramp of 1:4 slope (Table 6.2) to assess the aeration

efficiency (E) and jump characteristics for a set of discharges and bed gradients. Ramps were used to gain the desired velocity to form the jump in the rough bed. Five different flow rates as 15 l/s, 20 l/s, 25 l/s, 30 l/s, and 35 l/s were selected for the experiments and five different bed slopes were designated as Horizontal, 1.5°, 3°, 4.5°, and 6° variants.

The downstream water surface was repetitively rippled due to turbulence effect of the H-jump and the rough–bed profile. For further calculation to establish the depth at a certain location, the highest and lowest levels of these undulations were averaged. To solve the E by H-jumps, Eq. 5.1 is used, which is already discussed in the previous section 5.3. First, E is calculated using the Eq. 5.1 and then for standardization at 20°C temperature, this E is converted to E_{20} with the help of Eqs. 5.2 and 5.3 as described in chapter 5.3.

a) Ramp setup 1:3 slope

Table 6.1. Change in velocity ($\Delta V_{1\text{-}2}$) after H-jumps using ramp slope 1:3 at different experimental bed slopes and discharges.

Experiment number	Bed slope (Degree)	Discharge (lps)	Decrease in velocity after the jump, $\Delta V_{1\text{-}2}$ (%)
HJ1-RB	Horizontal	15	67.48
HJ2-RB	Horizontal	20	68.96
HJ3-RB	Horizontal	25	74.96
HJ4-RB	Horizontal	30	81.75
HJ5-RB	Horizontal	35	83.68
HJ6-RB	1.5°	15	77.60
HJ7-RB	1.5°	20	79.88
HJ8-RB	1.5°	25	80.34
HJ9-RB	1.5°	30	84.52
HJ10-RB	1.5°	35	86.74
HJ11-RB	3°	15	82.69
HJ12-RB	3°	20	84.09
HJ13-RB	3°	25	85.25
HJ14-RB	3°	30	86.71
HJ15-RB	3°	35	88.31
HJ16-RB	4.5°	15	83.59
HJ17-RB	4.5°	20	84.59
HJ18-RB	4.5°	25	86.76
HJ19-RB	4.5°	30	87.39
HJ20-RB	4.5°	35	89.03
HJ21-RB	6°	15	85.95
HJ22-RB	6°	20	86.67
HJ23-RB	6°	25	87.81
HJ24-RB	6°	30	88.43
HJ25-RB	6°	35	89.35

The inlet Froude number (Fr_1) varied from 2.24 to 8.33, while the flow depth before the jump (y_1) varied from 2.3 to 3.6 cm. Before the jump, the mean inlet velocity (V_1) was 2.42 m/s. After the development of the H-jump, choppy water was formed, and the post-jump velocity (V_2) was found to be significantly reduced. The patterns of the velocity percentage fluctuation, $\Delta V_{1\text{-}2} = (V_1 - V_2)/V_1$, before and after the jump are shown in Table 6.1. As the discharge and bed slope increase, the $\Delta V_{1\text{-}2}$ for this ramp setting increases. The Fr_1 also increases with the escalation of discharge as the inlet gate opening was identical for each experiment. For each discharge, the Fr_1 also improves with the development of the bed slope. It can be noticed from Table 6.1 that the minimum drop in velocity occurred in the horizontal slope of the bed with a flow of 15 lps and the maximum drop in velocity occurred in the slope of 6° with a flow of 35 lps. Therefore, for creating a hydraulic structure and to reduce the scour downstream for an advanced velocity drop an H-jump on a 6° bed slope with a 35 lps discharge can be produced.

(a)

(b)

(c)

(d)

(e)

Fig. 6.8. Jumps developed using ramp slope 1:3 under several experimental circumstances (a) discharge 15 lps, bed slope horizontal; (b) discharge 20 lps, bed slope 1.5°; (c) discharge 25 lps, bed slope 3°; (d) discharge 30 lps, bed slope 4.5°; (e) discharge 35 lps, bed slope 6°.

The aeration efficiency of the water is observed to fluctuate with the SD-Ratio in the H-jump. Here, a plot of the E_{20} with y_2/y_1, with respect to discharge for different bed slopes, is shown in Fig. 6.9(a) and then with respect to bed slope for different discharges, shown in Fig. 6.9(b). As the Fr_1 is increased with the increase of bed slopes and discharges, the SD-Ratio is also increased with these parameters. The improvement of the SD-Ratio indicates that more turbulence is created and as a result more air entrainment is occurred.

Therefore, with the increasing bed slope and discharge, the aeration efficiency and the SD-Ratio are observed to increase (Fig. 6.8). The improvement trend of E_{20} is almost similar for 15 lps and 20 lps. Also, a similar pattern is observed for 25 lps and 35 lps as shown in Fig. 6.9(a). Here, the tendency of E_{20} increase is almost identical for the 0° and 6° bed slopes, and also of a similar shape for the 3° and 4.5° bed slopes.

The average flow velocity is used to calculate Fr, which establishes whether a flow is super–critical or sub–critical. Initially, E_{20} with Fr_1 is plotted with respect to bed slopes for different discharges (Fig. 6.10a), and then with respect to discharges for different bed slopes (Fig. 6.10b). As the inlet velocity is increased for stepper slope and higher discharge, the Fr_1 and the E_{20} are also increased for these parameters. The change of E_{20} with the Fr_1 is plotted in Fig. 6.10. With respect to the Fr_1 the E_{20} improvement pattern is almost identical for 25 lps and 30 lps discharge and also for the 15 lps and 20 lps discharge, as shown in Fig. 6.10a. Similarly, in Fig. 6.10b, it is shown that the E_{20} improvement shape is likely similar to 1.5° and 3° bed slopes, and similar to the 4.5° and 6° bed slopes.

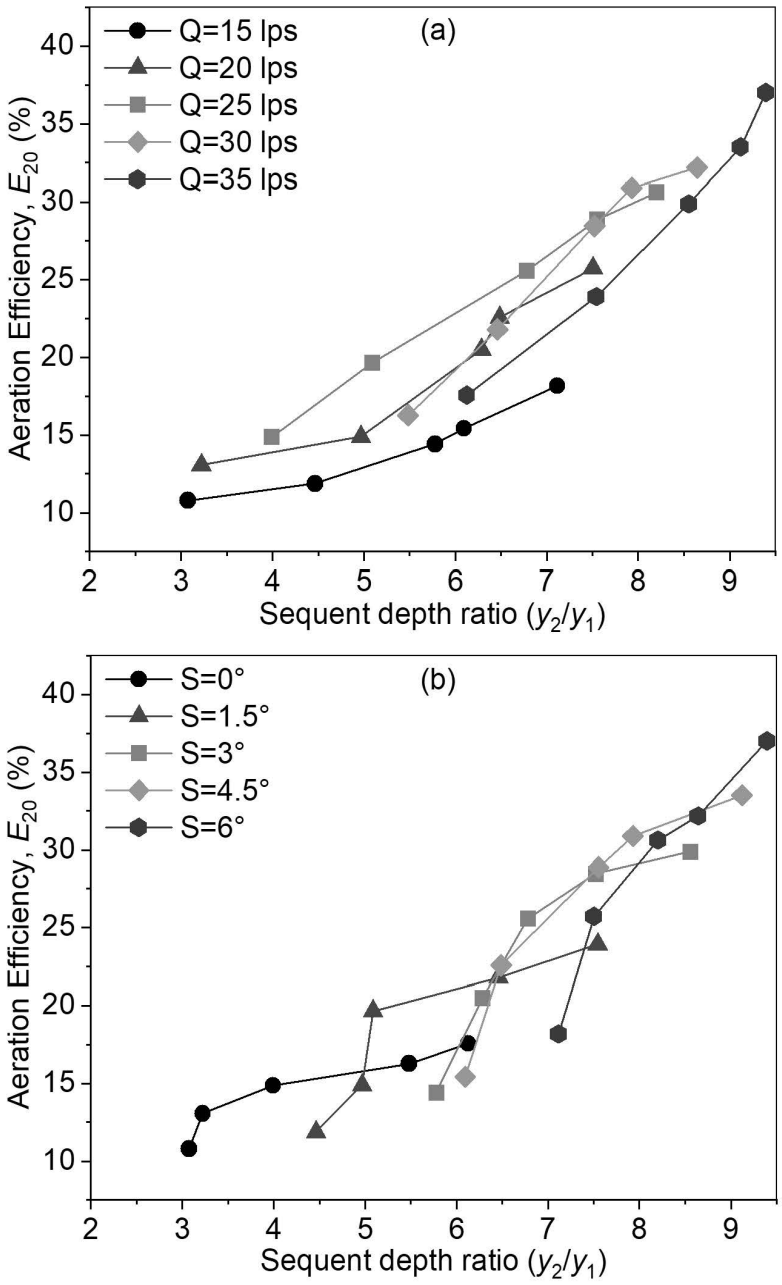

Fig. 6.9. Deviation of aeration efficiency during H-jumps using 1:3 ramp slope for different SD-Ratios for different (a) flows, and (b) bed slopes.

The correlation between the aeration– efficiency through H-jump and relative H-jump length (L_j/y_1) for various bed slopes and discharges, where the aeration efficiency is plotted along the ordinate and the relative jump length is plotted along the abscissa, shown in Fig 6.11. In this rough bed arrangement, through the H-jump, it is witnessed that the aeration efficiency strongly depends on the relative H-jump length (L_j/y_1). Along with the E_{20} improvement the relative H-jump length is also improved with improvement of bed stiffness and discharge. The E_{20} improvement pattern is near to similar for 15 lps and 35 lps discharges, and similar for 20 lps and 30 lps discharges, as shown in Fig 6.11a. Similarly, the E_{20} improvement pattern is identical for the 3° and 4.5° bed slopes, as in Fig 6.11b. The

maximum increase in aeration efficiency is found for the greater discharge and upper bed slope.

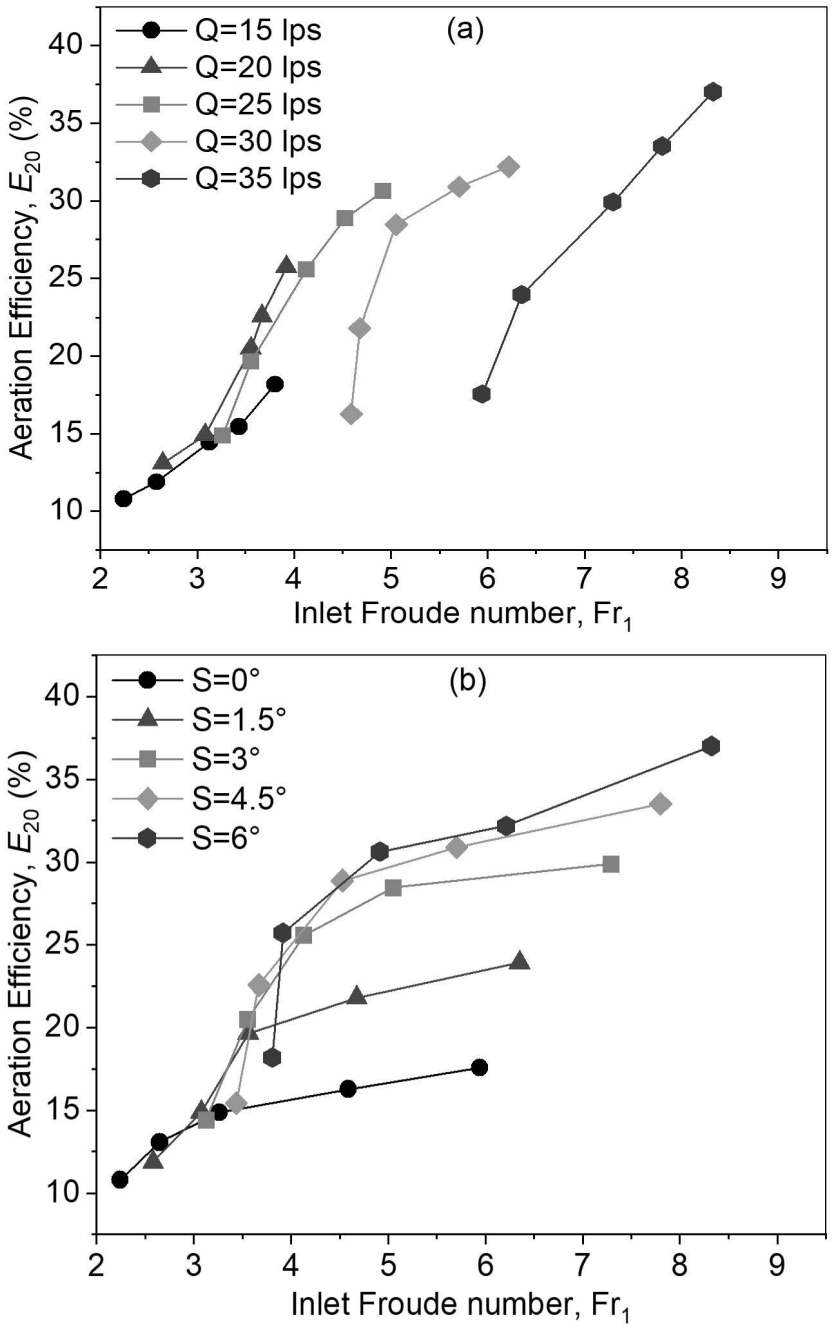

Fig. 6.10. Deviation of aeration efficiency during H-jumps using 1:3 ramp slope for different inlet Froude numbers for (a) different discharges and (b) different bed slopes.

In the present investigation on rough bed configuration, the Re is calculated at pre-jump conditions as an important non-dimensional parameter. Increasing the input discharge also increases the Re, which can range from about 51,000 to 120,000 for any given bed slope.

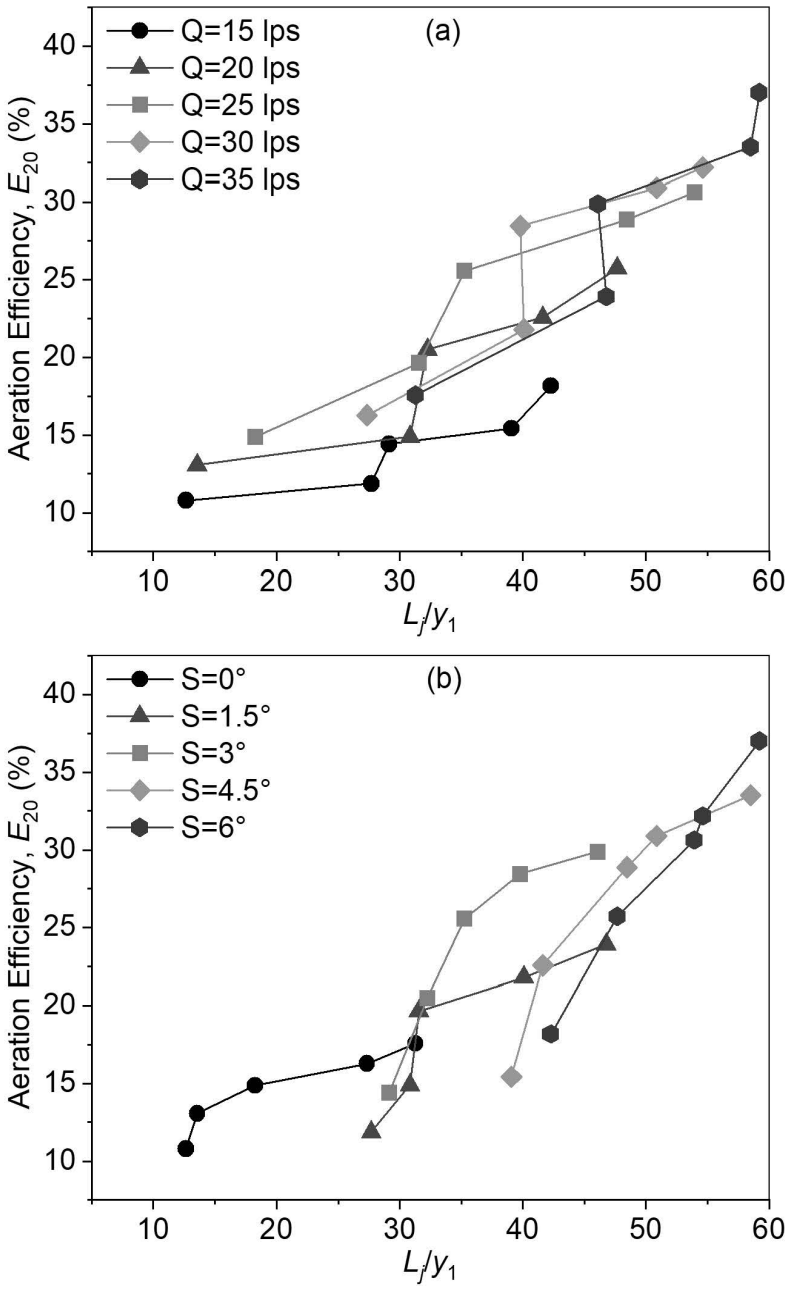

Fig. 6.11. Deviation of aeration efficiency during H-jumps using 1:3 ramp slope for different L_j/y_1 for (a) different discharges and (b) different bed slopes.

A comparison of E_{20} as a function of the Re for different bed slopes and different discharges is prepared (Fig. 6.12). As Re is dependent on inlet velocity, with the increase in discharge this parameter also varies. Additionally, with increased discharge, the E_{20} also improves. But with higher discharge, this alteration of Reynolds number with respect to E_{20} does not follow any proper trend (Fig. 6.12a), additional experiments with varying bed roughness are required to conclude a trend of improvement. In Fig. 6.12b, it is shown that the pattern of increasing Reynolds number with E_{20} is almost identical for improvement of bed stiffness except for the relational value of 6° bed slope and 30 lps discharge.

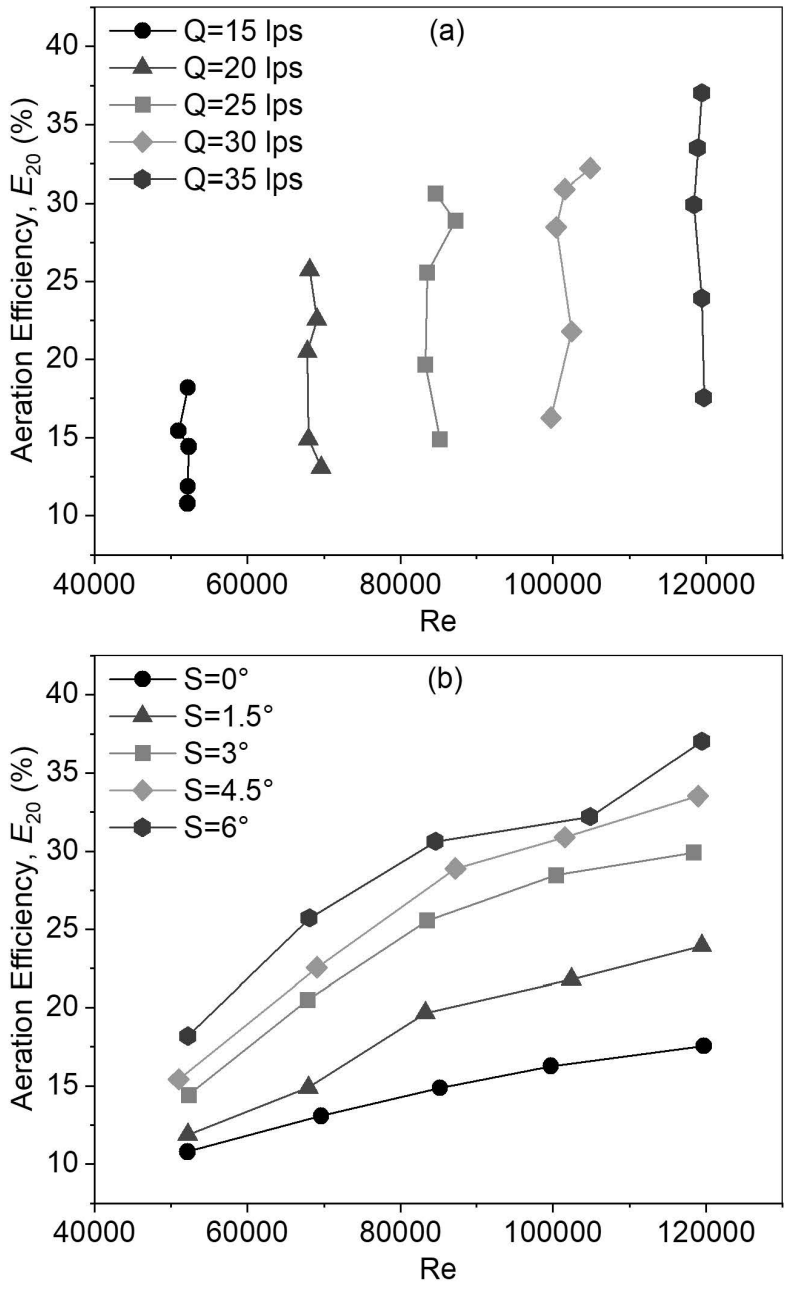

Fig. 6.12. Deviation of aeration efficiency during H-jumps using 1:3 ramp slope for different Reynolds numbers for (a) different flows, and (b) different bed slopes.

The energy–dissipation rate per unit width ($\Delta E_{loss}/H_1$) is plotted along the x-axis and the percentage of aeration efficiency (E_{20}) is plotted along y-axis, as shown in Fig. 6.13. The energy loss is a key factor of H-jump. In this rough bed experimental arrangement, the discharge and the bed slope have an enormous impact on E_{20}, at the same time these parameters have an influence on energy loss. With the variations in discharges and bed slopes the minimum $\Delta E_{loss}/H_1$ is found 0.15 and the maximum is found 0.98. With increasing bed slopes and discharges, the $\Delta E_{loss}/H_1$ and the E_{20} are also improved but this enhancement pattern is not identical for all the cases, especially for higher discharge and higher bed slopes.

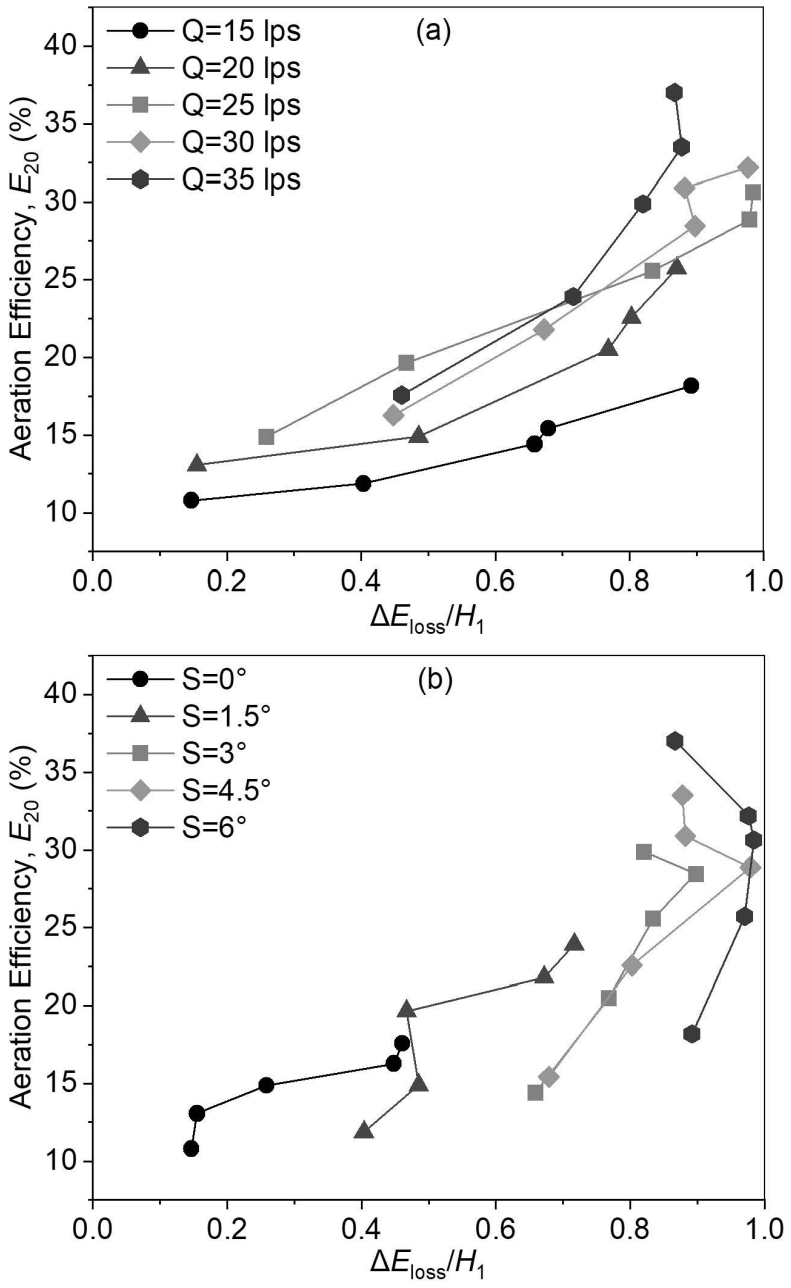

Fig. 6.13. Deviation of aeration efficiency during H-jumps using 1:3 ramp slope for different energy dissipation rates per unit width for (a) different discharges and (b) different bed slopes.

The bed slope is plotted along *x*-axis and the percentage of aeration efficiency at 20°C is plotted along *y*-axis, as depicted in Fig. 6.14(a). Again, the discharge is plotted along the abscissa and the percentage of aeration efficiency at 20°C is plotted along the ordinate, as shown in Fig. 6.14(b). As the bed slope and the discharge are increased the super-critical velocity is also increased, there is more turbulence and more air entrainment occurs. It is clearly visible from these two plots that aeration efficiency is increased with the enhancement of discharge and bed stiffness. As shown in Fig. 6.14(a), the improvement trend is almost identical for the 15 lps and 20 lps discharges and also the same for the 25

lps, 30 lps, and 35 lps discharges. The pattern of the plot is nearly similar for the 1.5° and 4.5° bed slopes, as well as for the 0° and 3° bed slopes [Fig. 6.14(b)].

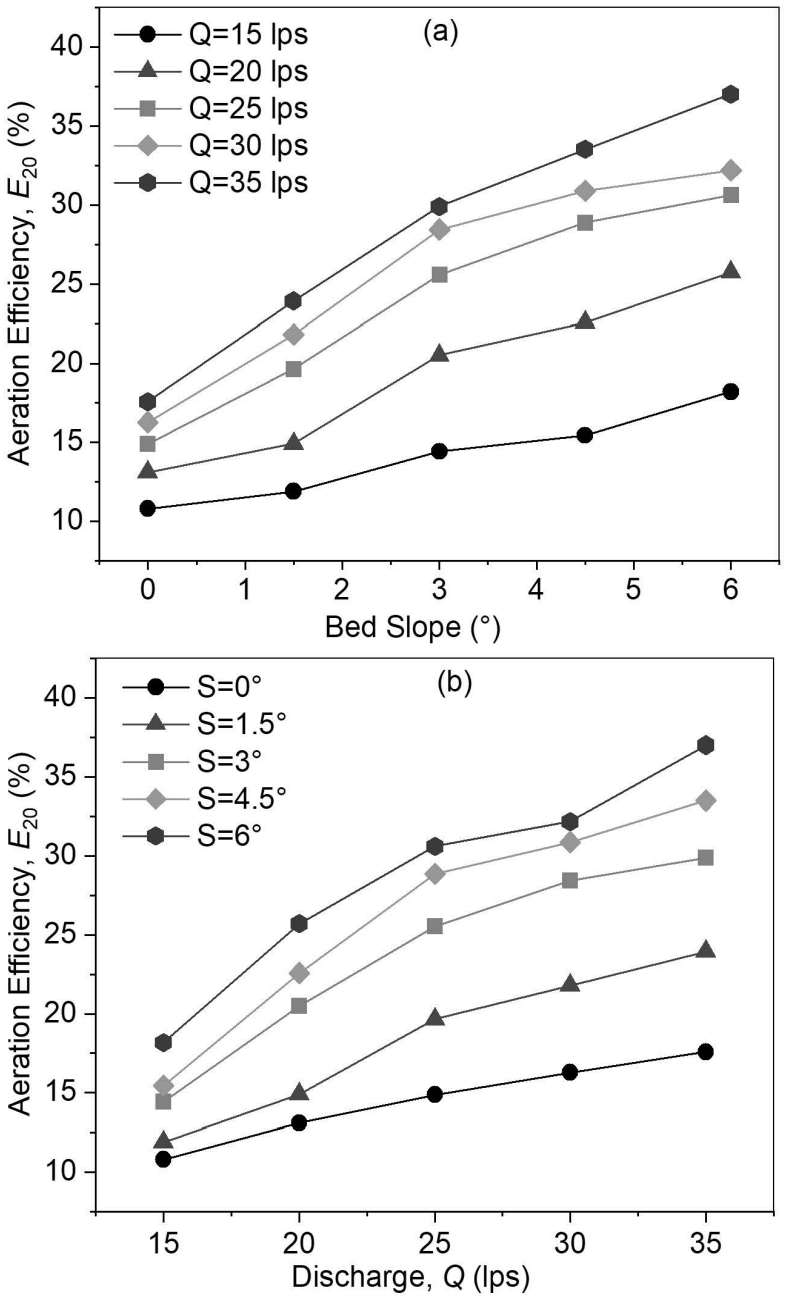

Fig. 6.14. Deviation of aeration efficiency during H-jumps using 1:3 ramp slope for (a) different discharges and (b) different bed slopes.

For 1.5° to 6° bed slopes, the aeration efficiency at 20°C is found to increase from 10.8% to 18.2% at 15 lps discharge. In addition, it is found that when the discharge is increased for a particular bed slope, such as 6°, the aeration efficiency at 20°C increases from 18.2% to 37.0% for the discharge of minimum to maximum. Therefore, for better E_{20} enhancement, in this rough bed arrangement, the 6° bed slope with 35 lps discharge has to be selected.

b) Ramp setup 1:4 slope

25 experiments were carried out using a ramp of 1:4 slope (Table 6.2) to assess the aeration efficiency (E) and jump characteristics for a set of discharges and bed gradients (Fig. 6.15). In this 1:4 ramp arrangement, the inlet Froude number ranged from 2.26 to 8.40, while the super-critical flow depths varied between 2.28 and 2.90 cm. The average inlet velocity (V_1) at the pre-jump position was 2.44 m/s. After the formation of the H-jump, turbulent flow occurs and the post-jump velocity (V_2) is drastically reduced. The velocity percentage variation, $\Delta V_{1\text{-}2} = (V_1 - V_2)/V_1$, before and after the jump is presented in Table 6.2.

Table 6.2. Change in velocity ($\Delta V_{1\text{-}2}$) after H-jumps using ramp slope 1:4 at different experimental bed slopes and discharges.

Experiment Number	Bed slope (Degree)	Discharge (lps)	Decrease in velocity after the jump, $\Delta V_{1\text{-}2}$ (%)
HJ26-RB	Horizontal	15	68.25
HJ27-RB	Horizontal	20	69.68
HJ28-RB	Horizontal	25	75.01
HJ29-RB	Horizontal	30	81.85
HJ30-RB	Horizontal	35	83.76
HJ31-RB	1.5°	15	78.03
HJ32-RB	1.5°	20	80.37
HJ33-RB	1.5°	25	80.53
HJ34-RB	1.5°	30	84.78
HJ35-RB	1.5°	35	86.89
HJ36-RB	3°	15	82.88
HJ37-RB	3°	20	84.18
HJ38-RB	3°	25	85.33
HJ39-RB	3°	30	86.79
HJ40-RB	3°	35	88.37
HJ41-RB	4.5°	15	83.65
HJ42-RB	4.5°	20	84.67
HJ43-RB	4.5°	25	86.81
HJ44-RB	4.5°	30	87.41
HJ45-RB	4.5°	35	89.89
HJ46-RB	6°	15	86.09
HJ47-RB	6°	20	86.85
HJ48-RB	6°	25	87.87
HJ49-RB	6°	30	88.49
HJ50-RB	6°	35	89.40

As both discharge and bed slope increase, the $\Delta V_{1\text{-}2}$ also increases for this ramp setup. The inlet Froude number (Fr_1) also increases with higher discharge, as the inlet gate opening is kept constant in all experiments. As a result, the inlet depth, as well as the relative depth (d^*/w), are almost identical for each experiment. Furthermore, for each discharge, the inlet Froude number also increases as the bed stiffness is increased. Table 6.2 clearly shows that the smallest velocity drop occurs with a horizontal bed slope at a 15 lps discharge, while the largest velocity drop is observed with a 6° bed slope at a 35 lps discharge. Therefore, for creating a hydraulic structure that minimizes downstream scour, erosion and endorses a significant velocity drop, an H-jump should be implemented on a 6° bed slope with a 35 lps discharge.

(a)

(b)

(c)

(d)

(e)

Fig. 6.15. Jump developed using ramp slope 1:4 under several experimental circumstances (a) discharge 35 lps, bed slope horizontal; (b) discharge 30 lps, bed slope 1.5°; (c) discharge 25 lps, bed slope 3°; (d) discharge 20 lps, bed slope 4.5°; (e) discharge 30 lps, bed slope 6°.

During the H-jump, it was found that the aeration efficiency (E_{20}) of water varied with the SD-Ratio (y_2/y_1). As bed slope and discharge increased, it was also observed that the aeration efficiency and the SD-Ratio increased, as shown in Fig. 6.16.

In Fig. 6.16(a), the improvement pattern is nearly similar for the 20 lps and 30 lps discharge. Similarly, the growth shape is almost identical for the 1.5° and 4.5° bed slope, as shown in Fig. 6.16(b). In Figs. 6.16(a-b), for higher discharge and bed slope the trend of the plot is not properly followed as for the highest discharge the jump profile is not fully developed in this investigational setup for the maximum bed slope.

In this rough bed experimental arrangement, the inlet Froude number (Fr_1) is an important jump parameter, so to identify its relation with aeration efficiency (E_{20}) a data series is plotted. The independent parameter Fr_1 is plotted along abscissa and the dependent parameter E_{20} is plotted along ordinate, Fig. 6.17.

In Fig. 6.17(a), the data series is plotted for an individual discharge with changed bed slopes and found that the E_{20} increase shape is nearly similar for 25 lps and 30 lps discharge. Again the data series is plotted for an individual bed slope with changed discharges and found that the E_{20} growth profile is closely similar for 3° and 4.5° bed slope, as in Fig. 6.17(b).

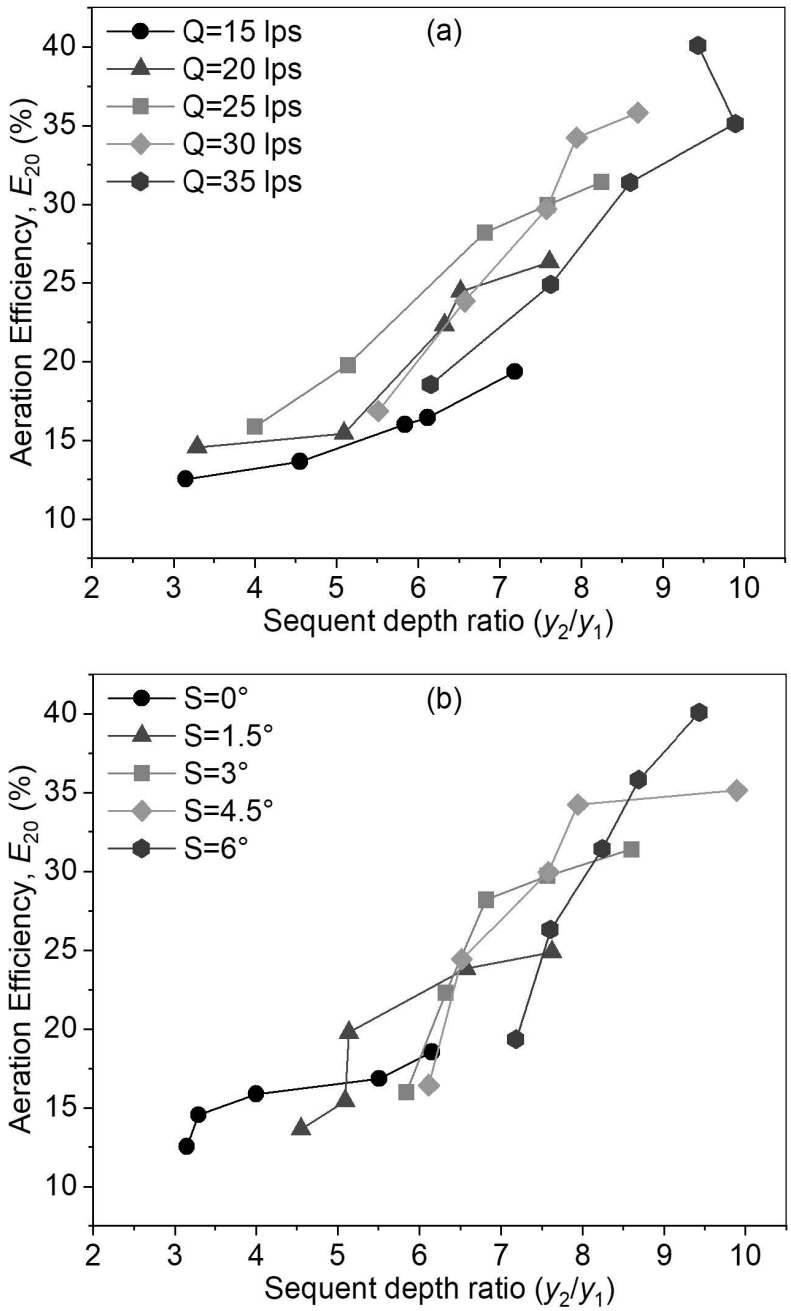

Fig. 6.16. Deviation of aeration efficiency during H-jumps using 1:4 ramp slope for different SD-Ratios for (a) different flows, and (b) different bed– slopes.

The relationship between the aeration efficiency (E_{20}) and the relative H-jump length (L_j/y_1) in the H-jump on rough– bed for different bed slopes and discharges where the relative jump length is plotted along the abscissa and aeration efficiency is plotted along the ordinate, Fig. 6.18. The relative jump length is a crucial parameter for the formation of the turbulence as it is dependent on the Fr_1. More turbulence indicates that more air water interaction occurred. Therefore, with the improvement of L_j/y_1 the E_{20} is also increased.

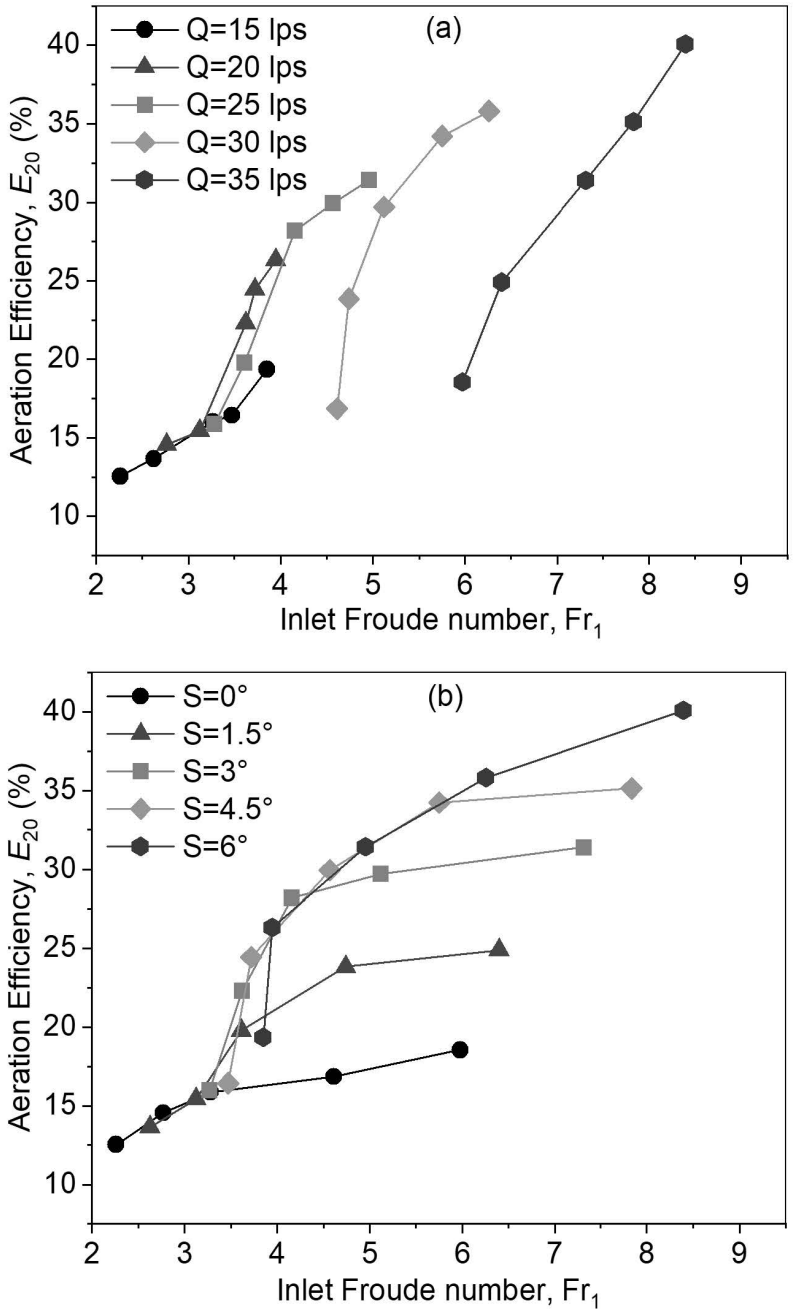

Fig. 6.17. Deviation of aeration efficiency during H-jumps using 1:4 ramp slope for different inlet Froude numbers for (a) different flows, and (b) different bed slopes.

In Fig. 6.18(a), it is visible that the E_{20} increment shape is nearly similar for 15 lps and 25 lps discharge. In another comparison mode, Fig. 6.18(b), it is observed that the E_{20} increment nature is almost similar for the 4.5° and 6° bed slopes.

In this rough bed and 1:4 ramp arrangement, the relationship between Re and aeration– efficiency (E_{20}) is plotted, in Fig. 6.19. In this typical experimental arrangement, the Reynolds number ranges between 47000 to 122000. In the aeration process, laminar flow is habitually not ideal because it limits the interaction between air and water. The oxygen transfer rate is low due to poor turbulence, reducing the efficiency of the aeration process.

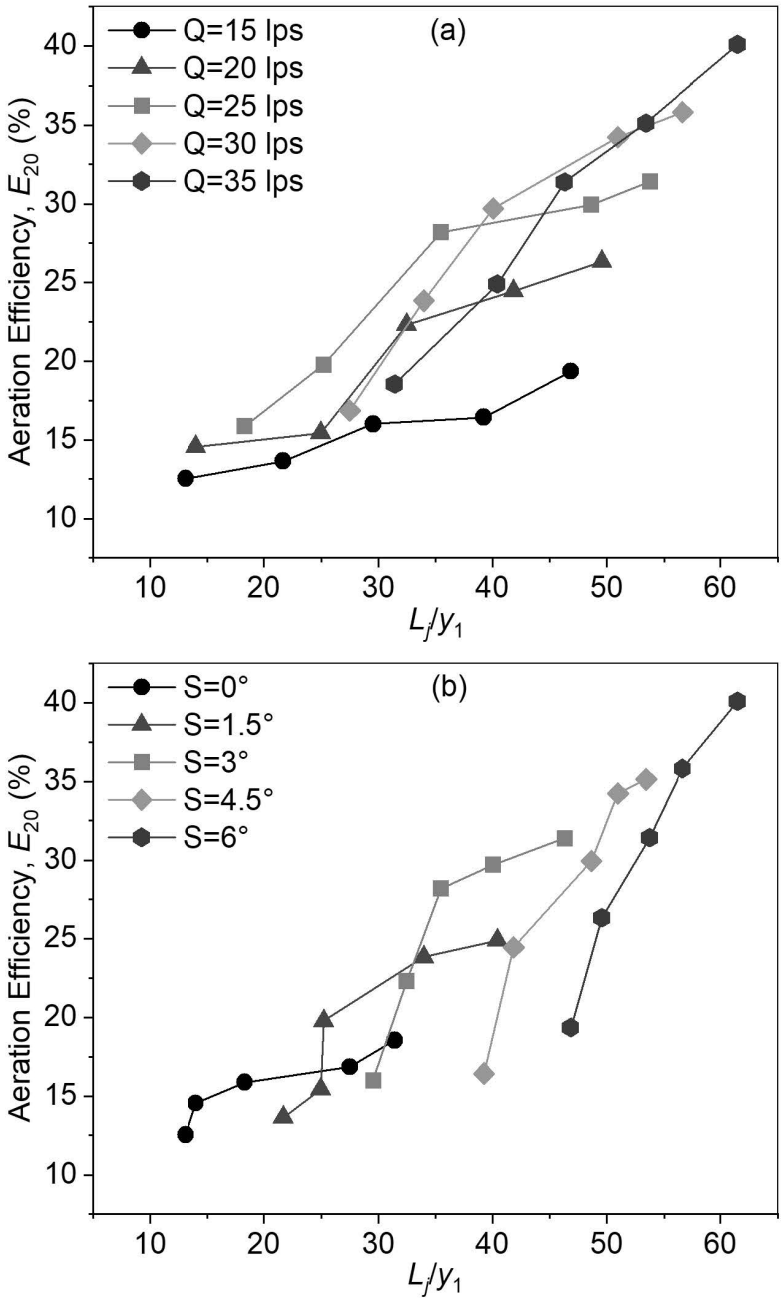

Fig. 6.18. Deviation of aeration efficiency during H-jumps using 1:4 ramp slope for different L_j/y_1 for (a) different flows, and (b) different bed slopes.

Therefore, with the increase of the Reynolds number strong turbulence is occurred and as a result, the oxygen transfer rate is increased. In Fig. 6.19(a) the aeration efficiency deviation with Reynolds number is plotted for a particular discharge with altered bed slopes in a divergence manner. The deviation is plotted for a particular bed slope with altered discharge in Fig. 6.19(b) and finds that with the improvement of Re, the E_{20} is increased as turbulence improves the air-water contact, breaks up air bubbles into smaller pieces, and increases the surface area of air bubbles.

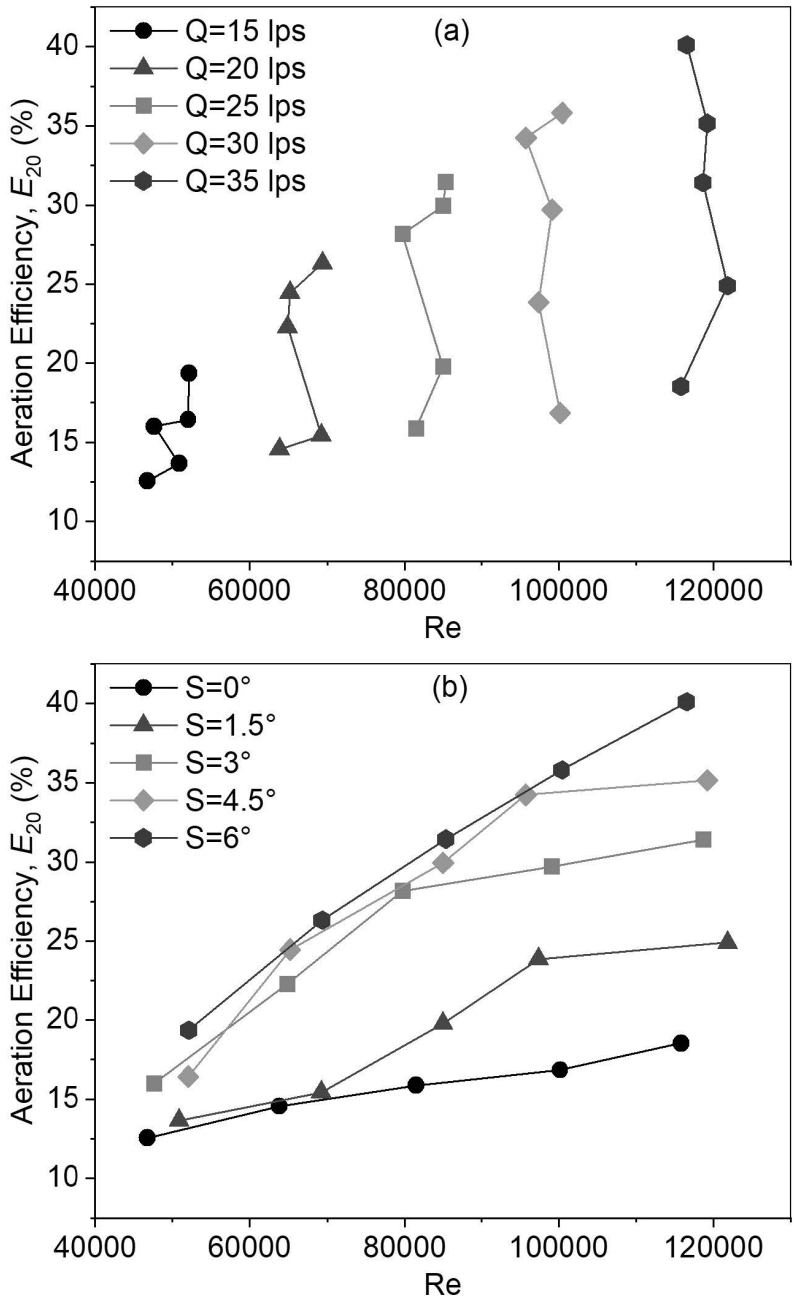

Fig. 6.19. Deviation of aeration efficiency during H-jumps using 1:4 ramp slope for different Reynolds numbers for (a) different flows, and (b) different bed slopes.

In systems like fermentation or wastewater treatment, the energy dissipation rate per unit width is a critical factor to determine aeration– efficiency. The energy dissipation rate has a direct impact on the oxygen transfer process by influencing the size of the gas bubbles and the intensity of mixing in the water. The relation of energy dissipation rates per unit width ($\Delta E_{loss}/H_1$) with aeration efficiency (E_{20}) is plotted in Fig. 6.20.

The amount of mixing and air diffusion is significantly influenced by the energy dissipation rate, which is a measurement of the energy lost in the fluid as a result of

turbulence. From Figs. 6.20(a-b), the minimum amount of $\Delta E_{loss}/H_1$ is found 0.15 for the lowest bed stiffness and minimum discharge and the maximum $\Delta E_{loss}/H_1$ is found 0.98 for the higher bed stiffness and maximum discharge.

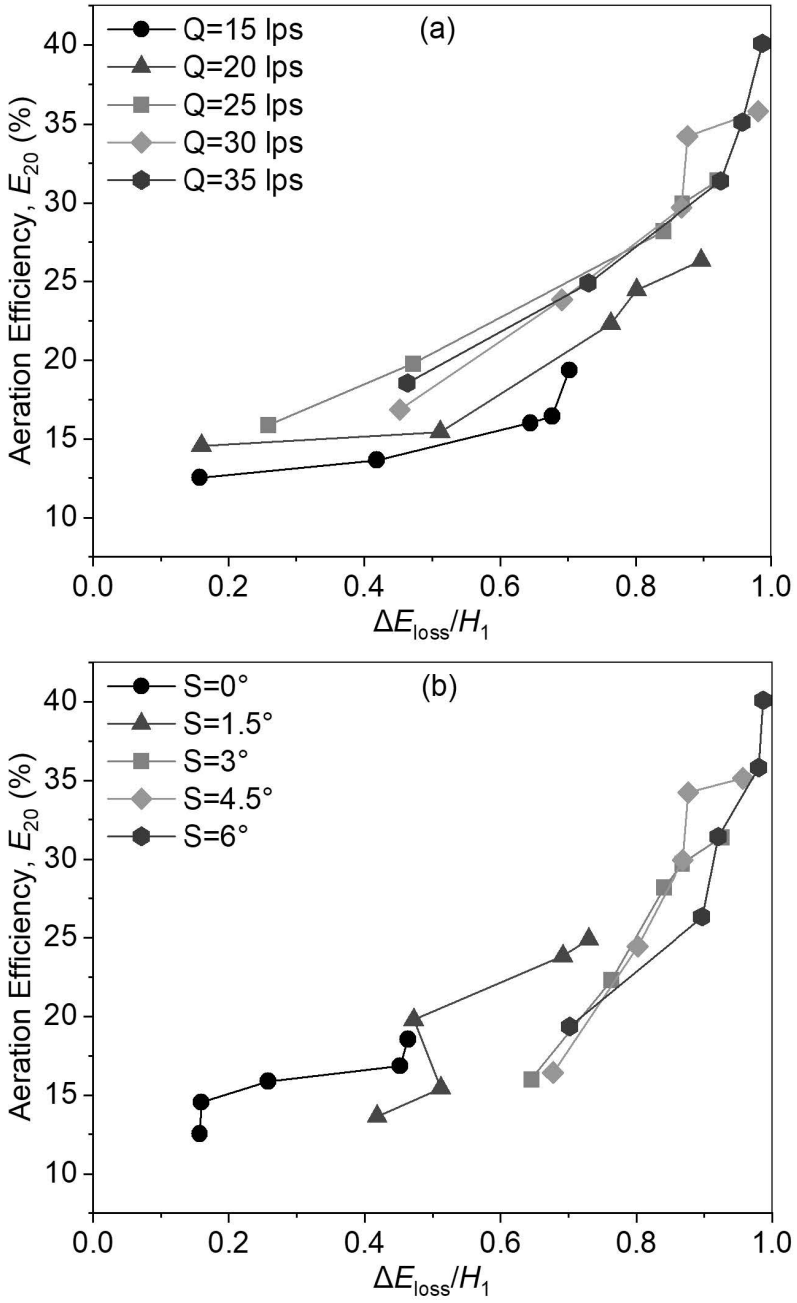

Fig. 6.20. Deviation of aeration efficiency during H-jumps using 1:4 ramp slope for different energy dissipation rates per unit width for (a) different flows, and (b) different bed slopes.

During H-jumps, a number of variables, like discharge and bed slope, affect the aeration– efficiency of a system. The oxygen– transfer efficiency, air-water interaction, and hydraulic conditions are all impacted by these two factors. Along with the higher discharge, the flow becomes more turbulent, which improves air water mixing and promotes air bubble

formation. As a result, the area of the water surface increases for better interaction with air. The bed slope is plotted along x-axis and percentage of aeration efficiency is plotted along y-axis, as shown in Fig. 6.21(a). Again, the discharge is plotted along the abscissa and the percentage of aeration efficiency is plotted along the ordinate [Fig. 6.21(b)].

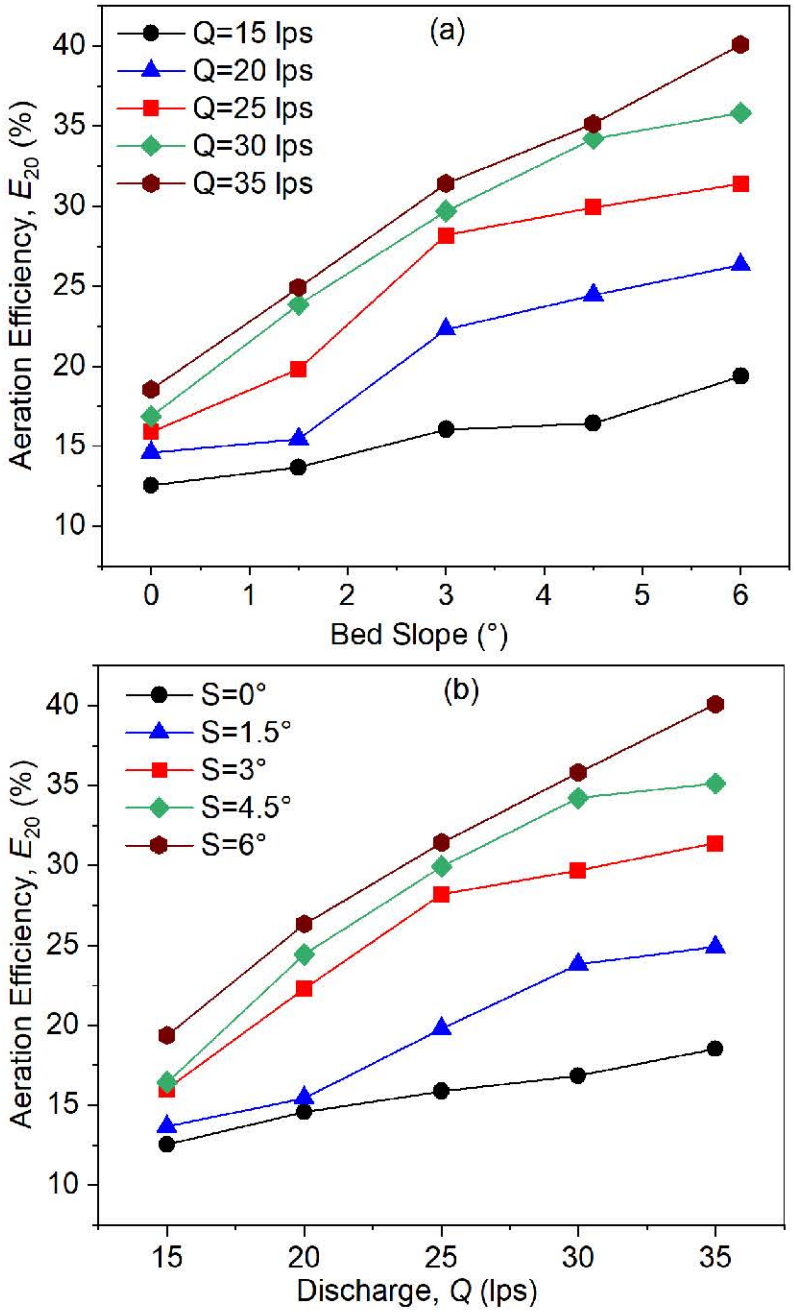

Fig. 6.21. Deviation of aeration efficiency during H-jumps using 1:4 ramp slope for (a) different discharges and (b) different bed slopes.

As in Fig. 6.21(a), the increasing pattern of E_{20} for different bed slopes seems to be the same for the discharge of 20 lps and 25 lps. Again the patterns are almost the same for the discharge of 15 lps and 35 lps. For the different discharges, the improvement shapes are nearly similar for the bed slope of 1.5° and 4.5° as shown in Fig. 6.21(b). The mixing

patterns in the aeration process can also be affected by a sloped bed. The bed slope is to produce more eddy currents or circulatory flows as a result the aeration efficiency is increased and mixing is improved due to better interaction between water and air. At 15 lps discharge, it is observed that E_{20} is increased from 12.6% to 19.4% for the minimum to maximum bed slopes and it is observed that as the discharge is increased for a specific bed slope like 6° the aeration efficiency is also on the rise from 19.4% to 40.1% for the discharge of 15 lps to 35 lps.

6.5. Conclusions

The study of H-jump characteristics in sloping rough beds through experimentation has great potential to further sustainable development by hydraulic engineering. A thorough examination of the H-jump phenomena on varying discharge and sloping rough beds has provided important new information about the intricate relationship between aeration efficiency and flow dynamics. This experimental study aims to investigate the impacts of aeration efficiency on jump features and establish the relationship between the dissolved oxygen (DO) variation and the most important H-jump parameters when the jump is formed in a rough bed using a ramp at the inlet. In order to accomplish this, 50 H-jump experiments are conducted using two different types of ramps, five distinct bed slopes, and five different discharges. Sequent depth, velocity, jump length, and DO measurements are made during tests conducted on rough beds for the experimental investigation.

- Large-scale eddies are generated during the H-jump formation on the rough bed. It is the undulations that are responsible for transporting air into the water as it flows.
- During open channel flows, the amount of DO measured after the H-jump improves quickly during the first several minutes and after a few occurrences, it starts to decline as it reaches its saturation.
- Reduced flow time from higher discharge rates may lead to inadequate mixing and decreased oxygen transfer when paired with an incorrect bed slope. However, higher discharge rates may aid in more efficient airflow distribution throughout the aeration system when combined with an ideal bed slope.
- The SD-Ratio is found to increase with the increase of experimental parameters. The aeration efficiency also improves with the escalation of the SD-Ratio as the inlet velocity has increased with the increase of discharge and bed slope. Compared to the 1:3 slope ramp, the setup of slope ramp 1:4 the SD-Ratio is more increased for the identical discharge and bed slope.
- Compared to the ramp slope of 1:3, the inlet velocity and the inlet Froude number are more in the 1:4 ramp slope. The upstream Froude number (Fr_1) is found as the primary factor influencing the aeration efficiency during the H-jump. For various upstream Froude numbers, fully developed H-jumps are always there. It is found that by raising the discharge and bed slope, the H-jump formation can improve the aeration efficiency. So with respect to Fr_1, the aeration efficiency is less in the 1:3 sloped ramp.

- For the same reason, the relative jump length plays a very crucial role in oxygen transfer. The Reynolds number has a direct correlation with aeration efficiency and is influenced by discharge and bed slope. The relative jump length and the range of Reynolds number are more for the 1:4 ramp slope.
- The maximum velocity drop for using the 1:3 bed slope as high as almost 89.4% is achieved for the experiment HJ25-RB and the 1:4 bed slope is 89.4% achieved for the experiment HJ50-RB. Maintaining a similar boundary condition is suggested to follow the experiment HJ25-RB and HJ50-RB for the best result in improving aeration efficiency for 1:3 slope and 1:4 slope respectively.
- In the present experimental condition using the 1:3 bed slope, the maximum energy dissipation rate per unit width is 97.6% for the experiment HJ24-RB.
- In the present experimental condition using the 1:4 bed slope, the maximum energy dissipation rate per unit width is 98.7% for the experiment HJ50-RB.
- Aeration efficiency in H-jumps through the experimental flume ranges from 10.8% to 37.0% for the 1:3 bed slope and for the 1:4 bed slope it ranges between 12.6% to 40.1%. The analysis of this experimental circumstance shows that discharge and bed slopes are the most influential parameters in aeration efficiency.
- These methodologies for the improvement of aeration efficiency can be applied to the re-aeration of wastewater treatment or fermentation to maintain a healthy DO concentration.

The discharge, bed material, channel shape, channel slope, and ramp slope may differ from the experimental setup with those in real-world scenarios. Therefore, when the water discharge, bed slope, and ramp slope are not constant, more rigorous research is necessary to arrive at a more distinct and reliable trend that illustrates the kind of fluctuation in these parameters.

References

Amaral, A., Bellandi, G., Rehman, U., Neves, R., Amerlinck, Y., & Nopens, I. (2018). Towards improved accuracy in modeling aeration efficiency through understanding bubble size distribution dynamics. *Water Research*, 131, 346-355.

Aras, E., & Berkun, M. (2012). Effects of tailwater depth on spillway aeration. *Water Sa*, 38(2), 307-312.

Baylar, A., & Bagatur, T. (2000). Study of aeration efficiency at weirs. *Turkish Journal of Engineering & Environmental Sciences*, 24(4), 255-264.

Baylar, A., & Bagatur, T. (2006). Experimental studies on air entrainment and oxygen content downstream of sharp-crested weirs. *Water and Environment Journal*, 20(4), 210-216.

Baylar, A., Bagatur, T., & Emiroglu, M. E. (2007). Aeration efficiency with nappe flow over stepped cascades. *Proceedings of the Institution of Civil Engineers - Water Management*, 160(1), 43-50.

Bunea, F., Nedelcu, A., & Ciocan, D. G. (2017). Prediction of water aeration efficiency in high turbulent flow. *Desalination and Water Treatment*, 85, 55-62.

Chanson, H. (1995). Air-water gas transfer at hydraulic jump with partially developed inflow. *Water Research*, 29(10), 2247-2254.

Chanson, H., & Qiao, G. L. (1994). Air bubble entrainment and gas transfer at hydraulic jumps. Research Report No. CE149, Department of Civil Engineering, University of Queensland, Australia.

Defina, A., Susin, F. M., & Viero, D. P. (2008). Bed friction effects on the stability of a stationary hydraulic jump in a rectangular upward sloping channel. *Physics of Fluids*, 20(3), 036601.

Esmaeili Varaki, M., Kamakoli, M., Biabani, R., & Navabian, M. (2022). Effect of large scale roughness of block ramps on dissolved oxygen efficiency in water. *Water Practice & Technology*, 17(7), 1490-1504.

Gulliver, J. S., Wilhelms, S. C., & Parkhill, K. L. (1998). Predictive Capabilities in Oxygen Transfer at Hydraulic Structures. *Journal of Hydraulic Engineering*, 124(7), 664-671.

Gupta, S. K., & Dwivedi, V. K. (2024). Experimental investigation of hydraulic jump characteristics in sloping rough surfaces for sustainable development. *Engineering Research Express*, 6(2), 025103.

Kucukali, S. (2005). Local Dissolved Oxygen (DO) Variations in The Vicinity of Different Boulder Arrangements Placed in A Flume. *Proceedings of the 31st IAHR World Congress*, Seoul. pp. 1464-1466.

Kucukali, S., & Cokgor, S. (2008). Boulder-flow interaction associated with self-aeration process. *Journal of Hydraulic Research*, 46(3), 415-419.

Palermo, M., & Pagliara, S. (2017). A review of hydraulic jump properties on both smooth and rough beds in sloping and adverse channels. *Acta Scientiarum Polonorum Formatio Circumiectus*, 16(1), 91-105.

Puri, D., Sihag, P., & Thakur, M. S. (2023). A review: Aeration efficiency of hydraulic structures in diffusing DO in water. *MethodsX*, 10, 102092.

Rajaratnam, N., & Kwan, A. Y. P. (1996). Air entrainment at drops. *Journal of Hydraulic Research*, 34(5), 579-588.

Rawat, V. S., Thendiyath, R., Bhatnagar, P., & Kumar, M. (2022). Hydro-environmental Characteristics for Flows Over Inclined Block Carpet. *Asian Journal of Water, Environment and Pollution*, 19(2), 33-40.

Sari, A., Bostan, T., Topçu, S., & Coşar, A. (2014). Determination of oxygen gain in hydraulic structures. 11th International Congress on Advances in Civil Engineering (ACE 2014), İstanbul, Turkey.

Wilhelms, S. C., Gulliver, J. S., & Parkhill, K. (1993). Reaeration at low-head hydraulic structures. Accession Number: ADA284089, US Army Engineer Waterways Experiment Station.

Overall Remarks

7.1. Conclusions and Remarks

In this research, experimental investigation and simulation of hydraulic jump in a rectangular laboratory channel at different flow directions was conducted. Several laboratory arrangements were prepared for this purpose. Firstly, the experiments were conducted to check the thermal dissipation during the hydraulic jump (H-jump) and correlate its key parameters with the thermal dissipation. The same phenomenon was numerically analysed through the Ansys Fluent 17 simulation model. Then another laboratory set up was prepared to identify the H-jump effects on aeration efficiency. This investigation was conducted in smooth bed as well as in rough bed conditions when the discharge and the bed slope were varied. Along with this during the rough bed experimentation, two different sloped ramps were utilized at the inlet position.

- It was observed that the specific energy varies with the pre-jump and post-jump depths.
- Under the same flow conditions, there is a significant change in the specific enthalpy of water as the temperature keeps on varying. Reynolds number also increases for the same conditions.
- Very limited literature has discussed the role of energy dissipation in terms of thermal dissipation during H-jumps. One simple way to examine thermal dissipation is by considering enthalpy, which is the method used here.
- Further experimentation is necessary to establish a clear trend to show the nature of variation of these parameters when the water temperature is not constant.
- The H-jump increased the heat dissipation from the water to the ambient i.e. the average temperature at a cross-section downstream of the H-jump was found to be less than the average temperature across the same section for a flow without the H-jump.
- The increase in specific enthalpy and specific entropy drops due to H-jumps was also a nonlinear function of the ambient temperature for the constant temperature of the water. Both the increase in specific enthalpy drop and specific entropy drop followed almost the same variation with ambient temperature.
- The amount of dissolved oxygen measured after the H-jump improves quickly during the first several minutes and after a few occurrences, it starts to decline.
- The SD-Ratio was found to increase with the increase in initial Froude number and bed slope and aeration efficiency at 20°C (E_{20}) was also improved with this escalation. For the same reason, the relative jump length plays a very crucial role in oxygen transfer. The Reynolds number has a direct correlation with E_{20} and is influenced by discharge and bed slope.

- In the case of rough bed, the SD-Ratio was also found to increase with the increase in inlet Froude number, and bed slope. The energy dissipation and aeration efficiency mainly depend on the bed roughness, discharge and channel bed slope. Compared to this ramp slope had a minimal effect on it.
- In this present study, the thermal dissipation through the H-jump was examined by considering the specific enthalpy. The relative energy dissipation was also calculated in this study. The thermal dissipation was close to 7% of the total energy dissipation for almost comparable flow parameters and similar boundary conditions.
- These methodologies for the improvement of E_{20} may be applied to the re-aeration of wastewater to maintain a healthy DO concentration.

7.2. Limitations

The H-jump characteristics under various flow circumstances can be predicted through the correlations between the key parameters as observed in this present study. In both experimental and simulation approaches, the relationship between the jump parameter and heat dissipation at various water temperatures and ambient temperatures has also been demonstrated. In both smooth bed and rough bed situations, a robust correlation has been found to predict aeration efficiency by the H-jump at various flow conditions. Despite these developments, there are a few limitations to take into account when implementing these discoveries in practical situations.

- The experimental models used in this study might not exactly represent the real-world circumstances where H-jumps occur, which may cause minor differences in the results when they are magnified.
- The study concentrates on a specific range of H-jump types which may not apply to other varieties or more intricate H-jump phenomena.
- The complexity of real-world systems may not be adequately captured by simulations, which frequently rely on idealised assumptions about fluid parameters, boundary conditions, or flow features.
- Particularly under turbulent flow circumstances, the study might not have taken into consideration every aspect of boundary layer interactions that can affect slightly heat dissipation and aeration efficiency.
- Measurements of heat dissipation and aeration efficiency may be marginally impacted by experimental error or inaccuracy because of sensor resolution limitations, calibration issues, or environmental variables such as changes in the ambient temperature.
- Initial conditions and simulation parameters such as fluid velocity, temperature, or geometry, may have an impact on the study and can lead to minor changes in the results.
- In a real-world channel bed, there may be several non-uniform sediment particles along with flora and fauna while in our experimental setup, we consider either a smooth bed or a uniformly rough bed.

- Real-world applications can be influenced by factors like weather, air pressure, humidity, and external turbulence, which may not be adequately captured in either experimental or simulation setups.
- In the aeration efficiency experiments, the dissolved oxygen was measured at five different locations with a single DO sensor probe. Results may vary slightly if multiple DO sensor probes were used simultaneously for data collection.

7.3. Future Scopes

After completing the thorough investigative analysis of the H-jump in a rectangular laboratory tilting flume, several parts of the study might have further been developed.

- In the laboratory setup, a fixed dimensional rectangular flume is used for the experiment. But in the real world, along with this rectangular shape, other cross-sectional shapes are also present. So in order to expand on this work a trapezoidal, circular or triangular shaped cross-sectional laboratory tilting flume might be used for the same experimental investigation.
- A natural channel bed may contain a number of non-uniform gravel or silt particles. All of these bed materials have the potential to alter the flow properties, energy dissipation rate, and atmospheric air entrainment level in the moving water. Presently, some experiments were conducted on a uniform bed roughness. Similar experiments may be carried out using different bed materials with distinct roughness heights and variations of results may be observed.
- Many other different arrangements of gravels with similar and different roughness heights may be made for experimentation.
- The experimental work of heat dissipation was conducted only on five specific water temperatures. For experimental research, a wider range of temperatures may be used.
- A laboratory flume with a smooth bed was used for the heat dissipation experiments. As a rough bed helps to increase turbulence, comparable studies might be conducted on a rough bed.
- Here the study of temperature simulation was done for a fixed water temperature along with several ambient temperatures. More simulations may be done with distinct water temperatures and can be compared the both experimental and simulated results.
- In this study, two different sloped ramps were utilized in the rough bed experimental setup. Using other ramp slopes, similar experiments could be conducted in the smooth bed, and varied outcomes may be seen.
- In the present research investigation, only five different discharges were used. For the air entrainment, there will be a minimum retention time of the turbulence. For a higher discharge value, if this retention time is less, the air entrainment due to turbulence does not take place properly. As a result, the aeration efficiency will not

increase with the increase of discharge. More experiments with higher ranges of discharge may be conducted to find out this point of singularity.

- Similarly, when the bed stiffness is too high this retention time of turbulence also decreases and the jump is not stable. Therefore, apart from these experimental bed slopes, higher slopes may be selected for future experimentation to identify the singular point of the improvement trend of aeration efficiency and energy dissipation rate with bed slopes.

Flow Measurement and Instrumentation 100 (2024) 102715

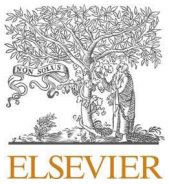

Contents lists available at ScienceDirect

Flow Measurement and Instrumentation

journal homepage: www.elsevier.com/locate/flowmeasinst

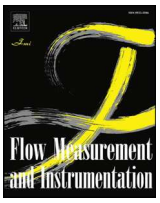

Experimental investigation of dissolved oxygen improving aeration efficiency by hydraulic jumps

Saikat Mondal [a], Rajib Das [a], Subhasish Das [a,*], Sanchayan Mukherjee [b]

[a] School of Water Resources Engineering, Jadavpur University, Kolkata, 700032, India
[b] Department of Mechanical Engineering, Kalyani Government Engineering College, Kalyani 741235, India

ARTICLE INFO

Keywords:
Hydraulic jump
Froude number
Reynolds number
Air entrainment
Dissolved oxygen
Aeration efficiency

ABSTRACT

The dissolved oxygen (DO) level in water is vital for water quality and supporting aquatic life. Hydraulic jumps involve rapid flow changes from super-critical to sub-critical, visible at abrupt bed slope shifts, like at spillway bases in rivers or canals. The hydraulic jump efficiently mixes oxygen from air into water and offers a cost-effective method of aeration by entraining air bubbles in the stream to improve oxygen transfer compared to traditional systems. The objective of this experimental research is to investigate the aeration performance with hydraulic jump parameters and establish correlations crucial to measuring aeration (or transfer) efficiency. Relationships between transfer efficiency, jump height, jump length, sequent depth ratio, discharge, inlet Froude number, and channel bed slope were determined. To investigate the nature of such relationships, a series of experiments were conducted in a rectangular tilt flume to test the aeration performance of forced submerged hydraulic jumps with five different discharges and five different smooth bed slopes. The inlet Froude number before the jump varied from 2.18 to 8.23. Experimental observation confirms a positive relationship between transfer efficiency and jump control parameters. During experimentation, transfer efficiency was found to vary between 9.4 % and 34 %. This research includes estimating the optimal transfer efficiency due to hydraulic jumps, which can help hydraulic engineers in building structures that can revitalize any degraded stream.

1. Introduction

It is not always necessary for solid boundaries to enclose a fluid's flow along all sides. Under these conditions of flow, the liquid's free surface serves as the topmost boundary. The continuous atmospheric pressure is the only force operating on the free surface. This top free atmospheric boundary causes the air water interaction in a fluid flow. Open channels include rivers, streams, irrigation ditches, man-made canals, and flumes. The phenomenon of an abrupt transition from a rapid flow to a tranquil flow is known as a hydraulic jump. A rapid flow could be triggered by a fast-moving liquid release in a channel beneath a sluice gate or at the base of a steep spillway. If this flow needs to be slowed to a uniform tranquil flow due to an obstruction downstream or the roughness of the boundary of a long channel with a mild slope, the only way to do so is to abruptly switch from rapid to tranquil flow at a specific point rather than gradually transitioning through the critical condition. In a hydraulic jump, the water surface abruptly discontinues at the jump position, and turbulence causes a significant quantity of energy to be dissipated. Large scale turbulence, surface waves and spray, energy dissipation, and air entrainment are its defining characteristics [1]. The term "roller" typically refers to this large-scale turbulence zone in hydraulic jumps. Strong mixing and extremely turbulent flows create an air-water contact in hydraulic jumps that assures gas transport.

Any body of water gets its dissolved oxygen (DO) from aerobic aquatic plants and atmospheric aeration. An increase in the concentration of dissolved oxygen in a river system can be attributed to hydraulic features. Rivers that flow, falling water via rapids, and wind-driven ripples all dissolve the free oxygen into the water. It is generally accepted that a substantial population of several fish species may be sustained within the minimal DO range of 4–5 mg/l [2]. Waterbody may have oxygen stratification in addition to temperature stratification. The DO typically has a high concentration in the higher sections close to the water's surface, falls in the thermocline zone, and is low or nonexistent in the water's lowest region. Since many types of aquatic life cannot thrive in environments with low DO, it is important to assess and identify the different re-oxygenation processes to develop structures that

* Corresponding author.
E-mail addresses: saikatm.swre.rs@jadavpuruniversity.in (S. Mondal), rajib.das@jadavpuruniversity.in (R. Das), subhasish.das@jadavpuruniversity.in (S. Das), sanchayan.mukherjee@kgec.edu.in (S. Mukherjee).

https://doi.org/10.1016/j.flowmeasinst.2024.102715
Received 17 June 2024; Received in revised form 5 October 2024; Accepted 14 October 2024
Available online 16 October 2024

DOI: 10.24906/isc/2020/v34/i4/205477

Search and Survey

Experimental Study of Thermal Effect on Oscillating Hydraulic Jump

Saikat Mondal[1], Sanchayan Mukherjee[2], Subhasish Das[3]

Abstract

Oscillating hydraulic jump experiments were conducted by increasing the temperature of water from minimum to maximum within a range of measurement. By varying temperature from 32-40°C, different jump characteristics were observed and noted. The varying temperature was measured throughout the jump profiles and dependence of jump parameters with varying temperature is measured and quantified. This study may find applications where a changing stream water temperature significantly affects the jump characteristics.

Key words: Rapidly Varied Flow; Subcritical Flow; Supercritical Flow; Froude Number; Sequent Depth Ratio

1. Introduction

A free surface channel is a ditch where the involved liquid flows over it maintaining atmospheric pressure. Gravity is the main force here which motivates the liquid flow. In open channel flow, the water acts as an incompressible liquid leads one to value the significance of energy due to gravity as the maximum force and the Froude number as the main number in the non-dimensional form, that govern the flow occurrence in the open channels. Rapidly varied flow is a type of open channel flows with high curvatures, the result of which is the incidence of non-hydrostatic type pressure distribution areas over a large part of the flow. Again, a rapidly varied flow phenomenon often occurs locally in the sense of friction rather than a small role. The jump is an important rapidly varied flow phenomenon. Hydraulic jump marks the flow conversion from supercritical to subcritical flow. Jumps are mostly served as energy dissipaters to disperse surplus kinetic energy of super-critically moving liquid downstream of typical hydraulic arrangements, like different spillways, and flow controlling sluice gates. The different uses of hydraulic jumps are: (i) well-organized procedure of flow-discharge measurement in flumes, (ii) incorporation of several chemicals, (iii) to assist intense assimilation and gas-transport in chemical practices, (iv) desalination of

[1]Ph.D. Student, School of Water Resources Engineering, Jadavpur University, Kolkata-700032, India. E-mail: saikatju86@gmail.com
[2]Associate Professor, Department of Mechanical Engineering, Kalyani Government Engineering College, Kalyani-741235, India. E-mail: sanchayan02@yahoo.com
[3]Assistant Professor, School of Water Resources Engineering, Jadavpur University, Kolkata-700032, India. E-mail: subhasishju@gmail.com
ORCID: Saikat Mondal:https://orcid.org/0000-0002-9851-9542
ORCID: Sanchayan Mukherjee: https://orcid.org/0000-0001-9606-1657
ORCID: Subhasish Das: https://orcid.org/0000-0002-6512-7454

An Approach to Improve Water Quality by Increasing Aeration Efficiency Through Hydraulic Jumps

Saikat Mondal, Subhasish Das, Rajib Das, and Sanchayan Mukherjee

Abstract A measure of a waterbody's water quality and, consequently, its ability to support aquatic life, is the dissolved oxygen (DO) concentration in the water. A hydraulic jump is caused by a swift or abrupt conversion of the flow commencing from supercritical form to subcritical. It can be found at the bottoms of spillways, in channels, canals beneath sluiceways, or when a slope suddenly becomes flatter after steepness. It causes abrupt rises in water level, surface-roller formation, and energy dissipation. Using these as a potent natural blender for oxygen transport can elevate DO levels in the water bodies, causing turbulence. The primary cause of this oxygen transmission is the entrainment of air into the stream through numerous air foams, which aids the air–water transfer. In this investigation, hydraulic jumps were developed in a rectangular laboratory channel, performing a series of experiments, to observe jump parameters and aeration efficiency varying discharge and bed slope. Hydraulic jump, herein, is formed by adjusting a tailgate and experiments are done at five different discharges and two different bed slopes. During experimentation, the inlet Froude number (F_{r1}) before the jump ranges between 2.18 to 7.95. Between the hydraulic jump controlling parameters with the rate of energy dissipation and aeration efficiency high correlations are observed. Throughout the series of experiments, it is found that the aeration efficiency varies from 0.1096 to 0.3333. Results conclude that the hydraulic jump effectively dissipates energy and transfers oxygen. This research has applications in estimating the efficiency of hydraulic jump aeration.

Keywords Hydraulic jump · Subcritical flow · Supercritical flow · Froude number · Dissolved oxygen · Aeration efficiency

S. Mondal (✉) · S. Das · R. Das
School of Water Resources Engineering, Jadavpur University, Kolkata, India
e-mail: Saikatju86@gmail.com

S. Mukherjee
Department of Mechanical Engineering, Kalyani Government Engineering College, Kalyani, India

A. Mukhopadhyay and K. Ghosh (eds.), *Advances in Thermo-Fluid Engineering*,
Lecture Notes in Mechanical Engineering,
https://doi.org/10.1007/978-981-97-7296-4_16

Effect of Hydraulic Jump on Aeration Efficiency in Terms of Dissolved Oxygen in an Experimental Channel

[1]Saikat Mondal*, [2]Rajib Das, [3]Subhasish Das,[4]Sanchayan Mukherjee
[1,2,3]School of Water Resources Engineering, Jadavpur University
[4]Mechanical Engineering, Kalyani Government Engineering College
*saikatju86@gmail.com

The content of dissolved oxygen (DO) in a waterbody is one of the most important parameters for determining water quality and, therefore, a measure of the ability of water to sustain aquatic life. Hydraulic jump is formed whenever there is a rapid or sudden change of flow from super-critical to sub-critical nature in open channels. In such transition, the water level rises suddenly, surface rollers form simultaneously, air enters rapidly, extreme mixing occurs, and energy dissipates. Taking advantage of these typical properties, the hydraulic jump is used as an effective natural mixer for oxygen transfer and can increase the amount of DO in a waterbody creating turbulent conditions. Hydraulic jump, in present study, is formed by adjusting a tailgate in a rectangular flume.Several experiments are conducted to determine jump characteristics and the aeration efficiency for different discharges and bed slopes. The aeration efficiency and energy dissipation rate are found to be strongly associated with the hydraulic jump data. From these results, the hydraulic jump is found to be effective for oxygen transfer and energy dissipation.

Saikat Mondal
27/01/2025

Ph.D. Thesis

ORIGINALITY REPORT

5%
SIMILARITY INDEX

PRIMARY SOURCES

1	pt.scribd.com Internet	398 words — 1%
2	www.researchgate.net Internet	136 words — < 1%
3	www.fedoa.unina.it Internet	120 words — < 1%
4	www.jaduniv.edu.in Internet	98 words — < 1%
5	mafiadoc.com Internet	91 words — < 1%
6	www.i-scholar.in Internet	82 words — < 1%
7	espace.library.uq.edu.au Internet	78 words — < 1%
8	www.tandfonline.com Internet	69 words — < 1%
9	archive.org Internet	62 words — < 1%
10	kupdf.net Internet	

Subhasish Das 27/01/25
Dr. Subhasish Das
Associate Professor & Joint Director
School of Water Resources Engineering
Jadavpur University
Kolkata - 700032

Sanchayan Mukherjee 27/1/2025
Associate Professor
Department of Mechanical Engineering
Kalyani Govt. Engg. College, Kalyani, Nadia

Saikat Mondal 27/01/2025
Rajib Das 27/01/2025
Dr. RAJIB DAS
Assistant Professor
School of Water Resources Engineering
Jadavpur University
Kolkata-700 032